UNIVERSITÉ DE STRASBOURG

ÉCOLE DOCTORALE EDSC (ED n°222)
Biophysique des Membranes et RMN

THÈSE

présentée par :

Patricia KEMAYO KOUMKOUA

soutenue le : **30 septembre 2015**
pour obtenir le grade de

Docteur de l'université de Strasbourg
Discipline/ Spécialité : Biochimie et biophysique des protéines

STRUCTURAL CHARACTERISATION OF HIGHLY SPECIFIC MEMBRANE PROTEIN-LIPID INTERACTIONS INVOLVED IN CELLULAR FUNCTION

THÈSE dirigée par:
M. BECHINGER Burkhard Professeur, Université de Strasbourg

RAPPORTEURS :
M. STURGIS James Nathaniel Professeur, University of the Mediterranean
M. DUFOURC Erick Joël Directeur de recherche, CNRS

AUTRES MEMBRES DU JURY :
Mme LEIZE-WAGNER Emmanuelle Directeur de recherche, CNRS
Mme Sizun Christina Chargé de recherche, CNRS

To the KING OF GLORY,

The LORD,

him who is able to do exceeding abundantly above all that we ask or think, according to the power that worketh in us (Ephesians 3:20).

Acknowledgements

This thesis work was achieved in the NMR and membrane biophysics laboratory (CNRS, UMR 7177) directed by Prof. Burkhard Bechinger my thesis director to whom I express all my gratitude for the opportunity he gave me and for the trust he testified me during these three years. I also sincerely thank our collaborators of Heidelberg who provided preliminary data and background to start this work: Prof. Dr. Felix Wieland, Pr. Britta Brügger, Dr. Andreas Ernst, Alexia Herrmann.

I would like to extend my appreciation to my committee members: Dr. Emmanuelle Leize-WAGNER, Prof. James Sturgis, Dr. Christina Sizun and Dr. Erick Dufourc for their useful comments during my defence. I'm especially grateful to Prof. Sturgis and Dr. Dufourc who agreed to revise the manuscript.

This thesis would not have been possible without the help and discussion with my collegues who agreed to share their scientific knowledge and experiences:
I first express my gratitude to Dr. Christopher Aisenbrey my supervisor for his tremendous help and initiation to a great number of biophysical methods: the solid- phase peptide synthesis, the ssNMR, the circular dichoism and fluorescence. I also thank him for his advices, availability, kindness and for the many interesting and stimulating discussions. I owe my deepest gratitude and special warm thanks to Dr. Elise Glattard with who I share a lot first as colleague and lately as the good friend, she became to me. Indeed, she has been a support at all times during this journey of three years. I thank her for the interesting and stimulating scientific discussions in molecular biology and for all her advices during the review of my defense. I also express my gratitude to Dr. Evgeniy Salnikov, who helped me with the ssNMR experiments and data analysis along with many critical discussions and review my thesis defence. It is also my pleasure to thank Dr. Jésus Raya who introduce me the ssNMR device, the bases of magnetization and contributed to my knowledge and understanding in this field. I would also like to thank Dr. Philippe Bertani for his help and discussion from time to time. I also thank the rest of our laboratory members including some students who defend their PhD and left: Delphine, Nicole, Omar, Anna, Mathias, Nataliia, Barbara, Arnaud... for exchanges and discussions. Caroline and specially Nadia for making me often facilitate administrative tasks and for the kind advices.

I am indebted to Prof. Michel Rohmer and his team members: Prof. Catherine Grosdemange-Billiard, Dr. Denis Tritsch, Aurore Dreneau, Mathilde Munier**,** for welcoming Elise and I in their building office, for sharing amazing and interesting discussion during the lunch and for the support during my thesis writting and defense. I specially thank Aurore and Mathilde the best singers I ever meet, who contributed to make the end of this journey pleasant.

I also thank Dr Martine Heinrich for her availability and advices for the circular dichroism experiments.

It is my fortune to thank Arsene Noume my treasure, my help and partner in life, my husband, and friend for his love, his encouragement, his precious help, his patience, his humour, and to stand by me at all times. I owe this thesis to my lovely mother, Justine Loudjoe for her love, her hard work and sacrifices to give me the best she had and her unconditional trust. She never stops encouraging me to give the best in life; she is a source of inspiration. I thank my sister Vanessa and my brother Franck for their encouragement and support. I also owe this thesis to my grandfather who has been very proud of me. I thank him for the trust in me and his encouragement to start this long academic journey. I am thankful to my uncle Hypollyte, his wife Béatrice and their children (Loïc and Chris) for their love, encouragement and support. My cousin Franck for the listening and support.

I would like to express also my gratitude to my sisters and brothers in church as well as my friend in Strasbourg who contributed in their own way to this work along encouragement, discussion and support: Clémentine, Francine, Jean-Claude, Ethan, Marie-Jeanne, Pamela, Matthieu, Bastien, Fatou.

I am also thankful to my wonderful friends in Switzerland for their support and encouragement: Nana, Isabelle, James, Deasun, Erika, Elsy.

Accomplishment of this PhD thesis was made possible with the financial support from the l'Agence National de la Recherche (ANR) to whom I express my gratitude.

Resumé

Les lipides sont des composants majeurs des membranes biologiques. La plupart d'entre eux sont synthétisés dans le reticulum endoplasmique (RE) à l'exception de la sphingomyéline (SM). En effet, la céramide molécule précurtrice, est d'abord synthétisée dans le RE ensuite transporté via des vésicules jusqu'à l'appareil de Golgi où la SM est synthétisée. Ce transport se fait par des vésicules spécialisées COP (**CO**at **P**rotein) I et II qui transportent respectivement les molécules dans le sens retrograde et antérograde entre le RE et le cis Golgi. Les vésicules COPI agissent activement dans les deux sens au niveau du Golgi.

Récemment, *Contreras et al* ont décrit une interaction protéine-lipide entre la SM et la protéine transmembranaire de typeI p24, fortement présente dans la membrane des vésicules COP I. Elle interagit spécifiquement parmi les différentes espèces moléculaires de SM avec la SM C 18 et cette interaction semble impliquer à la fois la tête lipidique et les chaînes aliphatiques. Il a été montré que l'interaction est conservée lorsque la protéine est réduite à son domaine transmembranaire (p24TMD, 21 résidus) et les résidus impliqués ont été identifié par mutagénèse : **V**XX**TL**XX**IY**. Une telle spécificité n'avait alors été identifiée que dans le cas d'interaction protéine-protéine et protéine-acide nucléique comme impliquée dans la régulation de fonctions cellulaires. En effet, il a été suggéré que l'interaction p24TMD-SM C18 serait potentiellement impliquée dans la régulation du mécanisme de formation des vésicules COPI. L'ensemble de ces travaux ont également permis de proposer un modèle du complexe p24TMD-SM C18 simulé par dynamique moléculaire. Nous avons voulu caractériser cette interaction en apportant des données structurales dans le but ultime de comprendre sa fonction.

Dans cet objectif, nous avons tout dabord procedé à l'obtention du peptide p24TMD, à sa reconstitution dans les liposomes après purification et à sa caractérisation par différentes méthodes spectroscopiques telles que la résonnance magnétique nucléaire (RMN), le dichroïsme circulaire (DC) et la fluorescence du tryptophane (Trp). Une étude de DC après reconstitution du peptide dans différentes membranes, nous a permis de caractériser l'interaction entre le p24TMD et la SM C18. Des études structurales obtenus par RMN du solide des écahntillons orientés, ont montré que cette interaction n'affecte pas de manière significative la topologie et la dynamique du peptide mais en revanche influencerait l'orientation de la chaîne latérale des acides aminés impliqués (leucine 23). Bien que l'ensemble des travaux présentés dans ce manuscrit ne permettent pas à ce jour de valider ou d'infirmer le modèle proposé, les résultats obtenus ont permis de comprendre caractériser cette interaction et ont apportés des informations structurales sur la topologie et la dynamique du p24TMD dans les membranes. D'autres études structurales par RMN du solide tel que la rotation à l'angle magique (MAS pour Magic Angle Spinning), le PISEMA (Polarization Inversion Spin Exchange at the Magic Angle) et le REDOR (Rotational Echo DOuble Resonance) sont necessaires pour compléter les résultats présentés dans ce manuscrit.

Abstract

The lipids are major components of biological membranes. Most of them are synthesized in the endoplasmic reticulum (ER) with the exception of sphingomyelin (SM). In fact, the ceramide (SM precursor) is first synthesized in the ER then transported via vesicles to the Golgi apparatus where the SM is synthesized. This transport is done by specialized vesicles COP (Coat Protein) I and II, which respectively carry the molecules in the direction retrograde and anterograde between the cis Golgi, and ER. The COPI vesicles actively act in both directions in the Golgi apparatus.

Recently, *Contreras et al* described a protein-lipid interaction between the SM and the type I transmembrane protein p24, mostly present in the membrane of the vesicles COP I. This protein specifically interacts among the different SM molecular species only with the SM C18 and this interaction seems to involve both the lipid head group and the aliphatic chains. It has been shown that the interaction is conserved when the protein is reduced to the transmembrane domain (p24TMD, 21 residues) and the residues involved were identified by mutagenesis: **V**XX**TL**XX**IY**. Such specificity was identified in the case of protein-protein interaction and protein-nucleic acid as involved in the regulation of cellular functions. Indeed, it has been suggested that the p24TMD-SM C18 interaction is potentially involved in the regulation of COPI vesicles biogenesis. Contreras et al proposed a molecular dynamics model of the p24TMD SM-C18 complex. To understanding the function of such specific interaction, here we proposed to investigate it by providing some structural data.

With this purpose, we first obtained the p24TMD peptide and after purification and reconstitution in liposomes, we proceed to his characterization using various spectroscopic methods such as nuclear magnetic resonance (NMR) spectroscopy, circular dichroism (CD) and the fluorescence of the tryptophan (Trp). CD investigation after reconstitution of the peptide in various membranes, has allowed us to characterize the interaction between the p24TMD and SM C18. Structural studies by solid state NMR of oriented samples showed that this interaction does not significantly affect the topology and dynamics of the whole peptide but influence the orientation of the amino acids side chains the involved in the interaction (leucine 23). Although all the work presented in this manuscript do not allow that day to validate or invalidate the proposed model, the results we obtained have allowed us to understand and characterize this interaction and have shed light on the topology and dynamics of p24TMD in membranes. Other structural solod state NMR studies such as the Magic Angle Spinning (MAS), the PISEMA (Spin Polarization Inversion Exchange at the Magic Angle) and REDOR (Rotational Echo Double Resonance) are needed to complete the results presented in this manuscript.

Publications

Some ideas and figures have appeared previously in the following publications:

Patricia Kemayo Koumkoua, Christopher Aisenbrey, Evgeniy Salnikov, Omar Rifi, Burkhard Bechinger, On the design of supramolecular assemblies made of peptides and lipid bilayers, *Journal of Peptide Science*, 2015, 21, 8

POSTERS

Kemayo K P, Aisenbrey C, Salnikov E, Bechinger B. Structural characterisation of highly specific membrane protein-lipid interactions involved in trafficking. A novel regulatory mechanism in membrane dynamics ? Conference of the société française de biophysique (SFB) and the société française de biochimie et de biologie moléculaire (SFBBM). Grenoble, France, 21-23 November 2012, (**winner of poster prize from the SFB and the SFBBM**).

PRESENTATIONS

Kemayo K P, Aisenbrey C, Salnikov E, Brügger B, Bechinger B. NMR studies of highly specific lipid-protein interactions in lipid bilayers. Réunion plénière GDR 3334 SupraMemBio : Assemblages supramoléculaires et membranes biologiques : Concepts, modèles et fonctions. Fournols, 14-17 October 2012.

Kemayo K P, Aisenbrey C, Glattard E, Salnikov E, and Bechinger B. Structural characterisation of highly specific membrane protein-lipid interactions involved in trafficking. A novel regulatory mechanism in membrane dynamics? Workshop of the German-French PhD College: "Membranes and Membrane Proteins" UFA 0407. Strasbourg, 30 November 2012.

Kemayo K P, Aisenbrey C, Glattard E, Salnikov E, and Bechinger B. Structural characterisation of highly specific membrane protein-lipid interactions involved in trafficking. A novel regulatory mechanism in membrane dynamics? ANR awardee mid-term workshop of the projects selected in 2010. Strasbourg, 7 December 2012.

Contents

Lists of figures

List of Abbreviations

Lipids:

PC: phosphatidylcholine
POPC: 1-palmitoyl-2-oleoyl-sn-glycero-3-phosphocholine
DPPC: di-palmitoyl-phosphatidylcholine
POPG: 1-palmitoyl-2-oleoyl-sn-glycero-3-[phospho-rac-(1-glycerol)]
POPE: 1-palmitoyl-2-oleoyl-sn-glycero-3-phosphoethanolamine
POPS: 1-palmitoyl-2-oleoyl-sn-glycero-3-phospho-L-serine
DOPC: 1,2-dioleoyl-sn-glycero-3-phosphocholine
SM: N-octadecanoyl-D-erythro-sphingosylphosphorylcholine (Sphingomyelin)
CL: cardiolipin

Others:

NMR: Nuclear Magnetic Resonance
ssNMR: solid state NMR
PAF: Principal Axis Frame
REDOR: Rotationnal Echo Double Resonnance
MAS: Magic Angle Spinning
PISEMA: Spin Polarization Inversion Exchange at the Magic Angle
MLV: multilamellar vesicle
SUV: small unilamellar vesicle
CP: Cross-Polarization
CD: Circular Dichroism
Fmoc: 9-Fluorenylmethoxycarbonyl
HPLC: High Performance Liquid Chromatography
RP-HPLC: Reverse Phase HPLC
CSA: Chemical Shift Anisotropy
CS: Chemical Shift
ppm: parts per million
LB: Lysogeny Broth
IPTG: IsoPropyl β-D-1-ThioGalactopyranoside
pTIPX-4: Taf12 Insoluble -mediated peptide eXpression
FID: Free Induction Decay
PAGE: Polyacrylamide Gel Electrophoresis
SDS: Sodium Dodecyl Sulfate
HRP: Horse Radish Peroxidase
AP: Alkaline Phosphatase
EtBr: Ethidium Bromide
TFA: Tri-Fluoro-Acetic acid
MALDI-TOF: Matrix-Assisted Laser Desorption/Ionization-Time-Of-Flight
LM : Linear Mode
RM : Reflectron Mode

CMC: Critical Micellar Concentration
AFC: AFfinity Chromatography
MCS: Multiple Cloning Site
MBP: Maltose-Binding Protein
SPPS: Solid Phase Peptide Synthesis
DMF: N,N-dimethylformamide
TMD: Trans Membrane Domain
P/L: Protein/ lipid ratio
OD : Optical Density
DPC: n-dodécylephospholine
EDTA : EthyleneDiamineTetraacetic Acid
IMAC: Immobilized Metal Afiinity Chromatography
DNA: Desoxyribonucleic Acid
E. coli : Escherichia coli

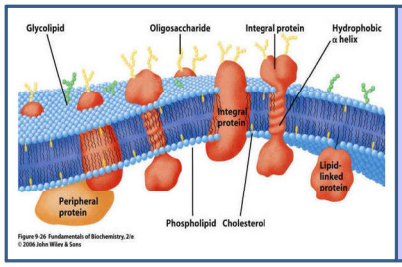

Chapter-I

GENERAL INTRODUCTION

This chapter is meant to give a general overview on biological membranes, and highlights the features that distinguish them from each other in terms of compositions and properties. As lipids represent the basic element of these membranes, their synthesis and sorting to the cellular plasma membrane are described here as well as their physical chemical properties. Furthermore, this part also emphasis on how lipids are used in model systems when we try to make sensible emulations of in vivo systems because the complexity of natural membranes hampers their biophysical investigation. Moreover, the properties that trigger their interaction with proteins within the membrane are also presented.

Chapter 1. General Introduction

1.1. Generalities on biomembranes

Biological membranes are essential for life as they play a central role in both the structure and function of all cells, prokaryotic and eukaryotic, plant and animal. They define the boundaries of the cell and are the point of contact between the cell and its environment. They also define cellular compartments, like numerous membranous organelles in eukaryotic cells (Figure 1) Membranes do not only define compartments, they also play an important role in all communication between the cell and its environment. They provide specialized permeability barriers for cells and cell organelles, in which the interplay of lipids and membranes proteins facilitates basic cellular processes as ions exchange. Moreover, most of the fundamental biochemical functions in cells involve membranes at some point, including such diverse processes as prokaryotic DNA replication, protein biosynthesis, protein secretion, bioenergetics, and signal transduction.

The structure and organization of biomembranes have been a matter of debate until the late 1970s. For many years, biologists thought the protein covered the outer surfaces of the phospholipid bilayer like a coat of paint. The initial model for membrane structure was proposed by Davson and Danielli in 1935. It portrayed the membrane as a phospholipid bilayer coated on both sides by protein. Thereafter, Michael Robertson proposed in 1960 the Unit Membrane Hypothesis which suggests that all biological membranes have a similar basic structure. This was consistent with what researchers were learning about the structure of membrane proteins. In 1972, S. Singer and G. Nicolson revised the Davson and Danielli model in a simple but profound way and proposed a new model called the **fluid mosaic model** (Figure 2). It suggested that proteins are inserted into the lipid bilayer, with their nonpolar segments in contact with the hydrophobic interior of the bilayer and their polar portions protruding out from the membrane surface. The lipid bilayer supplies the backbone of the membrane, and proteins associated with the membrane are not fixed in regular positions instead they float in the fluid lipid bilayer with occasional occurrence of proteins in this lipid matrix. The lipids forming the bilayer are also assumed to be dynamic and are randomly distributed in the membrane. This model is widely accepted till this date. However, through several later studies this model became more complex with the discovery of membrane ordered domains (Presti, 1982; Somerharju, 1985; Virtanen, 1995) named “raft”. These domains have a specific lipids and proteins composition. They are rich in cholesterol and sphingomyelin and are detergent resistant (Simons and Ikonen, 1997; Mukherjee and Maxfield, 2000; London, 2002; McMullen T.P.W and al 2003; Dufourc E.J, 2008; Pike L.J, 2009). They are believed to have certain specific functions such as lipid composition regulation (Virtanen, 1998), protein binding and lipid protein interaction (Simons and Ikonen 1997), enzyme regulation (Somerharju, 1999), proteolysis (Brown and London, 1998), signal transduction (Simons and Toomre, 2000; Brown and London, 1998), and intracellular trafficking (Mukherjee and Maxfield, 2000).

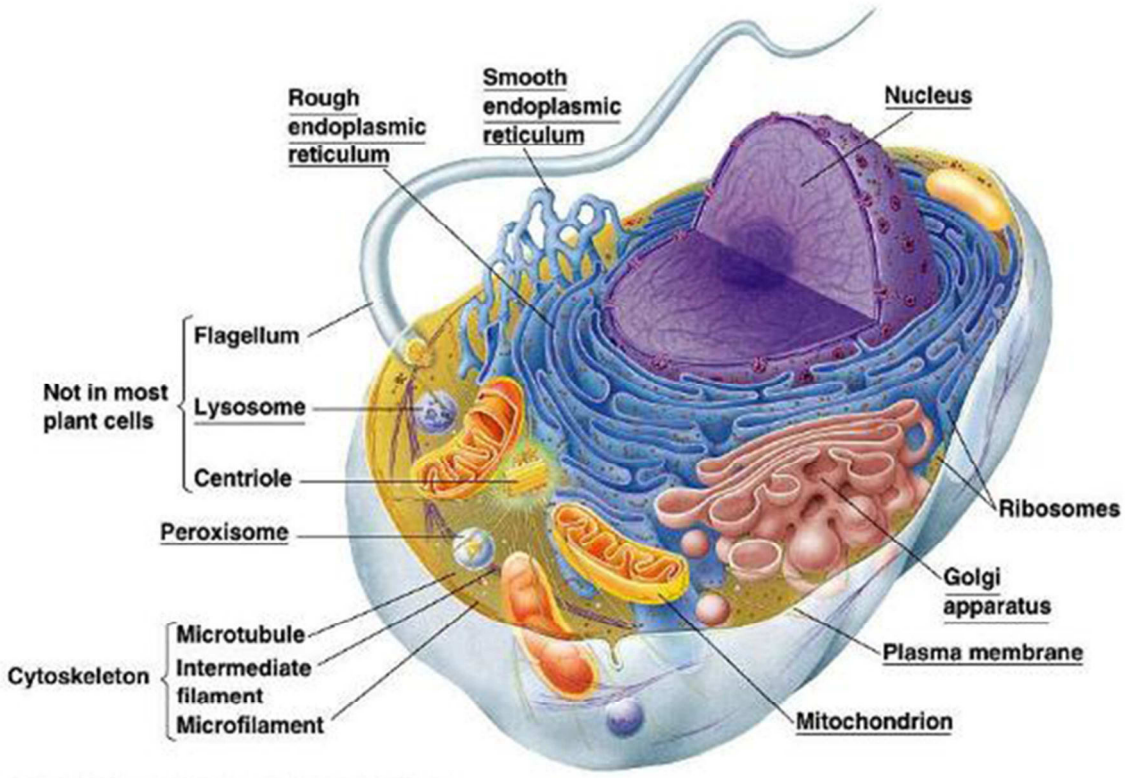

Figure 1: Representation of eukaryotic cell with the complex organization of organelles imbibed in the cytoplasm. Extract from Becker W.M and al, 2003.

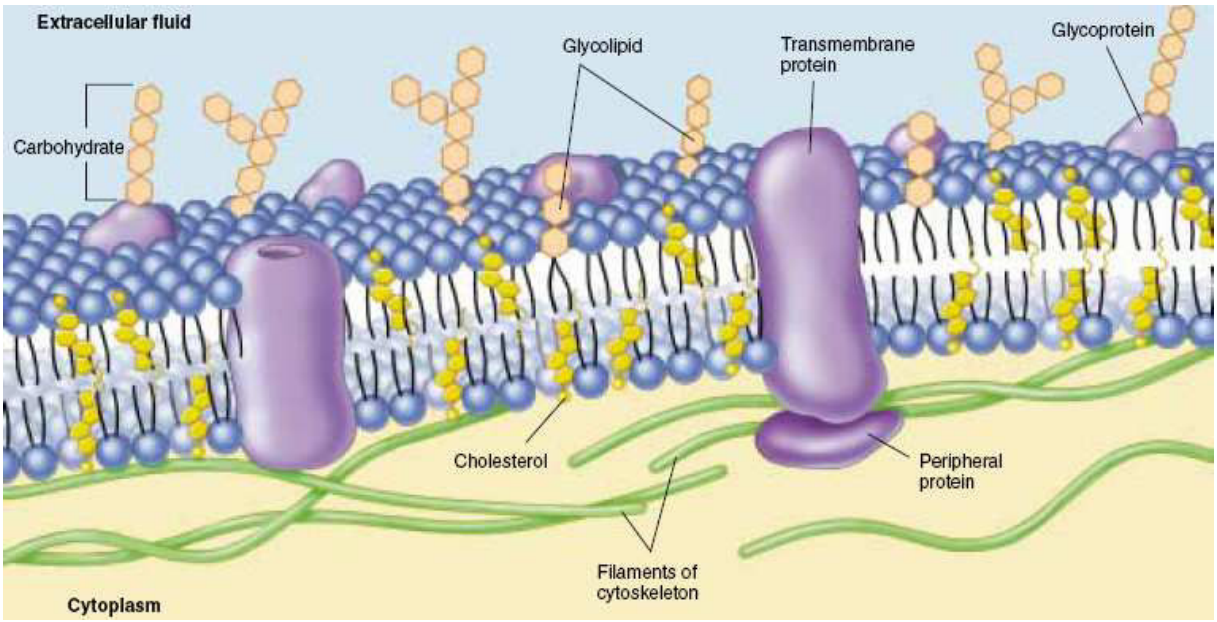

Figure 2: The fluid mosaic model of the plasma membrane proposed by Singer and Nicolson, in 1972. Extract from Biology of the cell, Part II chapiter 6.

1.2. Composition and organisation of biological membranes

This section gives an overview on biological membranes, their composition, how lipid components influence their physical properties and heterogeneity.

1.2.1. Membrane Components:

Biological membranes are composed of lipids, proteins and carbohydrates, with lipids as major component. Although lipids form most of the surface area of membranes, they account for only about 42% in weight for a typical human cell, while proteins account for roughly 55 wt% as they are much denser than lipids and carbohydrates for 3 wt%. The carbohydrates are generally bound either to the lipid or protein. In the cell membrane they are components of complex molecules such as proteoglycans, glycoproteins, and glycolipids.

1.2.1.1. Membrane Proteins:

Proteins are large polymers of natural amino acids amide bonded to each other. Early studies into the mechanism of protein secretion established the endoplasmic reticulum (ER) as the site of secretory and membrane protein synthesis (Palade and Siekevitz, 1956; Siekevitz and Palade, 1958). Membrane proteins form key nodes in mediating the cell's interaction with his envinronment, which is one of the main reasons why the majority of drug targets are membrane proteins. They represent an estimated 50% of the modern drugs targets, whereas 20-30% of all genes in most genomes encode membrane proteins (Krogh et al., 2001). Moreover, 15 to 39% of the human proteome is dedicated to be membrane proteins (Ahram et al., 2006). In January 2013, less than 0.1% of protein structures determined were those of membrane protein, although the deposit structures in the Protein Data Bank (PDB) continuously increase (*http://blanco.biomol.uci.edu/mpstruc/).* Membrane proteins are involved in many important cellular processus for instance molecules transport, energy provision, signal transduction and they also provide mechanical support to the bilayer. Accordingly, a large proportion of membrane proteins can be assigned a function either as receptors, transporters, or enzymes.
The amounts and types of proteins in a membrane are highly variable. For example, in the myelin membrane, 25% of the membrane mass is protein while it is approximately 75% in mitochondrial membranes. A typical plasma membrane is somewhere in between, with protein accounting for about 50% of its mass. Depending on how they associate with the lipid bilayer, membrane proteins fall into two broad categories: integral and peripheral proteins. While integral membrane proteins contain transmembrane domains that interact with membrane lipids, peripheral membrane proteins are associated with membranes via GPI-anchores or non-covalent binding (Figure 3 A and B respectively). Most biological membranes contain both of these categories.
Integral membrane proteins, also called intrinsic proteins, have one or more segments that cross the phospholipid bilayer. Although some integral proteins can anchor to one of the membrane leaflets, the most common type of integral membrane are those which span the entire membrane. They contain one or more domains that span entirely the membrane as

well as domains extending into the aqueous medium on each side of the bilayer. Membrane-spanning or transmembrane domains (TMD) are found in the so-called transmembrane proteins. They contain residues with hydrophobic side chains that interact with fatty acyl groups of the membrane lipids, thus anchoring the protein to the membrane. This anchoring is steered both by hydrophobic interactions between the phospholipids and the TMD, and likely by the polar lipid headgroups. In all the transmembrane proteins examined to date, two types of membrane-spanning domains are defined: either with one or more α helices, or less commonly with multiple β strands. Among them, proteins containing seven membrane-spanning α helices form a major class that includes bacteriorhodopsin and many cell-surface receptors. Proteins with multiple β strands are often found in porins present in the outer membrane of gram-negative bacteria such as *E. coli*.

The topology of transmembrane proteins can be describe by the number of segments passing through the membrane, as well as the orientation in the membrane (von Heijne, 2006) (Figure 3A) :

- Single pass TM proteins can be categorized as Type I or Type II, depending if their carboxy- terminus or their amino-terminus is positioned towards the cytosol, respectively
- Multi pass membrane proteins are divided in Type III and IV in which the multiple TMDs are present in a single polypeptide, or consist of several different polypeptide chains respectively. Type V proteins are anchored to the lipid bilayer through covalently linked lipids and Type VI through both TMDs and lipid anchors.

Peripheral membrane proteins, or extrinsic proteins, are weakly attached to the membrane and do not interact with the hydrophobic core of the phospholipid bilayer. Instead they are usually bound to the membrane either indirectly to integral membrane proteins or directly to the lipid bilayer. Their interactions with membranes mainly result on electrostatic forces with polar head groups of lipids or extending part of integral proteins. Thus, they are easily dissociated from membrane by changing of the pH or upon high salt concentrations. In contrary, integral membrane are removed from the membrane under chaotropic conditions such as > 6M urea or 6M guanidinium and the use of detergeant to disrupt the membrane.

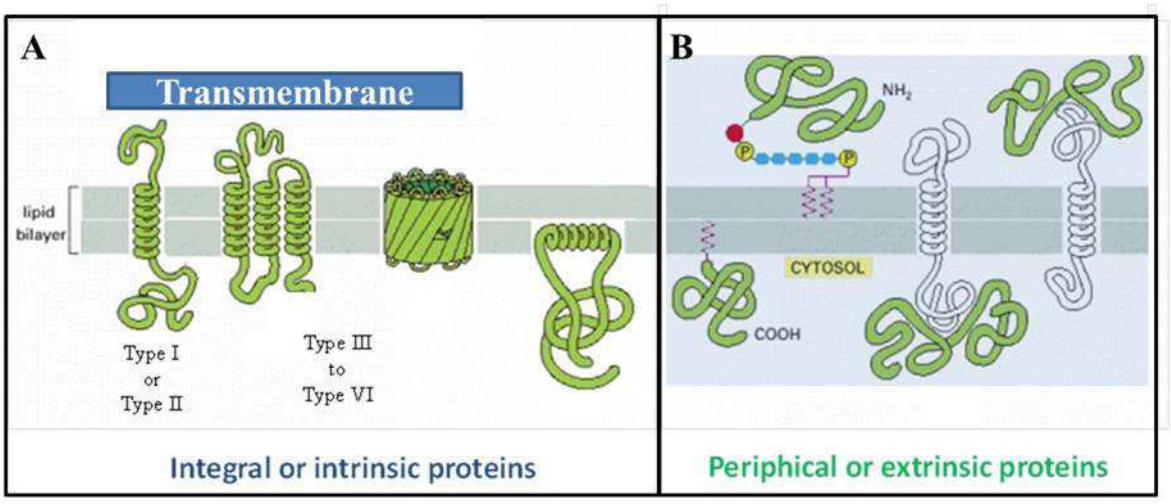

Figure 3: The different type of membrane proteins and the ways they bind to lipid bilayers. Adapted from (Alberts et al., 2002)

1.2.1.2. **Membrane lipids:**

Lipids are the main constituent of biological membranes. They are amphipathic molecules that are hydrophilic on one side and hydrophobic on the other side. When brought into contact with water, most lipids spontaneously form bilayer membranes due to the propensity of there hydrophobic moieties to self-associate by minimizing interaction with water, and their hydrophilic moieties to interact with water and with each others. The typical thickness of this lipid bilayer is 5 nm with a continuous surface area of hundreds of square microns. Lipids that are found in cellular membranes can be categorized into three major classes: the glycerophospholipids (GPLs), spingolipids (SLs) and sterols.

GPLs are the predominant lipids in most eukaryotic and prokaryotic membranes, excluding archaebacteria (by). They consist of a glycerol-3-phosphate esterified with fatty acids at the C1 and C2 positions. The phosphoryl group at the C3 position in addition is attached to various group 'x' as shown in the figure 3A, leading to a number of different phosphatidyl lipids headgroup such as phosphatidylcholine (PC), -ethanolamine (PE), -serine (PS), -glycerol (PG), -inositol (PI) or the unmodified phosphatidic acid (PA). PC accounts for more than 50% of the GPLs in most eucaryotic membranes while in PE is abundant in procaryotic membranes. The esterified fatty acid at position C1 and C2 contains saturated or cis-unsaturated acyl chains of varying lengths. Acyl chains ranging from 16 to 20 are commonly found in plants and animals; among them palmitate (C16, saturated), stearate (C18, saturated) and oleate (C18, one double bond) are predominant. The type of the linkage to the glycerol backbone varied also (ester or ether bonds) (Figure 4A). For example plasmogens are phosphoglycerides present in myelin and in cardic sarcoplasmic reticulum (Gross, 1985) which have hydrocarbon chains that are linked via ether bond.

Cardiolipids is another important class of GPLs that are significantly present in inner membranes of mitochondria, choraplast membranes, and some bacterial membranes, but rarely in other membranes.
The second class of membrane lipids SL, is a derivative of spingosine (Figure 4B). The amide bounded fatty acid to spingosine results in ceramides from which most of SLs are formed.
The ceramide can be further modified with phosphochloline or glycans to form sphingomyelin (SM) and glycosphingolipids (GSLs), respectively. GSLs can be classified as cerebrocides (containing a head group with a single sugar unit) and gangliocides (ceramides attached with oligosaccharides that contain at least one sialic acid residue). SM is the major sphingolipid in the plasma membrane. It represents for example 1/3 of the total lipids in myelin that protect and electrically isolate neurons. SLs acyl chain can be saturated or tans-unsaturated. Both glycerophospholipids and spingolipids thus have a polar head group and non-polar tails made up of acyl chains.
Another important class of lipid in membranes are sterols. Cholesterol is by far, the most commonly represented sterol in PM. Sterols are compact and rigid hydrophobic entity made of a saturated tetracyclic nucleus, with a polar hydroxyl headgroup. It has a four-ring structure with 17 carbon atoms, to which two methyl groups and an iso-octyl side chain are attached (Figure 4C). Whereas cholesterol is the major sterol in animal plasma membranes, other sterols are found in plants (sitosterol, stigmasterol), in yeast and other eukaryotic microorganisms (ergosterol) and in bacteria (hapanoids, a sterol-like).

The proportion of these lipids varies with the type of cells (Table 1). The variation in headgroups and aliphatic chain contribute to create the variety of lipid species; up to thousands different species in eukaryotic cells (Coskun and Simons, 2011; Sud et al., 2007). Their repartition between organelles and the leaflets of the same membrane varies (Figure 5). To generate such a huge variety of lipid species varying in head group and fatty acyl chain composition, a considerable part of our genome is required in order to synthetize, metabolize, and regulate such a complex array of lipids. Cells invest about 5% of their genes to create this diversity (van Meer et al., 2008). The reason why cells build such a large repertoire of lipids and the role of their heterogeneous distribution between organelles is a continuous topic of research in membrane biochemistry. The difference in membrane lipid composition is the base of membrane heterogeneity in cells that plays an important role in cellular process such as membrane trafficking, cellular homeostasis, etc. For example, the gradient of cholesterol along the secretory pathway from the ER to the PM (van Meer et al., 2008), has been shown to regulate the sorting of proteins (Coskun and Simons, 2011; Kaiser et al., 2011; Nilsson et al., 2001; Sharpe et al., 2010). The membrane asymmetry is also due the uneven distribution of lipids but also proteins, between the leaflets of membrane bilayers. The parameters that are though to create and maintain this membrane heterogeneity will be presented later.

Table 1 : Common genotype traits of bacteria related to protein expression. Adapted from BitesizeBio web site

Membrane	PC	PE	PS	PI	SM	CL	Glycolipid	Cholesterol	Others
Erythrocyte (human)	20	18	7	3	18	–	3	20	11
Plasma (rat liver)	18	12	7	3	12	–	8	19	21
Neurons	48	21	5	7	4	–	3	11	1
Myelin	11	17	9	1	8	–	20	28	6

Many cellular processes that take place at the membrane depend on its physical properties and these are influence by the lipid structure and the temperature. The following section will present some lipid properties and how they influence the characteristics of the membrane.

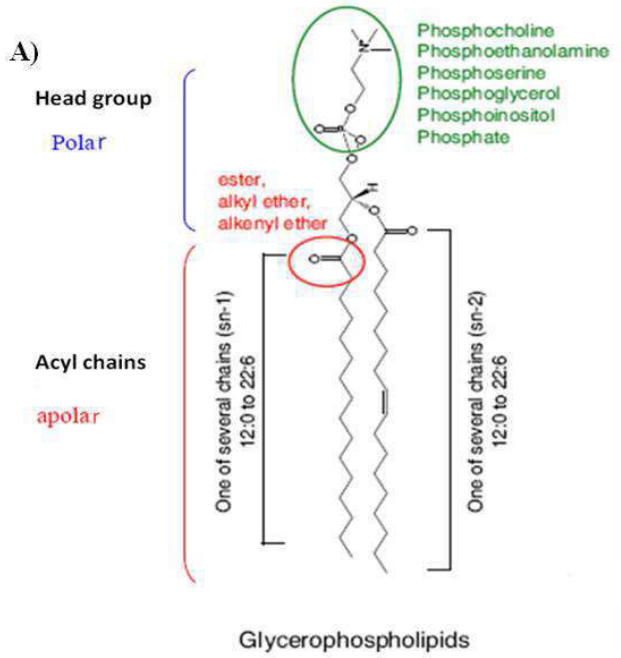

Glycerophospholipids

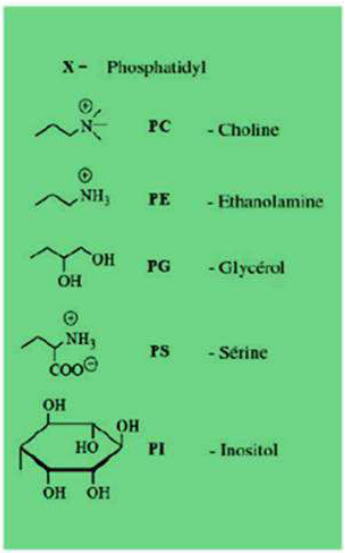

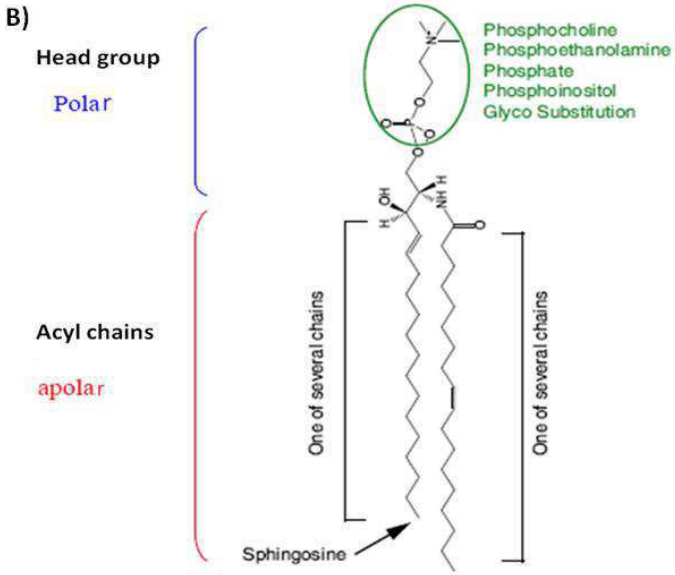

Sphingolipids

C)

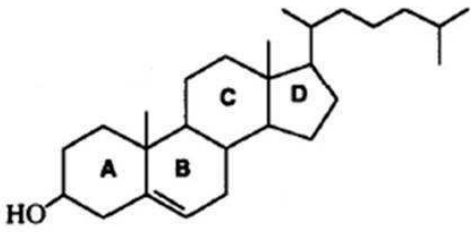

Figure 4: Chemical diversity of the different common classes of lipids in biological membranes. (A) Glycerophospholipids, (B) Sphingolipids. Possible chemical modifications of the head groups for these two classes are highlight in green (circle). The lists of groups that can be added to the head group are summed up into the green box. The type of linkage in glycerol at C1 position in glycerophospholipids is highlighted in red. (C) Sterols structure. Extracted and adapted from Ünal C and Kai S, 2011.

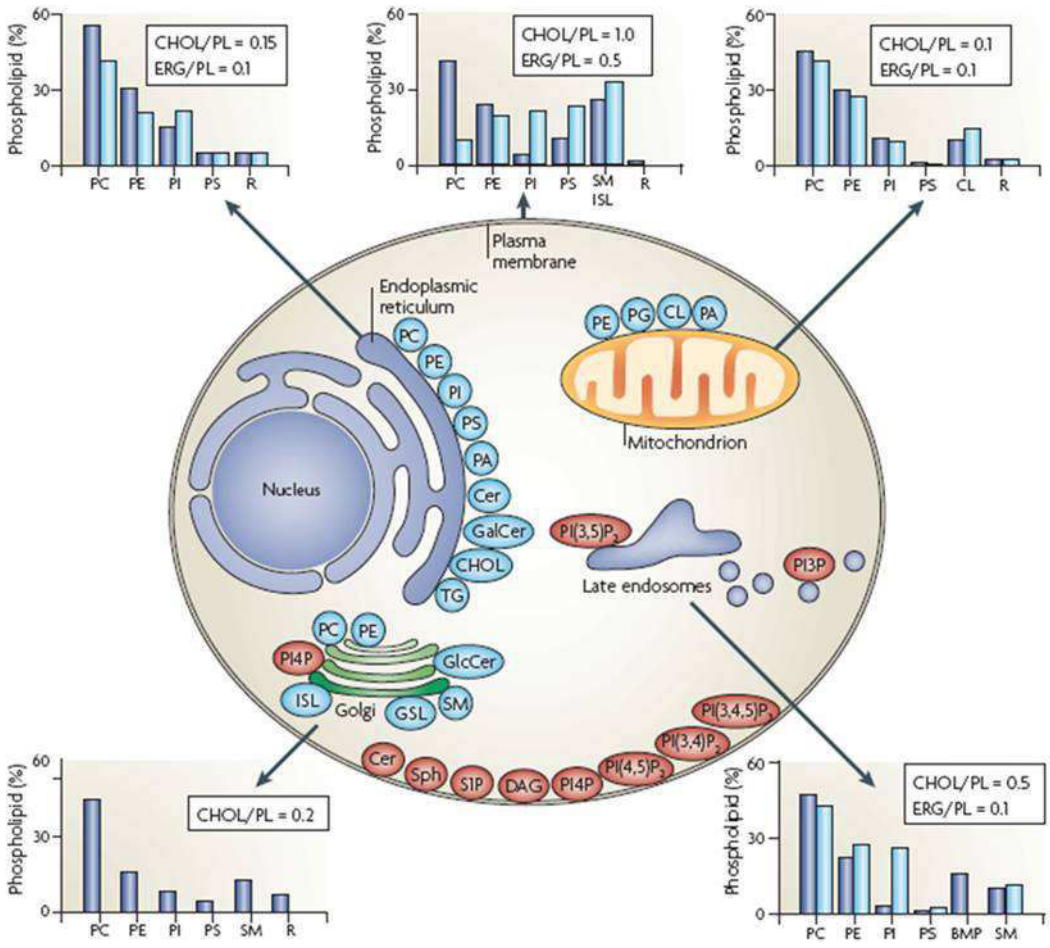

Figure 5: Typical lipid composition in the membranes of eukaryotic cell. Extracted from Van Meer G et al, 2008.

1.2.2. Physical properties of lipids in biological membranes:

Biological membranes are flexible, heterogeneous and permeable. These membrane properties depend on thermodynamic parameters such as temperature, pressure, pH, etc and lipid composition. Interetingly, the chemical nature of lipids controls the physical features of membranes. One of the most obvious characteristics being controlled by this chemical nature is the melting point of membranes. This is an important property as it

influences two others membrane features as for exemple phase behaviour. Another physical property that is inluenced by lipids is the electrostatic potential.

The constituent lipids forming the bilayer can be in different phases depending on the temperature and the lipid composition of the membrane. Most lipids possess two hydrocarbon chains as shown in Figure 4 except for cholesterol. These chains vary in length from 12 to about 24 carbons and in their degree of unsaturation. The acyl chain of lipids forming the bilayer can undergo transition order from a rigid (trans-configuration) into a liquid state (gauche-configuration) depending on the temperature. This transition order is the molecular basis of membrane melting that occurs at the melting temperature (Tm). At low temperature (below Tm), lipid chains are ordered into an all-trans configuration (Figure 6A, top left) while at higher temperature (above Tm), they are disordered due to rotations around the C-C bonds within the lipid chains (Figure 6A, top right). Unsaturated lipids have much lower melting temperatures than saturated lipids.
The melting events in membranes lead to changes in the distribution of lipids within the membrane plane, allowing the formation of phases with quite different composition and state. These phases differ in their physical properties and may display different elasticities, auto-diffusion constants or electrostatic potential. In biological membranes, several phases can coexist. The most commonly found in these membranes are: the solid ordered (SO) phase, the liquid ordered (LO) phase and the liquid disordered (LD) phase (Figure 6). 'Solid' means that the lipids arrange on a (typically triangular) lattice in the membrane plane while 'liquid' indicates the loss of lateral packing (Figure 6, bottom). The attributes 'ordered' and 'disordered' indicate the internal order of the lipid chains (Figure 6, top). The transition between ordered and disordered states is linked to the uptake of significant amounts of enthalpy (i.e., heat). The SO phase is also often called the 'gel phase' and the trivial name of the LD phase is the 'fluid phase'. Biological membranes often exist in a LD phase. However, this LD phase can be tuned by the organism depending on environmental conditions as for example, organisms adapt their lipid compositions to the temperature in order to maintain a particular physical state of their membranes. At low temperature, membranes are in an ordered 'gel' phase while at high temperatures they are in a disordered 'fluid phase' (Figure 6, center). Phases of microscopic or nanoscopic dimension are called domains. In biological membranes, these small scale domains are named 'rafts'. They were first proposed in the 1990's and described as membrane regions in a LO phase that are rich in cholesterol, sphingolipids and some GPI-anchored proteins (Brown and London, 1998; Edidin, 2003; London, 2002; Simons and Ikonen, 1997). The complex composition of membranes can lead to segregation of the constituent lipids into different phases thus, display phase coexistence that strongly influences membrane behavior. The presence of cholesterol and lipids having high Tm (such as spingolipids) for example in membranes favors the formation of an intermediate liquid ordered (lo) phase in which the acyl chains of the lipids are ordered as in the gel state but also have a greater lateral mobility.
In addition to the phase behaviour and melting transition also affects the elasticity of membranes. In particular, at their Tm, the membranes are very soft and easy to bend.

Furthermore, membranes display both fluctuations in area and curvature and their spontaneous curvature mainly depends on their asymmetry.

Biological membranes have an electrostatic potential, another important physical property. It depends on the charge density on the membrane surface and on the ionic strenght. Proteins and lipids provide these charges. Many soluble proteins are positively charged and therefore interact with negatively charged lipid membranes. For example, cytochrome c of the respiratory chain in mitochondria has a net positive charge of about 4 and binds to the highly charged mitochondrial membranes thereby reducing the overall electrostatic potential.
Membranes contain zwitterionic and negatively charged lipids at physiological pH. The zwitterionic lipids have head groups that are an electric dipole with a net charge equal to zero.
On average about 10% of all lipids are negatively charged. The relative amount of negative charge is very different depending on the particular organelle of a cell. Membranes of mitochondria contain for example up to 20% of cardiolipin that have two negative charges each. Further, the charges often distribute asymmetrically such that the inner membranes of cells and organelles are more charged (Rothman and Kennedy, 1977; Rothman and Lenard, 1977). This asymmetric distribution of charged lipids contributes to membrane heterogeneity as presented below.

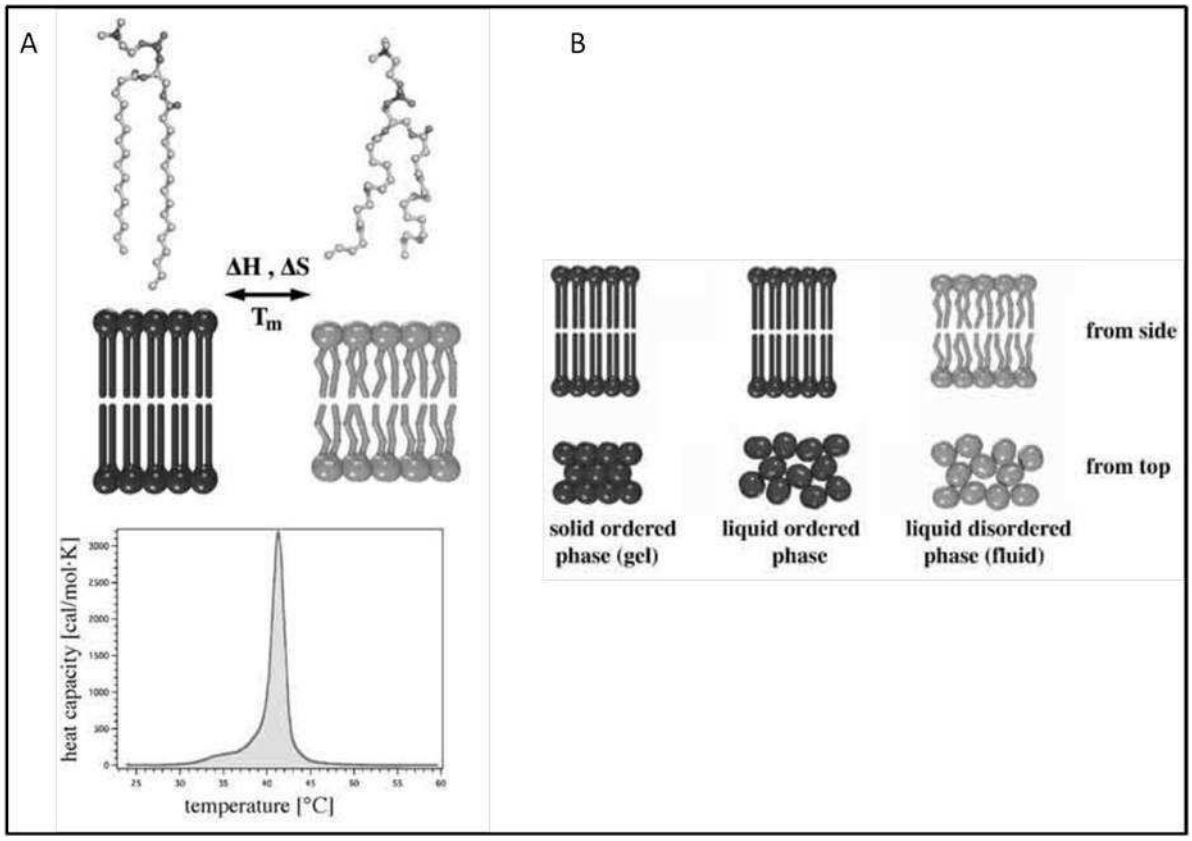

Figure 6: A) melting transition of lipid acyl chains under increase of the temperature. B) The three most common membrane phases seen as cross sections and from top. SO, LO, LD : solid ordered, liquid ordered, liquid disordered phases (Heimburg, 2009)

1.2.3. Membrane Heterogeneity:

The refined model of the fluid mosaic suggests a heterogeneous distribution of membrane components. This distribution is not symmetric between membrane leaflets (Kiessling et al., 2009) . It is related to heterogeneous repartition of lipids and proteins across the bilayer and their lateral organistion in membrane leaflets. This asymmetry has been extensively study and characterized in erythrocyte membrane (ref 2-6). In eukaryotic cells, lipid species are distributed heterogeleously between membranes of the different cellular compartments and across membrane bilayer except the ER (Kiessling et al., 2009; van Meer et al., 2008). Indeed, this organelle is assumed to have symmetric lipid distribution while post-ER membranes, show a clear asymmetric lipid arrangement. For instance in PM, glycosphingolipids and phosphatidylcholine are present in the exoplasmic leaflet and the aminophos-pholipids, phosphatidylserine and phosphatidylethanolamine (PE), on the cytoplasmic face (Zachowski, 1993). This assymetry is inherent to lipid biosynthesis and is governed by membrane components (protein and lipids), lipid-lipid and lipid-protein interactions. Furthermore, it is maintaining and regulate by continuous inward and outward lipid movement across the membrane monolayers and likely their lateral diffusion. This

section presents the factors that govern membrane heterogeneity how it is generated and maintained and the consequences of unregulation in some biological process.

1.2.3.1. **Elements that govern Membrane Heterogeneity:**

Natural membranes are heterogeneous patchworks of lipids species, membrane proteins and cholesterol. They are made of a huge variety of lipid species, typically hundreds (Coskun and Simons, 2011; Janmey and Kinnunen, 2006; van Meer et al., 2008) varying in head group and fatty acyl chain composition as described above. The acyl chains present different length and degree of unsaturation that both determine the thickness and ordering of the hydrophobic region of the membrane. The presence of unsaturated hydrocabon chains increase membrane fluidity while saturated hydrocarbon chains pack more tightly and lead to an ordered structure. Within the lipid bilayer, the differences in chain length and saturation of the hydrophobic chains in the membrane interior might introduce disorder (Killian, 1998). In addition to the acyl chains, lipids constituting membranes have different head groups with different charges and size. Charges mediate electrostatic interactions with membrane-associated proteins, specific lipids and lead to spatial organization of membranes (Janmey and Kinnunen, 2006b). On the other hand, the presence of a larger head group than the acyl chain causes the tails to be more loosely packed if the heads are placed close to each other. However, the presence of molecules like cholesterol which have a relatively small head group compared to its hydrophobic part might help in achieving a closer packing and an increase the acyl chain order.

Cholesterol is an important structural component of membranes. Its increases the rigidity of the membrane fluid and augments the fluidity of the gel phase, respectively. Cholesterol interacts more strongly with lipids that have a saturated acyl chain than with those that have unsaturations. Interaction with unsaturated lipids depends on the location of the double bond. As spingolipids usually have a long saturated acyl chain, they interact more favorably with cholesterol. For example, cholesterol preferentially associates with sphingolipids and when protein additionally interacts with this domain, it leads to the formation of dynamic nanoscale ‘raft’ domains (Lingwood and Simons, 2010; Simons and Ikonen, 1997) which are detergeant resistant (Brown and London, 1997).

Many proteins in membranes interact preferentially with certain lipids. Proteins in raft domains have been found for example to be anchored by saturated fatty acid chains (Simons and Vaz, 2004). As membrane proteins are amphipatic molecules, their interaction with the lipids can be based either on their hydrophilic (charge) or on their hydrophobic part. The hydrophobic part of the proteins that interacts with the lipid should match the membrane thickness. When this is not the case, hydrophobic mismatch occurs and lipid or proteins have to change their conformation in order to minimize this unfavourable energy contribution. The proteins can therefore stretch when the membrane thickness is smaller or they can fit themselves within the membrane by tilting their trans-membrane helices or by taking a different conformation. The lipids similarly can adapt by stretching their acyl chains.

1.2.3.2. **Generation, regulation and role of Membrane Heterogeneity**

Lipid asymmetry is inherent to *de novo* synthesis lipids as the enzymes responsible of their synthesis are distributed unevenly in membrane. This biosynthesis often occurs on the side of the membrane in which newly synthetized lipids will ultimately enriched in PM except PC and glucosylceramide (Daleke, 2003). Indeed, major glycerophospholipids (PS, PE, PC, PI) are synthetized on the cytosolic side of ER and accumulated on this side in PM while all SLs are synthetized on the luminal surface of ER or Golgi and accumulated on the external leaflet in PM. In addition to lipids, several lipids-anchored membrane proteins are also distributed asymmetrically across PM of eukaryotic cells as for exemple the GPI-anchored membrane proteins which are localized on the external side of PM. The asymmetry of these proteins is set by biosynthetic pathway.

Lipids asymmetry is maintained by a set of movement and protein-lipid interactions within membrane. Indeed, lipids can laterally diffuse, rotate, and exchange between membrane leaflets (flip-flop). However, compare to the rapid lateral movements of lipids within membrane leafleats, trans-bilayer movements are very slow processes and are governed by lipid nature (Lingwood and Simons, 2010). For instance, the half time for phospholipids flip-flop ranges from several hours to days (McConnell and Kornberg, 1971). Thus trans-bilayer movements are catalysed by proteins that significantly contributed to maintain or dissipate the trans-bilayer asymmetry. These proteins were classified according to the requirement of energy, the direction of transport within the membrane and the substrate specificity. The flippase and floppase are ATP-dependant lipid transporters which transfer lipid in opposite direction within the membrane. Flippase transports lipids from the outer to the the cytoplasmic side of PM. This enzyme is present in a variety of cells and PM. It selectively bind PS and was show to be essential to maintain this lipid asymmetry (Daleke, 2003). In contrast, floppase transfers lipids from the inner to the outer leaflet. This second class of lipid transporter involved the ABC transporters which are group of proteins responsible of the ATP-dependant export of amphipathic such as cytotoxic xenobitics. They are widely expressed in prokaryotes and play role in multi-drug resistance. Only some members of this protein family are implicated in lipid efflux and most of them are not involved in the maintenance of lipid asymmetry. More, not all of this lipid transporters class are floppases and most of them are nonspecific. However, among the well-characterized lipid floppase, the ABCC1 was suggest to be involved in the maintenance of choline and sphingolipid distribution in some cells (Daleke, 2003). The third class of lipid transporters is ATP-independent scramblases which catalysed bidirectional trans-bilayer transport of lipids thus, impairs asymmetry. Scramblase activity was found in the ER but not in post-Golgi membranes except in PM of activated cells. This may results in a symmetric distribution of newly synthetized lipids or lipid precursors in the ER membrane (Holthuis and Levine, 2005) and asymmetric distribution in the post-Golgi membranes (Daleke, 2007; Devaux and Morris, 2004). However, this trans-bilayer asymmetry is not strictly conserved, and likely to change over time.

In addition to trans-bilayer asymmetry, biological membranes are also heterogeneous with respect to the lateral organisation of both lipids and proteins (Mouritsen and Bloom, 1984).

These lateral assemblies have been put forward as evidence of rafts or other domains (Simons and Vaz, 2004). They are mainly modulated by cholesterol which is distribute in both leafleats but that seems to be more abundant in the outer leafleat. For instance, lateral segregation of cholesterol-induced microdomains in sphingomyelin bilayers (Coskun and Simons, 2010). These domains are stabilized by protein-lipid binding as to lipid–lipid interactions (García-Sáez and Schwille, 2010). Proteins are part of this raft domain. More, they also assemble in functional cluster such as the electron transfer complex in the inner mitochondrial membrane. In addition, acyl chain of lipids can be modify within the membrane by the actions of local enzymes (Hishikawa et al., 2014). Enzymes acting on membrane lipids can have consequences not only in causing changes in the lateral distribution but also in producing changes in the 3D organization of membranes. For example, removal of the phosphocholine headgroup of SM by sphingomyelinase (SMase) yields ceramide, a lipid with very different physicochemical properties that can alter spontaneous curvature and lateral packing.

Lipid asymmetry is essential for normal membrane function as it plays an important role in many biological processes such as signal transduction, molecular recognition, vesicular budding in membrane tracfficking process (Janmey and Kinnunen, 2006; van Meer et al., 2008). More, it is important for cell feature as for instance, the non-exposure of negatively charged lipids at the external membrane leaflet will distinguished eukaryotic from prokaryotic cells (Sato and Feix, 2006).Although, the loss of this asymmetry is associated with pathogenic conditions, it is also essential for normal cell development and homeostasis. For instance, exposure of PS in the external monolayer was shown to be induced in apoptisis early stage (Fadok et al., 1992). However, the unregulation of this loss is associated with cardiovascular disease such as diabetes. In addition lateral organisation of both lipids and proteins in domain such as raft, may regulate some cellular processes as for exemple the sorting of membrane proteins (Coskun and Simons, 2011; Simons and van Meer, 1988; van Meer and Lisman, 2002) or vesicle budding (Pomorski and Menon, 2006).

1.3. Cellular synthesis and trafficking of lipids

The biosynthetsis of many lipids in eukaryotic cells is initiated in the endoplasmic reticulum (ER). Thereafter, newly synthesized lipids are delivered to different cellular membrane compartments, each of which shows a unique lipid and protein composition. In their target location, lipids may be present as structural components or undergo modifications to generate new lipid species, contributing to the variety of membrane lipid composition. This section introduces de novo synthesis of the common membrane lipids as well as their cellular traffic.

1.3.1. De novo biosynthesis of major membrane lipids

In eukaryotic cells, several organelles are involved in lipid biosynthesis, including the ER, mitochondria and peroxisomes. The ER is the major site for biosynthesis of most membrane lipids whereas mitochondria and peroxisomes are responsible for cardiolipin, phosphatidylglycerol, and plasmalogens biosynthesis, respectively. As a rule, most of

membrane lipids are synthesized in the ER, except sphingolipids which are synthetized in the Golgi apparatus. Nevertheless, their precursors are synthetized in the ER, which contains multiple biosynthetic enzymes that catalyze the initial steps of de novo biosynthesis of the three major lipid classes in eukaryotes (Sprong et al., 2001).

1.3.1.1. Biosynthesis of Glycerophospholipids (GPLs)

GPLs represent the most abundant structural lipids of biological membranes in mammalian cells. The synthesis of the most common GPLs: PC, PE, PS, and PI is initiated at the ER from the same precursor; the phosphatidic acid (PA) (Hermansson et al., 2011) (Figure 7A). PA is obtained from glycerol 3-phosphate by two sequential acylation reactions mediated by two different enzymes: the glycerol phosphate acyltransferase (GPAT) and the acylglycerol-phosphate acyltransferase (AGPAT). De novo biosynthesis of PC and PE occur via the Kennedy pathway in the ER and require diacylglycerol (DAG) derived from PA by PA phosphatase (PAP). This pathway involves three sequential reactions: the first two which take place in the ER for PC and PE and in addition in the nuclear envelope for PE. These two first reactions are rate-limiting enzyme and lead sequentially to CDP-choline and CDP-ethanolamine. In the last reactions, PC and PE are obtained by the transfer of phosphocholine and phosphoethanolamine groups from CDP-choline and CDP-ethanolamnine, respectively, to DAG and are catalyzed in the ER by a dual specificity choline/ethanolamine (CPT/EPT) phosphotransferase (Vance, 2008; Vance and Steenbergen, 2005). This reaction can also occur for PC in the Golgi apparatus (Blom et al., 2011); in this case, the reaction is mediated by a specfic choline phosphotransferase. PC can also be obtained by sequential reactions of PE methylation that occur in the mitochondria in hepatocytes (Fagone and Jackowski, 2009). In addition to the Kennedy pathway, PE can also be produced by the PS decarboxylation pathway. This pathway takes place in the inner membrane of mitochondria and is mediated by the PS decarboxylase (PSD). Although most of the PE produced by this pathway stays in the mitochondria, some are transported to the ER and other organelles. The mechanism of this transport is not well established.

PS is synthetized in mammalian cells by the exchange of L-serine with either the polar head goup of PC (choline moiety) or PE (ethanolamine moiety). This reaction occurs in the “mitochondria-associated membranes” (MAM) and is catalyzed by the PS synthase 1 (PSS1) and PSS2 (Stone and Vance, 2000). From there, the newly synthesized PS is translocated to the plasma membrane or the mitochondria, where it undergoes decarboxylation to produce PE. This translocation seems to occur by lateral diffusion via membrane contact sites between mitochondria and ER membranes (Jasińska et al., 1993; Vance, 2008).

PI biosynthesis is initiated by the formation of CDP-DAG from PA follow by the production of PI from CDP-DAG. These sequential reactions are subsequently mediated by CDP-DAG synthase (CDS) and PI synthase (PIS) which are localized at the ER. However, recent studies, suggest that PI could be synthesized at the PM (Kim et al., 2011).

Although the biosynthesis site of GPLs in eukaryotes is the ER, various GPLs can also be produced in different membrane compartments by specific enzymes that modulate their head groups or fatty acyl chains.

1.3.1.2. **Biosynthesis of sphingolipids (SLs)**

The synthesis of SLs take place in the Golgi apparatus but their biosynthesis is initiated in the ER (Merrill, 2002). Ceramide is first synthetized at the cytosolic face of ER after subsequent steps from palmitoylCoA and serine (Figure 7B). It represents the central component in sphingolipids metabolism as it contains a sphingosine backbone and can therefore be metabolized to generate other sphingolipids. Most of the newly synthetized ceramide is then transferred to the Golgi, where it can be converted into sphingomyelin (SM), glucosylceramide (GlcCer), lactosylceramide (LacCer), and more complex glycosphingolipids (Tafesse et al., 2006). Therefore, the efficient de novo synthesis of GLs from the ceramide rely on its transport from the ER to the Golgi (Halter et al., 2007; Hanada et al., 2003). The ER to Golgi transport of ceramide in mammalian cells is mediated by ceramide transport proteins (CERT) which then regulate SL synthesis (Blom et al., 2011). Within the Golgi, SM is produced at the luminal leaflet of the trans-Golgi by SM synthase (SMS) which catalyzes the transfer of phosphocholine from PC to ceramide. The synthesis of most GSLs starts on the cytosolic side of Golgi membranes with the addition of a glycosyl moiety to the ceramide. Thereafter, the glycosylceramide is translocated to the luminal side of the trans-Golgi membranes to be converted in more complex GSLs.
The post-Golgi transport of complex SLs from the trans-Golgi to the plasma depends more on vesicular transport.

1.3.1.3. **Bionsyhnthesis of cholesterol**

Cholesterol is the major sterol in mammals, and is highly enriched at the PM (Blom et al., 2011). Mammalian cells as well as all nucleated cells are capable to produce their own cholesterol via de novo biosynthesis by using acetate as the sole carbon source. About 19 subsequent reactions are catalized by about 30 enzymes to obtain cholesterol (Figure 7C). Among them, the limited step is the one that leads to mevalonate, the first intermediate of the cholesterol pathway. The synthesis of this intermadiate is mediated by the HMG-CoA reductase, an integral ER membrane glycoprotein that catalyzes also the rate limiting step for the entire pathway. The whole process is highly energy dependent and is strongly regulated both at posttranslational and transcriptional level (Ye and DeBose-Boyd, 2011). Although the ER is the main site of cholesterol synthesis, several other cholesterol biosynthetic enzymes are also found in other celleular compartments, such as peroxysomes, nucleus or nuclear envelope (Zwerger et al., 2010), Golgi complex (Cotman et al., 2004). Many of the newly synthetized cholesterol and their intermediates are rapidly transported to other cellular membranes, which explains the low cholesterol concentration in the ER where they are mainly synthetized.

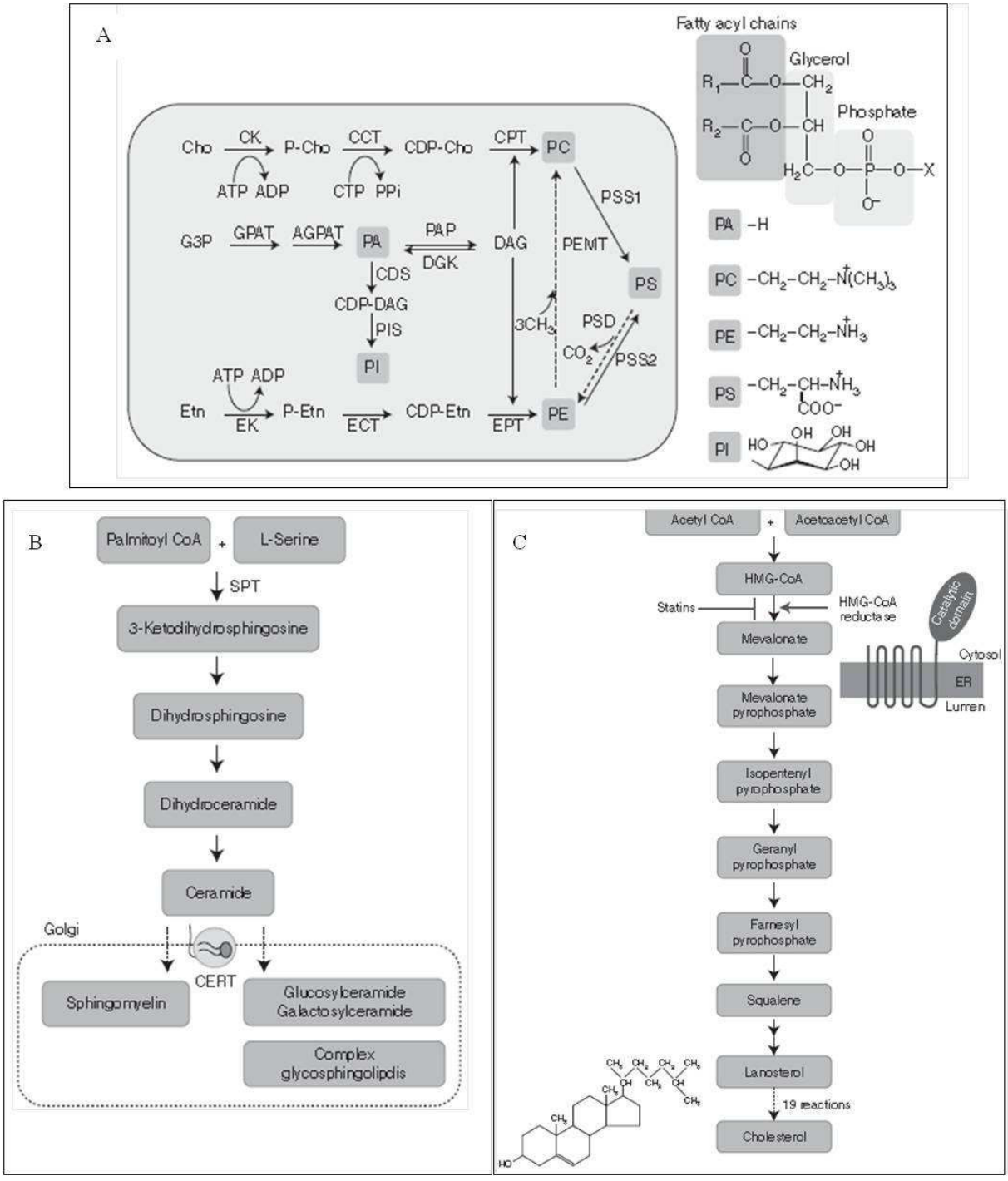

Figure 7: Biosynthetic pathways of the major classes of membrane lipids. A) Glycerophospholipids, biosynthetic pathway that take place in mitochondria are represented in dashed boxes. B) Sphingolipids and C) cholesterol the most abundant sterol. Extracted from (Lev, 2010).

1.3.2. Intracellular transport of membrane lipids

Membrane lipids transport occurs along the secretory pathway (Figure 8) from the ER to their final destination. Because of the hydrophobic nature of lipids, their free diffusion through the cytoplasm is very slow to be physiologically relevant for lipid transport (Mesmin and Maxfield, 2009). For example, spontaneous exchange of glycerolipids and sphingolipids between membranes occurs with half-times > 40 hrs (Prinz, 2010). Therefore, effective transport of lipids relies on active mechanisms that facilitate intercompartmental transport. These mechanisms are depicted as nonvesicular and vesicular lipid transport. Although transport of major lipids is mediated by vesicles, increasing evidence suggests that nonvesicular transport is the major route for certain lipid types (Lev, 2010) and in the past few years, considerable progress has been made in characterizing this alternate transport of lipids (reviewed in (Lev, 2010; Prinz, 2010)). This section will introduce these differents mechanims of lipid transport as well as the general intracellular trafficking of major membrane lipids.

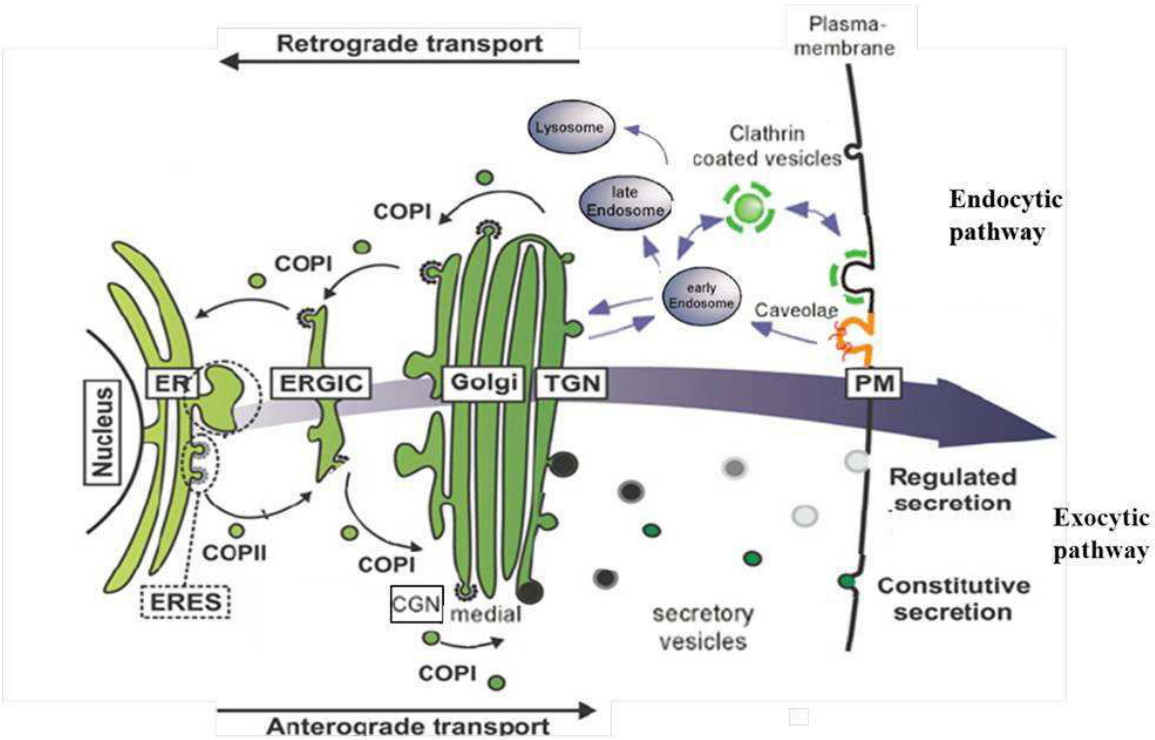

Figure 8: Schematic representation of the secretory pathway. The anterograde transport corresponds to the transport of molecules from the ER to the PM while retrograde transport is in the inverse direction. Arrows indicate the direction of transport. Extracted from (Strating and Martens, 2009) and adapted.

1.3.2.1. **Mechanisms of lipid transport**

From the ER, where they are synthetized, lipids transported via vesicles, or by nonvesicular mechanisms through membranes contact sites (MCSs) or proteins. In the

contrary to vesicular lipid transport, most nonvesicular transport mechanisms do not require metabolic energy.

1.3.2.1.1. **Nonvesicular transport:**

The evidence that lipids are transported by independent routes than vesicular transport have aroused from the observation that the rate of lipid transfer does not decrease when vesicular trafficking is blocked (Baumann et al., 2005; Kaplan and Simoni, 1985; Sleight and Pagano, 1983; Warnock et al., 1994). Surprisingly, this transport is mainly mediated by spontaneous exchange of lipid monomers (Figure 9A) through the aqueous cytoplasm from one compartment to another without assiatance of proteins. Nevertheless, as this process is very slow, it can be markedly accelerated by lipid-transfer proteins (LTPs) (D'Angelo et al., 2008; Lev, 2010) and at membrane contact sites MCSs (Holthuis and Levine, 2005). Lipids may exchange also during the collision of two membranes after activation of lipids (Prinz, 2010) (Figure 9B).

MCSs are small cytosolic gaps of 10–20 nm between the ER membranes and virtually all cellular organelles (Lebiedzinska et al., 2009), that allow lipids to exchange between two membranes when they come together in close proximity. In mammalian cells, this complex structure forms between the ER and the membranes of mitochondria and in plants between the ER and chloroplast. They are are highly enriched in proteins such as enzymes and LTPs, and are generally formed and/or stabilized by specialized tethering proteins (Lebiedzinska et al., 2009). The four mechanisms at MCSs that allow lipid transport are depicted in Figure 7D-G (Prinz, 2010). Active transport of lipids at MCSs is facilitate by protein complexes that form tunnels to allow lipid transfer, that promote lipid desorption from the donnor membrane, activate lipids prior to membrane collision or finally promote membrane hemifusion. A significant portion of this transport does not require soluble LTPs. MCSs have been proposed to be involved in the transfer of PS from the ER to the mitochondria and may be mediated by specific proteins at the ER/mitochondria contact sites (Vance, 2008).

Active nonvesicular transport of lipids is also mediated by proteins and it was postulated in the late 1960s that LTPs facilitate lipid exchange (Wirtz and Zilversmit, 1969). LTPs are cytosolic carrier proteins that facilitates lipid transport between membranes, likely by increasing the rate of lipid absorption from the bilayers (Lalanne and Ponsin, 2000). They are expressed in most cells and have been identified in all eukaryotes, plants, and bacteria. Many LTPs have been isolated, cloned, and crystallized. They selectively bing only one or closely related classes of lipids in a single hydrophobic pocket and may also have domains with varying functions such as peptides that target donnor and acceptor membranes (Lev, 2010) (Figure 9B). LTPs function in two distinct conformations: an open membrane-bound conformation and a closed conformation in which one lipid molecule is enclosed in the tunnel. Based on their lipid binding specificity, they can be broadly divided into three classes: glycephospholipid, sphingolipid and sterol transfer proteins. For exemple, among the sphingolipid transfer protein, the ceramide transfer protein (CERT) transports ceramide from the ER to the Golgi. They are involved in the transfer of PC from the ER to the Golgi and of sterols from the ER to the plasma membrane (PM).

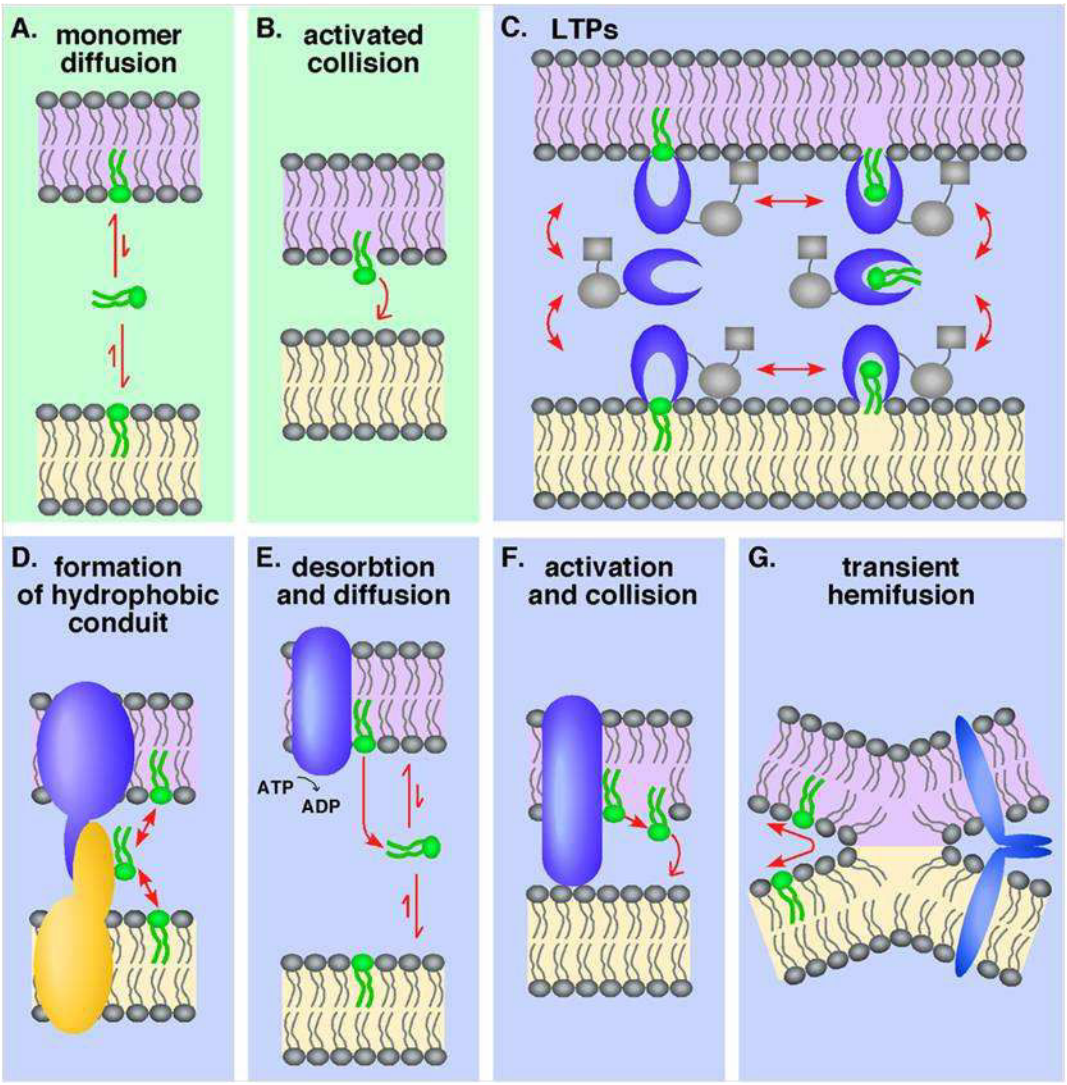

Figure 9 : Nonvesicular mechanisms of lipid transfer between membranes. A) and B) illustrate spontaneous diffusion of lipid monomer either through cytoplasm or during membrane collision. C. Mechanism of lipid transfer by LTPs. D to G. describe the differents mechanisms of lipid transfer at MCSs. Extracted from (Prinz, 2010).

1.3.2.1.2. **Vesicular transport**

It is generally assumed that the net transport of lipids occurs mainly via vesicular transport (Pagano, 1990; Rothman and Wieland, 1996; Trotter and Voelker, 1994). In this process, coated-enclosed sacks of about 50-100 nm diameter (Popoff et al., 2011) named vesicles form at a donor compartment, fused with and acceptor compartment with the help of specific adaptor proteins (eg. SNAREs). This fusion often occurs during the delivery of cargo molecules (proteins, lipids, signalling molecules, etc) to a specific endomembrane compartment and to the PM, or during the vesicles recycling. This membrane trafficking between organelles and the PM contributes to maintain the appropriate lipid and protein composition of these compartments. Vesicular lipid trafficking takes place along the

secretory pathway (Figure 8) and involves three classes of coated vesicles (reviewed in (Kirchhausen, 2000)): clathrin-coated vesicles mediate endocytic and the late secretory route (between the trans-Golgi and the PM) (Robinson, 2004), while the COat Protein I and II (COPI and COPII) vesicle trafficking routes are responsible for traffic between the ER and the Golgi apparatus. COPI vesicles appear to be involved in both the bidirectional intra-Golgi transport (Orci et al., 1997) as well as the Golgi-ER retrograde transport (Béthune et al., 2006a; Lee et al., 2004). There is evidence suggesting that COPI may also be involved in the endocytic pathway (Lowe and Kreis, 1998). COPII vesicles mediate the forward transport from the ER to the intermediate compartement membranes (IC or ERGIC) localized between the ER and the Golgi (Hughes and Stephens, 2008). Other vesicles that are not coated with COP or clathrin have been observed during macropinocytosis or phagocytosis that may occur through caveolae (Anderson, 1998).

Newly synthesized lipids escape the ER via COPII vesicles and are transported to the IC. In the anterograde transport, COPI vesicles bud from IC and enter the Golgi apparatus by fusion with the cis-Golgi cisternae (CGN). These vesicles also mediate transport within the Golgi cisternae toward the trans-Golgi (TGN). This fusion occurs either constitutively or, as in the case of regulated secretion, in response to an external signal. As the Golgi apparatus is the major sorting compartment of the cell, lipid vesicle carriers budding at the TGN do not sort lipid only to the PM for constitutive and regulated secretion, but also to endosomes and lysosomes, or back to the ER. This retrieval transport from the Golgi to the ER is mediated by COPI (Cosson and Letourneur 1994; Letourneur et al. 1994). There is evidence that lipids are sorted during vesicles budding (Brügger et al., 2000; Popoff et al., 2011). Moreover, proteins and lipids play an important role in the budding of these vesicles (McMahon and Gallop, 2005; Zimmerberg and Kozlov, 2006). For example, as a specific lipids serve as attachement sites for peripheral membrane proteins, modifications of the lipid composition can facilitate recruitment of proteins involved in membrane bending (e.g; ARF1 a GTPase involve in COPI biogenesis and coatomer protein complex). Recently, Contreras et al proposed the role of a specific sphingomyelin species in COPI biogenesis. In addition, as vesicular trafficking along the secretory pathway is coordinated by the exocytic and endocytic pathways (Figure 8), both are regulated by internal regulators and external signals that ensure fidelity and uninterrupted flow (Donaldson and Segev, 2000). For example, transport of membranes to and from the PM can be regulated by extracellular signaling molecules which bind membrane receptors and trigger intracellular cascade via intracellular signalling molecules. Phosphoinositol (PI), a second messager is one of these intracellular signalling molecules, has been found to regulate membrane trafficking (Lindmo and Stenmark, 2006; Odorizzi et al., 2000).

COPI vesicles have been used widely as a model system to study the molecular mechanism of transport vesicle biogenesis as they play an important role in lipid sorting. The following section COPI are presented intracellular trafficking as well as factors involved in this traffic during their biogenesis.

1.3.2.1.2.1. **COP I vesicles**

COPI-coated vesicles mediate protein and lipid transport in the early secretory pathway (Brügger et al., 2000; Rothman and Wieland, 1996). Their coat consists of a small Ras-like GTPase protein, the ADP-ribosylation factor 1 (ARF1) (Taylor et al., 1992), and the coatomer, a heterooligomeric protein complex of seven subunits (α, β, β′, γ, δ, ε and ζ COPs); both are cytosolic factors that are recruited at the Golgi membrane (Waters et al., 1991). Coat components are involved in multiple tasks such as cargo selection, vesicle budding at the donor membrane, vesicle fission and initiation of uncoating. For example, different binding sites exist in coatomer for the sorting of various classes of cargo such as membrane proteins with sorting motifs in their cytoplasmic domain (Cosson and Letourneur, 1994). Therefore, molecules to be transported are sorted and packed into these vesicles. Moreover, this sorting occured during COPI biogenesis. Interestingly, sorted molecules can also play a role in COPI formation as for example lipids which are also sorted to give a liquid-disordered phase composition during COPI vesicle budding, (Popoff et al., 2011).

A) COPI biogenesis

COPI vesicles budding takes place in the Golgi and the IC where components necessary for their biogenesis are abundant. The formation of these vesicles is achieved in several interdependent steps: coat recruitment, uptake of cargo, budding, membrane separation (scission), and uncoating (Figure 7). The minimal machinery for COPI vesicle formation consists of p24 family members (p23/p24), ARF-GTP and coatomer. Arf1 plays a central role in COPI biogenesis as its presence and activation is a pre requisite for the recrutement of coataomer to the membrane. Arf1 cycles between an inactive cytosolic GDP state and an active, membrane anchored, GTP state (Randazzo et al., 1993). These molecular states are regulated by Arf GTPase activating proteins (ArfGAPs) and guanine nucleotide exchange factors (ArfGEFs), respectively. Arf1 contains Golgi localization signals encoded in its sequence for his recruitement in the cis or the trans-Golgi. They are recruited in the trans-Golgi via homo dimeric complex of p24 family members (Gommel et al., 2001) and at the cis-Golgi by a SNARE protein. Once both Arf1 and its exchange factor are recruited to the membrane, a Sec7 domain within the Arf GEF triggers the activation of the small GTPase by exchange of GDP to GTP. This activation drives a conformational of Arf1 leading its anchorage in membrane via a myristoylated helix (Antonny et al., 1997; Franco et al., 1996). The cytosolic coatomer complex is then recruited at the membrane en bloc by Arf1 (Hara-Kuge et al., 1994) via interactions sites involving β, β′, γ, δ subunits. The cotaomer complex is stabilized by specific binding of γ -COP trunk domain to dimers of p23 and p24 proteins (Béthune et al., 2006b; Harter and Wieland, 1998) via dilysine and diphenylalanine motifs. Interaction with p24 members induces a conformational change in γ -COP (Béthune et al., 2006c; Reinhard et al., 1999) leading a spatial rearrangement that initiates aggregation and coatomer polymerization (Reinhard et al., 1999). This polymerization provides the energy to bend the membrane and generate a vesicle (Popoff et al., 2011), which dissociates from the donor membrane. After budding, these vesicles shed their coat.

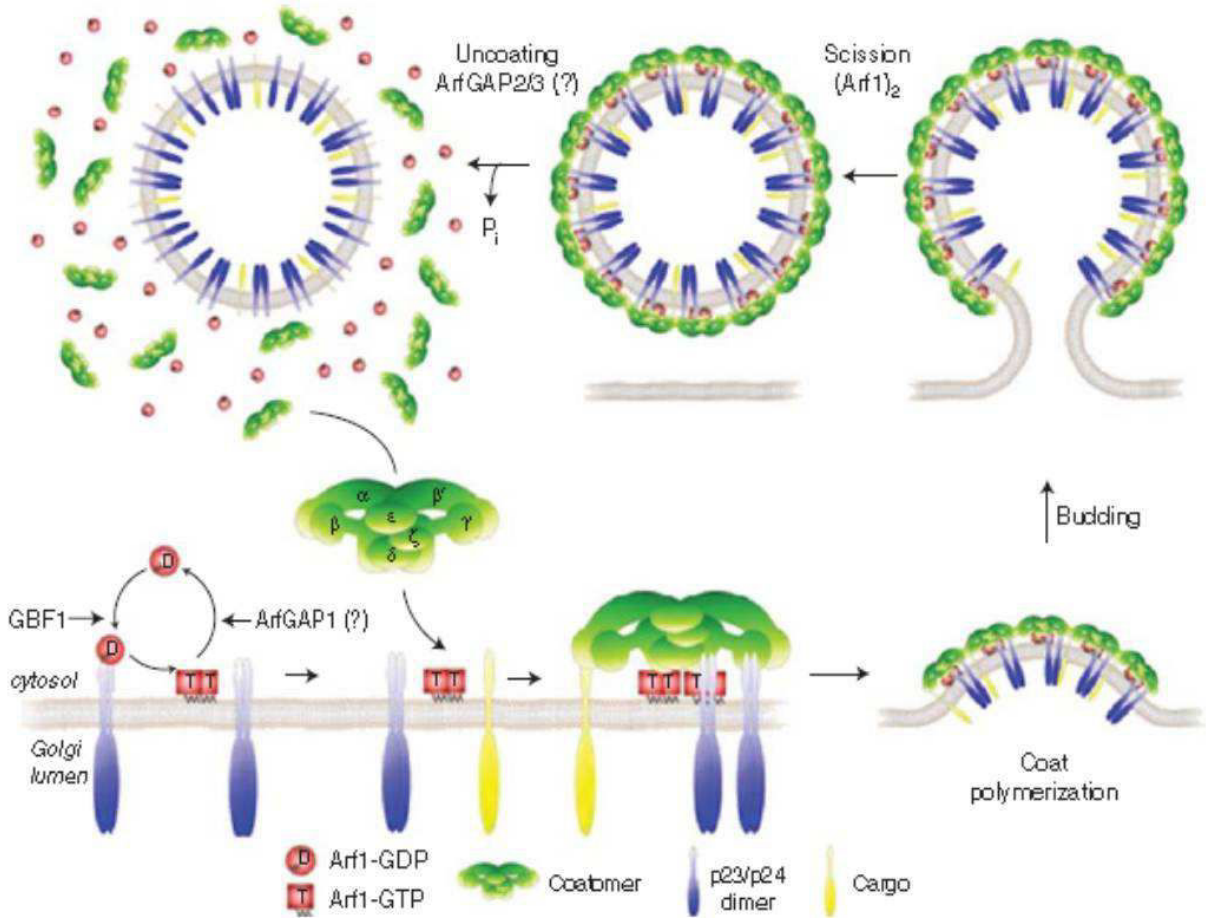

Figure 10: Schematic illustration of the different COPI biogenesis steps. Extracted from (Popoff et al., 2011).

B) Cargo sorting motifs

During COPI biogenesis, different cargo is sorted via specific signals that bind to the coatomer. The first signals characterized were dilysine motifs K(X)KXX present at the extreme carboxyl terminus of membrane proteins (Nilsson et al., 1989). This motif binds directly to coatomer and induces the retrieval from the Golgi to the ER of the host protein (Cosson and Letourneur, 1994; Letourneur et al., 1994). Various subsets of dilysine motifs exist that are recognized differentially by the coatomer complex (Schröder-Köhne et al., 1998) or by α or β′-COP subunits (Eugster et al., 2004). Another sorting motif consists of two positively charged arginine residues (usually in an RXR sequence) that can be found in cytoplasmic loops or tails of individual subunits of large oligomeric proteins such as ion channels. Diphenylalanine was also identified as a motif sorting involved in the forward transport. However, not all the membrane proteins transported within COPI vesicles carry coatomer-interacting motifs (Popoff et al., 2011). In addition, two coatomer subunits γ-COP and ζ- COP were found to exist in two isoforms, called γ1, γ2, and ζ1, ζ2, (Futatsumori et al., 2000) resulting in different heptameric protein complexes (Wegmann et al., 2004). It was proposed that these various coatomer complexes may bind to different members of p24 family protein thus contribute to generate different subpopulations of

COPI vesicles involved in different pathways that contribute to confer specialized sorting/trafficking properties to membranes of the early secretory pathway (Emery et al., 2000; Reinhard et al., 1999).

C) p24 family members involved in COPI biogenesis

An important family of transmembrane proteins that are found in COPI vesicles is the p24 family of proteins (reviewed in (Strating and Martens, 2009). The p24 family proteins are type I transmembrane proteins of roughly 24 kDa. They can be subdivided into four subfamilies (p24 α, β, γ and δ) (Dominguez et al., 1998) with the number of members in each subfamily and family varying among species. In higher eukaryotes, six family members have been identified, whereas eight are known in yeast (Emery et al., 1999). The first member was identified in 1991 (Wada et al., 1991), and the existence of a family of related proteins reported in 1995 (Stamnes et al., 1995). The six most-studied family members in mammalian systems are p23, p24, p25, p26, p27 and tp24. Most p24 proteins are ubiquitously expressed and only few proteins had a restricted expression pattern (Strating et al., 2009). Moreover, many p24 proteins from the same and from different subfamilies are coexpressed. Despite this coexpression, proteins of the same subfamilies display no functional redundancy except in yeast (Marzioch et al., 1999).

All p24 proteins share common structural features such as a large luminal domains (20 kDa), a single membrane-spanning domain and a short cytoplasmic tail (13–20 residues) [reviewed by (Emery et al., 1999)]. The luminal domain has been proposed to function as cargo receptor for transport of soluble proteins in the ER-Golgi shuttle. It is made of the N-terminal GOLD (Golgi dynamics) domain that harbours a presumed disulfide bridge (Anantharaman and Aravind, 2002) and the predicted coiled-coil region, which are thought to be involved in the oligomerization state of p24 proteins (Ciufo and Boyd, 2000). The cytoplasmic domains harbours several highly conserved motifs that mediate the binding to both the COPI and COPII coatomers namely, diphenylalanine and dilysine motif respectively close to the transmembrane region for all members and at the cytoplasmic terminus for some members. In cells, p24 proteins exist mostly as monomers and dimers of various composition depending on their subcellular localization (Jenne et al., 2002). Oligomeric state of p24 proteins is thought to be promote by the predicted coil-coil region and other regions such as the tail (Weidler et al., 2000). This oligomerization is required for their function and for the majority of their known interactions with other proteins, e.g. with γ-COP, Arf 1-GDP and TC48. Moreover, interactions between the members of these proteins are required for their stability and are important for the shuttling of p24 proteins in the ER–Golgi compartment (Dominguez et al., 1998; Emery et al., 2000).

The p24 proteins are localized in ER, IC and *cis*-Golgi membranes where they are abundant and they shuttle constantly between these compartments. Subsets of these proteins have been reported to be also localized at the post-Golgi compartement membranes in peroxisomes, secretory granules and PM (Blum and Lepier, 2008). Members of this family were identified as major transmembrane proteins of COPI vesicles.

Among them, p23 and p24 proteins are abundant in COPI membranes where they are present in various oligomeric forms to play function in biogenis of these vesicles. The p23 protein was identified as an ARF1-GDP receptor (Gommel et al., 2001) in the initiation step of COPI biogenesis and the dimeric p23 and p24 spontaneously form stable tetramers with bind coatomer complex via the γ subunit. It was shown that this heterodimer of p23 and p24 has a defined secondary structure (Weidler et al., 2000) that promote conformational change of coatomer leading to their polymerization and thus to the budding. Other members of the p24 family, that bind coatomer bear a diphenylalanine and dilysine motif, and may interact in an oligomerized state with this protein complex (Reinhard et al., 1999). The fact that various members of p24 proteins can bind to the coatomer allow different classes of COPI vesicle to exist, specified by the different p24 members they contain.

Members of the p24 family of proteins are conserved in many species such as yeast, mammalians, plants, Drosophilia and fungi; thus suggesting that they might play an essential role in cells. A p23-knockout in mice is for example embryonically lethal at the earliest possible stage (Denzel et al., 2000). Moreover, many studies have suggested the involvement of members of the p24 family in various human diseases such as nasopharyngeal carcinoma metastasis (Yang et al., 2005), pancreatic acinar atrophy, a degenerative disease of the exocrine pancreas leading to exocrine pancreatic insufficiency (Clark et al., 2005). Contreras et al, 2011 also show that mutation of p24 protein affects the early stage of development in zebrafish. Nevertheless, these proteins may be indirectly linked to disease as they may interact or influence proteins that are known to be involved in human pathology.

Despite the fact that the role of p24 proteins has been subject to much debate, many functions have been suggested among them, their implication in COPI vesicle biogenesis has been firmly established in mammalians (Béthune et al., 2006a). They are thought to act as cargo receptors and cargo selection via specific motifs, allowing their incorporation and transport into vesicles (Stamnes et al., 1995) (Figure 7). As such, p24 proteins were proposed to play a role for quality control proteins that need to be transported or retained in the ER (Wen and Greenwald, 1999). Another function proposed for p24 proteins concerns the organization of intracellular membranes in mammalian cell lines, as overexpression of p23/p24δ1 or p24/p24β1 was shown to induce expansion of ER membranes and fragmentation of the Golgi (Gommel et al., 1999). Recently, Strating et al also proposed a role of p24 proteins in supplying subsets of machinery proteins to furnish the various subcompartments of the early secretory pathway, allowing them to function properly during the biosynthesis of secretory cargo.

1.3.2.2. **Intracellular trafficking of membranes lipids**

From the ER where most of the membrane lipids are synthetized, they can be delivered to a specific compartment via nonvesicular pathways, vesicular pathways or both. As memtioned previously, this specific delivery can be regulated by internal regulators or external signals. The overview of the biosynthetic trafficking of the three classes of membrane lipids was proposed (Blom et al., 2011) as represented in Figure 11.
Glycerophospholipids are transported from the ER both along exocytic membrane transport and by nonvesicular transport. PC is the major lipid in most cellular membrane and their efficient delivery to these membranes is achieved by vesicles (Blom et al., 2011). In addition, several other possible nonvesicular mechanisms transport including MCSs, lipid diffusion mediated by proteins or not, were proposed to be involved, although their relative contributions are not determined (Voelker, 2009). For example the steroidogenic acute regulatory protein (StAR) was proposed to be potentially involved in PC transfer *in vitro* (Kang et al., 2010) but not *in vivo*. PEs are synthetized in the ER and in the inner mitochondrial membrane. Most PE synthetized in mitochondria stays in this compartment while, their transport from the ER to mitochondria, where they play an important role, is not efficient. PS is transported to other organelles via MCSs and spontaneous diffusion (Heikinheimo and Somerharju, 2002; Vance, 2008).
The second major class of membrane lipids is SLs. Their efficient de novo synthesis relies on the ER to Golgi transport of ceramide mediated by ceramide transport protein (CERT) (Halter et al., 2007; Hanada et al., 2003), except GSLs synthesis from sphingosine (D'Angelo et al., 2007) that is independent of CERT and may relie on vesicular tracfficking. CERTs are cytosolic proteins that transfer ceramide from the cytosolic leaflet of the ER to the trans-Golgi cisternae where it is converted to complex SLs species such as SM, and GSLs. They harbor a serine repeat motif that regulates CERT ceramide transfer activity depending on their phosphorylated state (Voelker, 2009). From the TG network, most synthelized SLs move in transport vesicles to the PM where they end up (van Meer et al., 2008). SLs also recyle in the late secretory pathway between PM and TGN via vesicular tracfficking in endosome/lysosome compartments and multivesicular bodies (Blom et al., 2011).

Cholesterol is the most abundant sterol in the mammalian PM where they are enriched.
They are mainly synthetized in the ER but are found there in low concentration because of the rapid transport of their precursors to other membranes. Most of newly synthetized cholesterol is transported to and from the PM via Golgi bypass routes (Baumann et al., 2005) with the help of soluble sterol carrier proteins that facilite their cellular trafficking. Two protein families are important in this process: the steroidogenic acute regulatory protein retated lipid tranfer (STAR) and the oxysterol-binding protein related protein (ORP) (Blom et al., 2011). Proteins of these families are encoded by almost 0.1% of the entire human genome (Ngo et al., 2010) and contain a sterol-binding motif and regulatory membrane target motifs. StAR a prototype of the START family regulated delivery of cholesterol to the mitochondria membrane for steroïd hormone synthesis while ORP2 one of the ORP family proteins enhance bidirectionnal trafficking of sterol between the ER and the plasma membrane (Hynynen et al., 2005; Jansen et al., 2011). In mammalian cells, the

transport of sterols via these soluble proteins is regulated by oxidation of sterols that increase their solubility and excretion in the extracellular milieu (Blom et al., 2011). Moreover, while StAR synthesis is tightly correlated with the steroid synthesis (Blom et al., 2011), ORPs sterol transfer function may be regulated by a phenylalanine (FFAT) motif (Kawano et al., 2006).

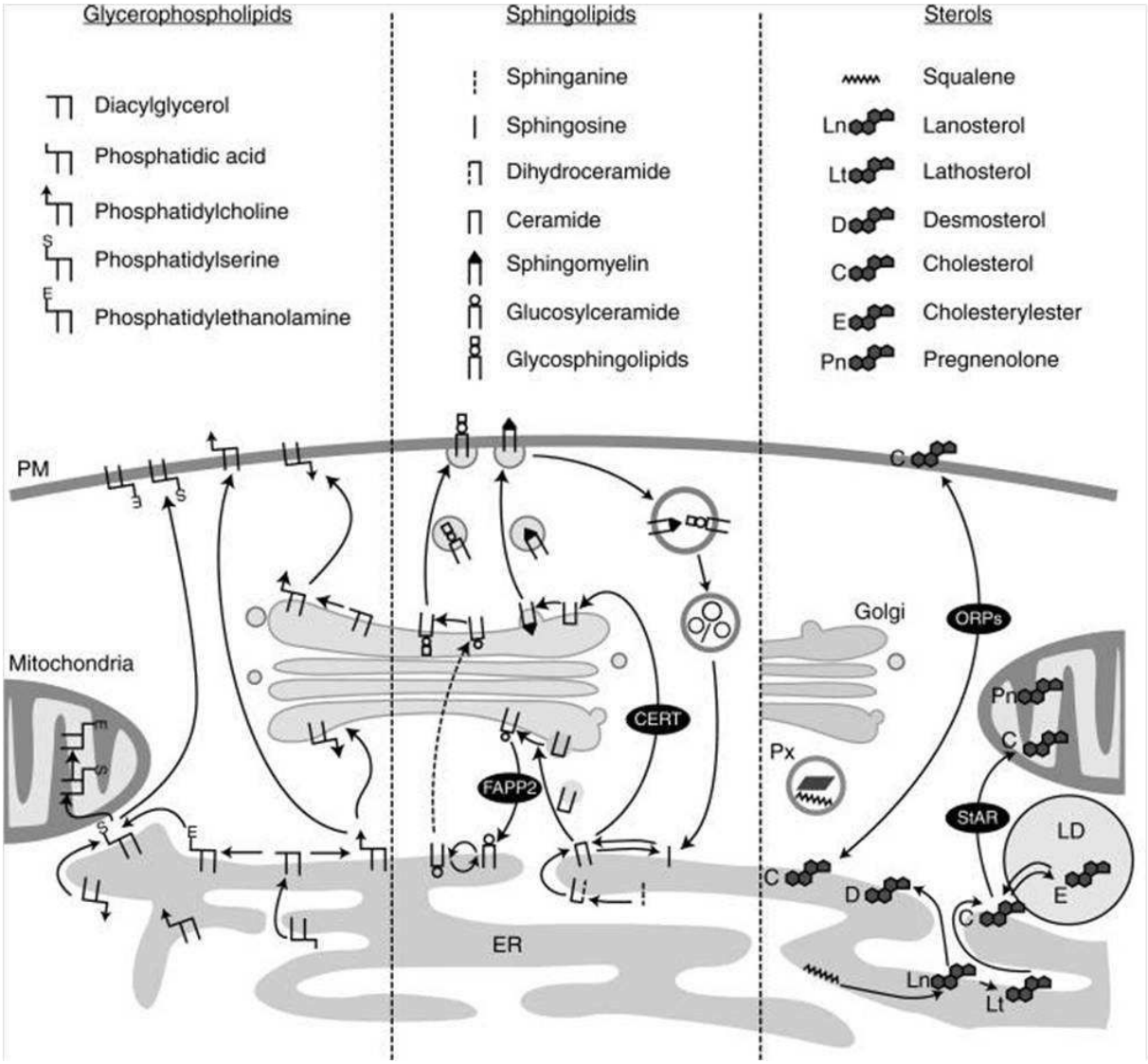

Figure 11 : Intracellular trafficking of the major classes of membrane lipids. Extracted from (Blom et al., 2011).

1.4. Membrane associated protein-lipid interactions in biological membranes

Membrane proteins rely on their interaction with membrane lipids to uphold their structure and functions. These interactions are involved in a number of impotant cellular processes such as membrane traffic, signal transduction, etc. Many membrane proteins interact

preferentially with certain lipids. This preferential interaction can favor the formation of lipid domains. The first information about how lipid molecules might interact with an intrinsic membrane protein was provided by electron spin resonance (ESR) studies (by; Contreras et al., 2011; Lee, 2003). The transmembrane domains of integral proteins present different sites of interaction with lipids: the hydrophobic surface, the protein-protein interface or protein segments. The hydrophobic surface of membrane protein is surrounded by a selected set of lipids that constitute a shell of highly immobilized 'annular' lipids. Polar headgroups of these lipids bind to the hydrophilic part of the membrane proteins and their chains to the hydrophobic surface of the membrane proteins. These lipids are mostly stabilized by polar and nonpolar interactions. The interaction with protein reduces their diffusion in the membrane compared to the 'bulk' lipids that diffuse rapidly. Annular lipids act as a solvent for membrane-spanning domains and have been observed in some crystal structures such as in the X-ray structure of the membrane rotor ring of the Na+ ATPase from *Enterococcus hirae* (Murata et al., 2005). Moreover, they were proposed to play a role in the orientation the membrane-spanning domain within the bilayer. The composition of this lipid shell depends on the local architecture of the TMD and the resident time of each lipid species at the protein-lipid interface (Contreras et al., 2011). Several parameters mediate the interaction of membrane proteins with lipids at the lipid-protein interface: the hydrophobic thickness of the lipids, the lateral pressure field of the membrane, the distribution of charges at the protein–lipid interface, and the presence of specific amino acid side chains. The lateral pressure field of membranes represents the influence of the lipid 'solvent' on a membrane protein. For example, its alteration was proposed as the molecular mechanism that provides the mechanical force to shift the channels from an open to a closed state (Perozo et al., 2002).
Integral membrane also presents binding sites within protein-protein complexes or between their transmembrane α-helices. Lipids that reside within these oligomeric membrane protein assemblies are referred as non-annular lipids. The presence of non-annular sites was first suggested for the Ca2 +-ATPase of sarcoplasmic reticulum (Lee, 2003) and most of them have been characterized in crystal structures of several other proteins. Cholesterol was reported as non-annular structural building block within GPCRs and other proteins. Moreover, cholesterol and other non-annular lipids have been suggested to play important role in modulating the structure, conformation, localization and activity within membrane protein complexes. For example, the regulation of caveolin-1 expression as well as its oligorimezation is related to cholesterol. Interestingly, a cholesterol-binding consensus motif was identified in these proteins complexes including caveloni-1 (Li and Papadopoulos, 1998a).

In addition to the role cited above, lipids involved in protein–lipid interactions were also proposed to act in a similar way than protein chaperones (Dowhan and Bogdanov, 2009). Moreover, the number of diseases related to lipids that interfere with protein folding is growing over the years (Kuznetsov and Nigam, 1998). For example, the formation of Aβ aggregates in the brain of patients with Alzheimer disease correlates with a specific peptide–lipid interaction (Wakabayashi et al., 2005).

1.5. Background & Aim of the thesis

This dissertation deals with some multi disciplinary work bridging the field of proteomics and lipodomics in the context of lipid bilayers. Although this area has been little explored in the last years, it is now a subject of intense research as it carries the potential for the discovery of new so far unknown regulatory mechanisms of membrane proteins function as well as for lipid sorting (Contreras et al., 2012; Dufourc, 2008; Jean-François et al., 2008; van Meer et al., 2008). Research has been focused in this area on the structural study of protein-protein and protein-lipid interactions when very little was known on the involvement of membrane lipids in fundamental regulatory mechanisms. Likewise, the sorting of membrane lipids has been mainly investigated from the view of dynamics of membrane microdomains (Dufourc, 2008; Rajendran and Simons, 2005). Nevertheless, recently interest has grown to understand the cellular function of lipid diversity and in a context of interaction with membrane proteins (Coskun and Simons, 2011; van Meer et al., 2008). In the continuous flow of this issue, this work has the potential to deliver new fundamental knowledge about the role of lipids and protein-lipid interactions in biological function and regulation; and could be helpful in understanding biological function in health and disease.

This thesis focuses on the investigation of a specific interaction between one SM species, SM C18 exclusively with the transmembrane domain of the COPI machinery protein p24 (p24TMD). The goal of this work is to have a better understanding of the role of this highly specific interaction. This project was initiated by the work of our collaborators at the Univesity of Heidelberg published in 2012 (Contreras et al., 2012a).

In a previous work, they had developed mass spectrometric methods to quantify lipids at a low picomole level (Brügger et al., 1997) and had found a surprising sorting of one SM molecular species, SM C18 into intracellular COPI transport vesicles (Brügger et al., 2000). In further studies, using FRET and lipid crosslinking (Haberkant et al., 2008) they were able to pinpoint this sorting to a single transmembrane domain (TMD) of the COPI machinery protein p24, with an almost exclusive specificity for SM C18:0 (Figure 12 A and B). When looked at the structural prerequisite for SM18 binding, they were able to define by mutagenesis a motif made of carboxy-terminus amino acids VxxTLxxIY of the p24 TMD, derterminant for the specific binding of SM C18. More important, when tranfert this motif to the amino-terminal half of the non-sphingomyelin-binding TMD of p23 another COPI machinery protein, this protein became able to bind SM C18. This signature was proposed to form a groove in which the SM C18 acyl chain pack.

Striking, amount all the SM species with acyl chain ranging from C14 to C22, only SM C18 could selectively bind this motif while steric effect between p24TMD and the others species avoid the binding. Moreover, the binding involves also the SM C18 headgroup. Based on molecular dynamic (MD) simulations a model of this interaction was proposed (Figure 12 C right).

Interaction of such pronounced specificity between a protein and sphingolipid involving both fatty acyl chain and headgroup has not been described before in membranes. Rather,

fatty acyl chains or head group fragments of lipids are known to be involved, for example, in cellular signalling (e.g. arachidonic acid and inositol-phosphates). Moreover, as p24 acts as membrane machinery for the formation of COPI vesicles, the effect of this interaction on the p24 oligomerization state and the transport of biosynthetic cargo (Scales et al., 1997) was investigated (Contreras et al., 2012a). Based on their data, it seems that the COPI retrograde transport depends on p24 binding to SM, and moreover, this interaction promotes and stabilizes the dimeric transport active state of p24. It seems therefore evident from such observations, that the characterization of the contact between the p24TMD and SM C18 at atomic level will provide insight on a specific lipid function in transport and sorting of other lipids. This will alson provide to a large extent first hints to understand the need for the complexity of membrane lipid composition at a functionnal level, and their importance in regulating protein function.

With the goal to understand molecular basis of this interaction, we investigated the structure of p24 with its bound lipid in a bilayer environment using a number of biophysical approaches including NMR and other spectroscopic methods. Solid-state NMR spectroscopy in particular has a long standing in characterising the structure and dynamics in a wide range of bio-membranes that are inaccessible to crystallography or solution NMR, such as membrane proteins and aggregates (Andronesi et al., 2005; Bechinger and Sizun, 2003a; Cross, 1997a; Hong, 2006; Opella et al., 2001). The dynamics and the topolgy of p24TMD in bilayers were investigated in the absence and presence of SM C18 using solid-state NMR on oriented samples. The perturbation of the peptide on membrane bilayers was also studied. Moreover, in order to determine the molecular distance between amino acids of the binding site and SM C18, we tested the REDOR approach. The whole structural data we recorded was used to shed light on the proposed model in order to test this model, and when necessary to propose a new model.

During this work, I had a proposition to continue a part of the PhD project of Dr Omar Rifi on interaction of cholesterol with the cholesterol binding motif (CRAC) of the human immunodeficiency virus (HIV) membrane protein gp41, with the aim to get insight on the mechanism of binding with cellular membrane during infection. To achieve this purpose, we investigate the structure, the dynamics and the topology of this binding motif in membrane containing cholesterol. We used a set of biophysical methods such as circular dichroism (CD), fluorescence and nuclear magnetic resonance (NMR) spectroscopy.

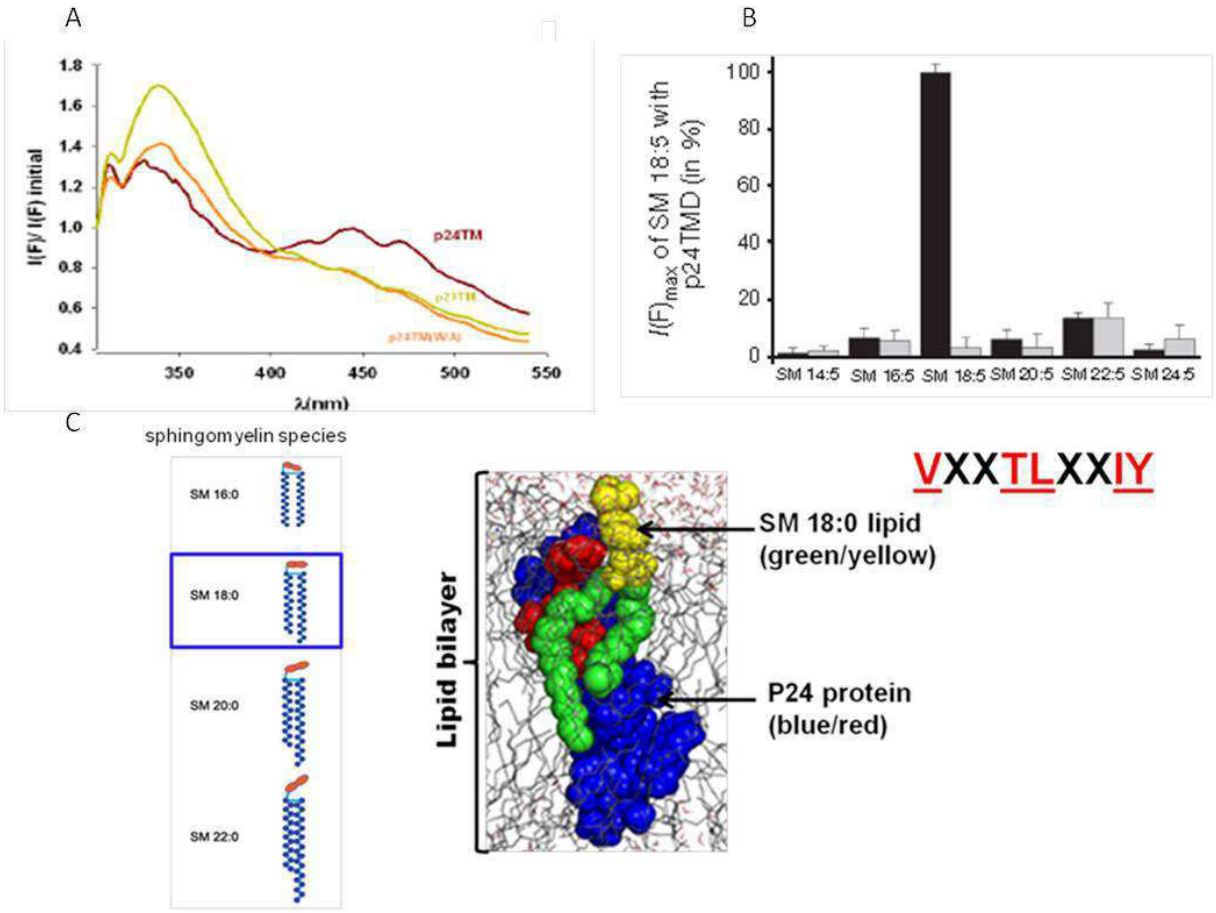

Figure 12 : p24TMD specific interaction with SM C18 (Contreras et al., 2012). A) In vitro FRET analysis of MBP–TMD fusion proteins and pentaenoyl-sphingomyelin (SM 18:5) in proteoliposomes. p24TMD (Red curve), p24TMD (greenyellow), p24TMDW4A (orange curve). B) Quantification of fluorence of p24TMD (black) or p23TMD (grey) in pentaenoyl-sphingomyelins liposomes mimicking liquid disordered phase. C) Molecular dynamic simulations: snapshot of a SM 18–p24TMD interaction.

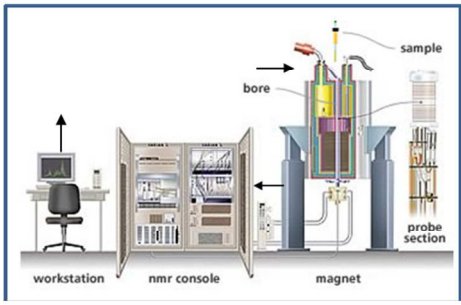

Chapter-2

THEORY : TECHNIQUES AND PRINCIPLES

This chapter focuses on the experimental techniques we used to achieve our goal. These techniques range from biochemistry to biophysics methods. The principles and the theoretical aspect of their contribution are presented.

Chapter 2. **Techniques and principles**

2.1. Strategies to obtain the peptide

Important prerequisites for characterization by solid-state NMR spectroscopy are a high level of polypeptide purity and its labelling with stable isotopes such as ^{15}N, ^{13}C. Two approaches were used for the production of the p24 peptide namely solid phase peptide synthesis (SPPS) and the recombinant over-expression in bacteria. Although both techniques are used to produce peptides, the later present advantage of potential higher yields of uniformly labelled protein at a lower cost. However, the setup of the experimental protocol for expression in bacteria can be laborious and time consuming without guarantee of result. In the following section, the principles and advantages/disadvantages of these methods will be presented.

2.1.1. Fmoc solid-phase peptide synthesis

SPPS pioneered by Robert Bruce Merrifield (Merrifield, 1963), is a widely accepted method to obtain peptides in a synthetic manner. It presents the advantage to allow specific labelling at defined positions of the peptide sequence, and to be less time consuming for smaller polypeptides. However, SPPS is expensive and cannot offer all the possibility of labelling as some labelled amino acids are not easily available. Moreover, the yield is limited by peptide length and sequence. In fact, increasing peptide lengths and/or having a hydrophobic sequence with β branch amino acids as valine, leucine etc… will lead to chain aggregation, truncated peptides, difficulty of purification resulting in low peptide yield.
SPPS consists of the sequential coupling of amino acids through peptide bonds. The peptides are synthesized on small porous beads made of a polymer resin usually in a direction opposite to that in the cell, i.e. from the carboxyl-terminus (C-ter) to the amino-terminus (N-ter). They are covalently attached to the resin via a linker that bears reactive groups such as –OH that will react easily with the carboxyl group of an N-α-protected amino acid. The amino protecting group (Fluorenylmethyloxycarbonyl (Fmoc)) will then be removed (deprotection) under basic treatment, usually piperidine, allowing a second N-α-protected amino acid to be coupled to the attached amino acid. At the end of each coupling step, the excess of amino acids are removed from the peptide-solid support matrix by washing with N,N-dimethylformamide (DMF) which is the main solvent used during all the different steps. In repeated steps of coupling-washing-deprotection SPPS proceeds until the desired peptide sequence is obtained. At the end of the synthesis, the peptide is cleaved from the resin under acidic conditions usually TFA (trifluoroacetic acid). As certain amino acids side chains contain functional groups that by reacting with the activated amino acids can interfere with the formation of the correct amide bound during the synthesis, these functional groups are protected. These protecting groups are removed during the cleavage of the peptide from the resin. TFA counter ions remain associated with the peptide to neutralize cationic side chains when the solvent is evaporated but can be exchanged by repeatedly resuspending the peptide in a solution of acetic acid 4% and evaporation. The general scheme of the Fmoc SPPS is outlined in Figure 13.

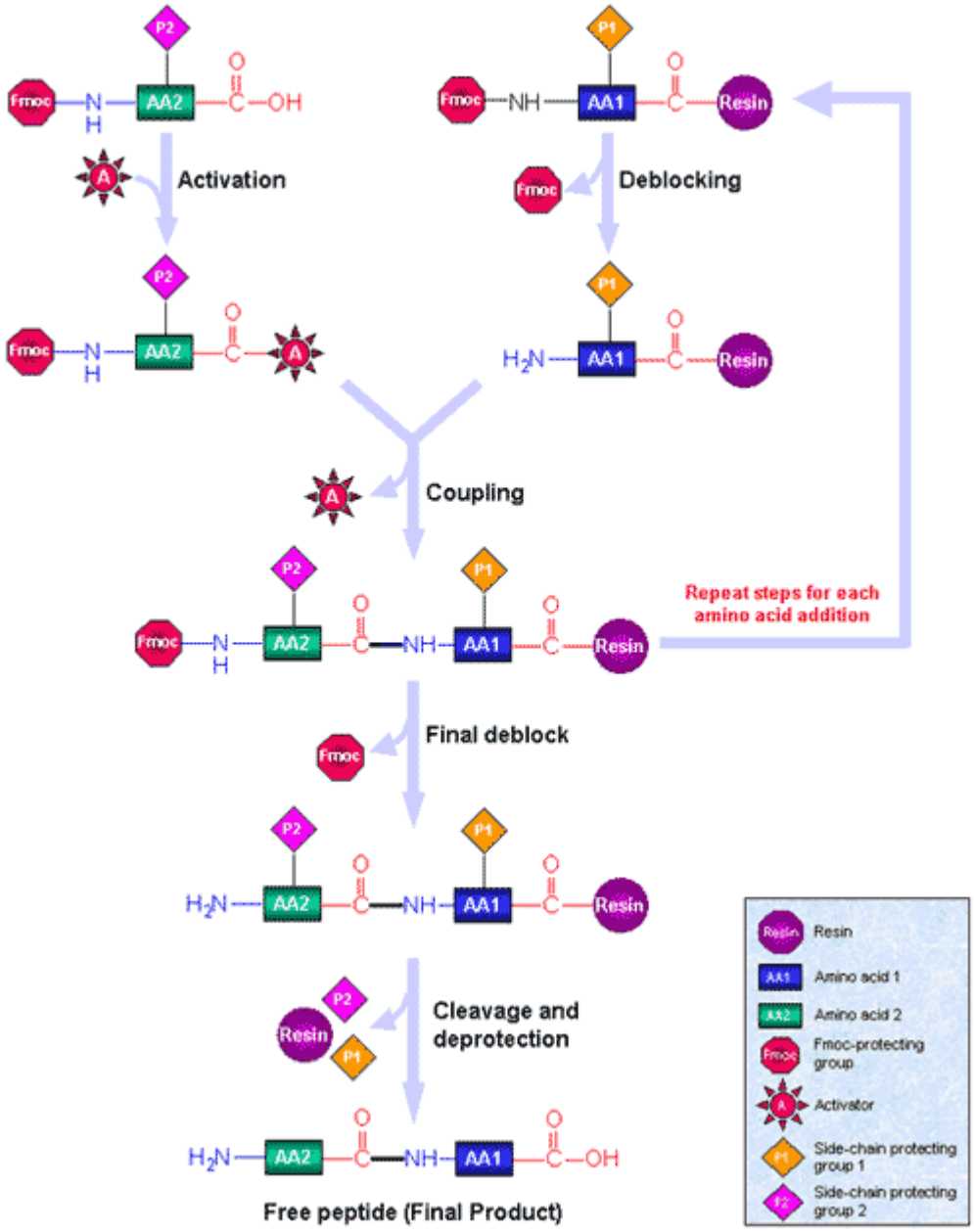

Figure 13: The general scheme of Fmoc SPPS. Reproduced from Sigma-Aldrich website

2.1.2. Expression strategy of recombinant protein in *E. coli*

In 1973, Stanley Cohen and Herbert Boyer pioneered the use of recombinant DNA technology for cloning and expression of genes in foreign organisms (Cohen et al., 1973). Bacterial expression systems are the method of choice for expression of many recombinant proteins. The reasons for this lie in the cost-effectiveness of producing proteins in bacteria, their easy manipulation and well-characterized genetics, the availability of many different bacterial expression systems, and the potentially high yield of uniformly or selectively labelled proteins at a cheaper cost.

Among the hosts available for recombinant expression, *Escherichia coli* is the most attractive strain. This strain is especially valued because of its rapid growth rate with high density in low costs media, its well-known genetics which offers a broad scope of biotechnological tools available for genetic engineering. Moreover, more than 70% of all proteins submitted to the protein data bank (PDB) in 2014 were expressed in *E. coli*. However, despite the advantages of this bacterial system, there is no guarantee that the protein will be produced in sufficient amount. This is essentially the case of membrane proteins or peptides whose expression is difficult and often leads to insufficient quantities needed for structural studies by NMR (Samuelson, 2011). In addition, the system presents limited ability for posttranslational modifications and occasional poor folding due to lack of specific molecular chaperones (Yin et al., 2007).

In general, to over-express a protein in *E. coli* it is necessary to clone the gene that encodes the protein of interest into an expression vector. The vector is then introduced into the host cell by physical (electroporation) or chemical ($CaCl_2$) methods. Commercial *E. coli* bacterial host cells, already in a competent state to take up foreign DNA, can be purchased. The expression of the protein of interest is then performed during bacterial growth in specific conditions of temperature and nutrients.
Despite all the recombinant expression technology available for *E. coli* strain, successful protein expression in this organism relies heavily on carefully choosing the expression system and its optimization. Interestingly, expression efficiency is regulated by several parameters which should be tested in order to maximize the yield of the recombinant protein. These parameters will be presented in the following sections as well as the chronological steps for the preparation of a recombinant protein.

2.1.2.1. **The expression vector**

The expression vector is designed for protein over expression and therefore contains several essential genetic elements to achieve this purpose:
The origin of replication (Ori): It initiates the replication of the vector independently of the bacterial chromosome and ensures that the cell contains many copies of the vector which are distributed between the daughter cells when the cell divides. The exact number of copies per cell varies according to the replicon. Most of the expression vectors are replicated by the ColE1 replicon and are defined as multi-copy plasmids with 10-50 copies per cell. Thus, the presence of the replicon expression vector increases the copy number of interest and consequently the performance of the overexpressed protein gene. However, other factors also play a role on the final amount of protein.
The gene for resistance to an antibiotic is used to select bacteria having the vector and allow this vector to be maintained in bacteria over generations during their growth. In fact, transformed bacteria will be resistant to a specific antibiotic (ampicillin, kanamycin, chloramphenicol, tetracycline ...). For example, a vector containing the gene for ampicillin resistance expresses a periplasmic enzyme called β-lactamase, which hydrolyses the β-lactam nucleus. Thus when ampicillin is added to a bacterial culture, vector-free bacteria will be killed while vector-containing bacteria will produce the enzyme to hydrolyse

ampicillin and therefore will not be killed. However, as this antibiotic will be hydrolysed, it is preferable to use other selection markers such as kanamycin or chloramphenicol which are not degraded but rather, inactivated.

The promoter is always positioned upstream of the coding sequence and drives its transcription. It contains the RNA polymerase binding site for initiation of the transcription and the operators (response elements). The promoter is often put under the control of a gene regulator (R) often localized upstream the promoter, that encodes a repressor. Its importance in the regulation of the production of heterologous proteins will be detailed later.

Downstream of the promoter is the translation initiation site which binds the ribosome (RBS) by complementarity to the 16S rRNA of the small ribosomal subunit. The site of translation termination (codon stop) is located at the end of the coding sequence to end the translation.

The site of transcription termination (TT) is located after the coding sequence and serves as both the termination site as well as a sequence which protects the mRNA from exonucleases.

All these regulatory elements (summarized in Figure 14) allow vectors to be replicated, maintained and to express the protein sequence that they contain to be expressed in the bacteria. Some of them are not present on cloning vectors as their first purpose is for vector amplification. Thus, the choice of vectors is done according to a specific purpose. Table 2 summarized the different elements of a vector and highlight differences between these two type of vectors.

2.1.2.2. *E. coli* host strains

The easy genetic manipulation and transformability of *E. coli* make it a host of choice for the propagation, manipulation, and characterization of recombinant vectors. A wide variety of *E. coli* mutants (strains) are available and as for the vectors, should be chosen according to the purpose. They are generally designed for cloning or for protein expression; although some strains are suitable for both purposes. Their genetic modifications can be made either via chromosomal modifications or the addition of plasmids. Among these mutations, some are essential to improve the yield of the heterologous protein. Table 3 summarizes the most common genotypes (bacteria traits) that are important for protein expression. Briefly, for example *lon* and *OmpT* mutations reduce proteolysis of the heterologous protein, DE3 allows the expression of the T7 RNA polymerase in *E. coli*, pLysS attenuates the protein basal expression and *rne131* stabilizes mRNA.

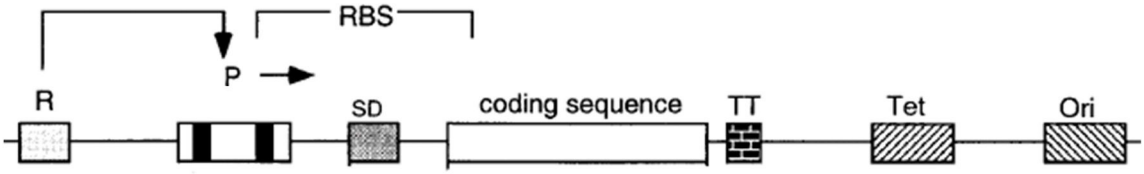

Figure 14: Schematic representation of the essential elements of a prokaryotic expression vector (Makrides, 1996). The promoter (P) is positioned upstream of the coding sequence and is often

under the control of a regulatory gene (R) that encodes a repressor. This gene may exist on the expression vector or on the chromosome of the host cell. The ribosomal binding site (RBS) sequence contains the Shine-Dalgarno (SD) which is complementary to the 16s RNA of the small subunit of ribosome. The termination sequence of transcription (TT) serves to stabilize the mRNA. The selectable marker (Tet) which encodes a gene for tetracycline resistance allows the selection of bacteria having the vector. The copy number of the vector in the cell is determined by the origin of replication (Ori). The arrow indicates the direction of the transcription. (Makrides, 1996)

Table 2: Common vectors elements and their characteristics. The combination of these elements determines the type of vector.

VECTOR ELEMENTS	CLONING VECTOR	EXPRESSION VECTOR	CHARACTERISTICS
Origin of replication (ORI)	Yes	Yes	Drives the replication of the vector and determines its copy number.
Antibiotic resistance gene	Yes	Yes	Selectable marker used to maintain the vector into bacteria and to select transformed bacteria.
Multiple cloning site (MCS)	Yes	Yes	Contains different enzymatic restriction sites to allow the insertion of foreign DNA called insert
Insert	Yes	Yes	Corresponds to a DNA sequence that encodes for a protein of interest (coding sequence)
Promoter region	No	Yes	Regulates the transcription of the coding sequence
Termination site of transcription and the initiate and termination site of translation	No	Yes	Regulate the end of the transcritpion and the translation initiation and end

Table 3: Common genotype traits of bacteria related to protein expression. Adapted from BitesizeBio web site.

GENOTYPE TRAITS OF BACTERIA RELATED TO PROTEIN EXPRESSION	DESCRIPTIONS	BENEFITS
DE3	Expression of the T7 RNA polymerase	Expression of the protein of interest under the control of the T7 promoter in E.coli
pLysS	Expression of the T7 lysozyme which destroys the T7 RNA polymerase produced from DE3.	Tight regulation of the basal expression from T7 promoter
lon	Deficiency in the Lon ATPase-dependent protease.	Reduced proteolysis of the recombinant proteins
ompT	Deficiency in an outer membrane protease.	Reduced proteolysis of the recombinant proteins
rne131	Expression a truncated RNase E that lacks its endonuclase function	Increased mRNA stability and then the yield of the heterologous protein
lacI q	Gives high levels of lac repressor expression	Tight regulation of gene expression under the control of the lac promoter

For molecular cloning, methyltransferase and endonuclease deficiency are important mutations that maintain the integrity and increase the stability of the vector. Thus, they improve the yields and maintain the quality of the manipulated DNA.

2.1.2.3. **Molecular cloning to obtain the expression vector**

Molecular cloning is the first stage of most genetic engineering experiments that aim to assemble the recombinant vector and direct it within a host cell (bacteria, yeast, insect…) for expression or for genetic manipulation. The recombinant expression vector, is obtained in two important steps: The first one is the amplification and the purification of the DNA fragment (insert) that encodes the protein of interest and the second step is the cloning of the insertion into the expression vector. The amplification step can be achieved either by polymerase chain reaction (PCR) or in bacteria. In the later case, as DNA fragments cannot be maintained in the host cells, it is often inserted first in a vector, usually a plasmid. In our case, as our insert (nucleic sequence coding for the p24TMD protein) was designed in a cloning plasmid (pMA), the amplification was achieved in bacteria; specifically, in XL1 blue an *E. coli* strain genetically modified for plasmid amplification.

Briefly, bacteria were transformed with the pMA-p24TMD vector and selected on agar plate with specific antibiotic as described above. Thereafter, they were grown in a rich medium to amplify the vector, usually the Lysogeny Broth (LB) medium either in small or large scale (minprep or maxiprep, respectively). Cells were harvested at a specific optical density (OD) at 600 nm and the vector extracted and purified with commercial kit for DNA extraction (Nucleospin Plasmid, Macherey-Nagel, Germany).

The pMa-p24TMD and the pTIPX4 expression vector were then separately digested with the same specific restriction enzymes in order to generate sticky ends that are complementary. The products of digestions are separated by agarose gel electrophoresis (described above) and DNA fragments corresponding to the insert and the digest expression vector are cut from the agarose gels and purified using commercial kits for DNA gel extraction (Nucleospin extract, Macherey-Nagel, Germany). Thereafter, they are mixed together in the presence of DNA ligase that connect their 3' and 5' ends to obtain the recombinant vector. As the ligation is done in small volumes with a tiny quantity of material, the recombinant vector needs to be amplified as described above to obtain sufficient amount of product. A quick check is often done by sequencing the recombinant vector and/or digestion with the same restriction enzymes that were previously used, to verify that the vector was constructed correctly with the insert.

2.1.2.4. **Regulation of the expression**

Overexpression of heterologous proteins are energy consuming for the host cell as it has to maintain and express the "foreign" gene. This causes a situation of stress for the bacteria which may results in a slower growth or proteolysis of the protein of interest. Thus, regulation of expression of the foreign gene is required to prevent bacterial stress and to produce high quality proteins in large quantities.

To achieve this, the ideal vector should not replicate too much (low copy number) and must have a strong promoter that initiates the transcription with a high frequency. However, strong promoters should be finely controlled to avoid the permanent expression of proteins which can impair bacterial growth. This control is achieved via inducible promoters which can be turned only at a specific stage of the bacteria growth, by the addition of a specific metabolite called inducer or by temperature changes. One of the most commonly used strong and inducible promoter for the expression of heterologous proteins is the lac operon. It is induced with by the Isopropyl β-D-1-thiogalactopyranoside (IPTG) which binds the repressor and activates the transcription as it will be describe later.

However, "leakage" of this system sometimes happens and results in basal expression before induction. This may lead to bacterial death in the case of toxic proteins. To restrain as much as possible this basal expression, specific bacterial strains such as BL21 (DE3) pLysS are preferentially used.

To regulate the expression of our protein of interest, we used two different vectors. The pTIPX-4 (Taf12 Insoluble -mediated Peptide eXpression) plasmid (see Figure 15), that was designed in our laboratory by Dr. Werten (Vidovic et al., 2009a) to allow the accumulation of the expressed protein in insoluble fraction called inclusion bodies. The other vector, the pMAL-c5X-p24TMD was designed and used by our collaborator (University of Heidelberg) for the expression of the p24TMD fusion protein in the soluble fraction. We have also used different *E. coli* strains to regulate the toxicity of this protein as it will be described. In the following paragraph, I will briefly describe the mechanism of regulation of these two expression systems.

The pTIPX-4 expression system

The pTIPX-4 is a modified pET-28b (Novagen) vector of 5577 bp in which a new DNA fragment BglII-Bpu1102l was introduced in the multiple cloning sites (MCS) (see Figure 16). This inserted fragment contains :

- The TAF12 sequence (TATA box binding protein (TBP)- Associated Factor 12 Histone fold Domain), a transcription factor used as a fusion protein with the desired sequence, where the non-soluble TAF12 directs the over-expressed protein into inclusion bodies to restrain their toxicity (Vidovic et al., 2009a)

- A new polylinker with unique restriction site which allows the insertion the gene that encodes the protein of interest. For the insertion of the p24TMD gene, we used the BamHI-SacI restriction sites

- This fragment was inserted downstream a stretch of six Histidines called His tag used for the purification of the fusion protein

- An enzymatic (enterokinase) and a chemical (formic acid) cleavage sites that allow the cleavage of the peptide from the fusion protein.

In addition, pTIPX4 (Figure 15) contains as all cis regulator elements of pET vectors: the *T7* promoter (*T7* promoter), a transcription terminator (*T7* terminator), and the gene that encodes the lacI repressor (lac I r) and the lac operator (lac O). It also contains a marker for resistance to kanamycin (Kan) and an ori for the replication of the vector.

The transcription of the gene of interest is regulated by the strong *T7* promoter present on the expression vector pTIPX4 via the binding with of the *T7* RNA polymerase. This transcription requires a bacterial strain which has integrated into its genome the gene that encodes the *T7* RNA polymerase (fragment of bacteriophage λDE3). This enzyme has a high processivity and is five times faster than the endogenous bacteria *T7* RNA polymerase. In general, the gene that encodes the *T7* RNA polymerase is under the control of the *lacUV5* promoter present on the bacterial chromosome. Both promoters *T7* and *lacUV5* are regulated by the *lacI* repressor via its binding to the lac O (inducible by IPTG). The *lacI* gene that encodes the *lacI* repressor is present on both the bacterial chromosome and the expression vector. In absence of IPTG, *lacI* binds to the operator and represses the lacUV5 promoter and the hybrid T7 / lac O promoter. Consequently, T7 RNA polymerase and the heterologous protein are not expressed. However, the T7 RNA polymerase can sometimes be produced even in the absence of IPTG, resulting in a basal protein expression. This basal expression can be suppressed by the presence of an inhibitor of the RNA polymerase *T7*: the *T7* lysozyme. For example the BL21 (DE3) pLysS strain carries a plasmid encoding the *T7* lysozyme (Samuelson, 2011) and was used for the expression of our fusion protein in order to restrain this basal expression.

In presence of IPTG, the repressor binds IPTG allowing the bacterial RNA polymerase to bind the lacUV5 promoter and express the *T7* RNA polymerase which will subsequently bind the *T7* promoter and allow the production of the heterologous protein (Baneyx, 1999; Chen, 2012; Hannig and Makrides, 1998; Studier et al., 1990). The T7 terminator allows the end of the transcription.

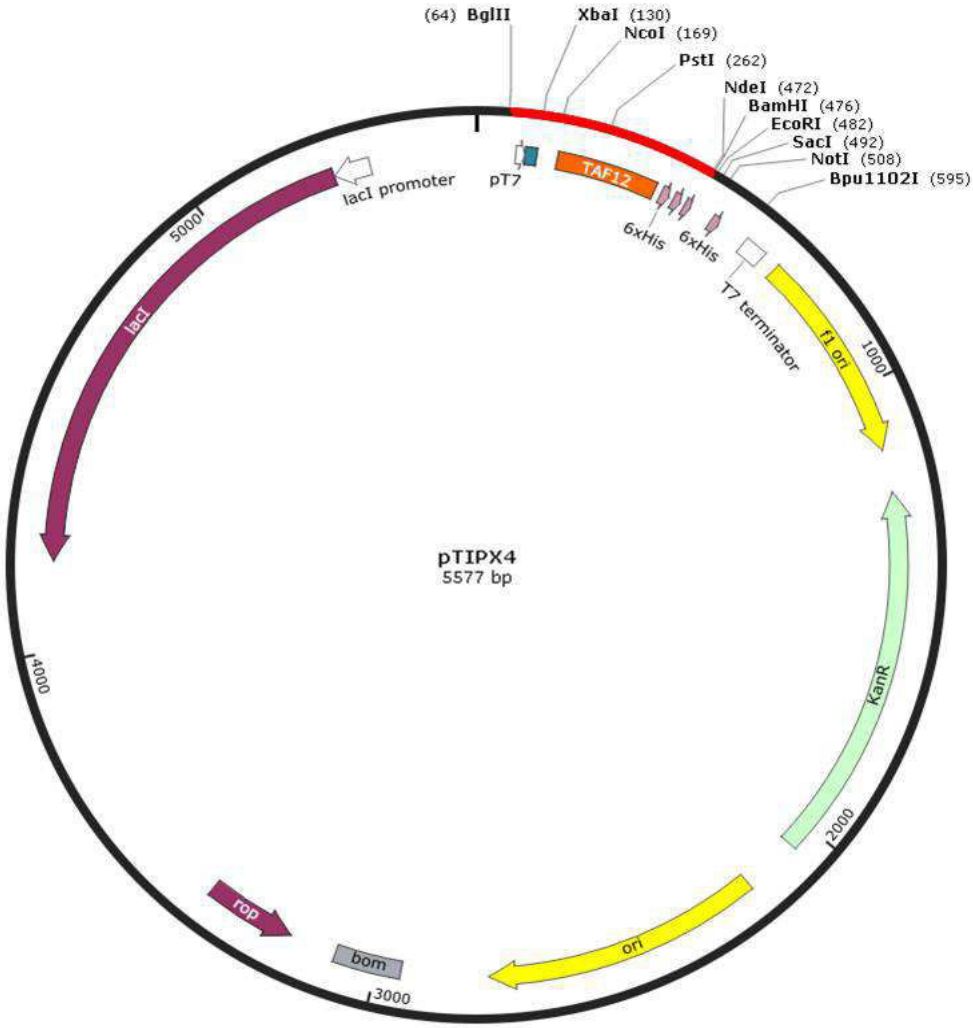

Figure 15: Schematic representation of the pTIPX-4 plasmid with its different regulatory elements. pTIPX-4 is a plasmid of 5577 bp that contains the resistance gene to the kanamycin, a MCS with the SacI and BamHI restriction sites, the cis regulatory elements and the nucleic sequence coding for the TAF12 fusion protein.

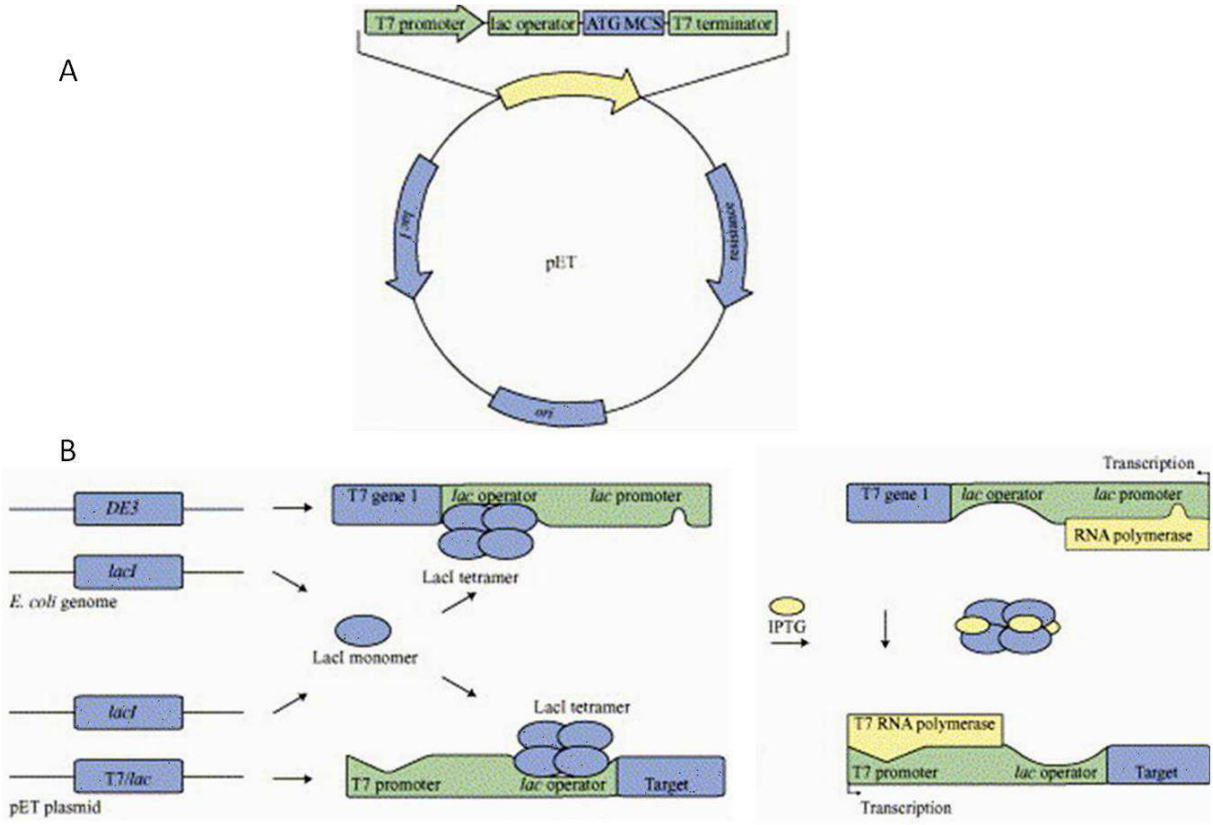

Figure 16 : General features of the pET expression system. A) A schematic representation of the pET vector with its important regulatory elements. B) Regulation of the inducible T7 and lacUV5 promoters. In absence of the inducer (ITPG), they are both repressed by LacI. The presence of IPTG allows the expression of the T7 polymerase that binds the T7 promoter and initiates the transcription. (Sørensen and Mortensen, 2005a)

The pMAL-c5X expression system

pMAL are commercial vectors designed to produce fusion proteins with the water soluble maltose-binding protein (MBP). This protein will direct the fusion protein either in the cytoplasm or the periplasm and allow their purification by amylase affinity chromatography. The gene of interest is inserted in the MCS downstream of the *malE* gene, which encodes MBP. The pMAL-c5X was designed with a deletion of the *malE* signal sequence, to allow a cytoplasmic expression of the fusion protein. To allow a correct folding of the MBP and a better access for the binding of amylose resin during protein purification, a spacer sequence coding for 10 asparagine residues was inserted between the *malE* sequence and the polylinker. This polylinker contains a sequence that allows the protein of interest to be cleaved from maltose-binding protein with the specific protease Factor Xa. In our construct pMAL-c5X-p24TMD, this cleavage site was replaced by the Tobacco Etch Virus (Tev) cleavage site.

The transcription of the gene of interest is under the control of the strong hybrid Ptac promoter. This promoter is not naturally found in bacteria but was designed by fusing the -35 region of the trp promoter and the -10 region of the lacUV5 promoter/operator to make

it more powerful than the parental promoters alone. The pMAL-c5X vector also carries the *lacIq* gene that codes the Lac repressor (Figure 17). This protein regulates the Ptac promoter which is inducible by IPTG. As for the T7 promoter, in presence of IPTG the LacI repressor will be inactivated allowing the production of the heterologous protein and in absence of IPTG, this production will be repressed.

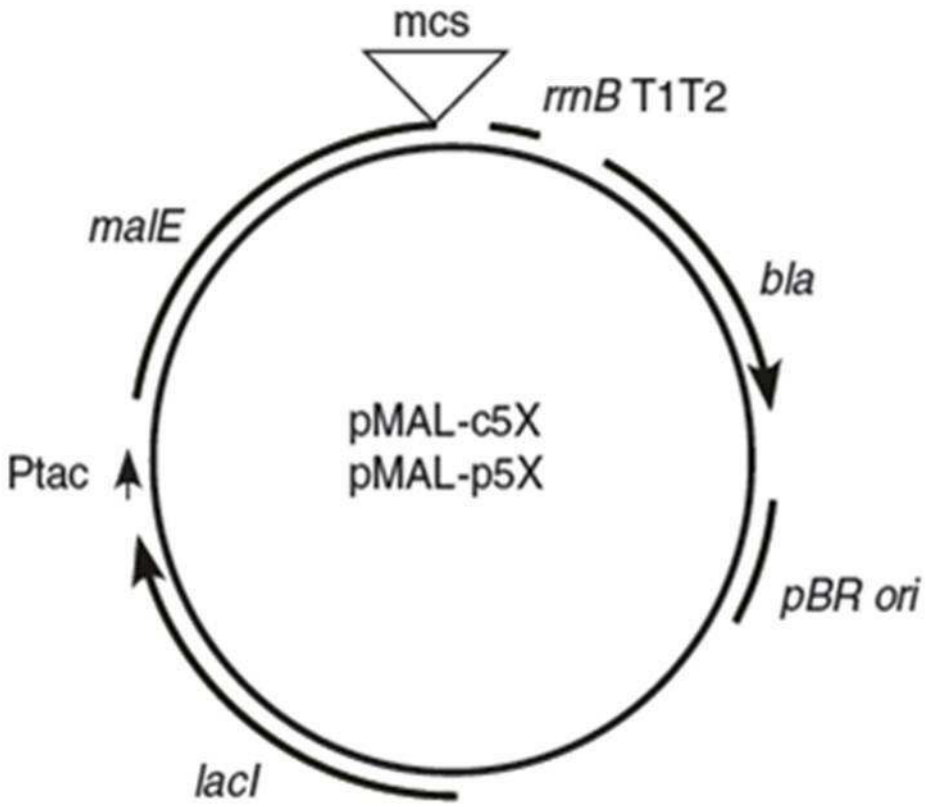

Figure 17: Schematic representation of the pMAL-c5X. It contains the hybrid Ptac promoter, the malE *gene that codes the MBP fusion protein, a pBR ori and the lacI gene that codes the LacI repressor. Reproduced from* New England Biolabs

2.1.2.5. **Cellular localization and purification of the protein**

Although most heterologous proteins are expressed in the cytoplasm, during expression they can also be directed to other cellular compartment such as the membrane or the periplasm. Over-expression of heterologous proteins is often accompanied by protein misfolding and aggregation leading to insoluble dense particles in cytoplasm of about 1 micron diameter, with an amyloid-like architecture known as inclusion bodies (García-Fruitós et al., 2011; Lilie et al., 1998). However, in case of toxic proteins such as antimicrobial peptides this can be an advantage. Their assembly into aggregates protects the expressed proteins against proteases and prevents them being toxic against the bacterial host cell (Vidovic et al., 2009a). For example, the TAF12 fusion protein was developed for

this purpose. However, to isolate the protein of interest these inclusion bodies need to be treated under denaturing conditions such
as 8M urea or 6M guanidine hydrochloride to solubilise the aggregate and recover the native folded protein.

Table 4 : List of the most common fusion partners, with their ligands and the competitors used during their purification by affinity chromatography

Fusion partners	Ligands	Competitors for elution
Gluthatione-S Transferase (GST)	Glutathione-Sepharose	Reduced glutathione
His_6-tag	Ni2+nitriloacetic acid	Imidazole
Maltose Binding Protein (MBP)	Amylose resin	Maltose
Thioredoxin	ThioBond resin	Ion exchange
Protein A	IgG-Sepharose	Low pH or specific ligand
Strep-tag	Streptavidin resin	2-Iminobiotin, diaminobiotin

Table 5 : List of the commonly used enzymatic and chemical cleavage sites with the corresponding sequences. ((*Hwang et al., 2014a)*; Vidovic et al., 2009).

	CLEAVAGE METHODS	CLEAVAGE SEQUENCES
ENZYMATIC/ CHIMICAL	Cyanogen bromide	-Met/X-
	Formic acid	-Asp/Pro-
	Enterokinase	-Asp-Asp-Asp-Asp-Lys/X-
	Thrombin	-Leu-Val-Pro-Arg/Gly-Ser-
	Tabacco Etch Virus protease	-Glu-Asn-Leu-Tyr-Phe-Gln\Gly-

Fusion partners were developed to improve the solubility of over-expressed proteins and thereby prevent the formation of these inclusion bodies (Costa et al., 2014). They can also be used to direct the fusion protein in a specific cellular compartment. Most fusion partners facilitated the detection and/or the purification of the fusion protein and protect them from

intracellular proteolysis (Hwang et al., 2014a). The most common fusion partners that are used to facilitate the purification are listed in Table 4. However, this function cannot be always fulfilled by some fusion partners. When it is the case, a "tag" is often introduced to allow the purification of the fusion protein. One of the most commonly used is the His-tag (HisX6) which corresponds to a sequence of six histidines. Proteins with this tag are purified by metal (cobalt or nickel) affinity chromatography. Using the His-tag in denaturing conditions such as 8 M urea or guanidine hydrochloride 6 M make them a good candidate for the purification of insoluble proteins.
However, these fusion partners usually need to be removed after purification to recover the peptide or the protein of interest. This is usually achieved by using cleavage sites between the fusion partner and the protein of interest in order to facilitate site-specific proteolysis (Sørensen and Mortensen, 2005a). Chemical or enzymatic cleavage can be achieved depending on the chosen site. Some commonly used cleavage sites are listed in Table 5.

2.2. Purification and characterization of the peptide

After obtaining the synthetic peptide or the peptide as a fusion protein, different sets of methods were used to purify and identify the products after purification. The general principle of these methods will be described in this section.

2.2.1. Chromatography

Chromatography is a technique that is widely used to separate and purify the different components in a sample mixture depending on their physico-chemical properties. It can be also used to quantify sample components. Although different forms of chromatography exist, they all work on the same principle, with a stationary phase which typically binds the components while the mobile phase flows through this stationary phase carrying the mixture. The components migrate through the stationary phase with a speed that depends on some properties for the stationary or mobile phase like affinity, molecular size etc... For example, components that do not have affinity for the stationary phase will not be retained on this stationary phase thus will migrate more rapidly, while components that have an affinity for the stationary phase will be retained and eluted later under specific conditions.
Liquid chromatography (LC) separates molecules in a liquid mobile phase using a solid stationary phase and is often carried out in a column either under gravity or high pressure. High performance liquid chromatography (HPLC) is a successful column LC used to purify and quantify biomolecules. In contrast to other types of column chromatography that are carried out under gravity, HPLC used a relatively high pressure of up to 400 bars that makes it much faster. Molecules are often adsorb on the stationary phase which is composed of very small (in the order of µm) particles packed in a column and the interactions of the molecules with these particles appear via various actions: adsorption, partitioning, ion exchange, molecular exclusion and affinity. In this work, reverse phase HPLC (RP-HPLC) and affinity chromatography (AFC) were used as preparative or analytic chromatography on synthetic peptides and biological sample. Both types of chromatography are briefly described below.

2.2.1.1. **Reverse-phase HPLC**

Depending on the relative polarity of the solvent and the stationary phase, there are at least two conceptually different variants in use of HPLC. The normal phase LC refers to a more polar stationary phase when compared to the mobile phase (e.g., toluene as the mobile phase, silica as the stationary phase) and the opposite for the reverse-phase LC. In both cases, the column is filled with tiny silica particles that are modified to be non-polar in the reverse HPLC as they bear hydrocarbon chains typically ranging from 4 to 18 carbons. Therefore, non-polar compounds in the mixture will tend to associate with the hydrocarbon groups because of van der Waals dispersion forces and will be less soluble in the polar mobile phase (for example a mixture of water and solvent such as acetonitrile). Consequently, they will spend more time on the column and will be eluted from the column later. The time it takes for each compound to travel through the column to the detector is known as its 'retention time'. Ideally it differs significantly for each compound and will vary depending on the pressure, the nature of the stationary phase, the exact composition of solvent and the temperature of the column. When exiting the column, molecules are detected by for example a UV detector. The output chart recorded display the time-dependent change in signal intensity as a result of the separation is called a "chromatogram" and the recording device a "chromatograph" (Figure 17).

2.2.1.2. **Affinity chromatography**

Affinity Chromatography (AFC) is based on reversible interactions between a target molecule and a specific ligand coupled to a chromatography matrix. These interactions can be the result of electrostatic or hydrophobic interactions, van der Waals forces and/or hydrogen bonding. The ligand is immobilized to the matrix via a spacer in order to overcome any steric effects and thus improve the binding with the target molecule. It is selected according to the compound to be isolated. The interaction from the affinity medium can be reversed to elute the target molecule, either specifically by using a competitive ligand, or non-specifically, by changing the pH, ionic strength or polarity.
This method is often used in biochemistry for the purification of fusion proteins which harbour target molecule called tag such as His-tags, biotin, Maltose binding protein (MBP) etc… and that can be usually removed after purification to obtain the protein of interest. It is suitable for specific separations, provides high purification yields and allows simple elution with a single-step gradient.
Briefly, in practice AFC media are made of a given volume of matrix in suspension that is prepared within a column according to the quantity of material to apply. When a biological sample is then applied on the column, target molecules bind specifically but reversibly to the ligand and unbound materials are washed through the column. The target molecules are then recovered by changing the conditions to favour their elution. Although AFC often used traditional column that allow the flow of the mobile phase by gravity, HPLC technique that utilises AFC properties also exist.

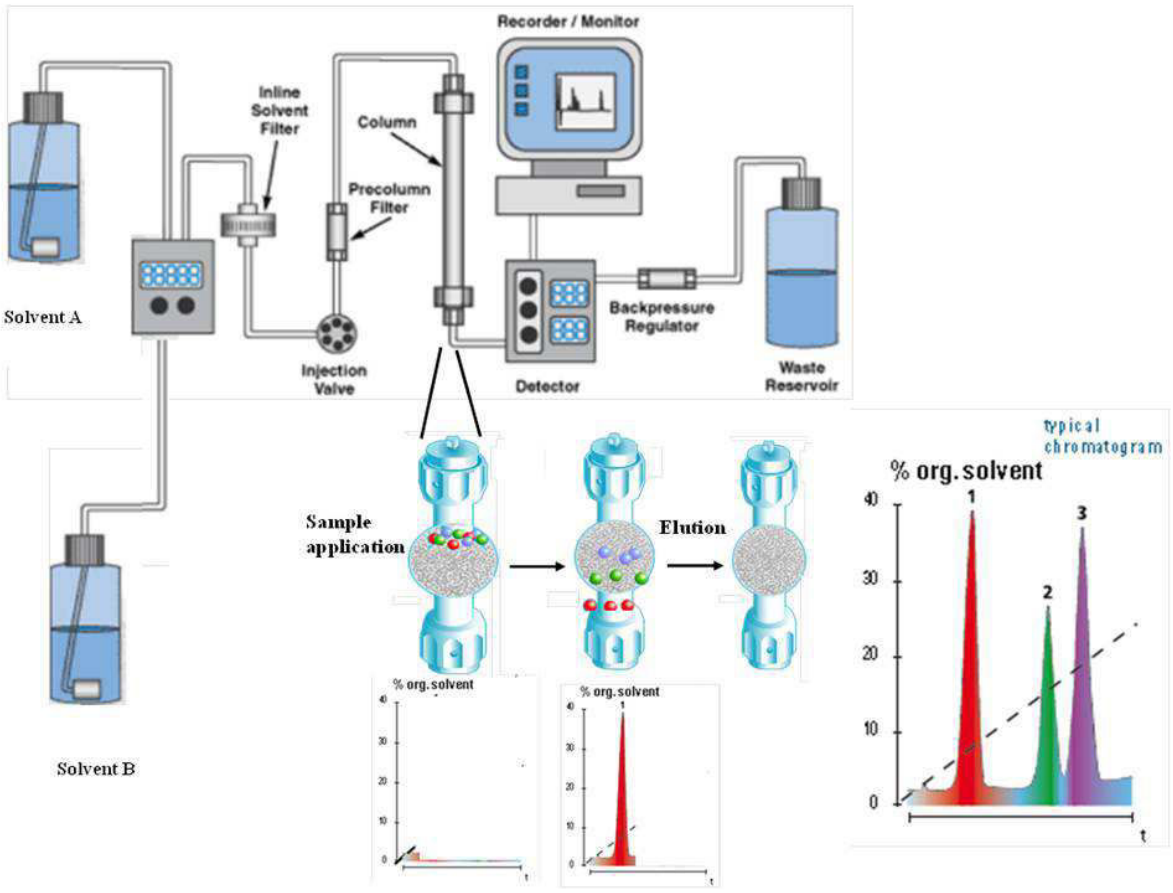

Figure 18: Schematic basic HPLC device with its components and typical RP-HPLC chromatograms. The different steps during the purification in the column are emphasized as well their corresponding chromatogram. Adapted from Tosoh Bioscience and Applied POROUS Technologies, Inc.

2.2.2. Electrophoresis

Electrophoresis is one of the most widely-used techniques in biochemistry and molecular biology to separate, characterize and sometimes purify macromolecules that differ in size, charge or conformation especially proteins and nucleic acids. Native electrophoresis relies on the separation of charged biomolecules within a matrix or gel, under an electric field. These molecules migrate toward either the positive (anode) or negative (cathode) electrode according to their charge. Proteins can have either a net positive or negative charge while nucleic acids have a consistent negative charge due to their phosphate backbone, and always migrate toward the anode. The gel in which these molecules migrate is composed of polymer either of agarose or polyacrylamide. It forms a network of meshes with sizes that are defined by the agarose or acrylamide concentration. The lower the concentration the more open will be the porous network, and adjusting the concentration helps in resolving biomolecules of different size, where a more open mesh is better for resolving high molecular weight molecules. Although both agarose and polyacrylamide can be used to separate proteins and nucleic acid, PolyAcrylamide Gel Electrophoresis (PAGE) is used extensively for separating and characterizing mixtures of proteins and agarose gels for

DNA. Polyacrylamide gels have a small range of separation, but very high resolving power compare to agarose gels.

SDS-PAGE is an analytical method that separate protein mixture based only on their size. As the mobility of molecules in the gel depends on their charge and size, this technique overcomes the charge dependence by using denaturing conditions in the presence of SDS (Sodium Dodecyl Sulphate) an anionic detergent. In the presence of SDS proteins lose their native structure, and their strong association with this anionic detergent makes the complexes negatively charged. Therefore, when loaded onto a gel and submitted to an electric field, they all migrate towards the anode and are separated based predominantly on their size. After the migration, proteins are visualized by staining usually Coomassie Blue or processed further for specific detection by Western blot. Proteins of known molecular weight (marker) are commonly run with the sample in a separate lane of the gel and used as a calibration to determine the apparent molecular mass of unknown biomolecules by comparing the distance travelled relative to the marker.
Agarose electrophoresis is often used to separate and purify DNA based only on their size. Agarose gel is typically prepared with buffer solution at concentrations ranging from 0.5 to 2% depending on the size of the DNA to separate. DNA markers are used to calibrate the gel and to determine the approximate size of unknown DNA. To visualize the separated DNA, gels are prepared with an intercalating agent, for example the ethidium bromide (EtBr) which fluoresces under UV light when bound to DNA. The part of the gel that contains the DNA fragments of interest can be cut and the DNA extracted from the gel using commercial kits for DNA gel extraction.

2.2.3. Western blot

Western blotting is an analytical technique in cell and molecular biology to identify specific proteins in a cell protein extract. It uses antibodies for the specific detection of a particular protein. Using SDS-PAGE, proteins are first separated by size and transferred to a nitrocellulose membrane under electric current in order to make the proteins accessible to antibody detection. To prevent non-specific interactions with others proteins, the membrane is saturated in non-fat dry milk solution (usually made up in Tris buffer) prior to incubation with the ‘primary antibodies’ that specifically recognized the protein of interest. After washing to eliminate the non specific binding, the membrane is "probed" with a ‘secondary antibody’ that recognized the primary antibody, and that is often conjugated with a reporter enzyme such as Horse Radish Peroxidase (HRP) or alkaline phosphatase (AP). The activities of these enzymes when exposed to suitable substrates allow colorimetric, chemiluminescent or fluorogenic detection. Western blot sensitivity depends on the enzyme substrate system used for detection.
In this work, we used the chemiluminescence detection (Figure 19). It used the HRP conjugated secondary antibodies to cleave a chemiluminescent agent leading to the production of luminescence (light) proportionally to the amount of protein. The light is then detected and a digital image of the Western blot is captured. Further analysis of the

image can allow the quantification of the detected proteins and the analysis of their molecular weight when appropriate standard are used.

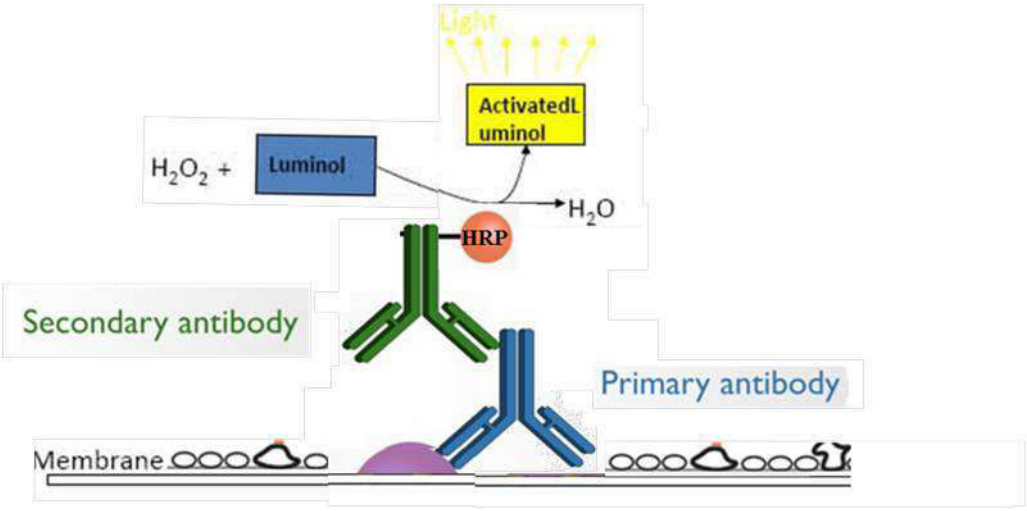

Figure 19 : Schematic representation of the principle of detection by chemiluminescence. The primary antibody specifically recognizes the protein of interest (in purple) which is then detected by a modified secondary antibody covalently link to the peroxidase. This enzyme produces an oxygen radical which activates luminol and allows the detection of the protein of interest.

2.2.4. Mass spectrometry

Mass spectrometry is a powerful analytical technique that is often used to identify unknown compounds within a sample, and to elucidate the structure and chemical properties of different molecules. It becomes a crucial in proteomics experiments as it allows protein identification, de novo sequencing, and identification of post-translational modifications. It is used for precise determination of the molecular mass of peptides and proteins as well as their sequences.

The complete process is schematically shown in Figure 20. It involves the conversion of the sample into gas phase ions, with or without fragmentation, which are separated in the mass spectrometer according to their mass-to-charge ratios (m/z) and are detected in proportion to their abundance. The resulting mass spectrum represents a plot of ion abundance versus the mass-to-charge ratio. Ions can be produced by different ionization techniques and provide information concerning the nature and the structure of their precursor molecule.

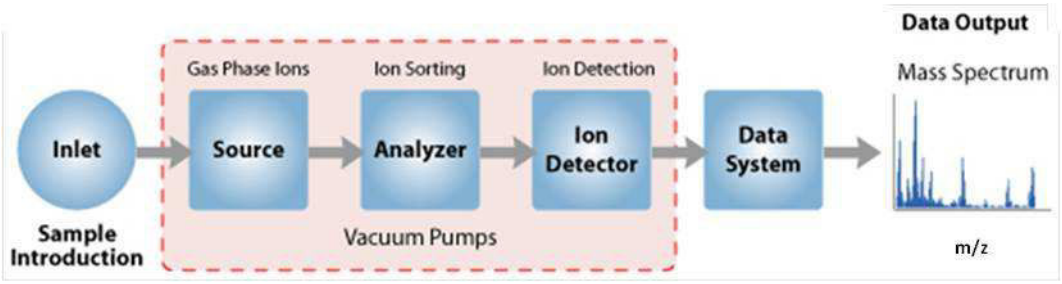

Figure 20: The different components of a Mass Spectrometer and the process to obtain a mass spectrum. Source: PREMIER Biosoft website.

Table 6: Common matrices that are often used in Matrix-assisted laser desorption/ionization (MALDI) mass spectrometry.

Matrix	Other names	Stuctures	Molecules
α-Cyano-4-hydroxycinnamic acid.	CHCA	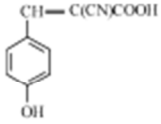	peptides
3,5-dimethoxy-4-hydroxycinnamic acetic acid.	Sinapinic acid, SA	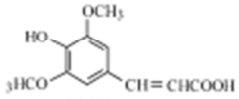	Proteins, polymers
2,5-dihydroxybenzoic acid.	Gentisic acid, DHB	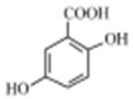	Peptides, proteins, lipids, nucleic acids saccharides
3-hydroxypicolinic acid.	HPA	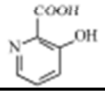	Nucleic acids

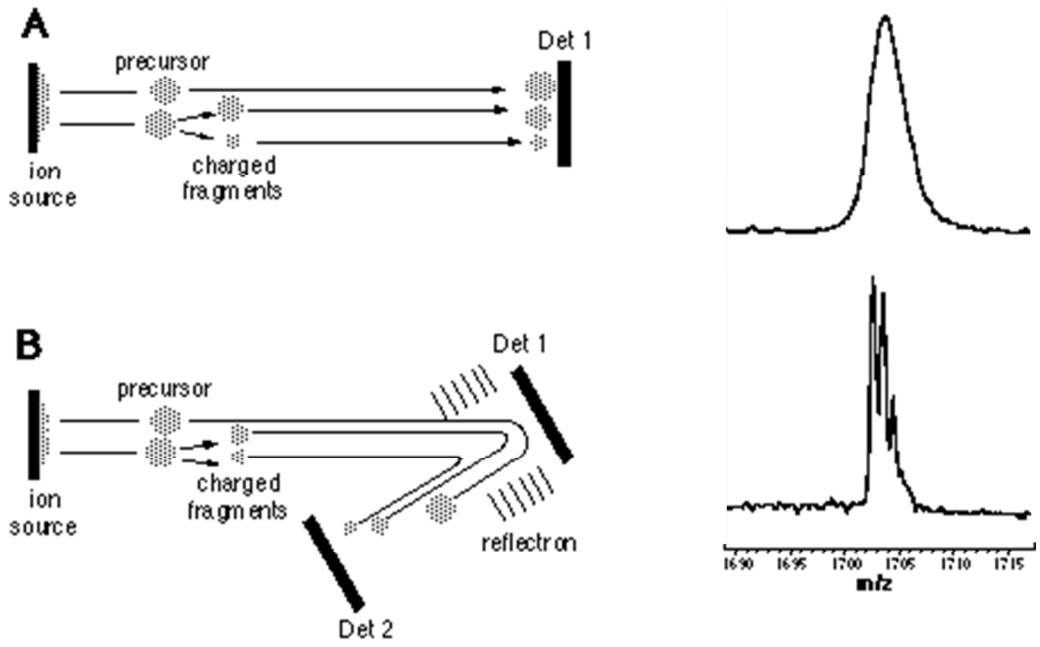

Figure 21: The different modes and the resulting spectrum. A) The basic path of ions in a linear mode (left) and the resulting broad spectrum (right). B) Components in a reflecting mode (left) and the more resolved spectrum that results (right). Det: abbreviation for detector. Source: R. S. Annan, SmithKline Beecham Pharmaceuticals.

Matrix-assisted laser desorption/ionization (MALDI) is the most popular analytic technique for peptide mass fingerprinting. It uses soft ionization technique which prevent sample damage after ionization. The analyte is dissolved in solution with an excess of matrix such as sinapinic acid that has a choromophore which absorbs at the laser wavelength. A drop of this solution is deposit on the laser target and irradiated. The matrix absorbs the energy from the laser pulse generating matrix ions. These primary ions react with the analyte via electron, proton or cation transfer resulting in sample ionization. This type of ionization presents the advantage to produce ions with little excess energy and thus yields spectra with less fragmentation in which the molecular species is easily recognized. Different matrices exist and have to be chosen according to the type of molecule to be studied in order to obtain mass spectra of good quality. The list of commonly used matrices is summarized in Table 6. The kind of ions that are generated (single or multiple charged ions) depends on the nature of the matrix, the laser intensity, and/or the voltage that are used. The desorbed ions are mainly analysed using a time-of-flight analyser (TOF-MS) working in a linear (LM) or reflection mode (RM) (represented in Figure 21). The TOF analyser uses an electric field to accelerate ions through the same potential and measures the time they take to reach the detector. For ions with the same charge, this time depends on their velocity that is related to their mass. Ions with smaller m/z value (lighter ions) and more highly charged ions move faster to the detector. The TOF mass spectrometry presents the advantage to analyse a wide mass range. Moreover, in the reflection mode the resolution is better than in the linear mode as the flight path of the ions is doubled.

2.3. Membrane model and peptide reconstitution

This section briefly presents lipid model membranes and the protocol to prepare them in presence (peptide reconstitution) or absence of peptide.

2.3.1. Lipid model membranes

The complex composition of biological membranes and their huge diversity make them complicated systems to work with. Model membranes have been developed with the aim to simplify this complexity and to allow their study, in order to understand the key parameters in the protein lipid interactions, and other processes that take place in natural membranes. These membranes are prepared with synthetic lipids such as POPC, DOPC, etc… that can be purchased from different companies (e.g. Avanti). The simplest model systems contain only a single pure synthetic lipid (e.g. POPC) while more physiologically relevant models can be made with mixtures of several lipids at different ratio comparable to those in natural membranes. Depending on the lipid shape, their concentration and the type of lipids in the mixture, they will organize into model membranes with different shape and physical properties. Some of these model membranes systems are micelles, vesicles with different size and number of layers, and flat bilayers. Two parameters drive the auto assembly of these lipids into supramolecular systems: their amphipathic property and the geometric approximation of the lipid shape. The amphipathic property allows lipids to be organized in aqueous environments in a way that hydrophobic surfaces come together in order to minimize their interaction with water, while the hydrophilic parts are exposed to water. This organization occurs above a critical concentration of amphiphile (CMC). In addition, the geometrical shape of lipid also influences their organization. This geometry is defined by the relative size of the lipid head group compared to the fatty acid moiety. According to the molecular shape concept, lipids with roughly equal diameters of head group and fatty acid moiety, such as PC, will be considered cylindrical, whereas lipids with small head groups, such as PE, PA are conical and lipids with large head groups, such as PIs, are inverse-conical. These different lipid shapes lead respectively to the formation of lamellar, hexagonal and spherical or cylindrical phases (Figure 22). In a planar membrane mostly built from cylindrical lipids, the introduction of lipids with conical or inverse-conical geometries might induce curvature strain. In addition, membrane lipids with a high degree of unsaturation in their fatty acid moieties will accumulate in areas of high curvature.
The following lipids were used in this thesis to model lipid membranes in presence or absence of peptides. There structures are represented in Figure 23.

1) 1-palmitoyl-2-oleoyl-*sn*-glycero-3-phosphocholine (POPC) (16:0-18:1) is typically considered one of the model lipids for biophysical experiments as it mimics mammalian phospholipid structure and properties. It consists of a phosphocholine headgroup and two acyl chains-one consisting of 16 carbons and another of 18 carbons with one double bond at position 9. Its polar head group presents a strong zwitterionic character over the entire pH range.

2) L-α-phosphatidylethanolamine (PE) is the major lipid constituent of bacterial membranes and only occurs in small amounts in mammalian and plant cells. The smaller size of the ethanolamine head group gives it a conical shape that imposes curvature stress which is utilized by cells for budding. PEs are zwitterionic at physiological pH.

3) L-α-phosphatidylserine (PS) is the only lipid in animal cells that contains an amino acid. It possesses three ionizable groups: a diester phosphoric acid, an amino group and a carboxyl moiety. At physiological pH, it is a negatively charged. It is typically located in the inner leaflet of cells membranes. The head group shape of PS is similar to that of PC and will also spontaneously form vesicles in an aqueous solution.

4) N-octadecanoyl-D-erythro-sphingosylphosphorylcholine (Sphingomyelin, SM) (18:0) is the major sphingolipid constituent of cell membranes. It is found at particularly high concentrations in the membranes of nerve cells. It was previously thought to have a purely structural role, similar to the function of phosphatidylcholine. However, it is now appreciated that sphingomyelin has a high affinity for cholesterol and that these two lipids pack tightly into liquid-ordered domains among a liquid-disordered phase to form lipid rafts (Milhas et al., 2010). These membrane micro domains are thought to function as signalling platforms that regulate the localization and interactions of proteins.

5) Cholesterol is an important component of lipid membranes as its presence changes the membrane characteristics. At high concentration it increases for example the rigidity of the membrane fluid phase or the fluidity of the gel phase. It plays a relevant role in membrane rafts domain. However, cholesterol cannot form a lipid bilayer by itself and hence its solubility in the bilayer is limited. It acts as a spacer between the phospholipid molecules that have a larger head group. The smaller head group of cholesterol (a hydroxyl group) favours the ordering of the phospholipid fatty acyl chains which are otherwise loosely packed below the level of the phospholipid head groups. The larger phospholipid head groups in turn cover the smaller cholesterol head group to protect the hydrophobic portion from getting exposed to water. Consequently, at higher concentrations of cholesterol, when there are not enough phospholipids to cover the cholesterol head groups, cholesterol solubility in the membrane decreases and it deposits as crystals. Therefore, the amount of cholesterol is critical during samples preparation and needs to be considered carefully.

The pure POPC is used as an emulator of the zwitterionic mammalian membranes while the PS is included to reproduce the negative charge. However, these lipids were mixed at different ratios to achieve the physiological composition of a given membrane compartment.
All these lipids were purchased from Avanti Polar Lipids (Alabama).

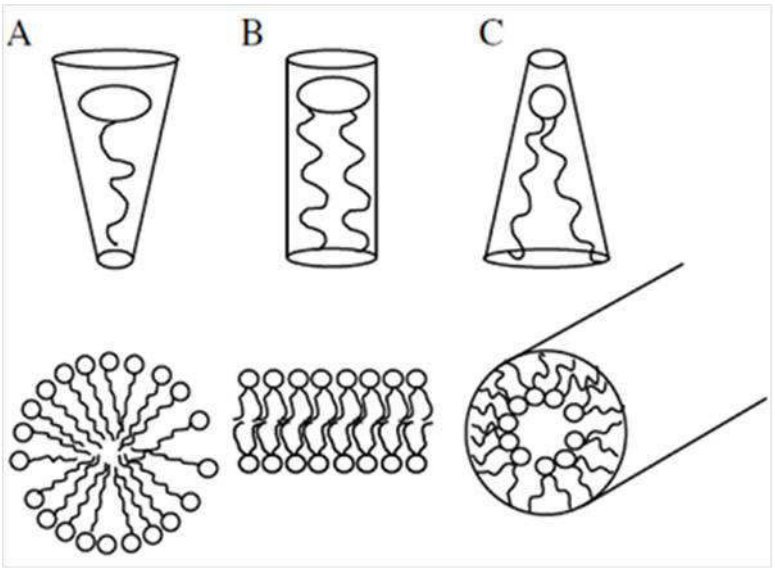

Figure 22: Geometrical models of lipid shapes. A) Inverse conical lipid, B) cylindrical lipid, and C) conical lipid. Bottom panels, simplified view of membrane curvature facilitated by lipids with different geometric shapes.

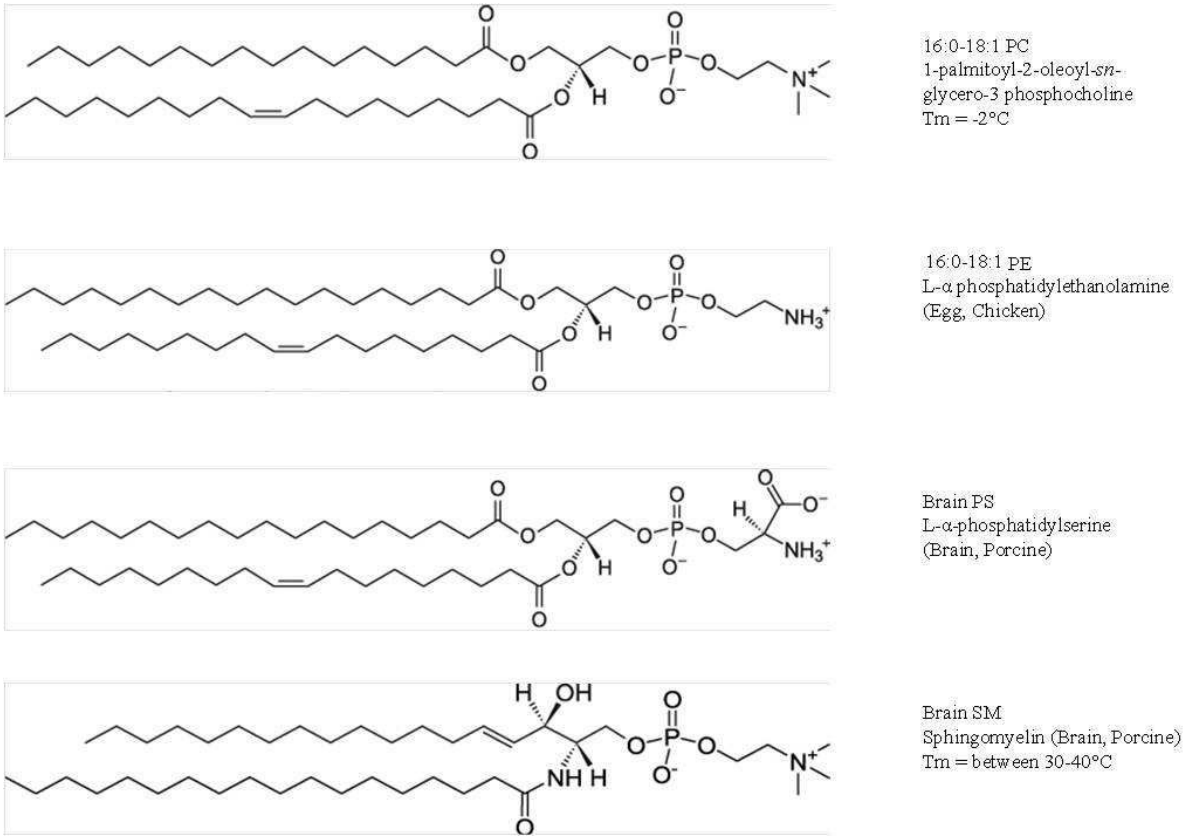

Figure 23: Structural representation of common lipids that were used in this work for preparation of model membranes: POPC, phosphatidylethanolamine (PE), phosphatidylserine (PS), and Sphingomyelin (SM).

2.3.2. Sample preparation with membrane model

Depending of the purpose of the experiment, different model lipid membranes can be prepared. Experiments in solution will be conducted with vesicles in suspension except for surface plasmon resonance which uses vesicles to form supported lipid bilayers. Different type of vesicles can be prepared but in this section we will only focus on the preparation of small unilamellar vesicles (SUV). Planar bilayers can be also prepared on supports (in this work we used glass plates). They are interesting as they are cell membrane mimetic and have been used for a wide variety of techniques.

2.3.2.1. Preparation of small unilamellar vesicles

Prior to preparation of membranes the lipids are dissolved in an organic solvent. This is because most lipids are soluble in organic solvent and will not mix homogeneously when dissolved in an aqueous phase. Usually chloroform is used because of their low vapour pressure and contrary to for example methanol they do not form hydrogen bonds with the polar head groups making it easier to evaporate. However, other solvents can be used and even mix at different volume ratio depending on the sample. Thereafter, solvent is evaporated and upon drying a thin film of the lipids forms on the glass surface of the container. The film is then hydrated under agitation, and the lipid films shear off into large disk. The exposed hydrophobic edges reseal leading to the formation of vesicles and by shaking or vortexing will result in a heterogeneous solution of multi lamellar vesicles (MLVs) that make the suspension appear milky white. These types of vesicles are the starting material for some of the other vesicle types, in particular when their extended size and their multi-layered nature interfere with spectroscopic experiments.
From the MLVs suspension, a homogeneous group of unilamellar vesicles with a diameter below 40 nm are prepared by sonication. The use of sonication for lipid sample preparation was reported early and is hence one of the first mechanical methods used during the formation of vesicles. Usually, sonication by insertion of a tip sonicator is preferred when compared to bath sonication, is the latter being less efficient. It results into a clear suspension essentially made of homogeneous small unilamellar vesicles (SUVs). These SUV´s are usually meta stable, the high energy curvature will by relaxed by fusing of vesicles into 60 to 80 nm vesicles over a period of days. Their size makes of them good candidates for spectroscopy experiments when compare to other vesicles as they are the smallest vesicles than can be produced.

2.3.2.2. Preparation of proteo-liposomes

When studying membrane peptides, proteo-liposomes are prepared in order to investigate them under conditions that mimic their natural environment. These vesicles are often prepared at a given protein/ lipid ratio (P/L). The steps of their preparation are the same than the one described above except than lipids are mixed from the beginning with the peptide or the protein of interest.

2.3.2.3. **Preparation of lipid bilayers for ssNMR of uniaxially oriented sample**

The general protocol to prepare uniaxially oriented when at the same time reconstituting peptides are documented in detail and illustrated in references (Aisenbrey et al., 2010a; Bechinger et al., 2011). Briefly, peptide and lipid are first dissolved in solvents and the solutions mixed together. Then the organic solvent is removed under a gentle stream of nitrogen until the solution turns viscous (to about 1 mL), which allows to deposit the sample onto the glass plates. Equal quantities of the sample are applied as small elongated droplets on the surface of individual ultra-thin cover glass plates (Figure 24A). The sample is first dried in air until the bulk solvent has evaporated and thereafter the sample is exposed to high vacuum overnight. In our laboratory, we have connected a dessicator to the lyophilizer to allow the drying of many samples simultaneously in their horizontal position. Thereafter the samples are hydrated in a closed chamber at 93% relative humidity (rh) and left to equilibrate for typically about 2 to 3 days. This can be achieved by establishing a closed atmosphere in contact with a saturated solution of KNO_3. Once the lipid films become translucent and soft, the glass plates are stacked on top of each other (Figure 24B). The stack is stabilized and protected from dehydration by wrapping with Teflon tape and the whole sample is sealed in a plastic wrapping using an impulse sealer (Figure 24C). Several membrane bilayers (about 10^4-10^6) are stacked on top of each other between two glass plates 00 (8x22mm) (Marienfeld, Germany).

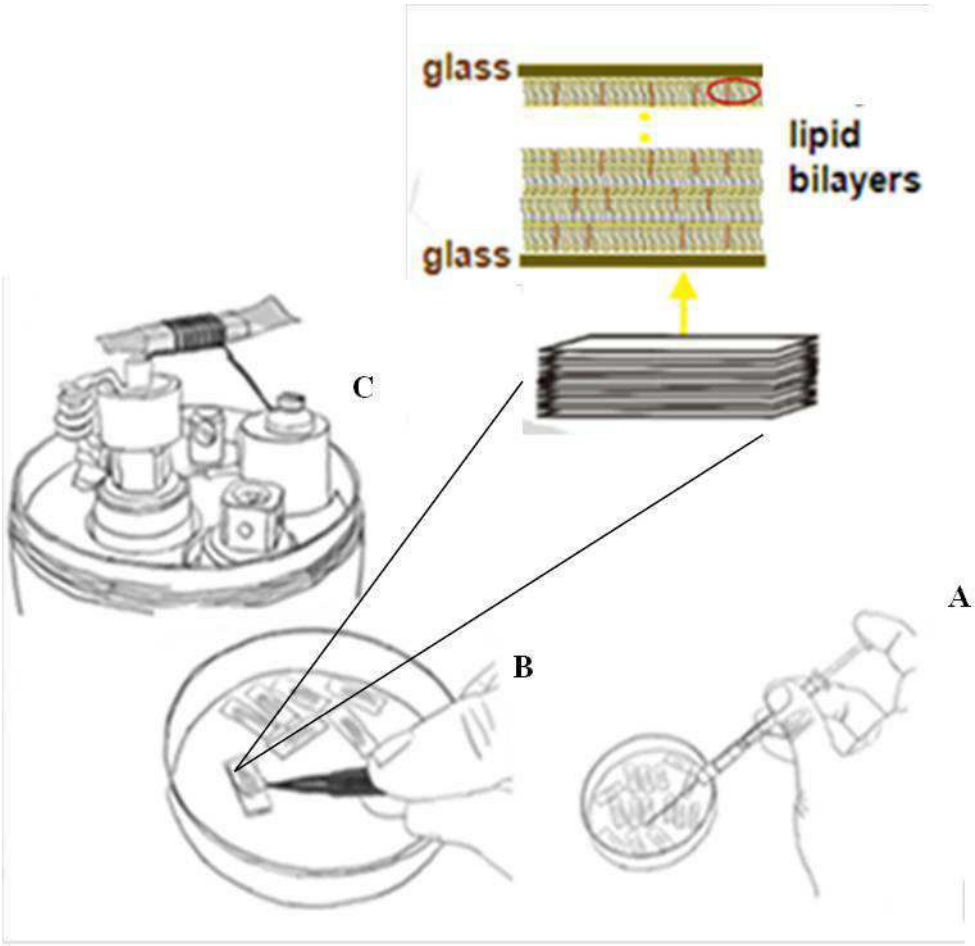

Figure 24: The different preparation steps of an oriented sample. (A) Application of viscous lipid/peptide solutions on glass plates. (B) Stacking of the glass plates on top of each other after elimination of the organic solvent and hydration of the membranes. Zoom on the stacked glass plates with several membranes bilayer stacking between two glass plates. (C) The sample is sealed into plastic foil for NMR measurement. (Aisenbrey et al., 2010b).

2.4. Structural characterization

The set of optical spectroscopy methods that will be described in the following paragraph were used for the characterization of the secondary structure of our peptide. These techniques also allowed us to investigate the interaction of this peptide with membranes. Furthermore, NMR spectroscopy was useful for the investigation of their topology and dynamics within the membrane. Here we briefly present these techniques.

2.4.1. Circular dichroism (CD)

CD is a light absorption spectroscopy extensively used in analyzing the secondary structures of proteins. It is particularly used to monitor the changes of structure elements under a given experimental conditions for example temperature, pH… as these molecules are sensitive to environment changes.

CD relies on the property of chiral molecules to differently absorb circularly polarized light turning in the right (RCP) and left direction (LCP). It measures the difference of absorption between LCP and RCP:

$$Circular\ dichroism = \Delta A(\lambda) = A(\lambda)LCP - A(\lambda)RCP \qquad (1)$$

λ corresponds to the wavelength.

The measurements on polypeptides are usually done in the far UV between 260 and 190 nm. In this range, absorption is dominated by the peptide bond and the resulting spectrum therefore reflects the secondary structure of proteins. Under 190 nm, data are not accessible by commercial CD apparatus but only by Synchrotron radiation due to light scattering and limitations in the light intensity. At 190 < λ < 260 nm characteristic spectra for each protein secondary structure are obtained (Figure 25). The contribution of each type of secondary structure (α helix, β turn, random coil) is estimate by deconvolution of CD spectra using different algorithms (CONTIN SELCON…) and data bases. Although CD spectra can be used to estimate the fraction of the different secondary structures, this estimation is not as accurate as the one obtain with Synchrotron radiation measurements. In addition, CD cannot give details on which part of the protein contains which structure. Despite this, CD is a valuable tool to investigate protein folding and conformational changes.

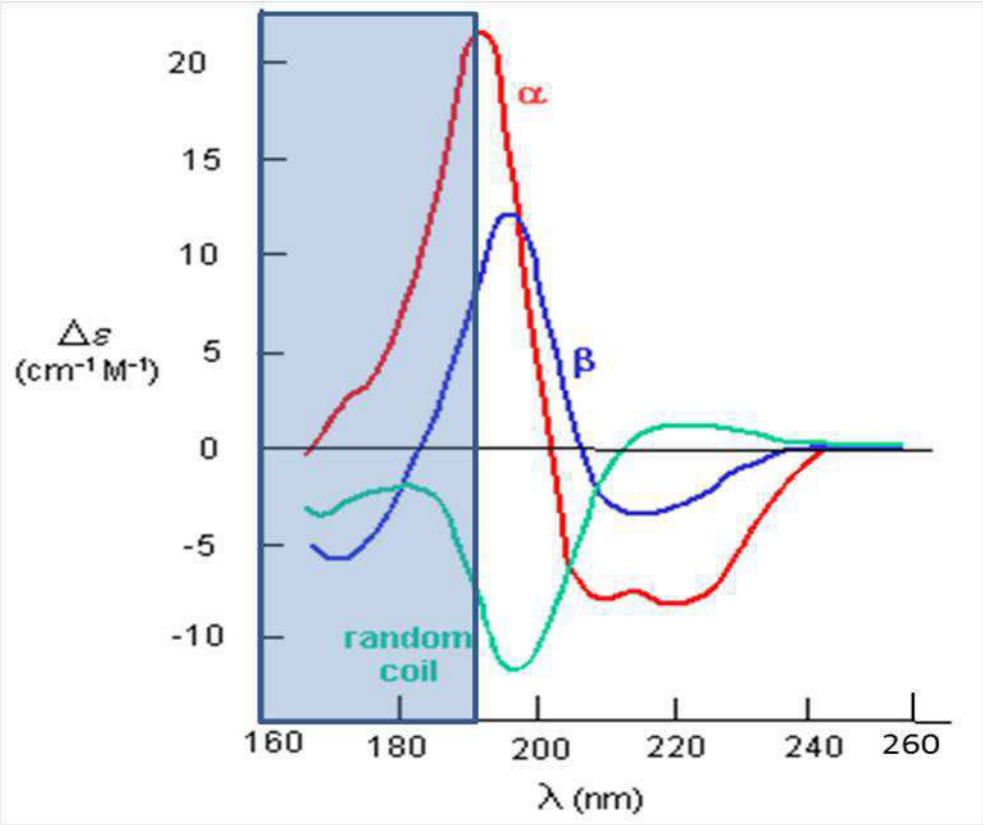

Figure 25: Representation of the characteristic CD spectra for the three common proteins secondary structures. α-helical (red), β-sheet (blue) and random coil (green). The area shaded in blue is not accessible by commercial CD apparatus but only by Synchrotron radiation CD´s.

2.4.2. Fluorescence spectroscopy

Fluorescence is a spectroscopic phenomenon in which a fluorophor molecule is excited by absorption of a photon and triggers the emission of a photon with a longer wavelength during the return to its normal state. Although specific fluorophore molecules can be added to the sample, natural fluorophores already exist in proteins. These are the aromatic residues tryptophan, tyrosin and phenylalanine (Figure 26). The fluorescence signal is usually a mixture of the fluorescence coming from these residues. However, most of the intrinsic fluorescence emissions are due to the excitation of tryptophan residues. The typical maximum absorbance of tryptophan (Trp) is at 280 nm and the maximum emission from 300 to 350 nm. Its maximum emission is sensitive to the solvent polarity of the local environment. Thus Trp fluorescence is used to monitor the conformational state of a protein. For example, Trp fluorescence was used in this work for the study of peptide and lipid membrane interactions for as the peptide inserts into the membrane, the polarity of the environment surrounding the tryptophan in the peptide change. Therefore, the shift in fluorescence can then be measured as a function of increasing lipid or peptide concentrations in order to describe the peptide binding to the membrane.

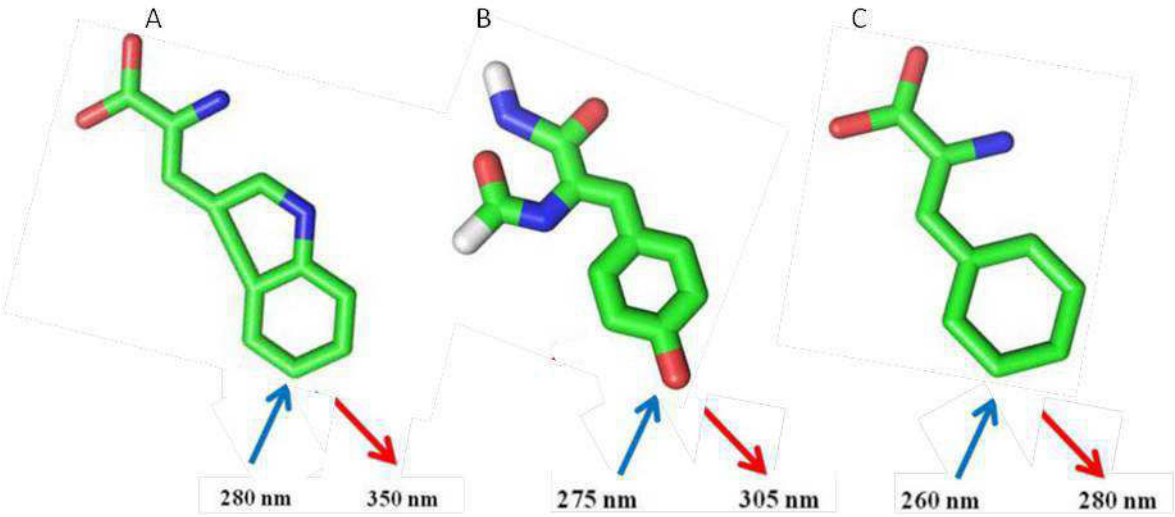

Figure 26: Stick representation of aromatic residues: tryptophan (A), tyrosine (B) and phenylalanine (C) with the maximum absorption (blue arrow) and fluorescence emission (red arrow) at pH 7.

2.4.3. NMR spectroscopy

Nuclear magnetic resonance (NMR) is a spectroscopic method which was detected in the late 1940s and early 1950s by *E.M Purcell and F. Bloch.* Over the decades it was

developed further to uses the magnetic properties of certain nuclei for the investigation of molecular structure and dynamics. It relies on physical phenomenon in which certain nuclei in a magnetic field, absorb and re-emit electromagnetic radiation which is recorded and analyzed to extract information on molecules in their environment. The nucleus is thus the key elementary particle.
This paragraph will introduce some NMR concepts and principles and the approaches used in solid state NMR.

2.4.3.1. Theory of the NMR phenomenon

Nuclear spin and magnetic properties associated

Nuclei contain an intrinsic property called spin generally associated with the angular momentum. Like electrons, the spin of a nucleus can be described using quantum numbers of I for the spin and m for the spin in a magnetic field. Nuclei which contain an odd number of protons and neutrons have a non-zero spin. Furthermore, all molecules with a non-zero spin have a magnetic moment, μ, and can be study by NMR. This magnetic moment, μ is correlated to the angular momentum by:

$$\mu = \gamma I \qquad (2)$$

With γ is the gyromagnetic ratio, a proportionality constant between the magnetic dipole moment and the angular momentum, specific to each nucleus. The gyromagnetic ratios of some commonly studied nuclei are listed below.

Table 7: Summary of gyromagnetic ratios, the nuclear spin I, the frequency at 9.4 Tesla and the natural abundance of some commonly studies nuclei.

Nuclei	Spin	γ10^8 rad.s-1T-1	ν/MHZ	Natural Abundance
^{1}H	1 / 2	26.75	400	99.985
^{13}C	1 / 2	6.73	100.6	1.108
^{15}N	1 / 2	-2.71	40.5	0.37
^{31}P	1 / 2	25.18	162.1	100.0
^{19}F	1 / 2	10.84	376.5	100.0

The magnetic moments are vectors and the net or bulk magnetization of a sample, called M is given by the sum of individual magnetic vectors:

$$M=\sum\mu \qquad (3)$$

Energy levels of spin ½ nuclei in a magnetic field

The most studied nuclei in biology are listed in Table 7 above, and they all possess spin I=1/2.

In the absence of an external magnetic field, the states of the spins are degenerate with random alignment and the bulk magnetization arising from the nucleus is zero.

During the NMR experiment, spins are placed in the presence of an external static magnetic field B_0. The interaction between the nuclear spins and the magnetic field B_0 breaks the degeneracy and leads to the splitting of spins into different populations either aligned with (low energy) or against (high energy) B_0. This effect is known as the Zeeman splitting (Figure 27) and results in a non-zero bulk magnetization.

For spin I= ½ nuclei, there are only two energy levels, the low energy level occupied by the spins which aligned with B_0 and the high energy level occupied by spins aligned against B_0. The difference between the two energy levels is:

$$\Delta E = \gamma h B_0 = h\upsilon_0, \qquad (4)$$

where E is the energy (in Joule), $\hbar$ Planks constant (1.054 10^{-34} JS), γ the gyromagnetic ratio (rad. s-1. T-1), B_0 the magnetic field (T) and $\boldsymbol{\upsilon_0}$ the resonance frequency or Larmor frequency which corresponds to the precession frequency of each nucleus around B_0 (Hertz, Hz)

At thermal equilibrium, the repartition of the different populations at each energy level is not equivalent and is given by the Boltzmann equation:

$$\mathbf{N^-/N^+ = e^{-E/kT}} \qquad (5)$$

With k corresponding to the Boltzmann constant (1.3805 10^{-23} J/Kelvin) and T to the temperature in Kelvin (K).

This repartition results in a slight excess of spin (N^+) at the high energy level (α) when compared to spins (N^-) at the low energy level (β) ; thus giving rise to a macroscopic net magnetization $\vec{\boldsymbol{M}}$ with the same orientation than B_0 (Figure 28). This net magnetization corresponds to the sum of all the elementary spin-moments.

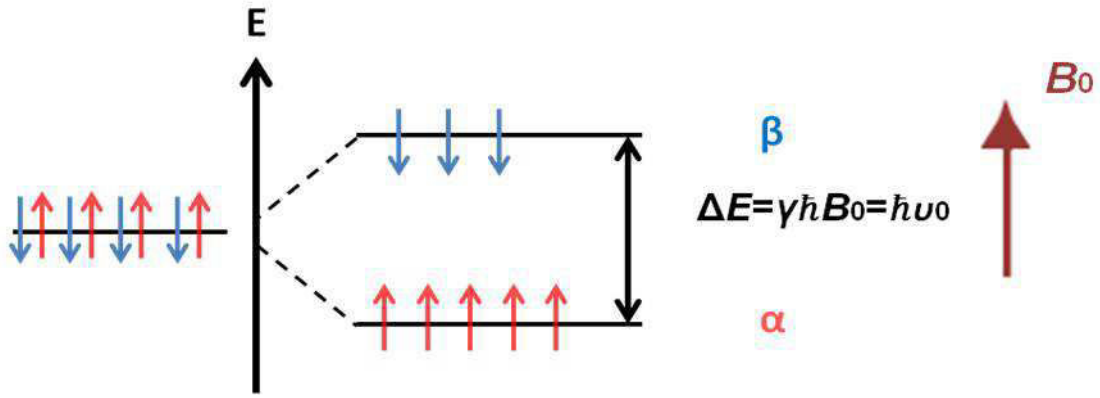

Figure 27: Splitting of spin population in presence of a magnetic field B_0 for spin ½: Zeeman Effect.

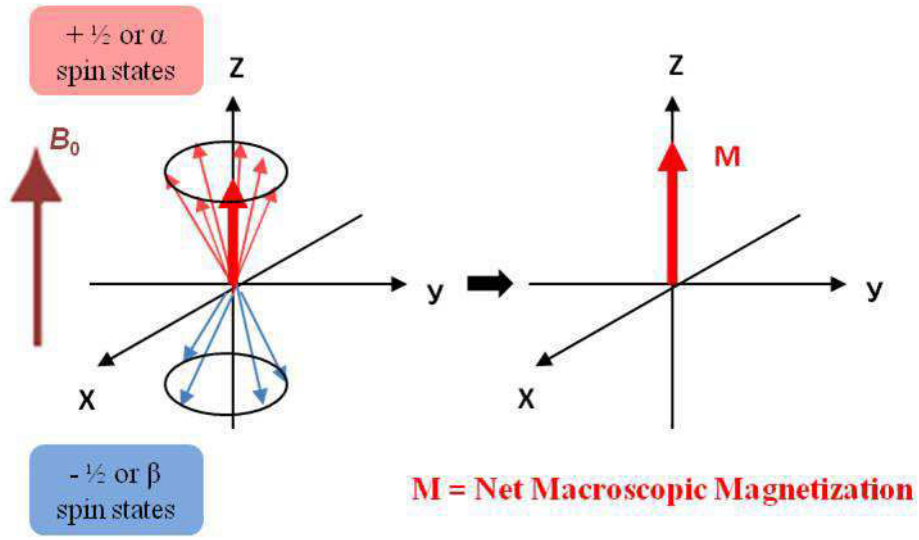

Figure 28: Representation of the creation of the net magnetization M at the equilibrium after B_0 is applied

How NMR signal is generated

The NMR signal is obtained in two main steps: the first step is the perturbation of the equilibrium of the magnetization and a second step in which the signal is recorded during the return of the magnetization to equilibrium.

a) Perturbation of the equilibrium:

At the equilibrium, the net magnetization is aligned along the z axis and is parallel to B_0; no signal is detected. Applying a radiofrequency (RF) B_1 pulse tilts the magnetization away from its equilibrium position in the transversal plane (x, y) by a specific angle θ depending on the applied magnetic field and the length of the pulse. The out-of-equilibrium position

of the net magnetization occurrs when the B_1 frequency is equal to the Larmor frequency υ_0 of the spins. When this condition is fulfilled, the interaction between the electromagnetic field B_1 and nuclei result in the switch of spins from low energy to high energy level as a consequence of energy absorption. After the pulse the magnetization vector precesses around the external magnetic field B_0 at the Larmor frequency and returns to the equilibrium.

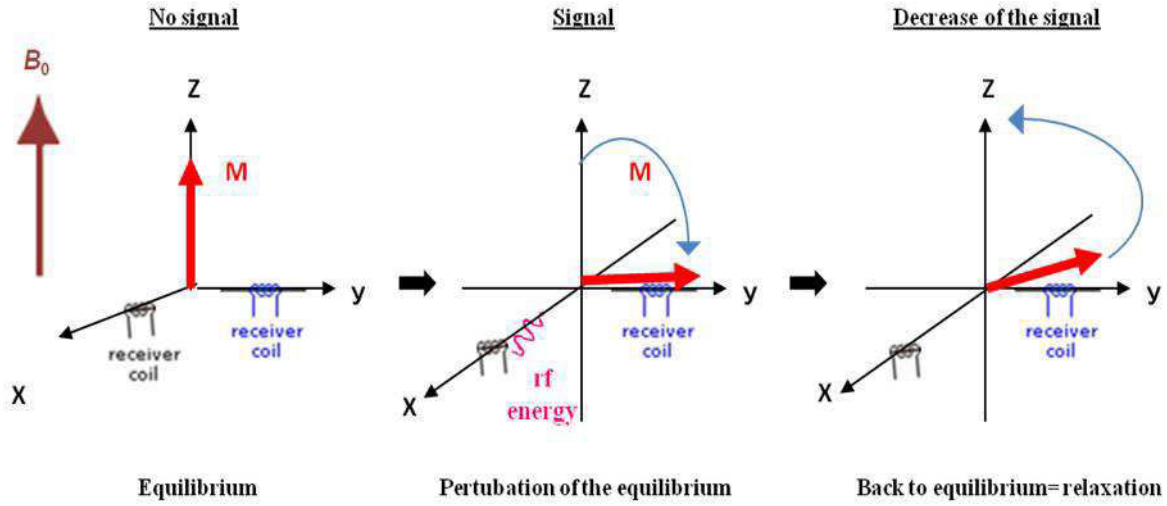

Figure 29: The different steps to obtain the NMR signal.

b) Relaxation:

The return of the magnetization to equilibrium is called relaxation. During this step, the absorbed energy is returned to the system. Two types of relaxation can be described:

- The spin-lattice relaxation (T_1) refers to the time needed for the magnetization to return at equilibrium along the Z axis. It depends on the size and the tumbling motions of the molecule.
- The spin-spin relaxation (T_2) describes the evolution of the precession in the (x, y) plane. It depends on interactions between nuclei. The additional effect of B_0 inhomogeneity is described by the parameter T2*.

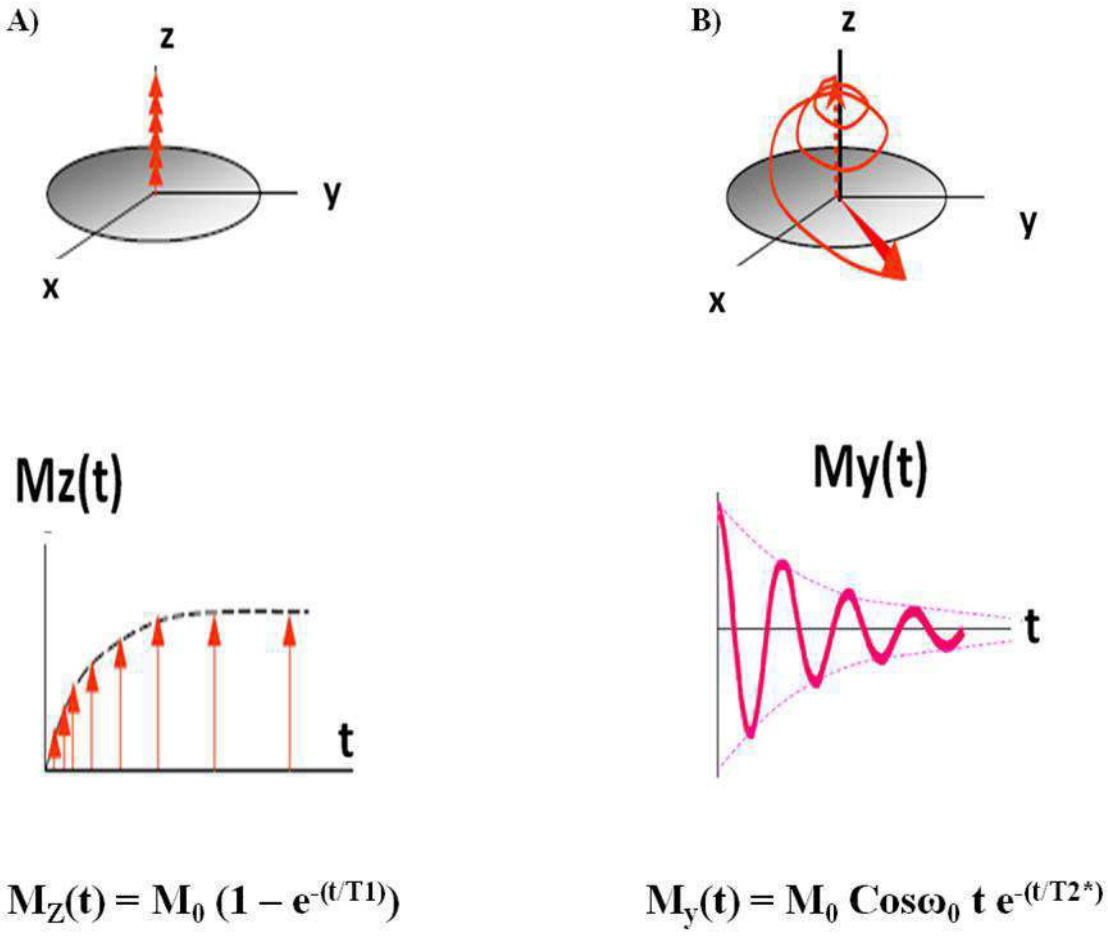

Figure 30: Representation of the different relaxation time with their respective equations. A) Representation of the spin-lattice relaxation. B) The spin-spin relaxation time T_2.*

c) The NMR signal:

The entire NMR signal is recorded during the spin-spin relaxation as the signal is detected in the (x, y) plane. The restitution of the absorbed energy leads to an oscillating magnetization vector which generates a current picked-up by the nearby coil. This current creates an electrical signal oscillating at the Larmor frequency known as the free decay induction (FID) which contains the vector sum of NMR responses from all the excited spins. To obtain the frequency-domain NMR spectrum, the raw signal recorded in a time-domain is Fourier transformed.

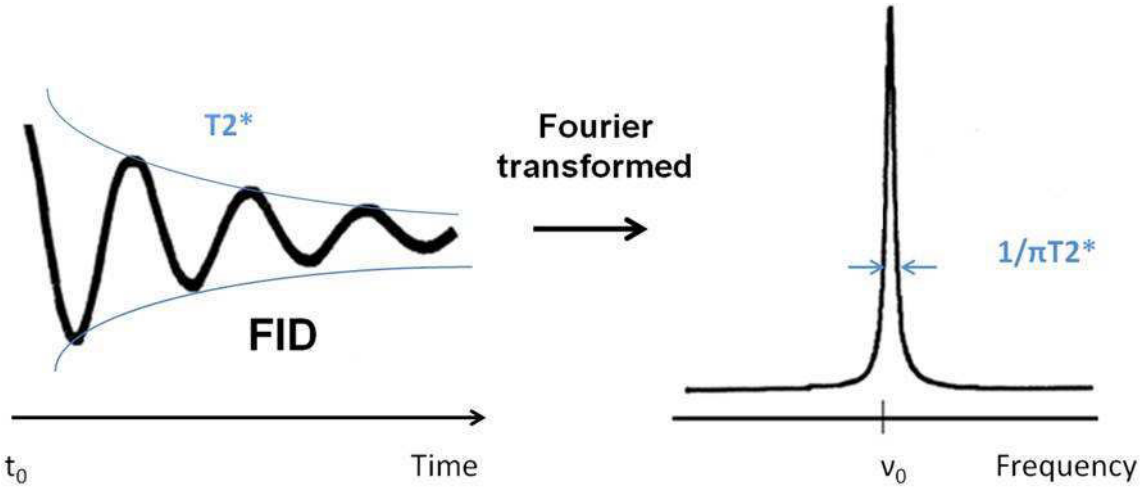

Figure 31: Transformation of the raw NMR signal to the observed final signal.

2.4.3.2. **The NMR interactions**

The NMR signal results from both interactions between nuclear spins and the magnetic field (external interaction) and between spins (internal interaction). The latter are responsible for magnetic field fluctuations that are felt by the nucleus and consequently perturb the Zeeman interaction, which is the most common interaction. These interactions are all expressed in the Hamiltonian $\hat{H}$ equation:

$$\hat{H} = \hat{H}_{zeeman} + \hat{H}_J + \hat{H}_{CS} + \hat{H}_{DD} + \hat{H}_Q \qquad (6)$$

where H_{Zeeman} is the Zeeman interaction, H_J is the J coupling, H_{CS} is the chemical shift coupling, H_{DD} is the dipolar coupling, and H_Q is the quadrupolar coupling.

The other interactions are weaker than the Zeeman interactions. In liquid state, the molecular reorientation occurring in solution average the dipolar interactions and the anisotropic contributions to the chemical shift, resulting in a characteristic narrow isotropic peak. In addition, quadrupole interactions are eliminated by such motions. Therefore, only the J coupling and isotropic part of the chemical shift remains. In the solid state, as molecular reorientation does not occur, solids may have a variety of bond lengths and angles of a given chemical site that result in NMR spectrum with broad peaks.

Chemical shift:

Nuclei in a molecule do not experience the same magnetic field. Indeed, electrons in the molecular orbital rotate around the nucleus; thereby shielding the magnetic field at the nucleus and reducing the effective magnetic field. This effective field is expressed as:

$$B_{eff} = B_0 (1-\sigma) \qquad (7)$$

with σ corresponding to the chemical shielding tensor

As the Larmor frequency described above is related to the magnetic field experienced by the observed nucleus, nuclei in different electronic environments resonate at different Larmor frequencies. The frequency shifts due to the interaction of the field produced by the electrons with the nucleus is called the chemical shift and when reported in ppm (part per million), is calculated as:

$$\delta = \frac{\upsilon - \upsilon_{ref}}{\upsilon_{ref}} 10^6 \qquad (8)$$

The electron distribution around the nucleus is not spherical thus the chemical shielding is not the same in all directions, but rather orientation dependent with respect to the magnetic field. This orientation dependence of nuclear spin is called chemical shift anisotropy (CSA) which is described by the chemical shielding tensor σ mathematically represented by a 3 x 3 matrix:

$$\sigma = \begin{pmatrix} \sigma_{XX} & \sigma_{XY} & \sigma_{XZ} \\ \sigma_{YX} & \sigma_{YY} & \sigma_{YZ} \\ \sigma_{ZX} & \sigma_{ZY} & \sigma_{ZZ} \end{pmatrix} \qquad (9)$$

Where X, Y, Z is an axis frame. When this axis frame is choosing such that the interaction tensor σ is defined with respect to the diagonal, it is called the principal axis frame (PAF):

$$\sigma_{PAF} = \begin{pmatrix} \sigma_{11} & 0 & 0 \\ 0 & \sigma_{22} & 0 \\ 0 & 0 & \sigma_{33} \end{pmatrix} \qquad (10)$$

The interaction tensor can be represented as an ellipsoid in which the principal axes of the ellipsoid coincide with the principal axis frame of the shielding tensor (Figure 32).

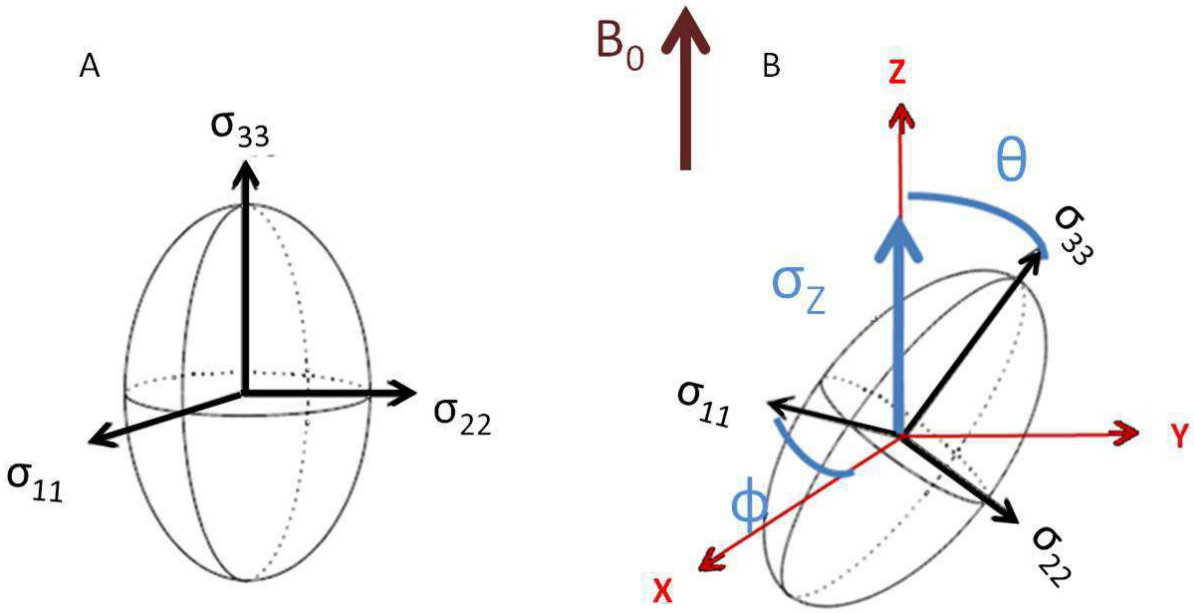

Figure 32: Graphical representation of the chemical shift anisotropy tensor A) in the PAF and B) in the laboratory frame with the Euler angles (θ and Φ).

The measured value of the CSA in an NMR experiment corresponds to the chemical shift tensor component oriented parallel in the laboratory frame (x, y, z) with respect to B_0 (σ_{ZZ}). Its value can be calculated using Euler angles ϕ and θ:

$$\sigma_{ZZ}(\phi,\theta) = \sigma_{iso} + \frac{\delta}{2}(3cos^2\theta - 1 - \eta sin^2\theta cos2\phi) \quad (11)$$

Where σ_{zz} is the chemical shift, θ and Φ the Euler angles, η the asymmetry parameter, δ the anisotropy parameter and σ_{iso} the isotropic chemical shift according to the Haeberlen-Mehring-Spiess convention:

$$\eta = \frac{(\sigma_{22} - \sigma_{11})}{\sigma_{33} - \sigma_{iso}} \quad (12)$$

$$\delta = (\sigma_{33} - \sigma_{iso}) \quad (13)$$

$$\sigma_{iso} = \frac{(\sigma_{11} + \sigma_{22} + \sigma_{33})}{3} \quad (14)$$

The line-shape of a powder spectrum change with the asymmetry of the CSA-interaction, described by the asymmetry parameter η of the chemical shift tensor.

For example, in a solid η is in general ≠ 0; while fast rotation of a molecule can average the tensor, thus η=0 corresponding to an axial symmetry (e.g; ^{31}P spectrum of phosphor lipids). In liquids the chemical shift average to the isotropic chemical shift σ_{iso} (Figure 33).

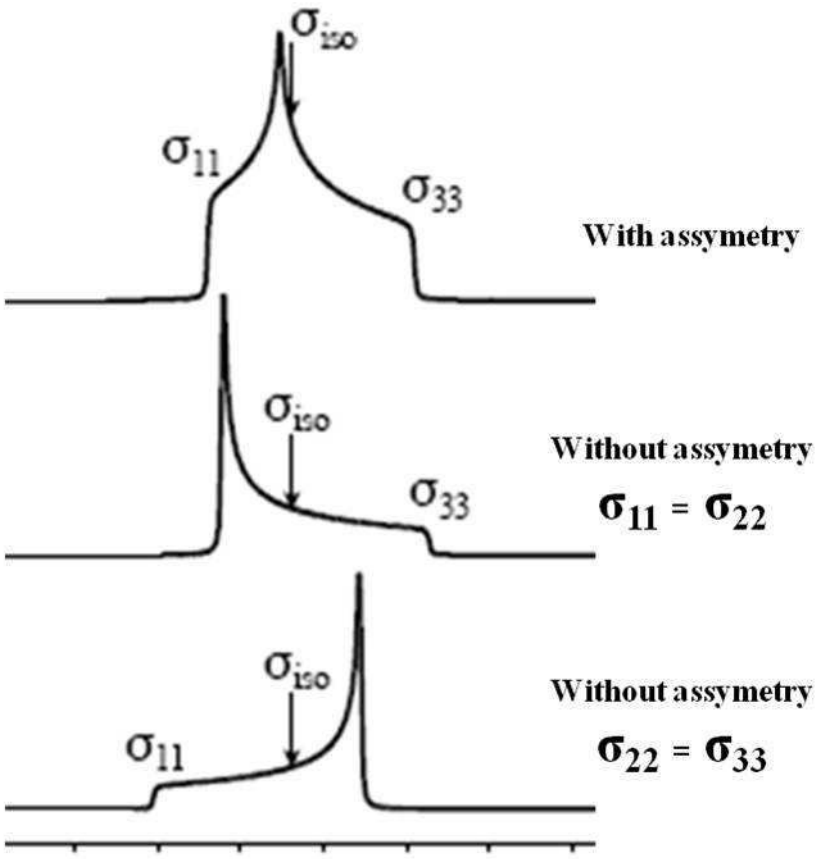

Figure 33: Representation of the influence of the asymmetry parameter on the anisotropic chemical shift tensor

Scalar and dipolar couplings:

Nuclear spins within macromolecules may interact directly or indirectly with each other. The interaction of nuclei mediated by electrons through covalent bonds is named scalar or J coupling. Its strength for two nuclei x, y separated by n covalent bonds is measured by the scalar coupling constant ${}^{n}J_{x\text{-}y}$. This constant represents the principal component of the J coupling Hamiltonian ($\hat{H}_J$).

Moreover, nuclear spin induced a local magnetic field which is felt by its neighbours. This direct interaction between neighbouring spins through space is called dipolar coupling. The strength of this interaction depends on the internuclear distance and the orientation of the vector related the two nuclei relative to the direction of the magnetic field B_0. If the interacting spins are from different species, the interaction is heteronuclear and if spins are from the same species, the interaction is homomonuclear. It is averaged in solution to zero due to the molecular tumbling. The interaction Hamiltonian is:

$$D_{zz} = \left(\frac{\mu_0}{4\pi}\right)\frac{\gamma_1\gamma_2}{r^3}(3cos^2\Theta - 1) \qquad (15)$$

Where $(3cos^2\Theta - 1)$ describes the angular dependence of the dipolar interaction.

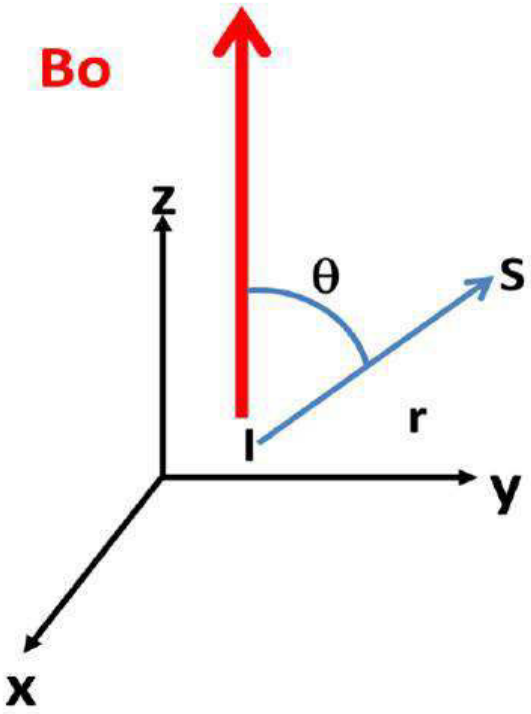

Figure 34: Graphic representation of dipolar coupling between two spins I et S

Quadrupolar coupling:

Nuclei with spin number I > 1/2 have an electrical quadrupolar moment which interacts with Electric Field Gradient (EFG) generated by uneven charge distribution within the nucleus. The coupling of this quadrupolar moment and the EFG are known as the quadrupolar coupling. The electrical quadrupolar moment is the consequence of the charge distribution within the nucleus. For a nucleus that has a spin I =1/2, the charge is spherically distributed about the nucleus and consequently no quadrupolar coupling is observed, but for spins with I > 1/2, the charge distribution in the nucleus is no longer spherical and a quadrupolar coupling occurs (Figure 34). For example, the ^{2}H isotope has a spin I =1 and therefore possesses an electrical quadrupolar moment (*eQ*).

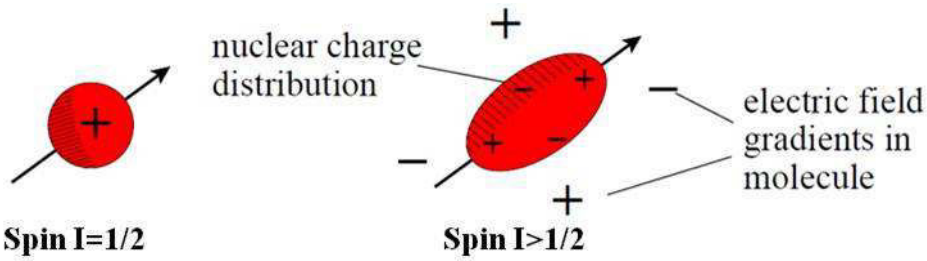

Figure 35: Symmetric and asymmetric distribution of charges for nucleus with spin I =1/2 and quadrupolar nucleus (I>1/2) respectively

2.4.3.3. **Solid state NMR (ssNMR)**

ssNMR is a powerful technique to study complex macromolecular systems such as amyloid fibrils and membrane-associated proteins. The nuclear spin interactions which affect solid state NMR spectra are all dependant on the molecular orientations and therefore anisotropic. In a solid the molecules are static with different molecular orientations, while in solution, with molecular tumbling, spin interactions undergo fast motional averaging. As a result of this, liquid sample results in sharp isotropic resonances while solid samples shows characteristic powder patterns and broad NMR spectra with all the different molecular orientations present in the sample, each giving rise to different spectral frequencies (illustrated for ^{13}C in Figure 36). However, these broad spectra contain valuable structural information. Different techniques have been developed to improve the resolution and the sensitivity of these spectra in order to recover this information.

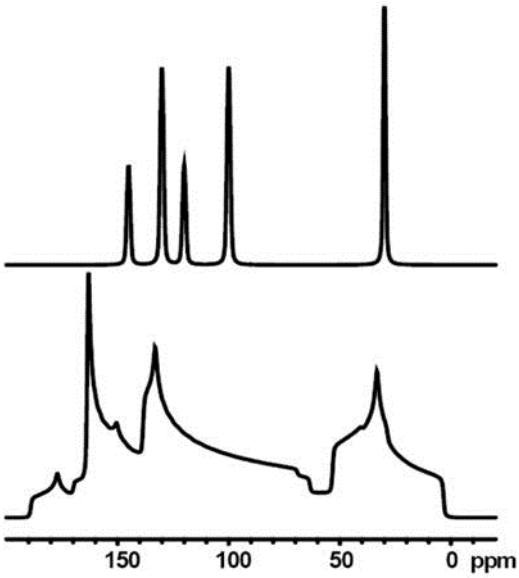

Figure 36: Differences between ^{13}C spectra recorded by solution (upper) and solid state NMR (down).

Solid-state NMR methods

a) ssNMR of oriented sample

NMR of static oriented sample is used in our and a few other laboratories to investigate the dynamics and the topology of peptides in membranes. It takes advantage on the fact that the NMR signal depends of the orientation of molecules relative to the magnetic field. An isotopically labelled peptide (^{15}N and/or ^{2}H) is often mixed with lipids and oriented between glass plates (Figure 24). The sample is then oriented with the membrane normal relative to the magnetic field B_0. These two isotopes are commonly used as they give information on the dynamics and the topology of the peptide within the membrane. In addition to the ^{15}N and ^{2}H experiences, ^{31}P is used to control the orientation of membrane relative to B_0.

- ^{15}N experience for oriented sample

When peptides are reconstituted in oriented phospholipids bilayers (with the normal parallel to B_0), it is possible to determine the approximate orientation of the helix by measuring the chemical shift of the ^{15}N belonging to the peptide bond. As represented on Figure 36A, the NH vector of the peptide bond and the chemical shift tensor σ_{33} form an angle between of about 18 °. They are both oriented almost parallel to the axis of the helix. The values of σ_{22}, σ_{11} and σ_{33} are respectively 85 ppm, 65 ppm and 230 ppm (Bechinger and Sizun, 2003b). Thanks to these particular features, the orientation of the peptide can be estimated. When peptides adopt a transmembrane orientation in oriented bilayers, the magnetic field B_0 is parallel to σ_{33} and assuming that the axis of the helix and σ33 coincide, the ^{15}N chemical shift value will be then > 200 ppm (Figure 37B). In contrast, when the helix adopts an in plane orientation, σ33 is perpendicular to B0 and consequently the value of the ^{15}N chemical shift nucleus is < 100 ppm due to the contribution of σ11 and σ22 (Figure 37C).

- ^{2}H NMR experience for oriented samples

The quadrupolar coupling of the ^{2}H nucleus results in a doublet in solid-state NMR spectra called quadrupolar splitting ($\Delta\nu_Q$) (Figure 37). This splitting depends on the strength of the interactions between the electric quadrupolar moment of the ^{2}H nucleus and the internal magnetic field gradients in the ^{2}H-C bonds. The line-shape of the ^{2}H quadrupolar splitting is very sensitive to the motional freedom of the ^{2}H-C bonds belonging to amino acid side chain and has been therefore used to investigate the topology and the dynamic of the peptide with membrane. For example, the side chain of alanine (methyl group) is directl yattached to the carbon α, and when deuterated used as a probe to investigate the interaction and the dynamics of the peptide within membranes. Moreover, the quadrupolar splitting has an orientational dependence:

$$\Delta\nu_Q = \frac{3}{2}\frac{e^2qQ}{h}\frac{1}{2}((3cos^2\theta - 1) + \eta sin^2\theta\, cos\, 2\phi) \qquad (16)$$

Where θ and ϕ are angles that characterize the ^{2}H-C bonds in the laboratory frame coordinates, and η the axial asymmetry parameter which determines the shape of ^{2}H spectra. η is assumed to be 0 for ^{2}H.

- ^{31}P experience for oriented sample

Phospholipids are predominant components of biological membrane. The phosphorous atoms present in phospholipid head groups are often used to assess the quality of membrane alignment relative to B_0. With a natural abundance of 100%, there is no need in isotopic labelling. Moreover, the high gyromagnetic ratio makes these nuclei a very sensitive probe and a spectrum can be measured within minutes whereas recording of a ^{15}N NMR spectrum of a labelled peptide in an oriented membrane may take overnight or days. In liquid crystalline bilayers in their fluid phase, because of the fast axial rotation of the phospholipids, the tensor singular axis ($\sigma_{\parallel}$) coincides with the rotational axis. Thus, correctly oriented phospholipids as POPC give rise to a ^{31}P spectrum with a peak at approximately 30 ppm when the normal to the bilayer is parallel to B0.

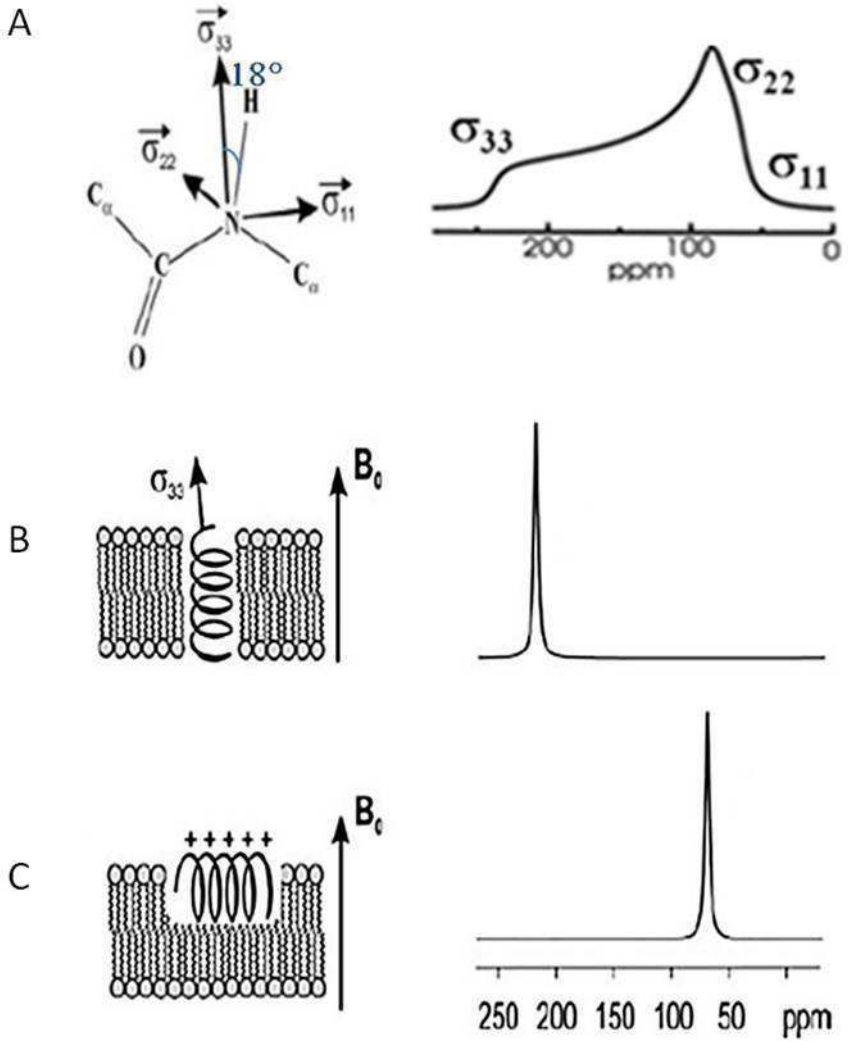

Figure 37: A) representation of the ^{15}N chemical shift tensors in a peptide reconstituted in a lipid bilayer and their representation for a powder sample. And the orientation of peptide in membrane: B) Tansmembrane and C) in plane orientation. (Bechinger and Sizun, 2003b).

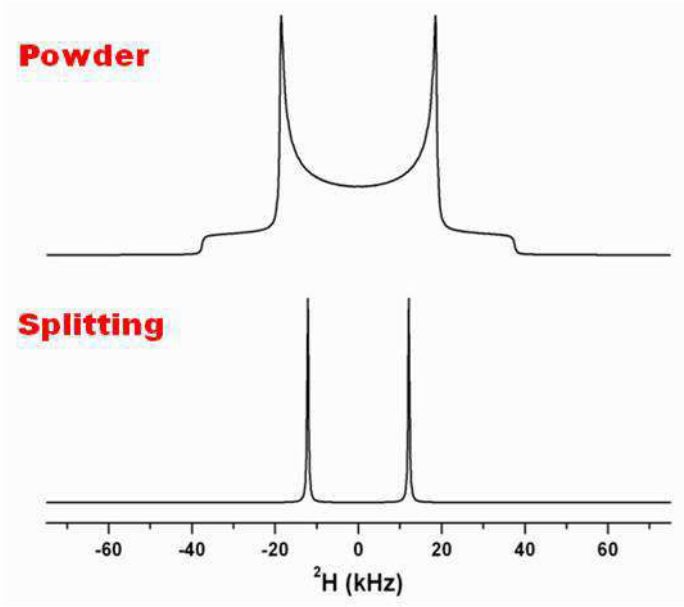

Figure 38: Simulated spectra of a powder and a well oriented sample. A peptide with a well defined orientation will give two sharp peaks corresponding to a splitting

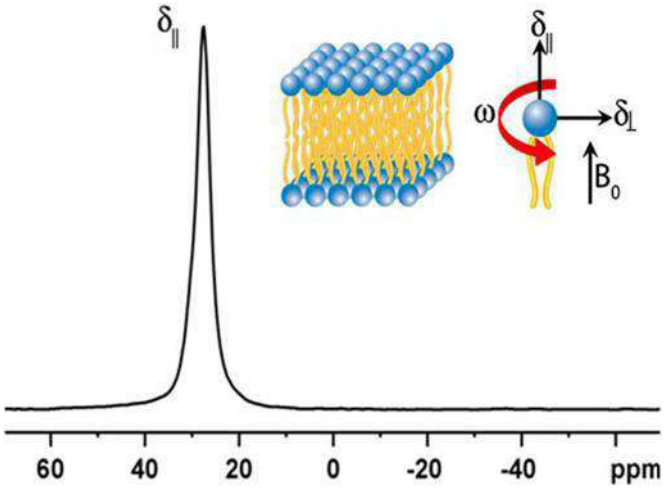

Figure 39: Proton decoupled ^{31}P spectra of well oriented POPC membrane with the normal parallel to B_0. Verica Vidovic Phd thesis, Univeristy of Strasbourg 2011.

b) Magic Angle Spinning solid-state NMR

Magic Angle Sample Spinning (MAS) averages molecular interaction anisotropies thereby giving rise to much better resolved NMR spectra. The averaging is achieved by mechanical spinning of sample that reproduces the molecular fast motion in solution in order to obtain spectra with resolution comparable to that of the liquid. The sample rotates about an axis forming an angle $\theta = 54.7\ ^\circ$ with respect to the B0, averaging dipolar interactions and chemical shift to their isotropic values. This angle θ is obtained from the spatial part of the Hamiltonian, namely $(1\text{-}3\cos^2\theta)$. This factor in solution disappears by averaging but it can also be cancelled when $\cos^2\theta = 1/3$, this gives $\theta = 54.7\ ^\circ$ called the magic angle. Figure 40 shows for example the comparison of the static ssNMR and MAS spectra of ^{13}C uniformly

labelled glycine powder. For MAS, spectra were measured at different rotational frequencies of 5 kHz and 10 kHz, respectively. When the speed of rotation of the sample is less than the value of the chemical shift anisotropy, "spinning sidebands" are observed (marked with an asterisk). The more the rotational frequency increase, the more spinning sidebands disappear.

Although this technique allows highly resolved spectra, this gain in resolution is done at the cost of losing important structural information. For example, the dipolar coupling which is important to determine internuclear distance is average to zero. However, this interaction can be reintroduced by the Rotational Echo Double Resonance (REDOR). This technique allows heteronuclear recoupling between two spins S and I. It then determines the value D of the dipolar interaction and consequently measured the internuclear distance between two spins S and I since it is proportional to the distance (1 / r3) (13).

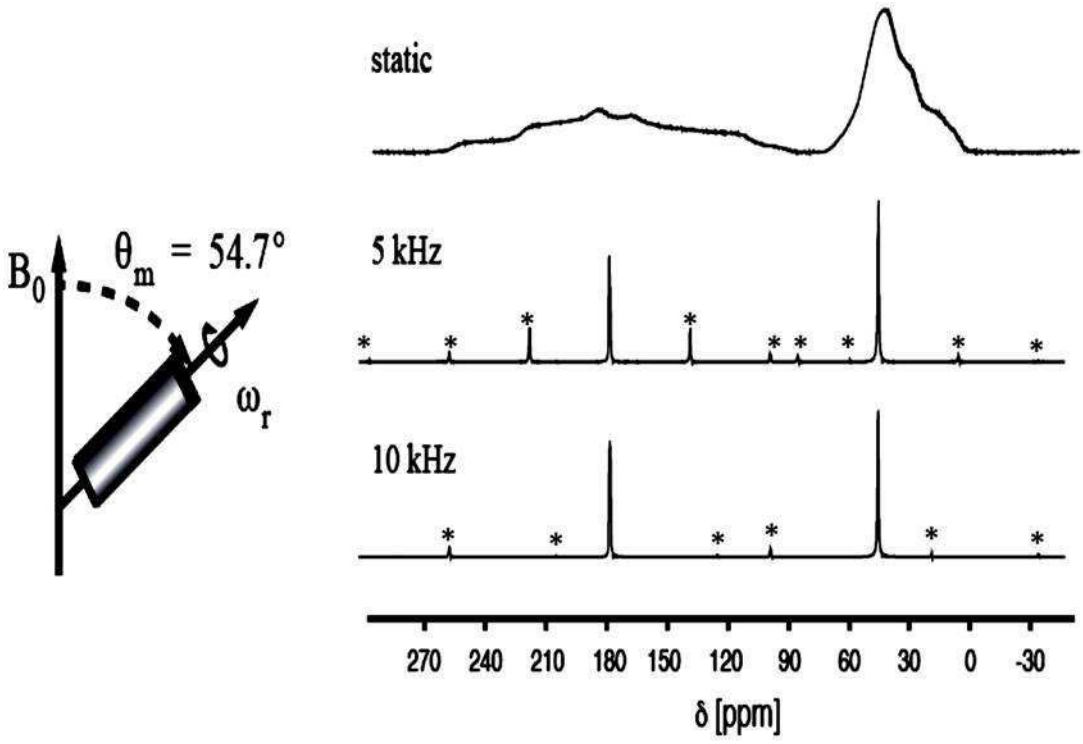

Figure 40: Static and MAS ^{13}C spectra at different rotational frequencies of ^{13}C uniformely labeled glycin powder. The stars represented the spinning side bands. (Laws et al., 2002).

C) Cross Polarization **(CP)**

CP is widely used in ssNMR to enhance the signals of isotopically dilute nuclear spins S (as ^{13}C and ^{15}N) by repeatedly transferring polarization from a species I of high abundance (typically ^{1}H) (Abragam A, 1961). These sparse nuclei interact strongly with the abundant ^{1}H which are more sensitive and will dominate the interactions. The transfer of polarization is mediated by dipolar heteronuclear coupling and the effect is a gain of sensitivity. This transfer obeys the Hartmann-Hahn condition:

$$\gamma_I H_{1I} = \gamma_S H_{1S}$$

And is more effective when the distances are short, the dipolar coupling is string and the connection is rigid between the two nuclei.

D) Dipolar decoupling

Considerable line-broadening of the NMR signals of sparse nuclei (^{13}C and ^{15}N) is due to their strong dipolar coupling interactions with protons. Therefore, proton decoupling is applied during the acquisition time.

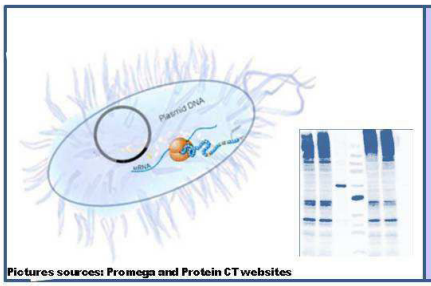

Chapter-3

EXPERIMENTAL RESULTS: EXPRESSION OF THE RECOMBINANT p24 TRANSMEMBRANE DOMAIN

Protein labeling with stable isotopes is a necessary condition for advanced NMR investigation. With this goal in mind, we expressed the p24 transmembrane domain (p24TMD) as a recombinant fusion protein in E.coli bacteria. As bacterial expression of membrane peptide/protein can be tricky, we tested two recombinant expression vectors (pMal c5X-p24TMDH and pTIPX4-p24TMD) to increase our chances to produce this peptide at high yields. Expression was first tested in rich medium to set up conditions and the thus defined experimental parameters were then used for the expression in minimum medium. Here we describe all the strategies we used to produce the p24TMD as well as the results we obtained, followed by a discussion.

Chapter 3. Experimental results: expression of the recombinant p24

Introduction:

In order to have more insights on the structure of p24TMD in a lipid membrane bound state, we decided to fully label the peptide with stable isotopes. Recombinant expression in bacteria is the method of choice to produce fully labelled protein/peptide because it is a much more economical way when compared to the peptide synthesis. Indeed, the amino acids and the solvents needed for the peptide synthesis are expensive thus the synthesis of a fully labelled peptide can be very expensive. Moreover, this method presents some limitations due to the fact that all labelled amino acids are not commercially available, and that the yield and efficiency depends on the size and the sequence of the peptide.

With regard to the bacterial expression system, among the available hosts, *Escherichia coli* (*E. coli*) is the most attractive strain because of its easy manipulation, it's well known genetics and low costs. However, the expression of foreign genes in *E. coli* often fails due to their toxicity for the host cells thus; there is no guarantee of the production of the protein of interest. The use of fusion partners was developed to avoid this problem and thus, improve and optimize the production of many recombinant peptides. Indeed, these fusion partners can be used to improve the solubility of the peptide of interest, enhance its stability, to direct the fusion protein in a specific cellular compartment and sometimes to facilitate its detection and/or the purification (Hwang et al., 2014b; Sørensen and Mortensen, 2005b). Interestingly, the peptide/protein of interest can be recovered by the cleavage of these fusion partners followed by a purification step.

As the expression of membrane proteins is tricky, here we tested two different constructs with a different strategy for the expression of our peptide in order to optimize its production. The first expression system was designed by our collaborator in Heidelberg. It used the pMal-c5X vector in which the gene that encodes the p24TMDH (H for Heidelberg) was cloned downstream the malE gene that encodes maltose-binding protein (MBP), resulting in the expression of a MBP fusion protein. MBP is a common fusion partner which significantly enhances the solubility of many recombinant proteins thus, allowing their secretion into the periplasm or their production in the cytoplasm. The recombinant vector pMal-c5X-p24TMDH allows for the expression of the MBP-p24TMDH fusion protein as a soluble protein that accumulates into the cytoplasm. Moreover, the MBP sequence in these vectors has been engineered for tighter binding to amylose thus, optimizing its purification. In addition, a cleavage site for the Tobacco Etch Virus (TEV) protease was added between the MBP and p24TMD as shown on Figure 41 (top) in order to remove the fusion partner and recover the peptide of interest.

In addition, another recombinant vector pTIPX4-p24TMD was designed in our laboratory to express p24TMD as a fusion to the histone fold domain of the human transcription factor TAF12 protein (TATA box binding protein (TBP) Associated Factor 12 Histone fold Domain). This fusion partner drives high-level expression of peptides and leads to their accumulation in an entirely insoluble form, thereby eliminating toxicity to the host and

optimizing consequently the stability and the yield of the expressed fusion protein. It has been shown for example to allow efficient expression of a wide range of antimicrobial peptides as for example LAH4 (Vidovic et al., 2009b). In contrast to the previous fusion partner, the TAF12 does not allow the purification of the fusion protein but it was designed to direct its accumulation in inclusion bodies. However, as shown on figure 68 (bottom), the TAF12 is followed by a tag of six histidines (HisTag) which allows for the purification of protein by Immobilized Metal Affinity Chromatography (IMAC) using divalent metal ion column affinity such as cobalt (Co2+), nickel (Ni2+). These histidines are followed by a formic acid cleavage site (DP) that allows the TAF12 cleavage and the purification of p24TMD peptide.

This chapter, we will then be organized in two parts. The first one will present the results we obtained with the pMalc5X-p24TMDH and the second with the pTIPX4-p24TMD expression vectors.

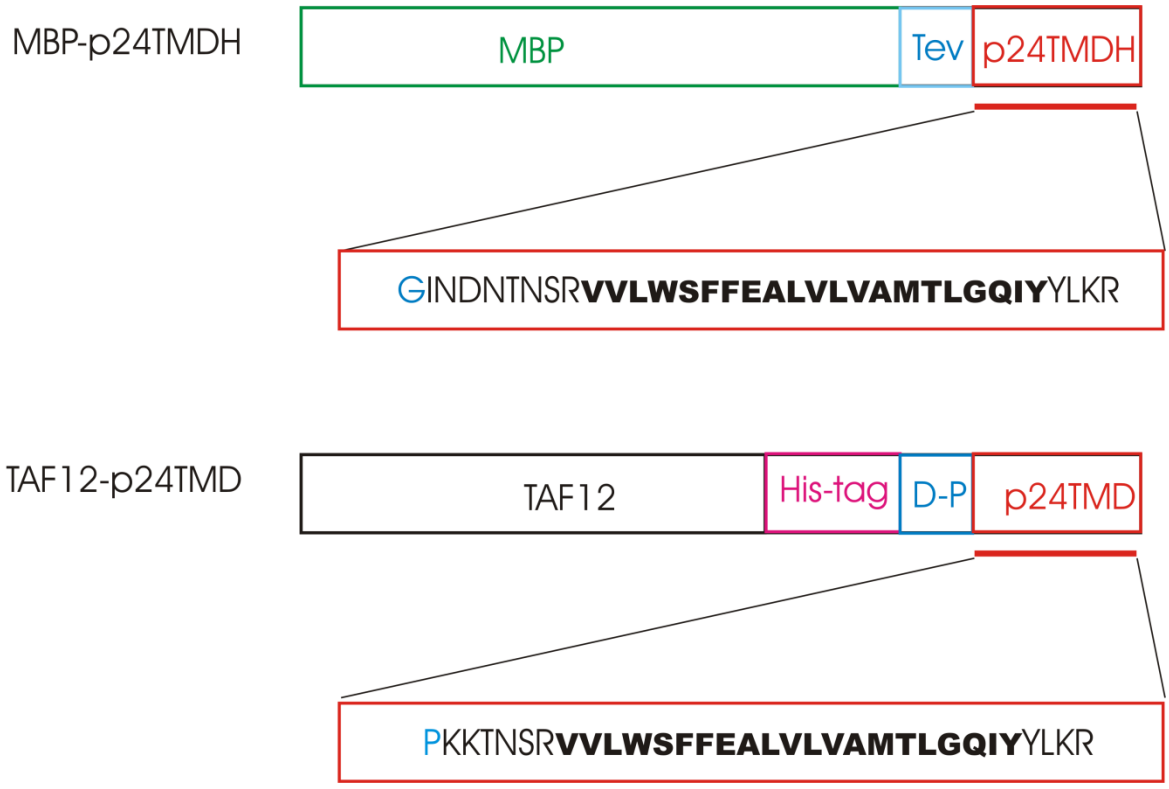

Figure 41 : Representation of MBP-p24TMDH and TAF12-p24TMD fusion proteins that were expressed and the respective p24TMDH and p24TMD peptide sequences.

3.1. Expression of p24TMDH as a MBP fusion protein.

3.1.1. Experimental

3.1.1.1. Amplification of the recombinant expression vector pMal-c5X-p24TMDH

The pMal-c5X-p24TMDH plasmid was designed by our collaborator and sent to us for protein expression. This vector carries the gene that encodes the β-lactamase enzyme which confers the resistance to the ampicillin antibiotic thus, allowing the selection of bacteria which carry this plasmid. To have enough amount of this vector, it was amplified by cloning in competent bacteria, the XL1 Blue (Competent Cells, 200249, Stratagene). 0.6µl of this vector (103ng) was used to transform 100µl of XL1 Blue suspension. After 20min kept in ice and 10min more at room temperature, the bacteria were grown in Luria Bertani (LB) medium for 1h at 37 °C under shaking (250rpm). The transformed bacteria were thereafter spread on agar plates containing ampicillin 100µg/ml in order to be selected and the plates incubated in an oven at 37 °C overnight. To amplify the vector 3ml of LB with ampicillin 100µg/ml was seeded with one colony of transformed bacteria and grown overnight at 37 °C under agitation (250rpm) until an OD 600nm of ~ 3-4 was reached. Cells were lysed and the plasmid DNA purified using a commercial kit for DNA extraction (Nucleospin Plasmid, Macherey-Nagel, Germany). The plasmid concentration was estimated by measuring the OD at 260nm on a nanodrop device (Nanodrop ND-1000 Spectrophotometer, Thermo Scientific, USA). The compliance of the expression vector was checked by nucleotide sequencing (Eurofins MWG Operon sending, Germany) and the product was stored at -20 ° C.

3.1.1.2. Overexpression of MBP-p24TMDH in rich medium

In order to express the protein of interest, *E.coli* bacteria strains specifically designed for protein over expression were transformed with 1µl of pMal-c5X-p24TMDH vector (122.7ng). To optimize the overexpression, different strains were transformed and tested: the competent bacteria BL21 (DE3) pLysS One Shot® (C6020-03, Invitrogen) and the BL21 (DE3) One Shot® (C6000-03, Invitrogen). The first strain harbours a pLysS plasmid that expresses T7 lysozyme to reduce basal level expression and confers resistance to chloramphenicol. Transformed bacteria were spread on agar plates containing ampicillin 100µg/ml and chloramphenicol 60µg/ml for the selection of the expression plasmid and the pLysS bacteria respectively. A preculture was obtained by inoculating a colony of transformed bacteria in 50ml LB medium and allowing for bacterial growth overnight at 37 ° C under shaking (200 rpm). 500 ml of culture media (LB: Luria Bertani, Yeast Extract, 20% glucose, chloramphenicol 34 µg/ml and/or ampicillin 100 µg/ml), was inoculated with the pre-culture at a volume ratio 1/100. The kinetics of bacteria growth were monitored each 30 min by measuring the optical density (OD) at 600 nm (Uvikon Spectrophotometer, New York, USA) and the protein expression induced between 0.8 < OD600nm <1 for 4 hours by adding IPTG at the final concentration of 1mM. Bacteria were

harvested by centrifugation at 5000 g for 15 min at 4°C, and the bacterial pellets frozen at -20 °C or directly treated for protein extraction.
Although LB is extensively used for bacteria culture, cells grown in this medium have substantial amounts of amylase that impair the protein purification. It likely interferes in the case of the MBP fusion protein with the binding allowing its flow through the column. The expression of these enzymes can be preventing by the addition of glucose in the medium.

3.1.1.3. **Overexpression of MBP-p24TMDH in M9 minimal medium**

BL21 (DE3) pLysS One Shot® (C6020-03, Invitrogen) harbouring the recombinant expression vector were first grown at 37 ° C under shaking (230 rpm) for 7 to 8 hours in 2 ml of LB medium supplemented with ampicillin 100µg/ml and chloramphenicol 34µl/ml. The bacteria were diluted to 1/100 in 50 ml M9 minimal medium (85.5 g/L $Na_2HPO_4 \cdot 12H_2O$, 15 g/L KH_2PO_4, 3 g/L NaCl, 5g/L $^{15}NH_4Cl$, 0.4 % glucose, 2 mM $MgSO_4$ and 0.1 mM $CaCl_2$). Ampicillin (100 µg/ml), kanamycin (50 µg/ml) or chloramphenicol (25 µg/ml) was added to the medium for bacterial selection and plasmid maintenance. Cells were incubated at 37 °C under shaking (230 rpm) until 0.8<OD260nm<1 and protein expression was then induced by addition of IPTG (1mM). After induction, cells were grown at different temperatures during several hours in order to test the optimal temperature. Bacteria growth was monitored every 30 min by measuring the optical density (OD) at 600 nm (Uvikon Spectrophotometer) and cells harvested by centrifugation at 5000 g for 15 min at 4°C. The bacterial pellets were frozen at -20 ° C or directly treated for the protein extraction.

3.1.1.4. **Protein extraction and purification of the fusion protein**

Bacteria pellets of a 1L culture were resuspended into 30ml column buffer (20 mM Tris; 200 mM NaCl; 100mM EDTA, pH 7.4) and 1 Tablet of Protease Inhibitor cocktail (Roche, Meylan, France) to reduce proteolysis. The suspension was sonicated twice for 5 min at 50% of the cycle time using a sonicator tip (Bandelin Sonopuls HD 200, probe MS70, Berlin, Germany). An aliquot of the cells lysate was collected for analysis by SDS-PAGE migration (Sodium Dodecyl Sodium-polyacrylamide gel electrophoresis). The lysate was spun down at 11000 g, 1 hour, 4 ° C and the soluble fraction (supernatant) incubated with 5ml of amylose beads in suspension (Amylose Resin, NEB, Ref.E8021L) for 1 hour at 4 °C on a rotary-wheel to allow the absorption of the fusion protein on the beads. The beads were spun down 5 min at 2000rpm, 4 °C and the supernatant (flow-through) kept. Beads were washed twice with 50ml column buffer and loaded on a column (Biorad Econo-Column Chromatography Columns, 0.7 x 10 cm, 4 ml, 4, Ref.737-4711). The fusion protein was then eluted with elution buffer (20 mM Tris; 200 mM NaCl; 100mM EDTA, pH 7.4; 10mM maltose) in 10 fractions of 2ml. Aliquots were prepared with Coomassie dye and analyzed on a 12% polyacrylamide gel by SDS-PAGE. Fractions containing the

fusion protein were collected and concentrated using centricon (Amicon Ultra 50.000 MW, Millipore, Molsheim, France).

3.1.1.5. Enzymatic cleavage with TEV-protease

The MBP was cleaved using a commercial TEV-protease (T4455 Sigma-Aldrich, Saint-Quentin, France). The cleavage was tested on the fusion protein in solution or attached to amylose beads. We first tested the different experimental conditions of cleavage of the fusion protein in solution and thereafter, the defined conditions were used for the cleavage of the attached fusion protein on amylose beads. The kinetic of cleavage was tested (30, 120, 180, 240 minutes and 24 hours) for different enzyme: fusion protein (E/P) ratios (1:20, 1:50, 1:100 and 1:150) at RT and 4 °C. The sample was spun down after the cleavage at 11000g for 15 min and the supernatant removed. 1µl (~ 47µg) aliquots of each cleavage product was prepared in Coomassie blue 1X final concentration and analyzed on 10% polyacrylamide gels (Biorad, Marne-la-coquette, France) by SDS-PAGE gel electrophoresis.
For the cleavage of MBP-p24TMDH on amylose beads, the fusion protein was incubated for 1 hour on amylose beads at 4 °C and the TEV-protease added to obtain the desired protein/enzyme ratio.

3.1.1.6. Purification of the peptide by reversed phase HPLC

The product of MBP-p24TMDH cleavage with the TEV protease was injected onto a ProntoSIL 300-3-C4 analytic reverse-phase HPLC column (Bischoff, Leonberg, Germany) equilibrated with the solvent A (acetonitrile/water/TFA, 10/90/0.1, v/v/v). This column is composed of silica beads grafted with chains of 4 carbons (C4). The choice of a short-chain is driven by the highly hydrophobic character of the peptide of interest as longer carbon chains lead to strong interactions with hydrophobic proteins/peptides and do not allow the dissociation and therefore their elution by the solvent. Adsorbed proteins and peptides were gradually eluted at different percentages of increasing solvent B (acetonitrile/TFA, 100/0.1, v/v) at 45, 50 and 53%. This was achieved on a semi-preparative reversed phase HPLC (Bischoff Chromatography, Leonberg, Germany) to develop the conditions for elution. Eluted fractions were thereafter analyzed by electrophoresis and MALDI-TOF mass spectrometry.

3.1.1.7. Purification of the peptide by butanol extraction

The butanol extraction was developed by our collaborator at the University of Heidelberg for the purification of p24TMDH peptide after cleavage. The different steps are presented below. Briefly, the sample was first spun-down at 11000g, 45 minutes after TEV protease cleavage. The supernatant (SN) was transferred into a new tube and butanol (B) added to the supernatant and the pellet. Both fractions were vortexed and spun-down at 11000g for

7minutes. The butanol fractions were transferred into a new tube and the liquid fractions spun-down for 20 minutes at 11000g and the SN and the pellet kept.

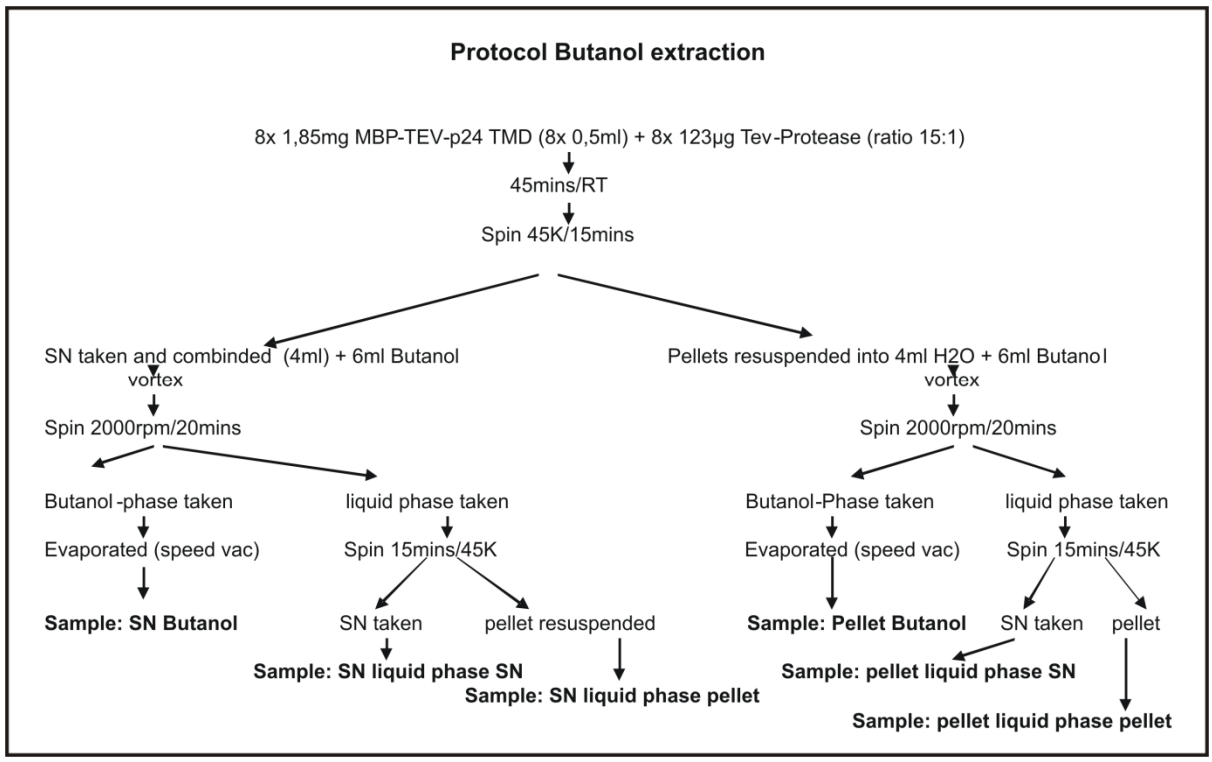

Figure 42:Protocol butanol extraction

3.1.1.8. **Electrophoresis:**

Proteins were separated by electrophoresis under denaturing conditions according to the "SDS-PAGE" technique. They were sequentially separated through two gels under electric current. The stacking gel with a low concentration of acrylamide (4%) was used to concentrated proteins at the limit of the second gel while the separating gel with a higher acrylamide concentration (10, 12, 15 or 16%) separate proteins. These gels were often prepared by us. For the peptide detection, we used commercial 10-20% or 4-20% precast polyacrylamide gradient gel (Biorad). Two Protein markers (Precision Plus Protein Dual Color Standards ™ Ref.161-0374 and/or Precision Plus Protein Dual Xtra Standards ™ Ref.161-0377) were used to estimate the apparent molecular weight of the proteins. The migration was in general achieved for 1 h to 1 h30 at 150V. Gels are stained with Coomassie blue (ROTI®-Blue 5X, A15.1, Carl Roth, Karlsruhe, Germany) or Brillant Blue R-250 (Carl Roth, Karlsruhe, Germany) and then destained with a solution of 25%

water and 75% Methanol. Gel pictures were taken with a gel reader (E-box VX2, Vilber, Eberhardzell, Germany).

3.1.1.9. **Mass Spectrometry**

The sinapinic acid (SA) or α-cyano-4-hydroxycinnamic acid (α-cyano) matrix was prepared at 10 mg/ml final concentration in acetonirile 30% and TFA 0.1%. They were used to analyze protein and peptide, respectively. 1µl of sample was mixed to 1µl matrix on the sample target (05 174, Bruker, Leipzig, Germany) and analyzed in the MALDI-TOF (Matrix Assisted Laser Desorption-/ Ionization -Time-Of-Flight; Bruker Daltonics Autoflex modelm Leipzig, Germany) spectrometer. Samples were analyzed under linear mode detection.
A part of MALDI-TOF spectrometry with or without fragmentation was achieved by the mass spectrometry service of the Molecular and Cellular Biology Institute (IBMC).
The expected theoretical masses for the fusion protein MBP-p24TMDH, the cleaved MBP-TEV and the peptide p24TMDH are respectively 48176.62, 44262.04, 3932.60 Da.

3.1.1.10. **Protein quantification:**

The Thermo Scientific NanoDrop™ 1000 spectrophotometer (Wilmington, USA) was used to quantify the purified protein. Absorbance at 280nm was measured using 1µl of diluted or concentrated sample and the protein concentration determined with the p24TMD extinction coefficient ξ= 8250 $cm^{-1}M^{-1}$. Beer Lambert equation: $A=\xi \times l \times C$ (with l corresponding to the cuvette length, 1cm)

3.1.2. Results and discussion:

3.1.2.1. **Bacterial over expression of MBP-p24TMDH**

3.1.2.1.1. **Expression in rich medium**

The recombinant vector pMal-c5X-p24TMDH was obtained from our collaborator with a protocol of expression of the protein of interest. Therefore, we did not test the concentration of the inducer, the temperature of induction but rather, only the bacterial strains as their initial protocol was set up with the *E.coli* DH5α strain. The tests were performed in rich medium and thereafter the best conditions were used for the expression in M9 minimum medium for the protein labelling. The tests in rich medium were performed on a small scale (10 ml) and a large scale (500 ml) to obtain unlabelled fusion protein for testing purification, cleavage and protein characterization.

The expression was first tested in different bacteria strains, BL21 DE3 and BL21 DE3 pLysS. They were transformed with the recombinant vector pMal-c5X-p24TMDH and a pre-culture of each strain was prepared by inoculating separately 50 ml LB with one transformed colony. Bacteria precultures were first grown at 37°C and seed in 500ml LB for the main culture. Expression of MBP-p24TMDH was induced with 1 mM IPTG at OD 1 and 1.3 for BL21 DE3 and BL21 DE3 pLysS respectively. The bacteria growth was followed each 30 min and cells were harvested by centrifugation after 4 hours of induction. The kinetic curves of bacterial growth are shown on figure 69. For both bacteria strains, the expression of the fusion protein MBP-p24TMDH at 37 °C slows down the bacterial growth after induction compared to the uninduced cells. However, bacterial growth seems to increase for the induced BL21 DE3 compared to the uninduced cells after 2h30 (Figure 43A). This result suggests that the uninduced bacteria reached their stationary phase earlier while the induced were still growing. In contrast, induced and uninduced BL21 DE3 pLys S seem to reach a plateau simultaneously (Figure 43B).

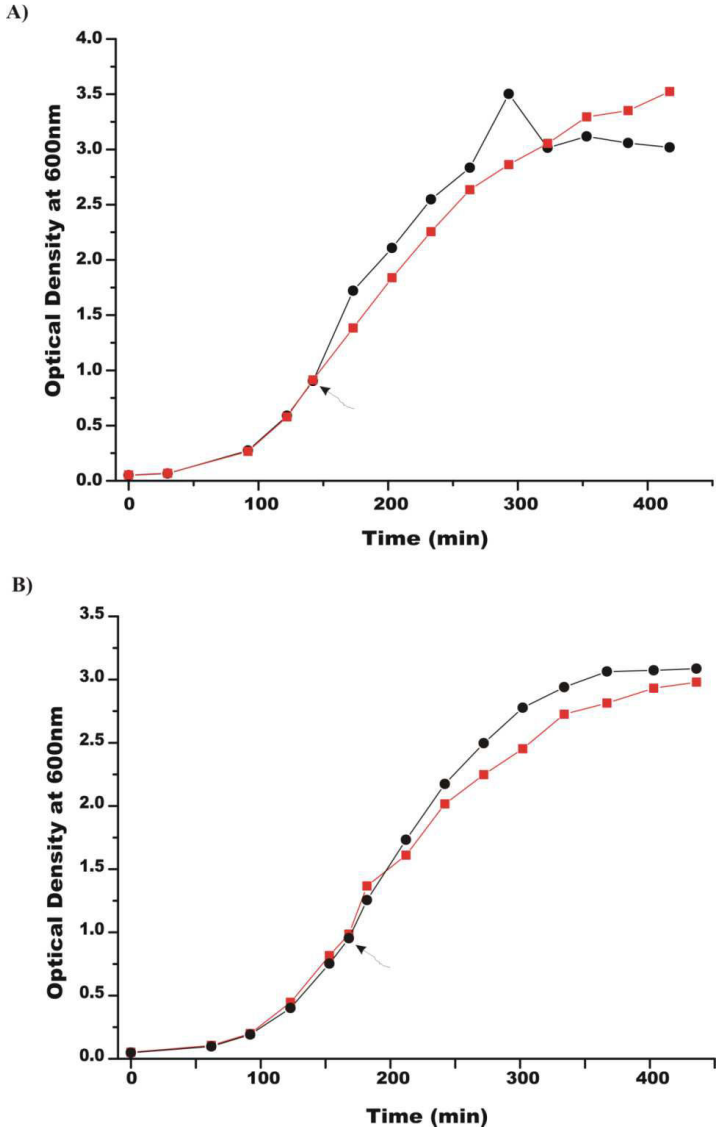

Figure 43: Kinetics of bacterial growth (A) BL21 DE3 and (B) BL21 DE3 pLysS in LB medium before and during expression of MBP-p24TMDH at 37°C. Bacterial growth is monitored by measuring the OD 600 nm versus time. The arrow indicates the induction by the addition of IPTG (final concentration 1 mM) at OD = 1 and 1.4 respectively. The red curve corresponds to the induced and the black one to the uninduced condition

In order to characterize the MBP-p24TMDH fusion protein, after lysis of the bacteria proteins were extracted and purified by affinity chromatography on amylose resin. Briefly, the insoluble fraction was pelleted by centrifugation and the supernatant corresponding to the total soluble protein extract was incubated with amylose resin in order to allow the adsorption of MBP-p24TMDH. Beads were washed prior to the elution in order to remove weakly attached proteins. Aliquots of the different purification steps were sampled and proteins separated on polyacrylamide gel under denaturing conditions (SDS-PAGE) to identify and follow the presence MBP-p24TMDH during the purification.

Figure 44A and B correspond to the SDS-PAGE profile of protein expression in BL21 DE3 pLysS and BL21 DE3, respectively. In both cases, we clearly identify a band around the

expected apparent molecular weight (48.2 kDa) which is present in the total protein extract (SN) and during the different steps of purification. As the band presents a high intensity in the induced conditions compared to the uninduced, we thus conclude that it corresponds to MBP-p24TMDH which is overexpressed in induced bacteria and presents a basal expression in uninduced bacteria. Interestingly, the elution fractions (En) indicated that we recovered pure fractions of MBP-p24TMDH fusion protein (Figure 44A and B middle and bottom). However, we noticed the presence of two bands with the upper corresponding to the full length protein. The lower band likely corresponds to protein degradation thus indicating that the fusion protein is instable. In elution fractions which present low amount of protein, we still identify the two bands on the SDS-PAGE expression profile of BL21 DE3 but not on that of BL21 DE3 pLysS suggesting that the protein is more stable or submit to less degradation in the later strain. In addition, as expected with this strain, we do not observe any basal expression. Moreover, we yield more protein after purification compared to BL21 DE3 (Figure 45). Although expression in DH5α that was achieved by our collaborator yield more protein compared BL21 DE3 pLysS, it presents important protein degradation. Based on these observations, we choose to express MBP-p24TMDH in BL21 DE3 pLysS.

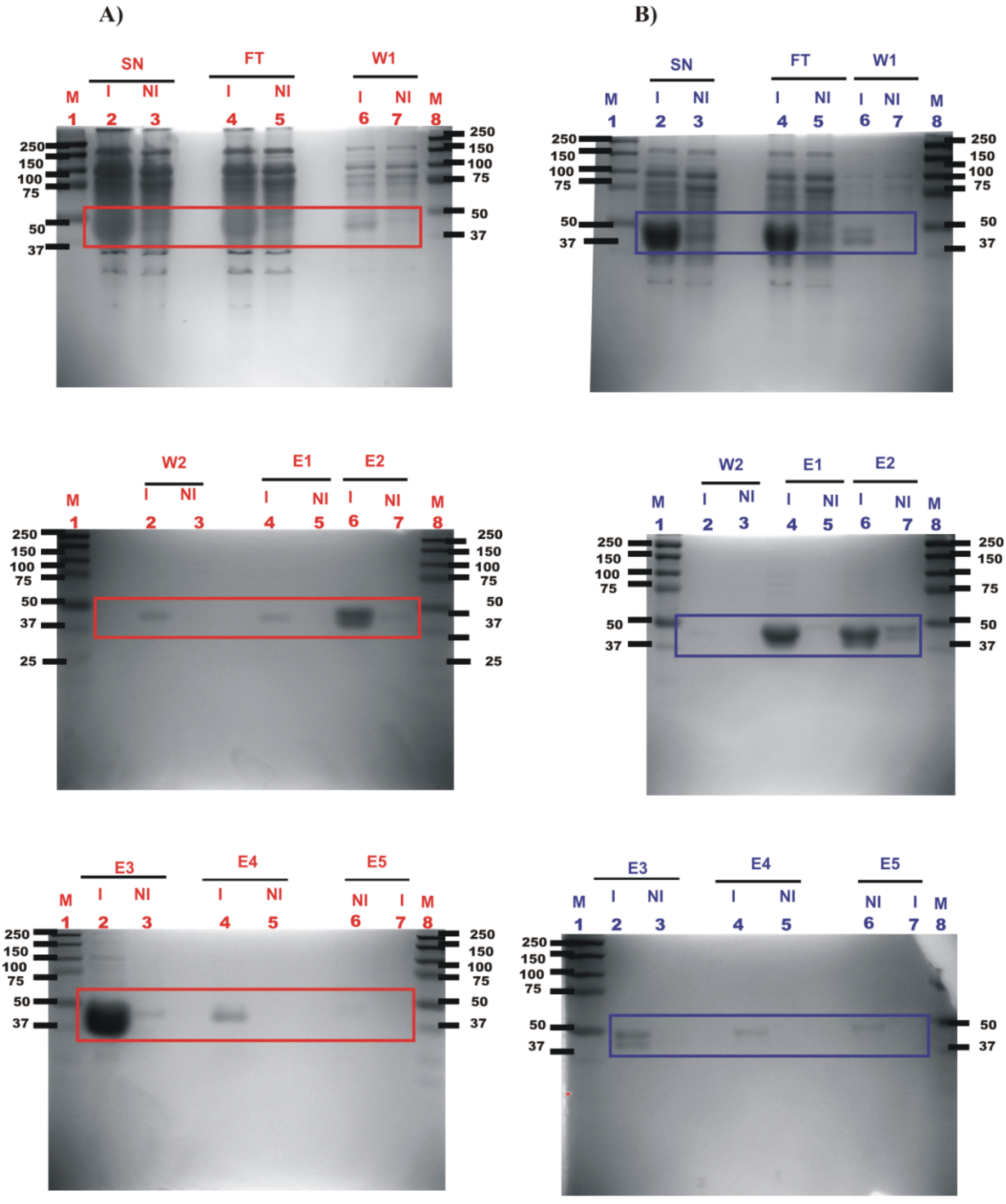

	MBP-p24TMDH	MBP5
Monomer (Da)	48176.62	42500
Dimer (Da)	9635.24	85000

Figure 44: SDS PAGE gel electrophoresis of the different fractions of protein extraction for MBP-p24TMD after expression in (A) BL21 DE3 pLysS and (B) BL21 DE3. The different fractions from the protein extraction induced conditions (I) and non-induced (NI) were deposited on 12% polyacrylamide gel SDS-PAGE. Deposits volumes are: 15µL for the different fractions (equivalent

to 500µl of culture). After electrophoresis migration for 1h at 150V, gels were stained with Coomassie blue. The different bands are defined as follow: SN: supernatant after cells lysis and centrifugation, FT: flowthrough after incubation of the SN with amylose beads, W_n: correspond the wash of the beads in order to remove weakly or unbound proteins with n corresponding to the number of washing step, E_n for elution fraction with n corresponding to the fraction, M: molecular weight marker. The table below contain the theoretical masses of different forms of MBP-p24TMDH. They were obtained from the sequence through the Software ProtParam Site ExPASy (http://web.expasy.org/protparam/).

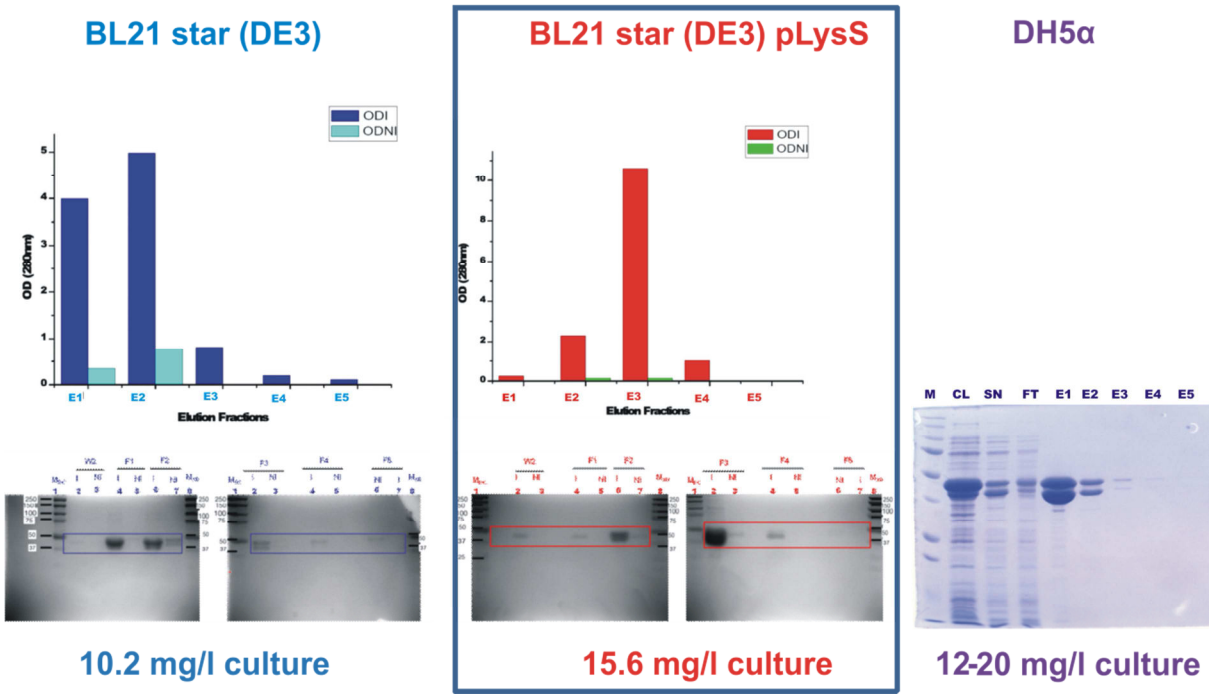

Figure 45: Summary of the yield in the different bacteria strains and the elution profiles of MBP-p24TMD. The protein elution profiles of MBP-p24TMDH are represented as a function of the optical density at 280nm. The SDS-PAGE after expression in DH5α was obtained from our collaborators at the University of Heidelberg. The different concentrations were estimated from the measured OD 280nm values on a Nanodrop-1000 spectrophotometer

3.1.2.1.2. Expression in minimum medium

When grown in minimal medium, bacteria culture was started in LB and used to seed a M9 minimal medium. After overnight growth at 37°C this pre culture was used for the main culture. Bacteria were induced at OD 600nm > 0.8 with 1mM IPTG during longer incubation time (between 8 to 16 h) which is required to achieve comparable protein yield than in LB medium. In addition, as lower bacterial growth temperature is frequently found to be helpful to increase the yield of soluble protein (Ouzzine et al., 1996; Sørensen and Mortensen, 2005b), we therefore tested different temperatures including lower temperature (37, 30, and 18 °C).

At 37 °C, as shown on the bacterial curve (Figure 46A), cells growth is significantly slowed down after protein induction when compared to the uninduced cells. This result indicates that the expressed protein might be toxic for the cells. At low temperatures (30 and 18 °C), bacteria were grown during a longer time (22 and 24 h respectively) after induction. We did not achieve bacterial growth at these two temperatures under non-induced conditions. However, when the induced bacteria are grown at lowered tmeperatures a higher cell density is obtained (Figure 46A).
The analysis of the protein expression by electrophoresis revealed the presence of a band with an apparent molecular weight around 50 kDa which is only present in induced and not in non-induced conditions (Figure 46B). We therefore concluded that it should correspond to the MBP-p24TMDH. Interestingly, the fusion protein is expressed for all the different temperatures that we tested. When comparing the protein expression levels of the different incubation times after induction, it seems that the maximal expression was achieved at 18 °C as shown on the SDS-PAGE gel (Figure 46B, elution fractions (E1)). Moreover, when elution fractions of the different conditions were pooled, concentrated and the protein concentration estimated, for one liter of culture we obtained 0.29, 0.44 and 0.57mg of protein respectively for the induction at 37, 30 and 18 °C. Unfortunately, more than 30% of the expressed protein is loss in the flow-through (Figure 46B, FT). This could come from a low accessibility of the MBP to the amylose beads.
When the protein was expressed on a larger scale (6 times 500ml in M9 minimal medium culture in 2L flask) with the same experimental conditions (18 °C, 24 h, 230rpm in BL21 DE3 pLysS), we obtained around 3mg of protein per liter of culture. However, the SDS-PAGE gel analysis revealed the presence of two bands as we previously observed for the expression of the protein in BL21 DE3 and DH5α (see Figure 44). Moreover, even for the expression on a small scale, for which we obtained only one band at the expected molecular weight, we noticed that after one or a few days, we started to detect a second band on the electrophoresis gels (Figure 47). This observation indicates that the protein undergoes proteolysis during and after the purification, although protease inhibitor (Roche) was used during the extraction and purification steps. Unfortunately, the lower band which corresponds to the truncated protein seems to be ~3/4 of the total protein (Figure 47) thus, reducing the yield of the full length protein. As it will be shown later from the tandem mass spectrometry MS/MS results, this band contains truncated protein at the C terminus.

In conclusion, we were able to set up the expression of MPB-p24TMDH in M9 minimal medium. Using amylose affinity chromatography, we obtained about 3mg of pure protein per litre. But we noticed important protein degradation that reduced the total yield of the full length protein. However, BL21 DE3 and BL21 (DE3) pLys S we used are *E. coli* strains that are deficient in Lon and the outer membrane OmpT protease to reduce degradation of the expressed heterologous protein. Moreover, an important part of the protein was lost during the affinity chromatography and flow through the column. This problem could be the consequence of the presence of factors in the crude protein extract or cellular components that interfered with the binding. The presence of other proteins in the

washing fraction (Figure 46A & B, lines W1) suggests that these proteins can indeed compete with the binding of MBP-p24TMDH. Finally, interaction between the peptide of interest and MBP can reduced the affinity to amylose beads.

A)

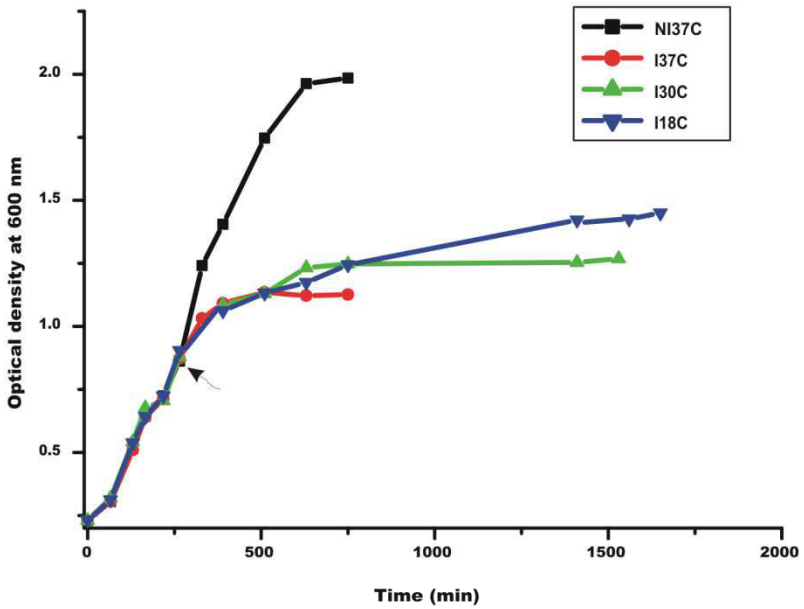
NI37C
I37C
I30C
I18C
Optical density at 600 nm
2.0
1.5
1.0
0.5
0
500
1000
1500
2000
Time (min)

B)

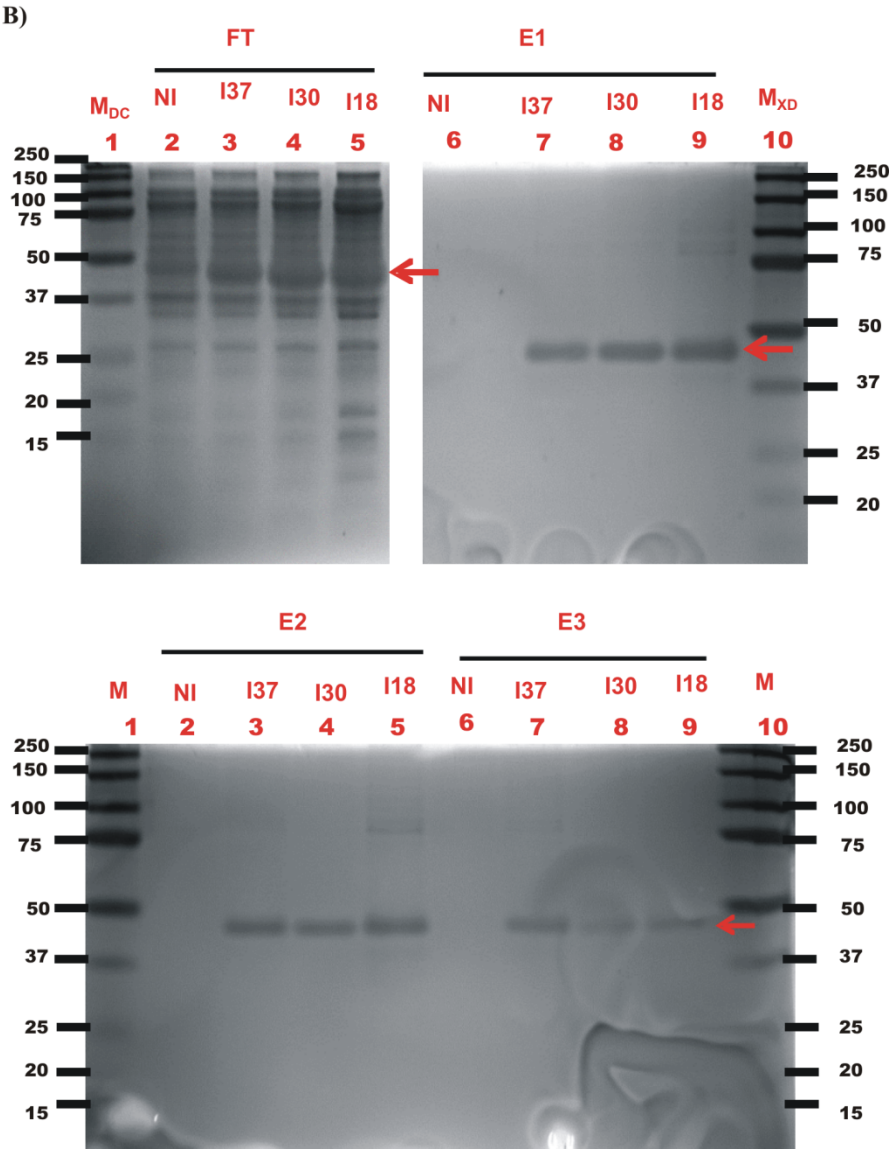
FT
E1
M_DC
NI
I37
I30
I18
NI
I37
I30
I18
M_XD
1
2
3
4
5
6
7
8
9
10
250
150
100
75
50
37
25
20
15
E2
E3
M
NI
I37
I30
I18
NI
I37
I30
I18
M
1
2
3
4
5
6
7
8
9
10
250
150
100
75
50
37
25
20
15

Figure 46: Expression and purification of MBP-p24TMDH. (A) Bacterial growth curve in M9 minimum medium. Bacteria were grown at 37°C until OD 600nm 0.8-0.9 and protein expression induced by addition of IPTG 1mM (see arrow). After induction, cells were grown at 18, 30 and 37 °C under shaking (230 rpm) during 24, 22 and 8 hours respectively. (B) SDS-PAGE analysis of the expression of MBP-TMDH during the purification steps. The total cell lysates were centrifugated and the supernatant corresponding to the total protein extract, was incubated with amylase beads 1h at 4 °C. Beads were settle down by centrifugation at 2000g, 5min and the supernatant (FT) recovered. Beads were thereafter washed to remove the excess of protein and the MBP eluted with the elution buffer (20 mM Tris; 200 mM NaCl; 100mM EDTA, pH 7.4; 10mM maltose). 15µl of FT (equivalent to 500µl of culture) and 20µl the different elution fractions (En) (equivalent to 600µl of culture) were loaded on 12% SDS-PAGE gel. Gels were stained with Coomassie blue after 1h electrophoresis migration at 150V. NI37 corresponds to the non-induced conditions at 37 °C; I37, I30 and I18 to the induced conditions at 37, 30, and 18 °C respectively. M indicates the molecular weight marker

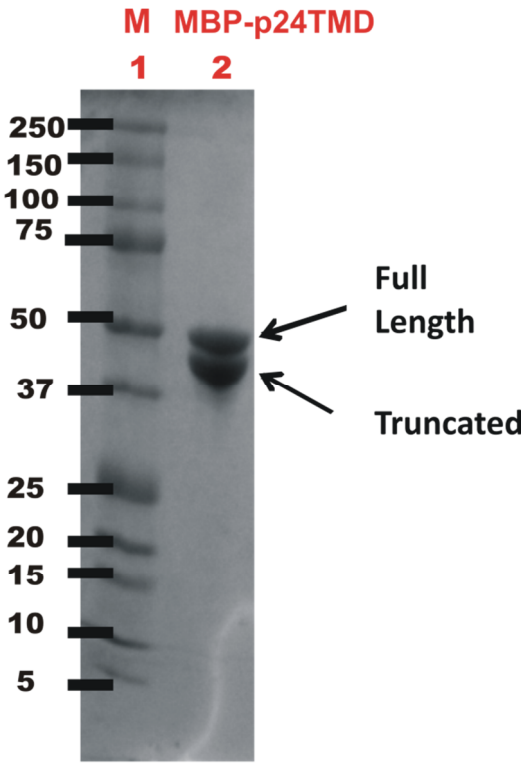

Figure 47: SDS-PAGE profile of the full and truncated MBP-p24TMDH after Coomassie

3.1.2.2. MBP-p24TMDH cleavage and purification of p24TMDH peptide

3.1.2.2.1. Setting of MBP-p24TMDH cleavage

In order to obtain the p24TMDH peptide, MBP-p24TMDH was cleaved using a 52 kDa commercial Tobacco Etch Virus (TEV) protease that contains a histidine and a Glutathione *S*-transferase (GST) tag to facilitate its removal after the cleavage. To set up the best conditions of cleavage, we tested the kinetics of cleavage at different temperatures (RT~25 °C, 4 °C) and protease-to-target protein ratio (w/w) ranging from 1:20 to 1:150. 47µg of purified MBP-p24TMDH in solution was digested with the corresponding amount of enzyme to have the different enzyme to protein ratios at RT or 4 °C during several hours. The products of digestion were sampled at different times and analysed on a 10% polyacrylamide gel by SDS-PAGE (Figure 48A). At T=0, the purified protein contains two bands with the upper one corresponding to the full length protein and the lower one to the truncated protein (MBP5) as shown on Figure 48A (Lane 2). After 30 minutes of digestion, we observed a reduction in the intensity of the full length protein for the ratio 1:20 at RT compared to the other conditions suggesting that the cleavage has started in this condition but is not yet complete. After 4 hours, the digestion is almost total compared to the other ratios. At 4 °C the digestion is nearly total after 24 hours for the same ratio. Based on these results, we therefore deduced that the MBP-p24TMDH digestion is efficient for the ratio 1:20 RT during 4h at or 24h or 4 °C, respectively. However, as our protein is not stable, we choose to achieve the cleavage at 4 °C during 24 h to restrict unwanted proteolysis.

In order to optimize the purification of the peptide and reduce the loss of the fusion protein during the purification steps, we also tested the cleavage on the resin-attached protein thus, reducing the number of steps. This test was performed at 4 °C during 24h for the ratio 1:20 and 1:15 as the later was tested by our collaborator with an expressed TEV-protease. To achieve these ratios, the protein was first purified to estimate its concentration and incubated 1h at 4 °C with amylose resin under gentle agitation. Thereafter, TEV-protease was added for the cleavage. Beads were settled down by centrifugation 5 min at 700g after the cleavage and the supernatant recovered. An aliquot was sampled for electrophoresis analysis and separated on a 10-20% gradient gel to detect the peptide. As shown in Figure 48B, we did not observe low molecular weight band suggesting that the quantity of peptide is likely not detectable. However, we detected bands with high molecular weights indicating that not all proteins that were attached to the amylose resin (Figure 48B, lanes 3 and 4). The two lower bands likely correspond to the truncated and the cleaved MBP as indicated (Figure 48B, lanes 3 and 4 zoom). Even if we did not achieve the control of the supernatant before the cleavage, these observations suggest that a part of the fusion protein is not attached to the resin and the presence of the intermediate band (between the degradation product and the full length protein) indicate that the protein was cleaved and

could correspond to the cleaved MBP. Moreover, the intensity of the bands obtained with ratio 1: 15 and 1:20 are not different.

As the molecular weight of the TEV-protease is 52 kDa, we checked also if the upper band does correspond to this enzyme. With this purpose, the recovered supernatant was incubated for 1h at 4 °C with cobalt resin to get-rid-off TEV-protease as this enzyme contains a His-tag. Beads were settled down by centrifugation and the supernatant recovered. When analysed on SDS-PAGE gel, no difference of intensity was observed for the upper band before and after the incubation with the cobalt resin confirming that this band corresponds to the full length protein MBP-p24TMDH (Figure 48B, lanes 6 and 7).

In conclusion, we set up the conditions of MBP-p24TMDH cleavage in solution and tested these conditions for cleavage on resin in order to optimize the purification of the peptide. Although we showed that the cleavage works in both cases, it was not total. Cleavage on resin did not bring considerable advantages compared to that in solution. It first required a quantification of the protein before a new incubation with amylose thus, a supplementary step of binding to amylose resin which increases the loss of the protein. Therefore, we choose to cleave the protein in directly solution and to follow by the peptide purification. For this purpose, we tested two different methods of purification: the butanol extraction and reverse phase HPLC as it will be presented in the section below.

Notably, although proteins were detected on the gel, we did not detect the peptide even on gradient polyacrylamide gel (Figure 48B), as the total fusion protein (48.2 kDa) is 12 times bigger than the peptide (3.9 kDa). Therefore, for a given molar quantity after the cleavage, only a comparatively small amount of the peptide is produced (by wt).

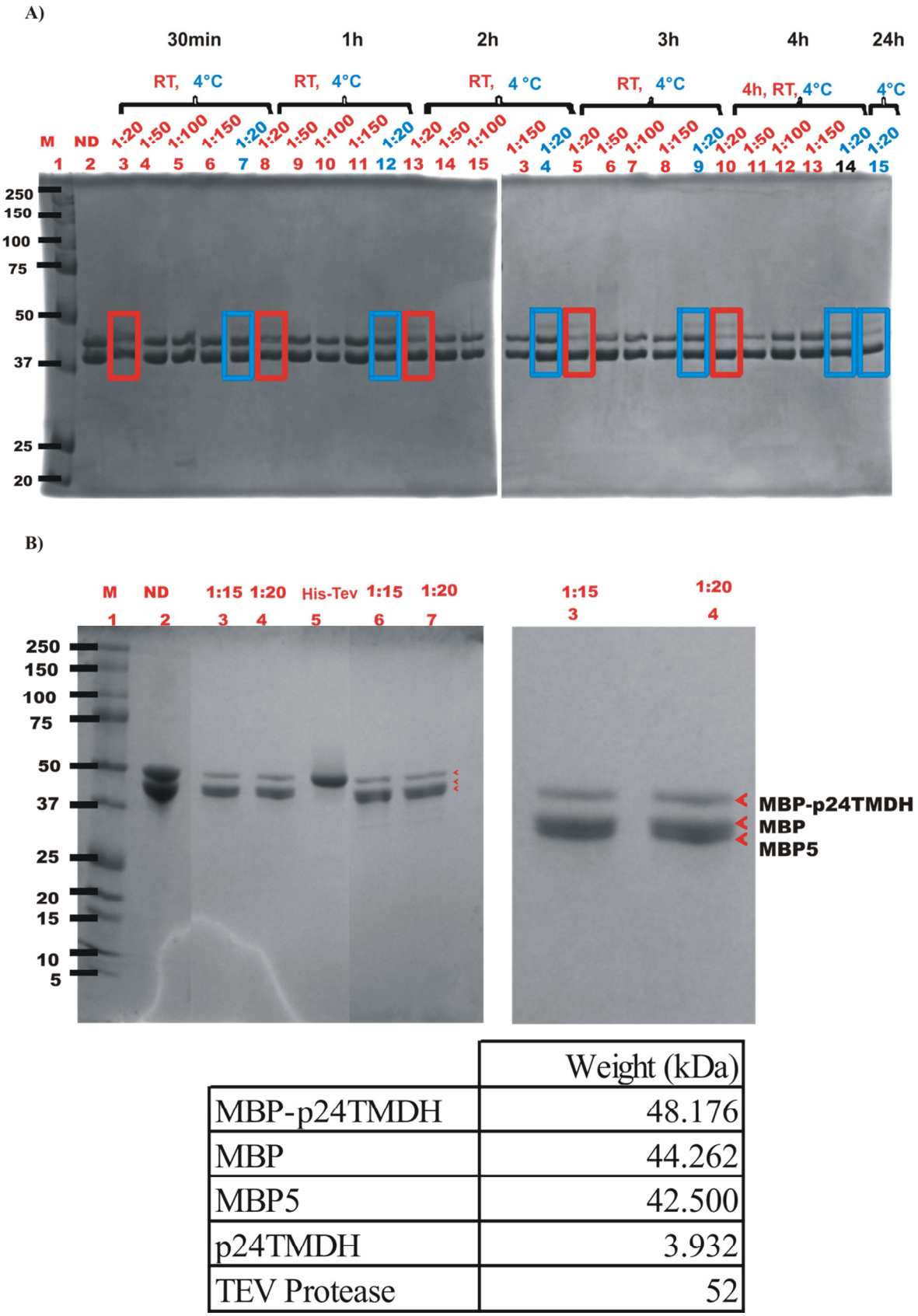

	Weight (kDa)
MBP-p24TMDH	48.176
MBP	44.262
MBP5	42.500
p24TMDH	3.932
TEV Protease	52

Figure 48: SDS-PAGE profile of MBP-p24TMDH cleavage. (A) Kinetic of cleavage in solution at different protease-to-target protein ratios and different temperatures. For each condition, 47µg of

purified protein was digested with the corresponding amount of TEV protease to obtain the different ratios (w:w; 1:20, 1:50, 1:100, and 1:150). The cleavage was then achieved at RT~25°C (red) or 4°C (blue). 1µl (1.6µg) of the different products of digestion and non-digest (ND) protein were sampled at different times (30min, 1h, 2h, 3h, 4h and 24h) and separated on a 10% polyacrylamide gel for 1h at 200V. (B) Cleavage of the resin-bound protein. After incubation of MBP-p24TMDH 1h at 4°C with amylose beads, TEV protease was added and the sample incubated for 24h at 4°C under gentle agitation. Beads were settled-down by centrifugation and the supernatant recovered and incubated with cobalt resin to get-rid-off the TEV protease. Lanes 3 and 4 correspond to the supernatant before incubation with cobalt resin and 6 and 7 to the supernatant after incubation. 5µl (8.5µg) of supernatant was loaded on a 10-20% gradient gel and separated for 1h at 200V with the purpose of identifying the peptide. The well 5 corresponds to the pure His-TEV protease (0.2µg) as reference (or as control). A zoom of lanes 3 and 4 is shown (right) with arrows indicating the MBP-p24TMDH, MBP after cleavage of p24TMD (44.3 kDa) and the MBP-5 (42kDa) corresponding to the truncated MBP. The table summarizes the theoretical molecular weight of the expected protein and peptide

3.1.2.2.2. **Purification and characterization of p24TMDH**

The purification of p24TMDH was tested using analytical reverse phase HPLC or butanol extraction as mentioned above. The later method relies on the separation of molecules based on their physico-chemical properties during solvent phase partitioning. Butanol is often added to samples in solution and molecules separate between two phases after vortex and centrifugation. Hydrophobic molecules will concentrate in the butanol phase while the hydrophilic molecules will stay in the polar solvent.

After purification, the characterization of the peptide was achieved by electrophoresis and/or MALDI-TOF (Matrix-Assisted Laser Desorption/Ionization Time-Of-Flight) spectrometry. For the later, the best conditions to detect the peptide were first set up using the two main butanol extraction fractions named SNB (butanol supernatant) and PB (butanol pellet) that were received from our collaborator in which they identified p24TMDH by mass spectrometry. These fractions were obtained as described in the experimental butanol extraction protocol (Figure 42). When prepared with α-cyano-4-hydroxycinnamic (α-cyano) matrix and analyzed by MALDI-TOF using linear mode detection, the resulting spectra displayed peaks corresponding to the expected mass of the peptide with and without Na+ ions adduct (Figure 49). These results confirmed the presence of p24TMDH in these fractions. We therefore used these conditions for further detection of the peptide.

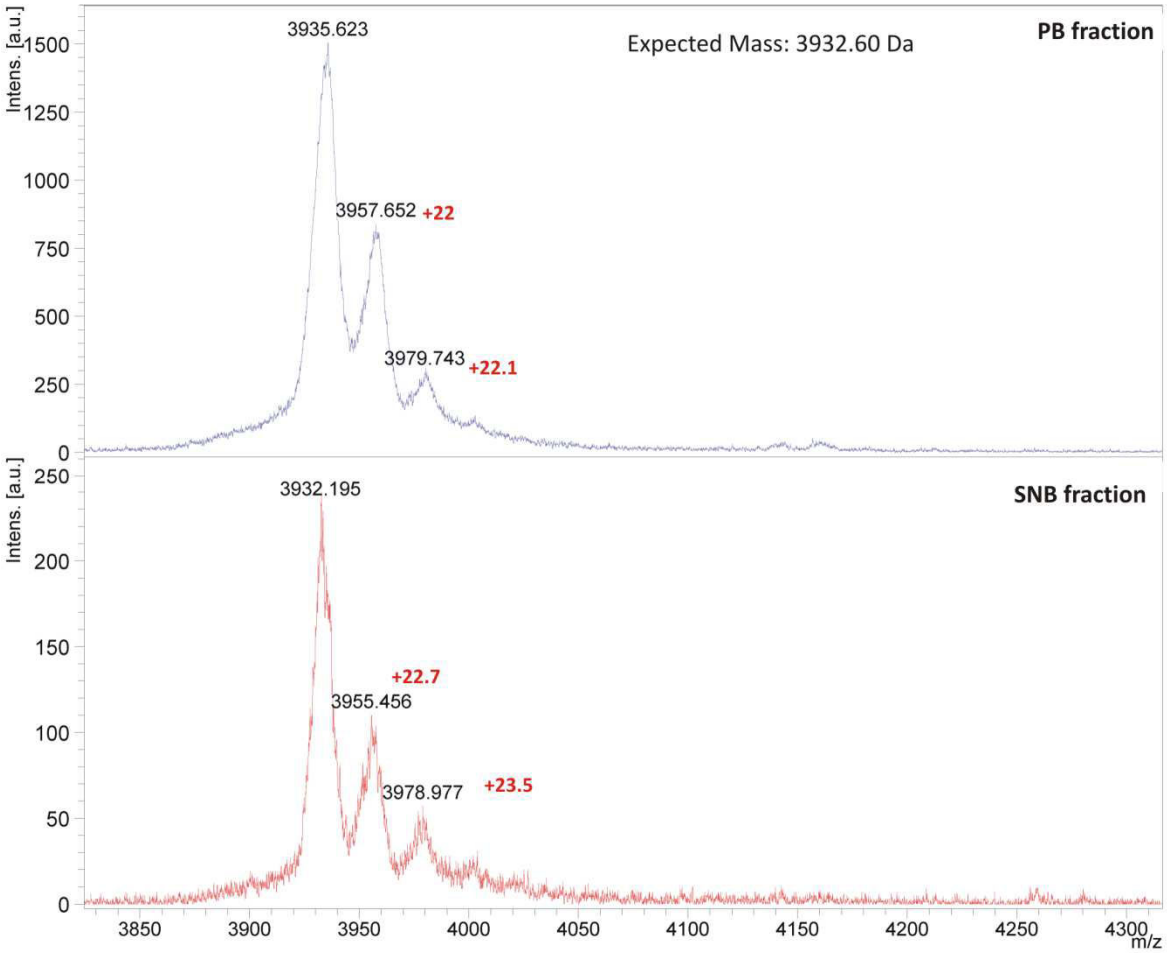

Figure 49: p24TMDH mass spectrometry. The main butanol extraction fractions containing the peptide (butanol phase supernatant and pellet) were received from our collaborators. These fractions were resuspended in 30% acetonitrile/ 0.1% TFA/water and 1µl mixed to 1µl α-Cyano matrix on the target. The sample was dried at air and analyzed on a MALDI-TOF spectrometer using linear mode detection. The spectrometer was calibrated with a mixture of peptide ranging between 1000 and 3500 Da (peptide calibration standard, Bruker, Bremen, Germany). Abbreviations: PB (pellet of the butanol phase); SNB (supernatant of the butanol phase).

3.1.2.2.2.1. Characterization of p24TMDH after butanol extraction

Butanol extraction purification was developed by our collaborators and the protocol sent to us. Our first test was achieved from a small scale protein expression in LB after TEV protease cleavage at ratio 1:50 24 h at 4 °C as this new condition of cleavage as described above was not yet tested. Butanol was added to the product of cleavage to achieve the final volume ratio 2:3 (aqueous solution: butanol, v/v) and the different fractions were obtained after subsequent steps of vortex, centrifugation as described below (Figure 50A). These fractions were loaded on a 15% polyacrylamide gel and the proteins separated in denaturing conditions by SDS-PAGE. As shown on the gel electrophoresis Figure 50B, the product of cleavage (lane 2) presents two bands with the lower one of more important

intensity indicating that the protein was cleaved. However, the cleavage was not total as an important part of full length protein remains in the upper band. Among the butanol extraction fractions that were deposited, the peptide was not observed in any of them but some of the non cleaved protein (lanes 7) and the truncated protein (lanes 6 and 7) were detected in the aqueous phases. When all the fractions were analyzed by mass spectrometry for the presence of the peptide, as our collaborator, the peptide was identified only into the SNB and SP fractions and not in the others (Figure 50C). Indeed, the mass spectra present peaks with the expected mass of peptide and closely related masses of peptide with Na+ ions adduct, thereby confirming that the peptide accumulated in SNB and SP fractions. Although we did not detect the peptide on SDS-PAGE gel, MALDI-TOF allowed us to characterize its presence.

However, these set conditions did not allow the detection of the peptide in a reproducible way which is an important prerequisite for further expression studies.

Indeed, when the fusion protein was expressed later in large quantities, after purification and cleavage, we did not detect the presence of the peptide neither by electrophoresis (Figure 51A) nor by MALDI MS (not shown). However, when compared the electrophoresis profile of the product of cleavage to the one of the uncleaved protein (Figure 51A lane 3 and 1 respectively), the presence of a much more intense lower band for the first indicated that the protein was cleaved. Moreover, the mass spectrum of the cleavage product revealed the presence of a peak with a mass close to the one expected for the cleaved MBP with an addition of ~ 186 Da. Unfortunately, we could not explain this difference (Figure 51B). Together with gel electrophoresis analysis, this result is consistent with the fact that the cleavage worked.

Thereafter, the peptide was purified by butanol extraction and the main fractions in which the peptide was expected (SNB, PB) separated on SDS-PAGE gel. In order to have an idea of the apparent molecular weight of the peptide on the gel, synthetic p24TMD (with a sequence slightly different from the one of p24TMDH peptide) was separated on the same gel as we did not succeed to purify the later as mentioned earlier.

Given that the theoretical molecular weight of the two peptides p24TMD and p24TMDH differ by about 0.3 kDa, we expected that they migrate at the same size. As shown on the gel, a band corresponding to the synthetic p24TMD was identified around 5kDa (Figure 51A, lane 7). A negative control of the peptide stability during the TEV protease cleavage was achieved during 24h at 4 °C and loaded on the same gel (Figure 51A, lane 8). As it separated at the same apparent molecular weight than the previous, we therefore concluded that this enzyme does not cleave the peptide. We did not observe any lower band for the two butanol fractions suggesting that the peptide is not present. However, as the theoretical total amount of peptide expected in these fractions was 0.34mg, which is more than the protein detection limit from a polyacrylamide gel using the coomassie-R250 staining (100ng), we cannot really explain why the peptide was not detected. Therefore, we can only speculate that the peptide could aggregate as we previously suggested due to its hydrophobicity. Its presence was not characterized by MALDI-TOF using the previous

conditions of detection (data not shown). This complication with detection could also be related to the difficulty of the peptide to be ionized.

Therefore, we decided to use in addition another mass spectrometry technique, the tandem mass spectrometry with a MALDI source to analyse the different bands observed on the gel to detect the peptide. In addition, to characterize the difference in sequence between the truncated and the full length protein, the uncleaved protein was also analyzed. The different bands highlighted on the gel shown Figure 51A with arrows (numbered from 1 to 8) were cut and sent for analyses by the mass spectrometry service of the molecular and cellular biology institute (IBMC).

In order to analyse the sequences of the bands 1 to 3 (Figure 51A, lane 1) which correspond to the uncleaved fusion protein, they first performed a trypsin digestion of the protein in solution in order to generate a bank of fragments that wash used for comparison with the fragments obtained from the trypsin digestion of the cut-out bands. Here, we only focused our analysis on the C terminus of the MBP-p24TMDH fusion protein. The mass spectra of the different C-terminal fragments that were generated from trypsin digestion of MBP-p24TMDH are shown Figure 51C (spectra on top). When compared to the mass spectra of trypsin digestion of the bands 1, 2 and 3, we noticed that they all shared the presence of the peptides with the following molecular weight: 3459.546, 975.462 and 184.859 Da. These peptides correspond to the cleaved fragments of the MBP protein between residues 368 to 413. The peptide at 2959.663 Da is a part of the p24TMDH peptide as present on Figure 51C. This later fragment was not identified in bands 2 and 3 but only in band 1, thus, indicating that the truncated version of the fusion protein lacks the C-terminus of our peptide of interest. Interestingly, as this fragment is common to p24TMD and p24TMDH peptides, its presence could have be found in bands 4, 5, 6 and 8. As shown in Figure 51D, this fragment was not identified in any of these bands but only for p24TMD synthetic peptide digested with trypsin suggesting that the peptide is not present or is hardly detectable even in butanol extraction fractions in which they were previously identified. Interestingly, the presence of the other expected fragments were also characterized as shown on the full MALDI spectra confirming that the trypsin digestion of the synthetic peptide was efficient (Figure 51D). However, we only looked for the presence of the monomeric peptide and it would have been interesting to search in the range of the dimeric peptide. The band 7 was identified as the TEV protease.

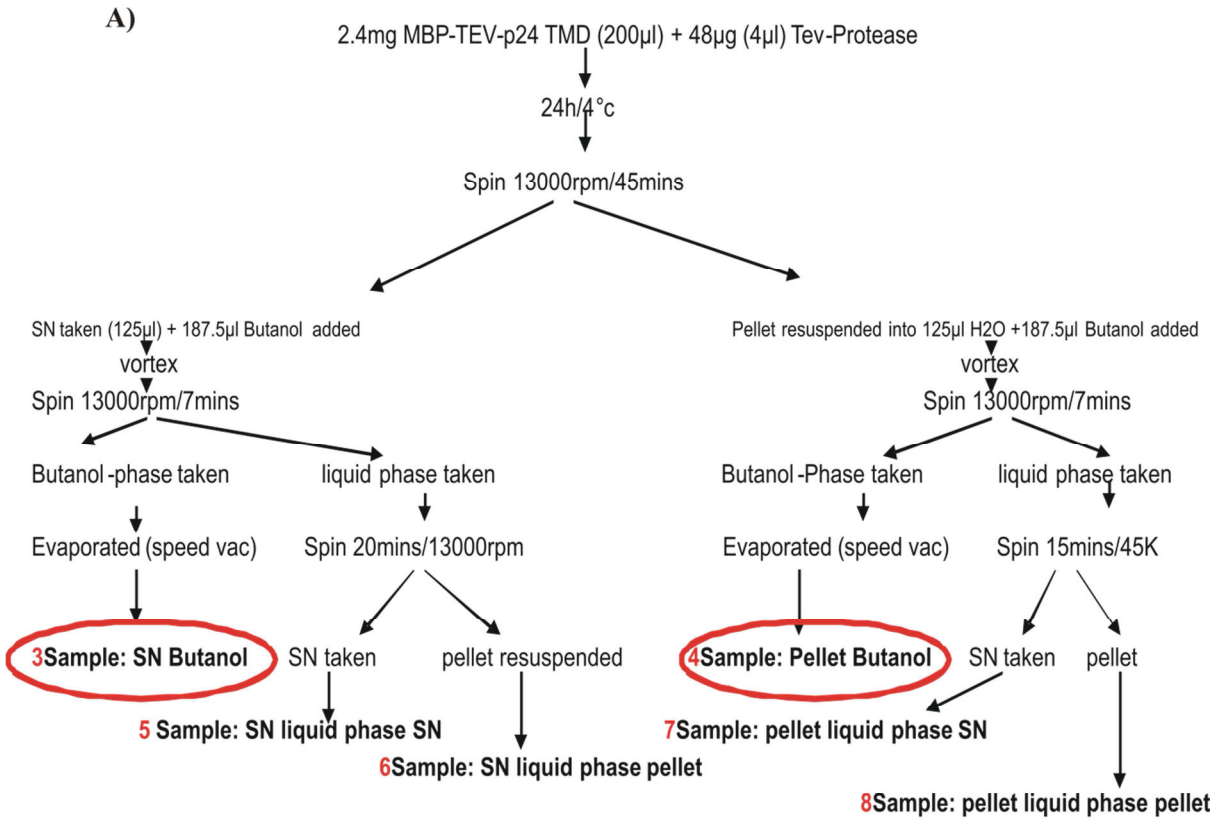
A)
2.4mg MBP-TEV-p24 TMD (200µl) + 48µg (4µl) Tev-Protease
24h/4°c
Spin 13000rpm/45mins
SN taken (125µl) + 187.5µl Butanol added
vortex
Spin 13000rpm/7mins
Butanol -phase taken
liquid phase taken
Evaporated (speed vac)
Spin 20mins/13000rpm
3Sample: SN Butanol
SN taken
pellet resuspended
5 Sample: SN liquid phase SN
6Sample: SN liquid phase pellet
Pellet resuspended into 125µl H2O +187.5µl Butanol added
vortex
Spin 13000rpm/7mins
Butanol -Phase taken
liquid phase taken
Evaporated (speed vac)
Spin 15mins/45K
4Sample: Pellet Butanol
SN taken
pellet
7Sample: pellet liquid phase SN
8Sample: pellet liquid phase pellet

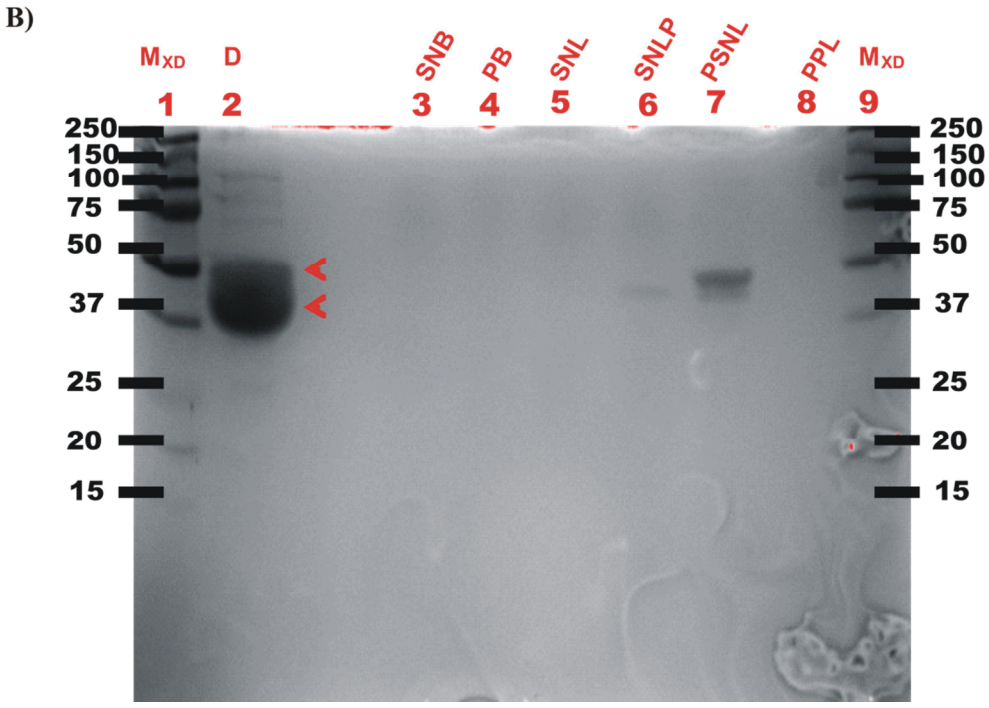
B)
MXD
D
SNB
PB
SNL
SNLP
PSNL
PPL
MXD
1
2
3
4
5
6
7
8
9
250
150
100
75
50
37
25
20
15

C)

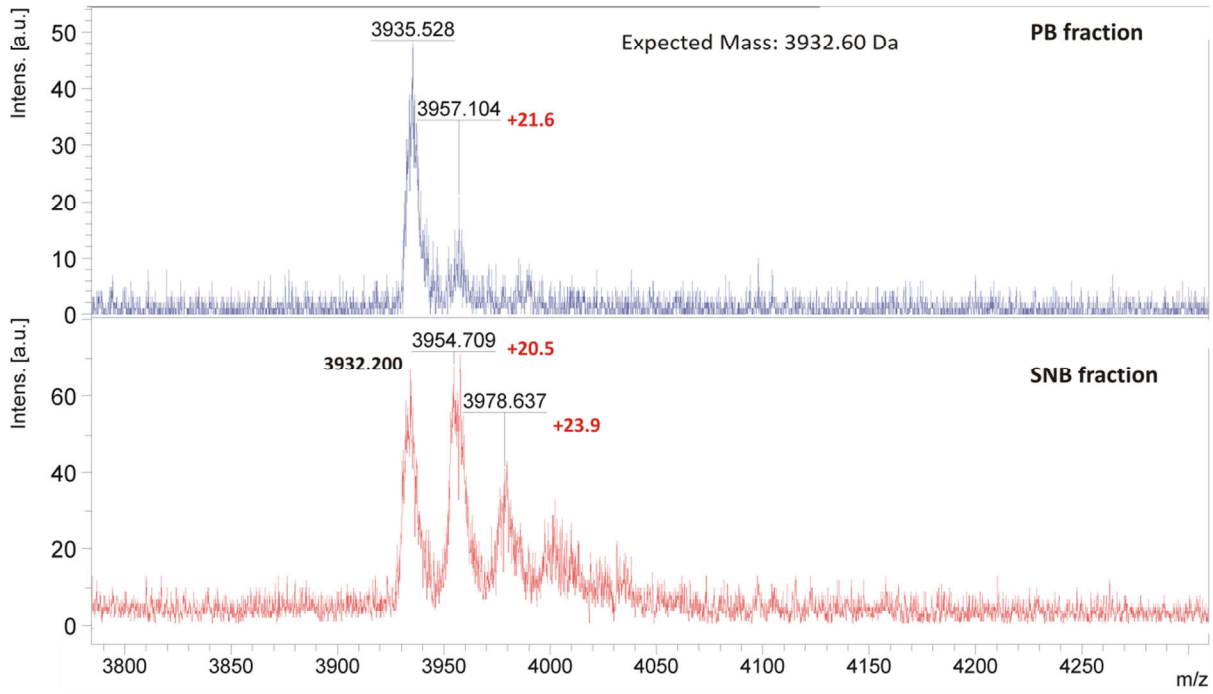

Figure 50: p24TMDH purification and characterization by SDS-PAGE and mass spectrometry. 2.5mg of MBP-p24TMDH was cleaved with 48µg of TEV protease achieving the ratio (50:1). (A) The peptide was thereafter purified as described on the butanol extraction protocol above. (B)1.5µl of each fraction and 15µl (180µg) of the cleavage product were loaded on a 15% polyacrylamide gel and protein separated for 1h under 150V, 300mA. The Protein ladder (M_{XD}) was separated simultaneously and the gel stained with Coomassie blue. The different abbreviations are defined in the butanol extraction protocol; D is for the digest product. (C) In parallel, 1µl of each fraction was mixed to 1µl α-Cyano matrix on the target, dried at air and analyzed by MALDI-TOF mass spectrometry using linear mode detection. The spectrometer was calibrated with a mixture of peptide ranging between 1000 and 3500 Da (peptide calibration standard, Bruker)

These results show that butanol extraction allows in some cases the purification of the peptide. However, its detection seems to be difficult due to the peptide's hydrophobic character. Indeed, when the cleavage product was mixed with HFIP to achieve a 50% HFIP/water ratio, that was shown as we will see in the next chapter to promote the helical conformation of the peptide, it results in aggregation as shown Figure 51E. We observed two phases with a white film in between and a precipitate. When the different phases including the white pellet were analyzed by SDS-PAGE and MALDI, we did not detect the peptide but rather the cleaved and uncleaved MBP (not shown). This observation is consistent with the synthetic p24TMDH peptide aggregation we encountered and which impaired its purification after solid phase peptide synthesis. However, as we did not analyse the presence of oligomeric peptide, we cannot really say if the peptide aggregates by forming oligomers during the purification. In addition, we also considered that the

peptide could also stick on the wall of the Eppendorf tubes due to its hydrophobic properties. For this reason, special tubes that prevent this adhesion on the wall were used to avoid this problem.

A)

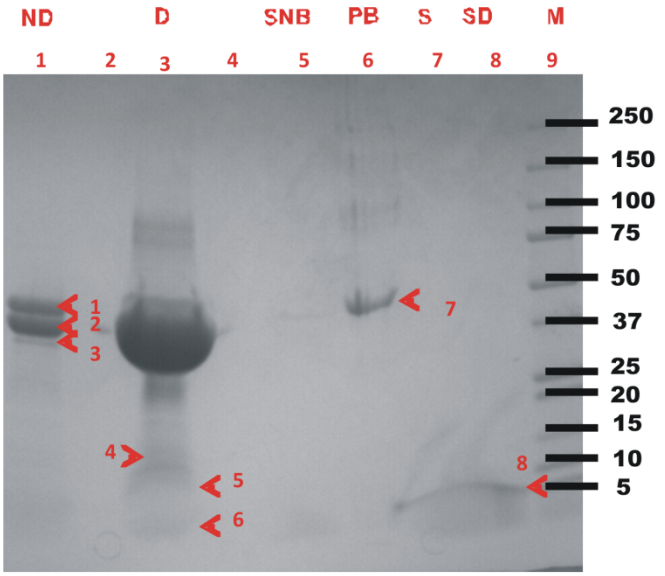

B)

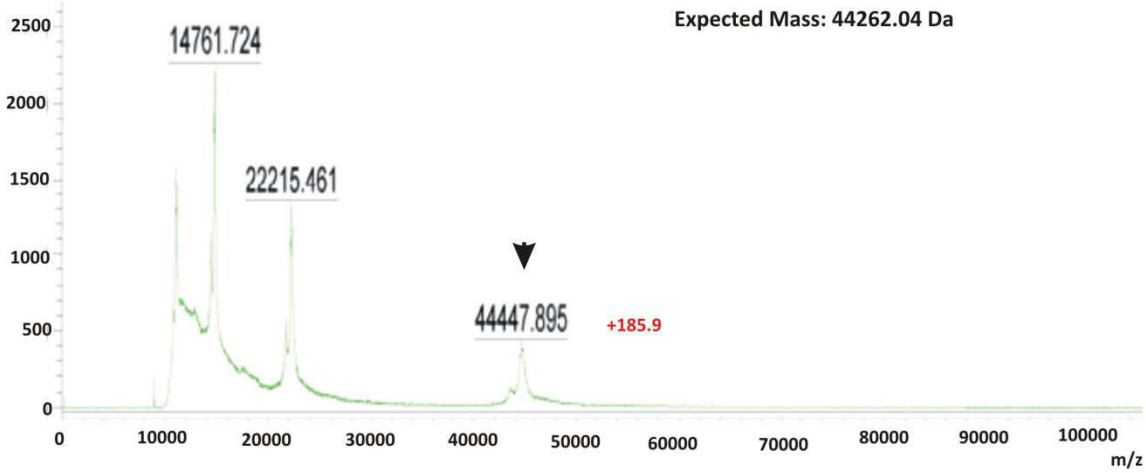

C)

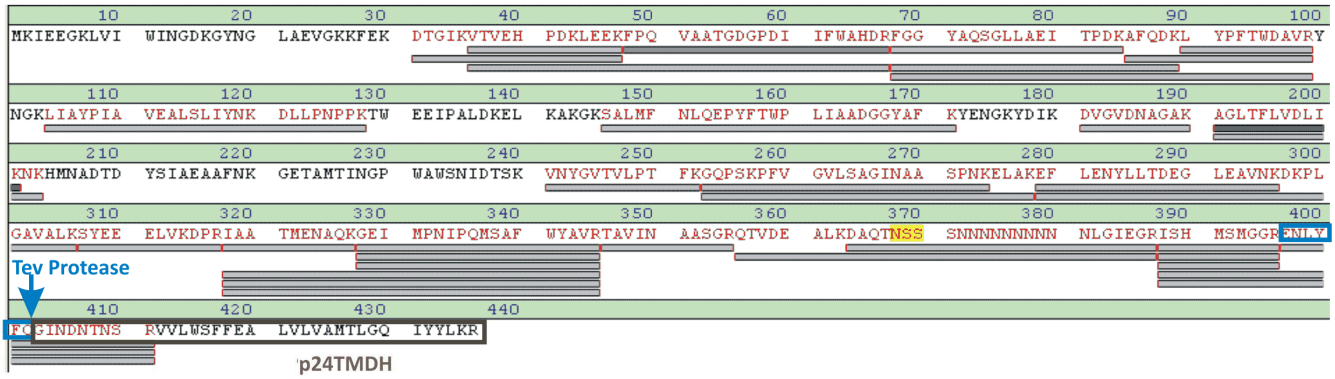
MKIEEGKLVI WINGDKGYNG LAEVGKKFEK DTGIKVTVEH PDKLEEKFPQ VAATGDGPDI IFWAHDRFGG YAQSGLLAEI TPDKAFQDKL YPFTWDAVRY
NGKLIAYPIA VEALSLIYNK DLLPNPPKTW EEIPALDKEL KAKGKSALMF NLQEPYFTWP LIAADGGYAF KYENGKYDIK DVGVDNAGAK AGLTFLVDLI
KNKHMNADTD YSIAEAAFNK GETAMTINGP WAWSNIDTSK VNYGVTVLPT FKGQPSKPFV GVLSAGINAA SPNKELAKEF LENYLLTDEG LEAVNKDKPL
GAVALKSYEE ELVKDPRIAA TMENAQKGEI MPNIPQMSAF WYAVRTAVIN AASGRQTVDE ALKDAQTNSS SNNNNNNNNN NLGIEGRISH MSMGGRENLY
Tev Protease
FQGINDNTNS RVVLWSFFEA LVLVAMTLGQ IYYLKR
p24TMDH


3459.610212
356 - 387 QTVDEALKDAQTNSSSNNNNNNNNNNLGIEGR
Intensity: 4.33%
975.456413
388 - 396 ISHMSMGGR
Intensity: 9.54%
1784.858516
397 - 411 ENLYFQGINDNTNSR
Intensity: 6.61%
2959.663182
412 - 436 VVLWSFFEALVLVAMTLGQIYYLKR
Intensity: 0.93%

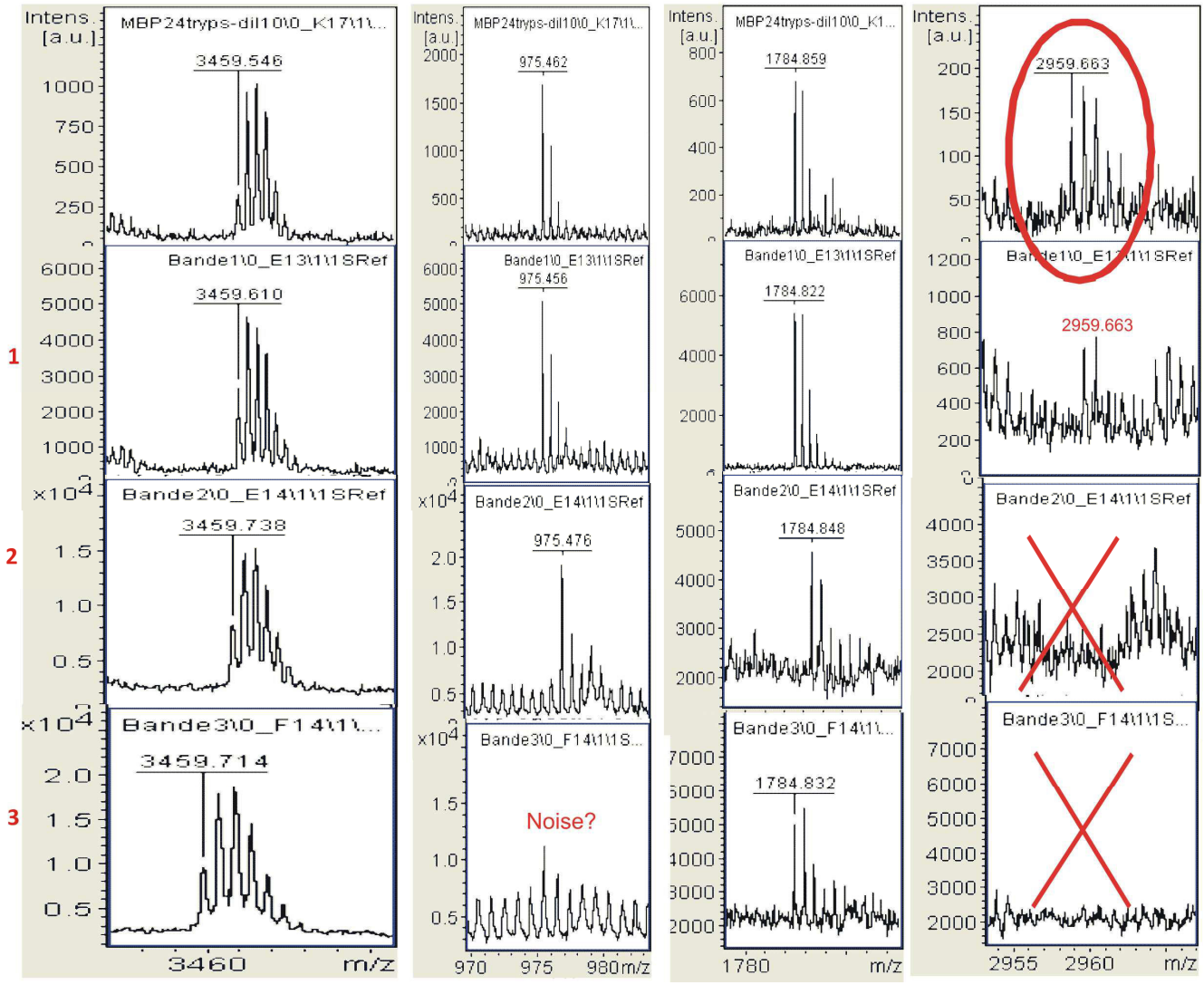
Intens. [a.u.]
MBP24tryps-dil10\0_K17\1\...
3459.546
Bande1\0_E13\1\1SRef
3459.610
Bande2\0_E14\1\1SRef
3459.738
Bande3\0_F14\1\...
3459.714
m/z
975.462
975.456
975.476
Noise?
970 975 980 m/z
MBP24tryps-dil10\0_K1...
1784.859
1784.822
1784.848
1784.832
1780 m/z
2959.663
2959.663
2955 2960 m/z
1
2
3

D)

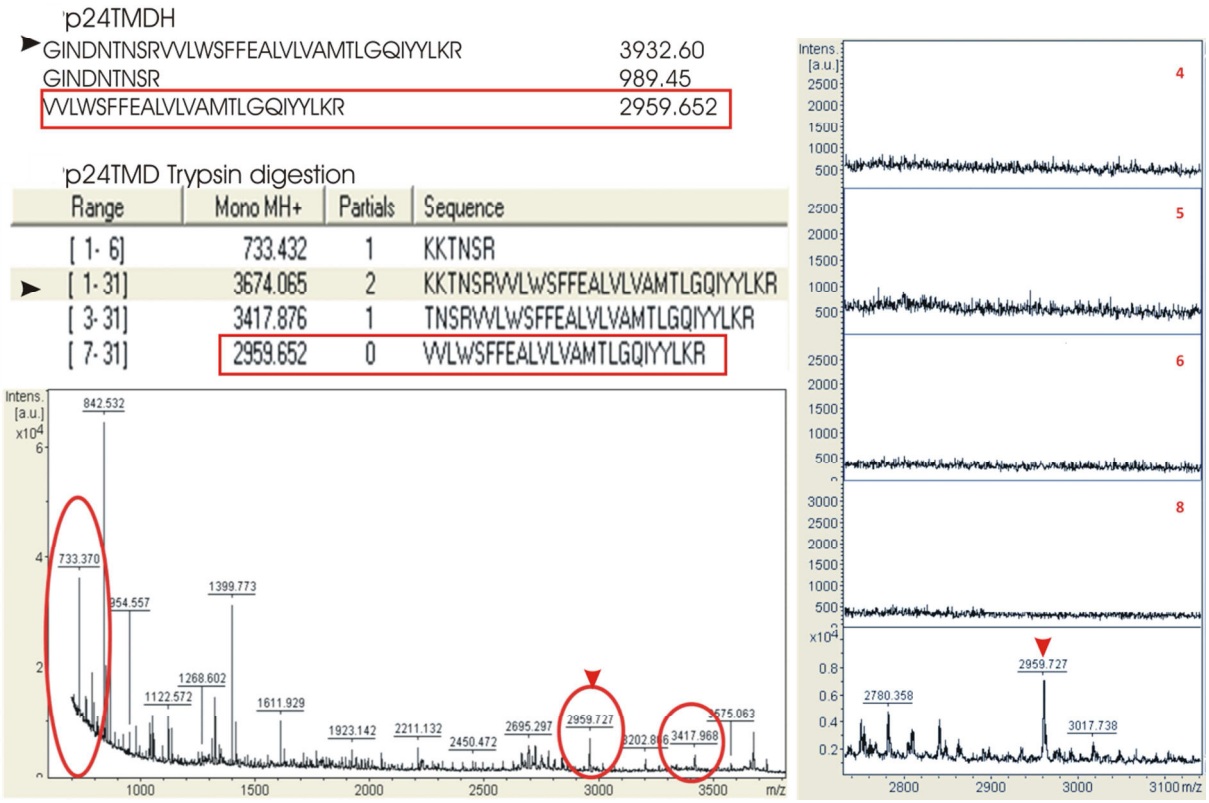

E)

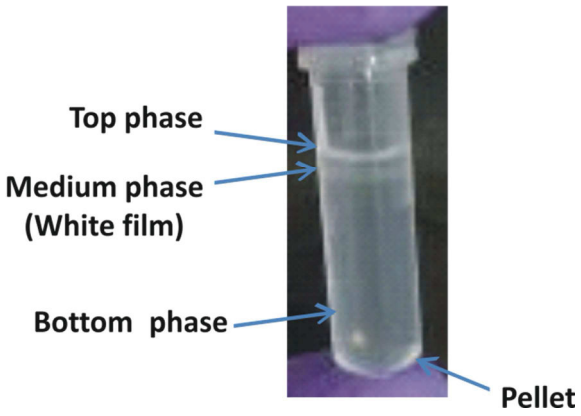

Figure 51: (A) SDS-PAGE of the uncleaved (ND, 15µg) and cleaved (D, 185µg) MBP-p24TMDH fusion protein, the butanol fractions (SNB and PB), the cleaved (SD, 30µg) and uncleaved (S, 30µg) p24TMD synthetic peptide. The different samples were separated in a 4-20% polyacrylamide gel in denaturing conditions. Protein ladder (M) was separated simultaneously and the gel stained with Coomassie blue. (B) 1µl of the product of MBP-p24TMDH cleavage was mixed to 1µl SA matrix on the target, dried at air and analyzed by MALDI-TOF mass spectrometry using linear mode detection. The spectrometer was calibrated with a mixture of proteins ranging between 4000 and 20000 Da (protein calibration standard I, Bruker). (C) Mass spectrometry spectra of the MBP-p24TMDH digested with trypsin (control, top) and that of the bands 1, 2 and 3 cut from the gel are shown (A). The MBP-p24TMDH was first digested with the trypsin and the generated fragments

used to provide a bank of peptides. Their presence was thereafter found after the trypsin digestion of the bands cut on the gel by comparison of the mass spectra. (D) Mass spectrometry of p24TMD synthetic peptide and the bands 4, 5, 6, 8 after trypsin digestion. The spectra C and D were obtained by MALDI without fragmentation with a reflectron mode and provided by the mass spectrometry service at the molecular and cellular biology institute. The black arrows pinpoint the p24TMD and p24TMDH sequences with their expected masses. (E) Product of cleavage with 50% HFIP (v/v). 9 mg of purified MBP-p24TMDH from M9 medium culture was cleaved in solution with TEV protease with the final protein/enzyme ratio 20:1. Addition of HFIP to 7.714 mg of total cleaved protein, (1:1, v/v), lead to different phases and a white precipitate after vortexing and centrifugation

3.1.2.2.2.2. Characterization of p24TMDH after reverse phase HPLC

As for the butanol extraction, the first test of peptide purification by reverse phase HPLC was achieved starting from a small scale LB protein expression. After cleavage on resin, amylose beads were settled down by centrifugation at 700g for 5min and the supernatant injected on an analytic column (ProntoSIL 300-3-C4). HPLC was performed using an acetonitrile/water gradient during 30min. The resulting chromatogram is shown in Figure 52A. The different fractions 1, 2 and 3 were eluted at 45, 50 and 53% of solvent B (100% acetonitrile + 0.1% TFA) respectively. Intriguingly, although they were eluted at different percentage of solvent B, the mass spectra revealed the presence of peptides with quite close mass (Figure 76B). However, these masses do not correspond to the expected one but could correspond to p24TMDH lacking three residues at the N-terminus (3648.28 Da). However, we can only speculate as we showed above that the peptide is stable during TEV cleavage (Figure 51A) and the possible trypsin cleavage sites in p24TMDH do not predict the detected masses. Therefore, these peptides could also result from the digestion of the MBP of the protein. Again, these peptides were not detected on an SDS-PAGE gel but rather a high molecular weight protein was observed in fraction 1 and likely corresponds to the cleaved MBP (Figure 50B).

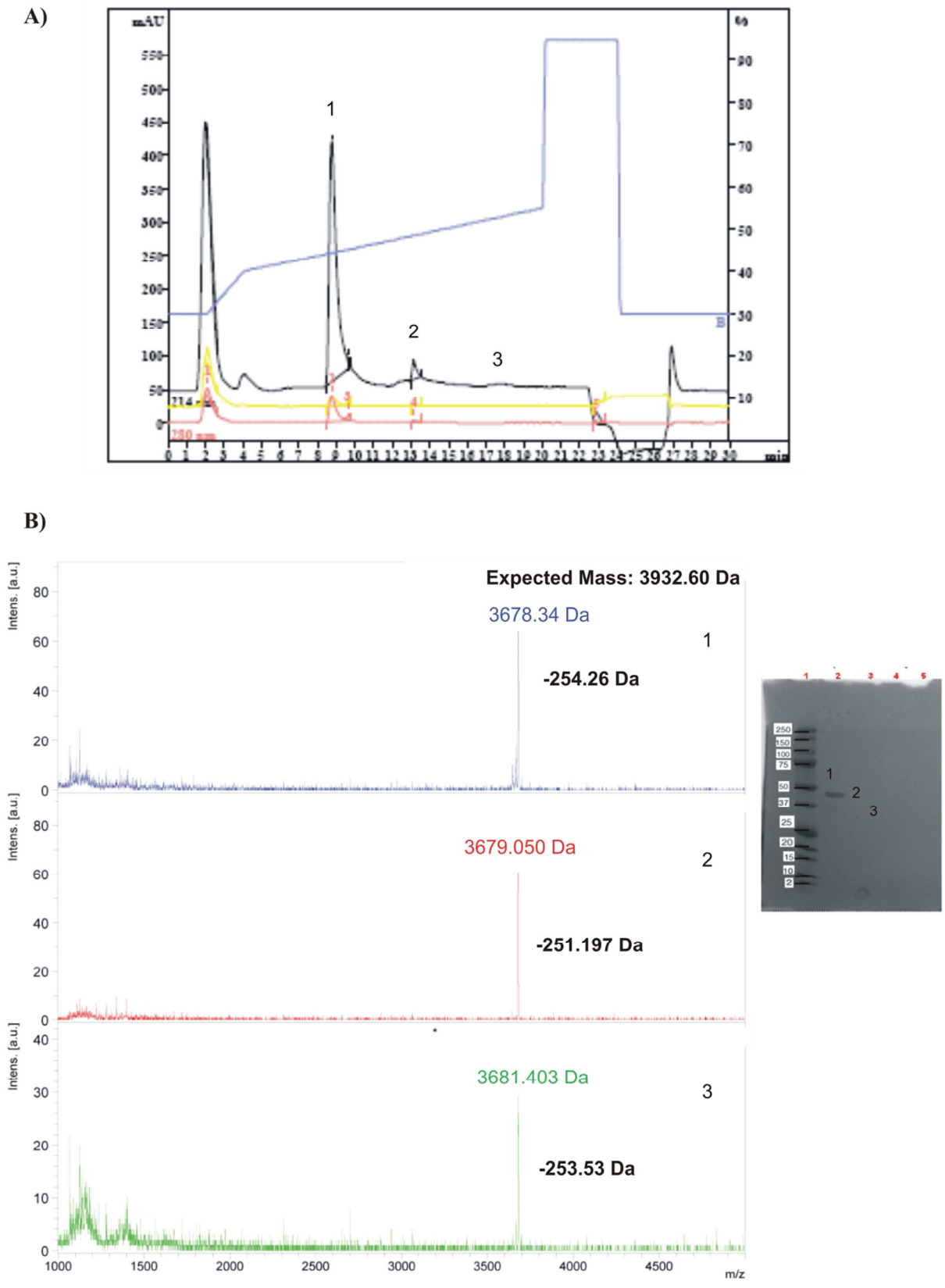

Figure 52: Purification and characterization of p24TMDH after cleavage of the resin-attached MBP-p24TMDH. (A) The reverse phase HPLC chromatogram of the supernatant that was recovered after cleavage from the amylose resin. After cleavage on resin (1:20 protease-to-protein

ratio), beads were settled down and the supernatant (equivalent of 148µg of protein) was injected a ProntoSIL 300-3-C4 analytic column. The sample was purified under a 10-95% acetonitrile/water gradient on Bischoff device. (C) 0.5µl of the different elution fractions were mixed to the same volume of α-cyano matrix and analyzed using a linear mode on a MALDI-TOF spectrometer. HPLC fractions were lyophilized, loaded on a 10-20% gradient polyacrylamide gel and separated for 1h at 200mV. The gel was stained with Coomassie blue

3.1.3. Conclusion

In summary, we set up the conditions of expression of MBP-p24TMDH in rich and minimum medium with the purpose of protein labelling in the later. Although the electrophoresis profile revealed that the protein was overexpressed, we noticed the presence of a truncated version of the protein. Unfortunately, this protein was more abundant (2/3) than the full length protein. In addition, a considerable part of proteins was lost in the flow through due to the weak interaction with amylose resin thus, reducing the final yield of proteins and peptides. However, although we set up the conditions of cleavage; we could hardly detect the peptide after purification by butanol extraction or reverse phase HPLC. The first explanation to that is the important molecular weight ratio between the full length protein and the peptide that contributes to reduce the final amount of peptide. In addition, as the truncated protein was shown by MALDI to lack a part of the peptide (C-terminus); it thus also affects the final yield of the peptide. Furthermore, the peptide likely also aggregates due to its hydrophobic character as we shown. All these problems emphasize our difficulty to detect the peptide in a reproducible manner.
With the purpose to optimize our chance to produce the peptide, another expression vector system commonly used in our laboratory, the pTIPX4 was also tested. It allows the expression of peptides with fusion protein partner TAF12 which drives proteins into inclusion bodies. The results we obtained are presented in the following section.

3.2. Expression **of** p24TMD as a TAF12 fusion protein

3.2.1. Experimental

3.2.1.1. Construction of the recombinant expression vector pTIPX4-p24TMD*

The pTIPX4-p24TMD* (5632 pb) vector was obtained from the pTIPX4-fpTM (5713 pb) expression vector which is used in our laboratory to express the fusion peptide (fp) of the HIV gp41. The pMA-p24TMD (2480 pb) cloning vector was purchased from GeneArt® harboring the nucleotide sequence encoding for p24TMD. 3µg of pTIPX4-fpTM and 10µg of pMA-p24TMD were first double digested separately for 2h at 37 °C by *BamH*I (1U/µg) and *Sac*I (5U/µg) (New England Biolabs) restriction enzymes generating incompatible ends that prevent the recircularization of the vector. After the digestion, enzymes were inactivated for 20 min at 65 °C. The digest pTIPX4 was dephosphorylated with antartic phosphatase (5U/3µg) (New England Biolabs) for 1h at 37 °C and the enzyme was inactivated for 10 min at 65 °C. The pTIPX4-fpTM and pMA-p24TMD products of digestion were separated on a 1 and 2% agarose (Agarose high resolution 1000bp, Carl Roth) gel for 30 min at 100V. The pTIPX4 (5522 pb) and p24TMD (110pb) fragments of interest were purified and ligated in the presence of the T4 DNA ligase (New England Biolabs) at 16 °C overnight. The compliance of the vector was confirmed by *BamH*I and *Sac*I double digestion and nucleotide sequencing.

3.2.1.2. Agarose electrophoresis

This method was used to separate nucleotide fragments after digestion with restriction enzymes. Product of digestion was mixed with the Orange G xylenecyanolblue 6X HP05.1 (Carl Roth, Karlsruhe, Germany) a loading buffer which contains a dye that helps to follow the migration. Samples were loaded on a 1 or 2% agarose gel, respectively, and separated in TAE 1X (40 mM Tris acetate, 1 mM EDTA, pH 8.2) for 35 min at 100V. 5µl of 50pb and 1kb DNA ladders were separated simultaneously to determine the apparent molecular weight of the nucleotide fragment. Agarose gels were prepared with ethydium bromide (EtBr) which is a commonly used for DNA detection. Indeed, this dye is more fluorescent under UV excitation when it intercalates between DNA base pairs. A picture of the gel was performed with the reader (E-box VX2, Vilber, Eberhardzell).

3.2.1.3. TAF12-p24TMD expression

A pre culture of 8 ml LB medium (0.1% glucose, kanamycin 50µg/ml) was inoculated with a colony of BL21 AI transformed with pTIPX4-p24TMD*. After overnight incubation at 37 ° C, this pre culture was used to seed 50 ml LB medium (0.1% glucose, kan 50 µg/ml) at a 1/25 dilution. The kinetics of bacterial growth at 37 °C was monitored each 30 min by measurement of the optical density (OD) at 600nm (Uvikon spectrometer). Protein

expression was induced by addition of IPTG and arabinose when the bacteria are in the exponential phase of growth (OD 600nm ~ 1). Induction was achieved with the final concentrations of 0.8mM IPTG and 1% arabinose during 3 hours at 37 °C. Before the induction, a part of the bacterial suspension was collected for the negative control of expression. Bacteria were thereafter harvested by centrifugation for 15 min 5000 g at 4 °C at the pellet kept at -20 °C for protein extraction.

3.2.1.4. **Protein extraction**

Before cells were harvested, 10 ml of induced and uninduced bacteria culture were sampled and protein extracted as described here for this given volume of culture. The thawed bacterial pellets were taken up in 2 ml of lysis buffer (50 mM Tris; 300 mM NaCl; 0.5% Triton, pH 8) and then sonicated twice for 5 min at 50% of the time cycle (Tip sonicator, Bandelin Sonopuls HD 200, Berlin, Germany). 10 µl (equivalent of 50 µl culture) of obtained lysate are collected and constitute the total sample lysate (ET). After centrifugation at 11000 g, for 30 min at 4 °C, 24 µl (equivalent of 120 µl culture) of the supernatant named soluble fraction (FS) was sampled. The bacterial pellet which corresponds to the insoluble fraction (membrane + inclusion body) was washed twice with washing buffer (50 mM Tris; 300 mM NaCl, pH 8) to remove Triton. In order to separate membrane (Mbe) from inclusion bodies (CI), the pellet was finally resuspended in denaturing buffer (50 mM Tris; 300 mM NaCl, 6 M Guanidine at pH 8) and the suspension incubated on the wheel (20 rpm) at RT overnight. After centrifugation at 12,900 g for 20 min at 20 °C, the supernatant (inclusion bodies) was collected and 12 µl (equivalent of 60 µl culture) sampled. The pellet (membrane fraction) was resuspended with the loading buffer 1X and 12µl (equivalent of 1.2 ml culture) was loaded on the gel for SDS-PAGE. All the other aliquots were also prepared with the loading buffer 5X (0.25 M tris-HCl pH 6.8; 0.5% bromophenol blue; 0.5 M DTT; 50% glycerol; 10% SDS) for SDS-PAGE analysis.

3.2.1.5. **Protein purification by cobalt affinity chromatography**

After solubilisation of the insoluble fraction (bacteria pellet made of membrane and inclusion bodies) in Guanidine 6M, inclusion bodies fraction (from 10 ml culture) was incubated with 100 µl cobalt resin (in suspension) for 1h at room temperature on the wheel (rotation 250 rpm) to fix our protein of interest which harbours a Histidine tag (His tag). Thereafter, resin was settled by centrifugation at 750 g for 5 min at RT and the supernatant (Flow Through, FT) recovered and 15µl (equivalent of 75µl culture) sampled for SDS-PAGE analysis. The resin pellet was washed to remove proteins weakly attached to resin and then successive elution of 2ml were achieved with the elution buffer (330 mM imidazole, 50 mM Tris, 300 mM NaCl, pH 7) to recover the proteins of interest. Ethylenediamine tetraacetic acid (EDTA) 100mM pH 8 was used in the last elution to get everything that is retained on the resin.

3.2.1.6. Protein purification by reverse phase HPLC

The TAF12-p24TMD fusion protein was purified from the cobalt affinity chromatography elution fractions or directly from the insoluble fraction. When starting from elution fraction, the solvent was first evaporated under vacuum and proteins resuspended in acetonitrile/water (80/20, v/v) while the insoluble pellet was solubilised in formic acid/water (75/25, v/v). Samples were spun-down for 10 min at 12857 g (Eppendorf centrifuge 5804R, Hamburg, Germany) at 4 °C prior to purification. The purification tests were performed on a semi-preparative HPLC (Bischoff) using an analytical column (Phenomenex Jupiter C4 Particule 300Å, 5µm, Column 4.60mm x 150mm) under a continuous 10-95% acetonitrile/water or sloped 10-95% isopropanol/water gradient (see appendix) to develop the conditions of purification. Proteins were purified thereafter on a preparative HPLC (Gilson, Villiers-le-bel, France) using a preparative column (Phenomenex Jupiter Particle C4 300 Å, 5 µm, Column 30mm x 150mm, Le Pecq, France) under slope 10-95% isopropanol/water gradient (see appendix). Acetonitrile/water gradient was prepared by mixing solvents A (acetonitrile/water/TFA, 10/90/0.1, v/v/v) and B (acetonitrile/water/TFA, 90/10/0.1, v/v/v) and for the isopropanol/water gradient with solvents A' (water/TFA, 90/0.1, v/v) and B' (isopropanol/water/TFA, 90/10/0.1, v/v/v). Proteins eluted with increased percentage of solvents B and B', respectively.

3.2.1.7. Characterization by electrophoresis

Proteins were separated by electrophoresis under denaturing conditions. Liquid samples were mixed to the loading buffer 5X (0.25 M Tris-HCl pH 6.8; 0.5% bromophenol blue; 0.5 M DTT; 50% glycerol; 10% SDS) prior to the loading on the gel in order to weigh down the sample and denature proteins. Samples were loaded on a 4% stacking gel and proteins separated in a 16% polyacrylamide tris-glycine gels. The migration was performed for 1 h10 at 150V successively through these two gels. They were stained with Coomassie blue (Blue ROTI® 5X, A15.1, Karlsruhe) and then destained with a solution of methanol 25% and water 75%. Photos gels are made with the E-box VX2 gel reader (Vilber, Eberhardzell, Germany).

3.2.2. Characterization by mass Spectrometry

The matrix (sinapinic acid, SA, or α-cyano-4-hydroxycinnamic acid, α-cyano, Sigma-Aldrich, Saint-Quentin, France) was prepared at a final concentration of 10 mg / mL in acetonirile 30% and TFA 0.1%. These matrices were used to analyze protein and peptide samples, respectively. 1µl of sample was mixed to 1µl matrix on the sample target (05 174, Bruker, Leipzig, Germany) and analyzed in the spectrometer MALDI-TOF (Matrix

Assisted Laser Desorption-/ Ionization - Time Of Flight; Bruker Daltonics Autoflex model). Samples were most often ionized with 20-30% laser and analyzed under linear mode detection.

3.2.2.1. **Cleavage of the TAF12-p24TMD fusion protein**

The TAF12-p24TMD was designed with a formic acid cleavage site (DP, Asp-Pro site) between the fusion protein partner and the p24TMD peptide. The cleavage was tested directly on the insoluble fraction or on HPLC fraction obtained after a preliminary step of purification. In the later, the solvents were first removed under vacuum and proteins resuspended in formic acid/water (75/25, v/v) while insoluble fraction was directly solubilized in this solvent mixture. Samples were thereafter incubated for 24 hours at 50 °C in a water bath to perform the cleavage. The product of cleavage was spun-down for 10 min 12857 g (Eppendorf centrifuge 5804R, Hamburg, Germany) at 4 °C prior to the purification by reverse HPLC and the eluted fractions analyzed by MALDI-TOF for the presence of the peptide.

3.2.3. Results and discussion:

The expression of TAF12-p24TMD was first performed with the pTIPX4-p24TMD recombinant vector that was obtained by molecular cloning from the pTIPX4 vector from our laboratory. However, as we encountered some major difficulties for the expression, a new vector the pTIPX4-p24TMD* was obtained from the pTIPX4-fpTM acceptor vector for which we already knew that the expression works. Indeed, this vector is used in our laboratory to express the fusion peptide of the HIV gp41 (fpTM) as a TAF12 fusion protein. The fpTM insert was replaced by the p24TMD nucleotide sequence as described in the experimental section. Here we will only present results that were obtained with this new vector.

3.2.3.1. **Expression of the fusion protein TAF12-p24TMD**

Different bacterial strains (BL21 DE3, BL21 DE3 pLys S, BL21 AI) were first tested (data not shown) and TAF12-p24TMD expression seems to work better in BL21AI. Thereafter, different parameters (inducer, OD of induction and temperature) were tested in order to set up the conditions of expression.

An overnight pre culture of BL21 AI transformed with pTIPX4-p24TMD* was used to seed 50 ml LB supplemented with 0.1% glucose and 50 µg/ml kanamycin and bacteria were grown at 37 °C under agitation. The optical density of bacteria was monitored at 600 nm each 30 min and at OD ~ 1, protein expression was induced by the addition of IPTG and arabinose (see Figure 53A & B respectively). Different IPTG concentrations were tested in parallel at 0.2% arabinose (see Figure 53A) and arabinose at 1mM IPTG (Figure 53B). Uninduced bacteria were collected before induction for the negative control

of expression. Induction was performed for 3 hours at 37 °C and bacteria harvested by centrifugation. As shown in Figure 53A & B, bacterial growth significantly slows down 30 min after of induction compared to the non-induced bacteria and all reached the stationary phase. This result suggests an important expression activity that requires important metabolic resources and thus, slows the bacteria growth. Bacterial growth was not significantly different between the tested IPTG and arabinose concentrations.

Cells were lysed and proteins extracted during different steps of separation/purification. As p24TMD was expressed as a TAF12 fusion protein, it was expected in inclusion body. Thus the insoluble fraction (pellet after cell lysis named Mbe+CI) was solubilised with 6M guanidine and the inclusion bodies (supernatant, CI) separated from the membranes (pellet, Mbe) by centrifugation. As the fusion protein contains the His-tag, inclusion bodies were first incubated with cobalt resin and the protein was eluted with 330mM imidazole. Aliquots of each purification step were analyzed on a 16% SDS-PAGE to identify the protein of interest. The different fractions that were analyzed for increasing concentration of IPTG are shown in Figure 53C. When comparing the electrophoresis profile of these fractions, we could hardly observe any differences between the induced and the non-induced conditions except for the elution fractions. Indeed, for the different IPTG concentrations and not for the non-induced, a band between 15 and 20 kDa was identified. As the expected molecular weight is 15.624 kDa, we deduced that it corresponds to the TAF12-p24TMD. In addition, as the intensities of the bands increased from 0.8 to 1.2mM IPTG and seems to be important at 1% arabinose (Figure 53D), we deduced that the expression works better at 0.8 mM IPTG and 1% arabinose. These results confirmed that our protein indeed accumulated in inclusion bodies as expected and not in membranes (data not shown). However, the presence of other proteins in the elution fraction was an obstacle for its quantification after cobalt affinity chromatography. These proteins could come from the interaction with our protein or directly with the resin. Moreover, a part of the protein is lost in the flow through (data not shown). In addition, we also noticed some protein degradation (Figure 53C & D) despite the use of BL21 AI which is a protease deficient strain and dedicated for the expression of toxic proteins.

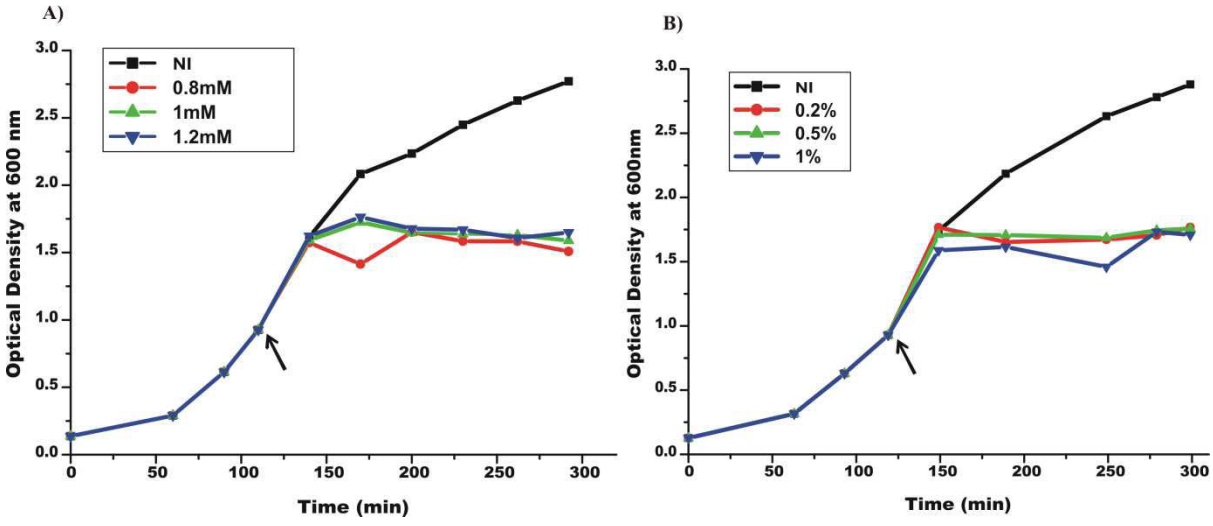

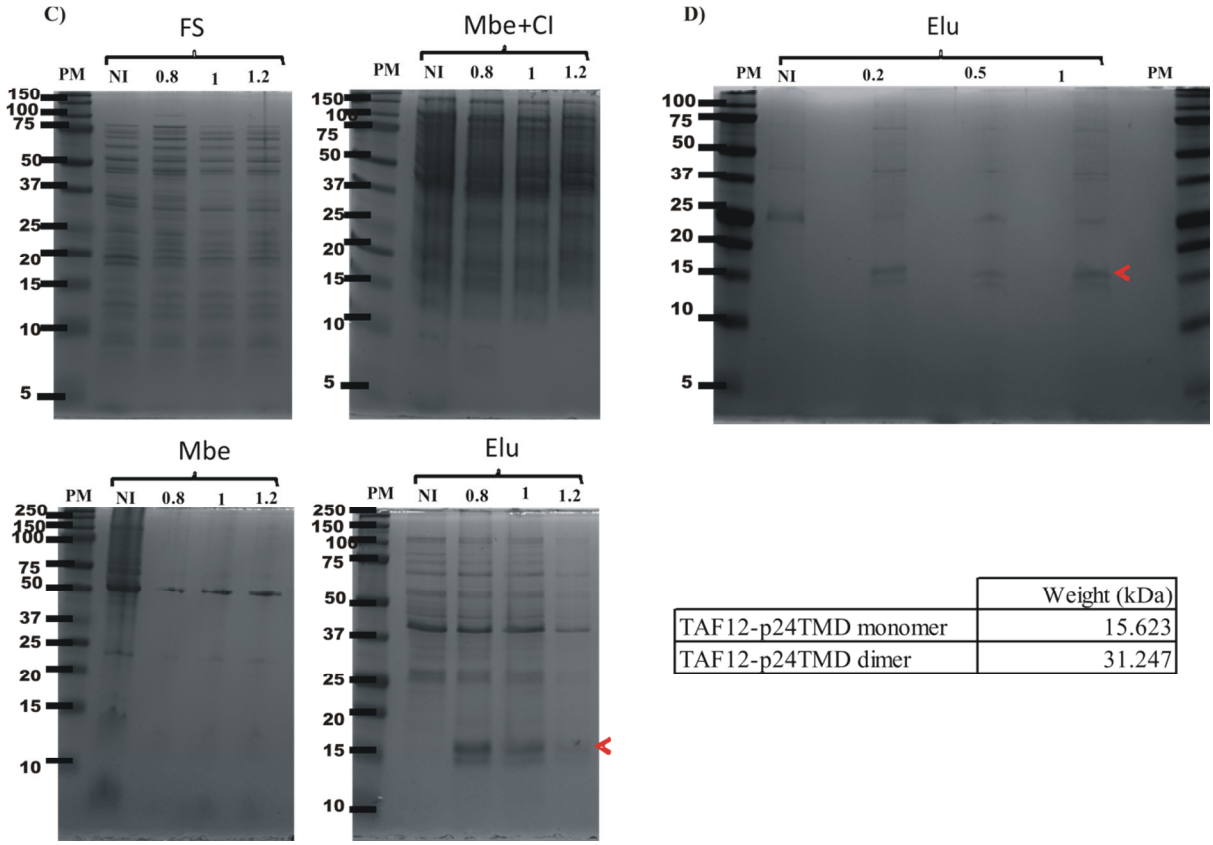

	Weight (kDa)
TAF12-p24TMD monomer	15.623
TAF12-p24TMD dimer	31.247

Figure 53: Influence of IPTG and arabinose on bacterial growth and TAF12-p24TMD expression. Kinetics of bacterial growth was achieved by monitoring of the OD 600nm every 30min. They were grown at 37 °C until OD = 1 (arrows) and the expression induced with (A) different concentrations of IPTG (0.8, 1 and 1.2 mM) and a fixed concentration of arabinose (0.2%) or (B) different concentrations of arabinose (0.2, 0.5 and 1%) and a fixed concentration of IPTG (1mM). The different fractions during protein extraction for the IPTG test (C) and the elution fractions for arabinose test (D) in induced (I) or non-induced (NI) conditions were analysed by SDS-PAGE. Samples were separated on a 16% Tris glycine gel during 1h10 at 150V and the gels stained with Rotiblue. The loaded volumes are the following: 24µl for soluble (FS) and insoluble fractions (Mbe + CI: membrane and inclusion bodies) (equivalent to 120 µl of culture), 12 µl for membrane fractions (Mbe) (equivalent to 1.2 ml of culture) and 25 µl for elution fractions (Elu) (equivalent to 1.2 ml of culture) for IPTG test and 60µl (equivalent to 6 ml of culture) for arabinose test and 12µl of protein ladder (PM) (Precision Plus Protein Dual Color Standards ™). The red arrows indicate the protein of interest. The theoretical masses in the table were obtained through the web software ProtParam Site ExPASy.

Protein expression was also induced at different OD 600 nm values ~1, 1.5 and 2 during 3h at 37 °C with final concentration of 0.8mM IPTG and 1% arabinose. As shown on the elution fractions electrophoresis profile in Figure 54A, the intensities of the bands seems to decrease while the ODs of induction increase suggesting that the expression is less efficient at higher OD induction. We thus decided to perform the induction of expression at OD~1.

In addition, as temperature is an important parameter to take in account for the expression, different temperatures (15, 20, 28 and 37 °C) were tested. Protein expression was induced during 4h at 28 and 37 °C, and for 24h at 15 and 20 °C with the previously defined conditions (OD 600nm ~1, 0.8mM IPTG, 1% arabinose). In order to follow the kinetics of protein expression and to determine the best induction time, 10ml of bacterial culture was sampled every hour during the first 4 hours of induction and every 2 hours or more at higher (37, 28 °C) and lower (15, 20 °C) temperatures, respectively. The SDS-PAGE profile of cobalt affinity elution fractions is shown in Figure 54B. At temperature 28 and 37 °C, the expression starts after 1 hour of induction and seems to be effective during 3 hours before it decreases (Figure 54B, left). As protein expression is slowed down at low temperatures, the presence of our protein of interest is detected only after 4 hours of induction (Figure 54B, right). Surprisingly, while at high temperatures (28, 37 °C) the expressed protein accumulates only in inclusion bodies, its presence is detected in both inclusion bodies and membrane fraction at low temperatures (15, 20 °C) (Figure 54C). This result suggests an affinity of the protein for the membranes at low temperature. Indeed, in this case as the expression is lower, it appears to be less toxic for bacteria and thus, protein may fix to the membrane and with its accumulation drive into inclusion bodies. While at high temperature, the fast expression of proteins allows their accumulation which appears to be likely toxic for bacteria and thus, may drive them directly into inclusion bodies to overcome this toxicity. However, it is difficult to say if the accumulation in both fractions at low temperature occurred simultaneously or at different moments.

When the electrophoresis profiles are compared, the expression seems to work better at 37 °C thus, this temperature was maintained for TAF12-p24TMD expression.

In summary, we were able to define the best conditions of expression for TAF12-p24TMD. We show that the protein is addressed to inclusion bodies at 37 °C and 28 °C and at lower temperature (15, 20°C) additionally into membranes. However, its quantification was not possible after cobalt affinity chromatography as the eluted fractions were not pure thus, requiring a supplement step of purification. For this purpose, reverse phase HPLC was used.

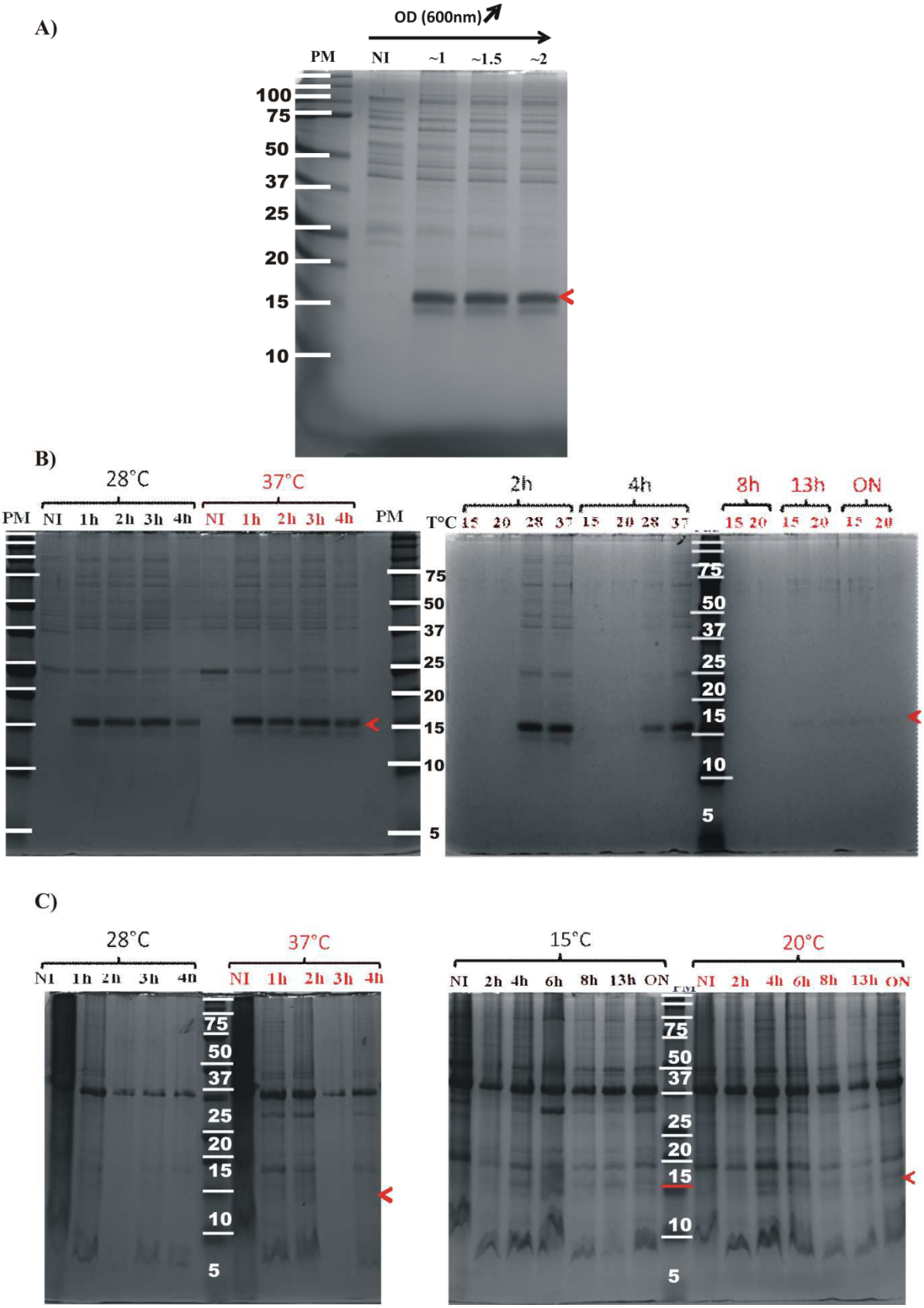

Figure 54: Influence of OD 600nm at induction and temperatures on TAF12-p24TMD expression. (A) Bacteria were grown until OD (600nm) ~ 1, 1.5 and 2 and the expression induced during 3 hours at 37 °C with 0. 8 mM IPTG and 1% arabinose. After purification of the fusion protein, 45µl

of each elution fraction (equivalent to 4.5 ml culture) were analyzed by SDS-PAGE. For the temperature test, induction was performed with the same concentration of inducers during 4h at 28, 37°C and for longer time at 15, 20°C. (B) 25µl of elution fractions (equivalent to 2.5 ml culture) and (C) 12µl (equivalent to 1.2ml) were analyzed. Samples were separated on a 16% Tris glycine gel during 1h10 at 150V and the gels stained with Rotiblue. 12µl of molecular weight marker was deposit. The red arrows indicate the protein of interest

3.2.3.2. **Purification by reverse phase HPLC:**

TAF12-p24TMD was purified starting from the cobalt affinity chromatography elution fractions under a 10-95% acetonitrile/water gradient. The chromatogram shown Figure 55A was obtained for the injection of an equivalent of 125ml culture. Proteins were eluted at different percentage of solvent B (acetonitrile/TFA, 100/0.1, v/v) ~ 30, 42, 52 and 60% of B (Figure 55A). These elution peaks were analyzed by MALDI-TOF. Different mode of detection (reflectron and linear) and matrices (SA and α-cyano) were tested. The mass spectrometry spectra shown in Figure 55B were obtained when samples were prepared with SA matrix and analyzed in a linear mode. As shown, we did not detect any peak with the expected mass of our protein in these elution fractions. Nevertheless, as the protein was identified in these fractions on the SDS-PAGE, we deduced that it may hardly ionize. In addition, the presence of other proteins as well as peptides that were detected in the different HPLC fractions indicates that they are not pure (Figure 55B). Thus, this could impair the detection of our protein. Based on this result and as we did not succeed to purify our protein by performing subsequent purification of inclusion bodies by cobalt affinity chromatography and elution fractions by reverse phase HPLC, we decided to purify our protein directly from the insoluble fraction.

This fraction was solubilised in formic acid/water (75/25, v/v), and TAF12-p24TMD purified under a 10-95% isopropanol/water gradient. The chromatograms shown in Figure 56A were obtained for 1 L and 500 ml of induced and uninduced culture respectively. Proteins eluted in the same range of isopropanol percentage starting from 38 to 62%. However, although both chromatograms follow the same profile, they present some differences suggesting the presence of different proteins that eluted from the column at different percentage of solvent. When these elution fractions were analysed by MALDI-TOF, we could clearly identify peaks with a close mass to that we expected for the fusion protein (15623.85 Da). Interestingly, these peaks were identified as shown in the induced and not in the uninduced sample (Figure 56B). The zoom of this region indeed revealed the presence of a peak with the expected mass (Figure 56B, arrow) as well as peaks than could correspond to the protein lacking some residues at the C terminus.

A)

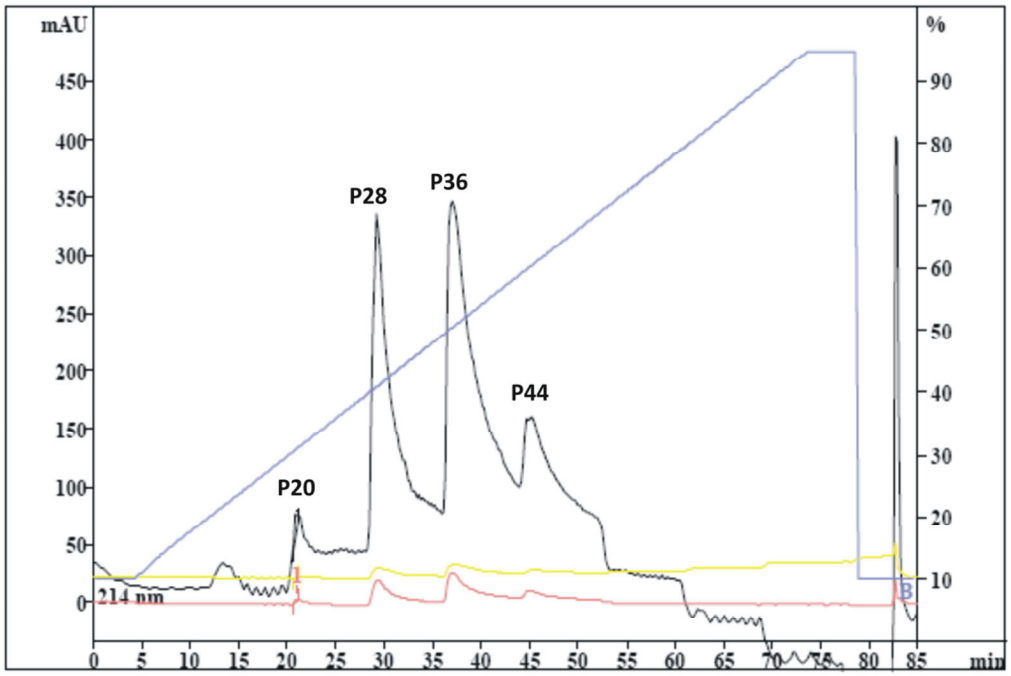
mAU
%
P28
P36
P44
P20
214 nm
min

B)

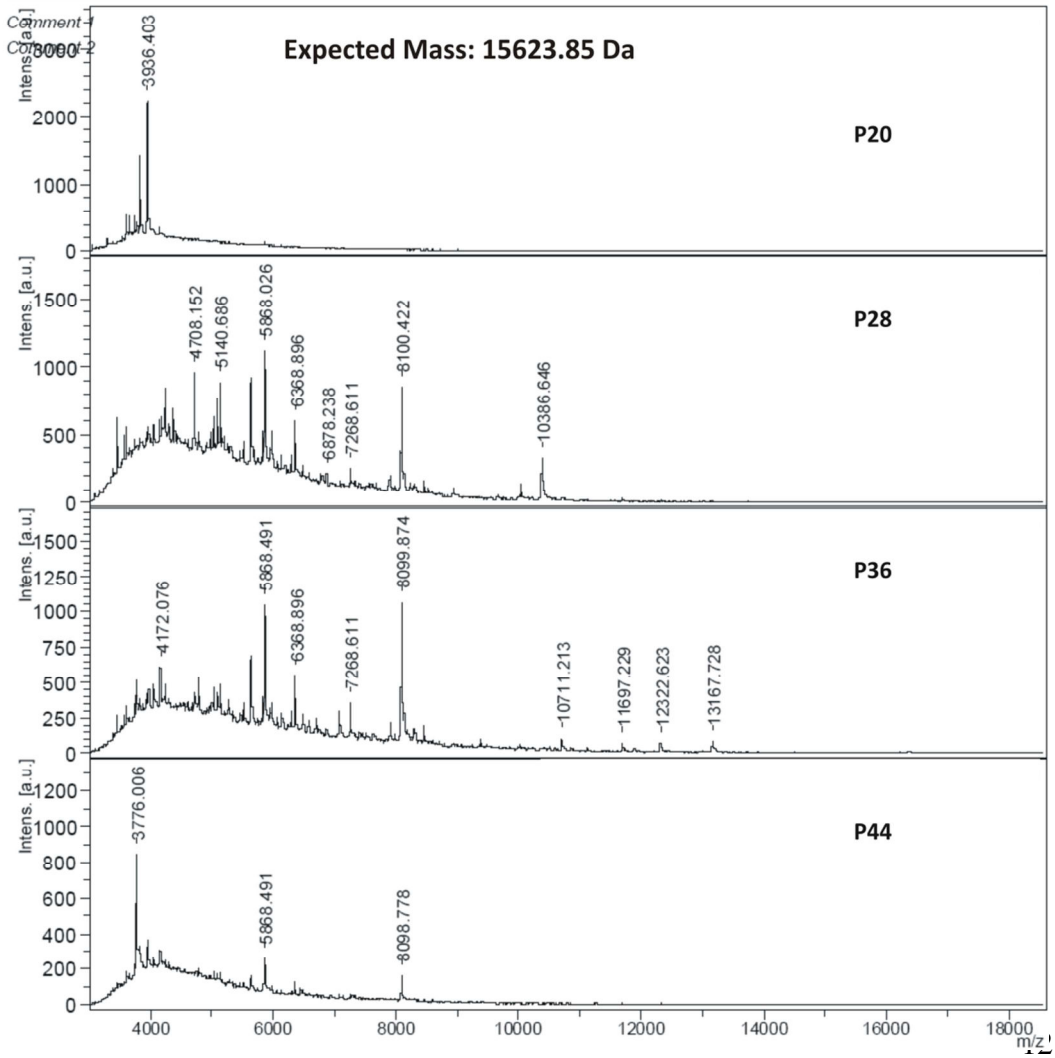
Expected Mass: 15623.85 Da
P20
P28
P36
P44
Intens. [a.u.]
m/z

Figure 55: Chromatogram of elution fractions after cobalt affinity and MALDI-TOF mass spectra of the HPLC fractions. (A) The pool of cobalt affinity elution fractions (equivalent of 125ml culture) were purified under a 10-95% acetonitile/water gradient during 85min on Bischoff HPLC using Jupiter C4 HPLC analytic column. The chromatogram shows the absorbance at 214nm (black), 280nm (red) and 253nm (yellow) as a function of time (min). The peaks correspond to the eluted proteins at different acetonitrile gradients: ~ 30, 42, 52 and 60%. (B) 1µl of each eluted fraction was mixed with 1µl of SA matrix and analyzed MALDI-TOF using linear mode detection under 30% laser power. The calibration was performed with the protein calibration standard I (Bruker)

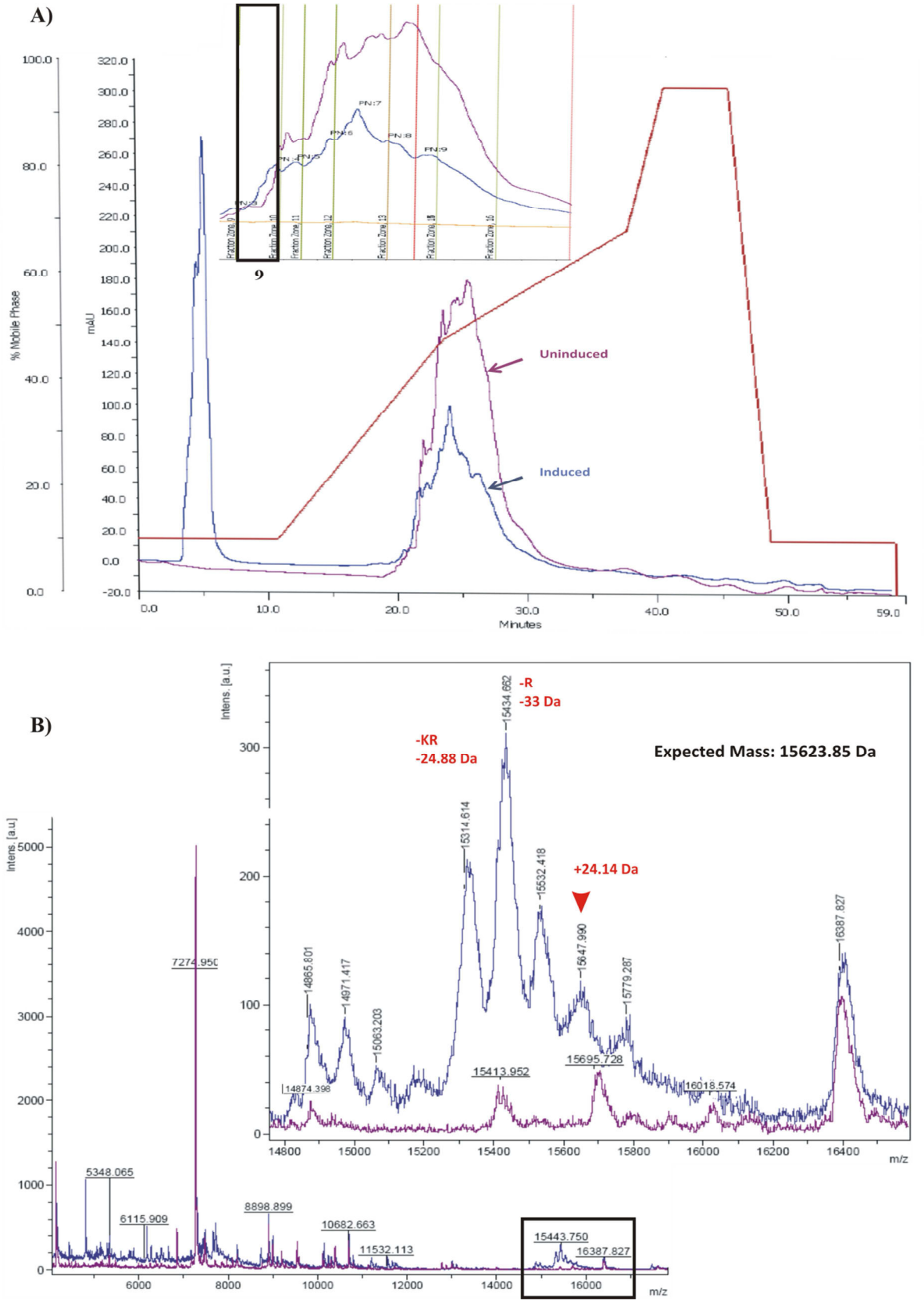

Figure 56: Reverse phase HPLC chromatogram of insoluble fraction and mass spectra. (A) The insoluble fraction of 1L and 500ml equivalent culture for the induced and non-induced conditions, respectively, was purified under a 10-95% isopropanol/water gradient during 60min on Gilson

HPLC using a Jupiter C4 preparative column. The chromatogram shows the absorbance at 214nm as a function of the time (min) for the induced (blue) and non-induced (purple) conditions. Proteins were eluted in both conditions between 38 and 62% isopropanol. (B) 1µl of each eluted fraction was mixed with 1µl of SA matrix and analyzed by MALDI-TOF using linear mode detection under 30% laser power. The calibration was performed with the protein calibration standard I. Only the full spectra of the HPLC fraction 9 (highlight in the black frame) in which our protein of interest was identified is represented. The region of the expected mass (frame in black) was zoomed. The red arrow pinpoints the peak that could correspond to the TAF12-p24TMD. The –KR or –R indicate that the peak could correspond to the peptide lacking the KR (Lysine and Arginine) residues or R (Arginine) residue

In fact, because of the presence of arginine and lysine residues, our protein is likely sensitive to enzymatic digestion. However, we observed some differences in mass which can be explained by the broadening of peaks that impaired the precision of mass determination. Although we were able to identify our protein of interest, we did not quantify it because of the presence of other proteins in this fraction.
In summary, we tried to purify TAF12-p24TMD starting from the elution fraction after cobalt affinity chromatography or from insoluble bacterial pellets. In both cases, we did not recover a pure fraction of our protein. Nevertheless, as we are more interested by the peptide, we decided to go forward with the cleavage of the protein follow by the purification of the peptide.

3.2.3.3. **TAF12-p24TMD cleavage and purification of p24TMD:**

The TAF12-p24TMD fusion protein was designed with a chemical formic acid cleavage site. As we could not obtain the pure protein, the cleavage was first tested on the HPLC fraction that contains the protein and later directly on the insoluble fraction. Starting from the HPLC fraction, the solvent was first evaporated under vacuum and the sample resuspended in formic acid/water (75/25, v/v). The cleavage was performed for 24 hours at 50 °C and the product of cleavage purified by reverse phase HPLC to recover the peptide. The chromatograms for the induced and non-induced conditions are shown in Figure 57A. Although proteins are eluted in both conditions between 30 and 68% isopropanol and they followed the same profile, there are some differences that suggest that different peptides may elute from the column. When HPLC fractions were analyzed, peaks around 3547.26 Da which correspond to the peptide lacking two residues (PK) at the N terminus were identified only in the induced sample (Figure 57B) with additional posttranslational modifications (methylation and hydroxylation). Interestingly, these peaks were identified in a reproducible manner even when the cleavage was performed in the same conditions directly on the insoluble fraction and purified by reverse phase HPLC (Figure 57C). In addition, as the injection peaks present an absorbance at 280nm during elution, we decided to analyse these peaks. As shown in Figure 57B (cyan), it contains different peptides including some with masses that could correspond to our peptide lacking an arginine at the C terminus with or without some post translational modifications. However, we can only

speculate about this hypothesis. Surprisingly, a peak with the expected mass of the peptide was identified in the non induced sample (Figure 57B).

A)

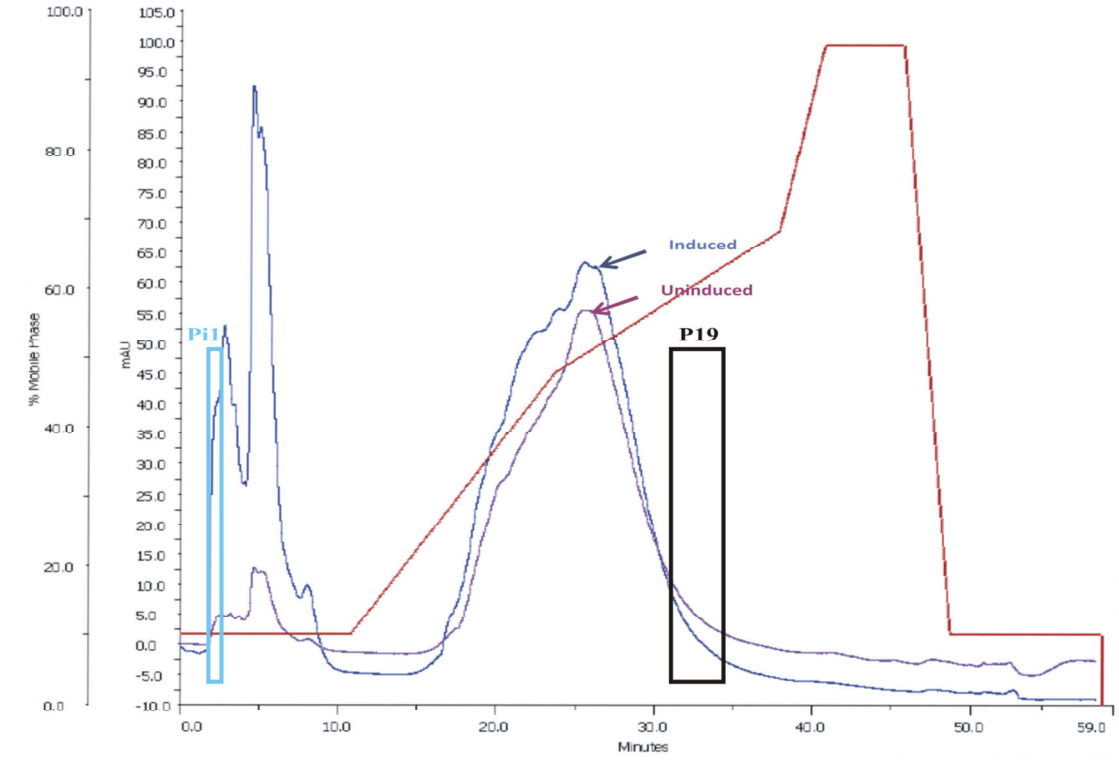

B)

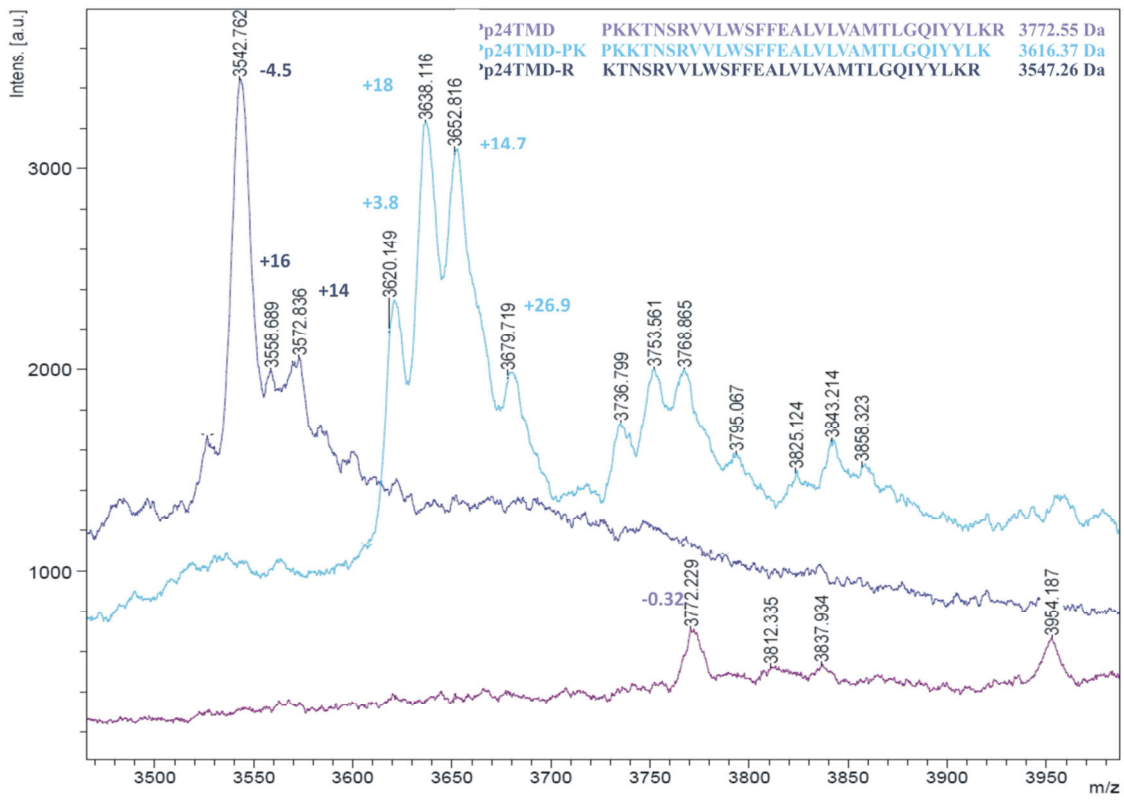

C)

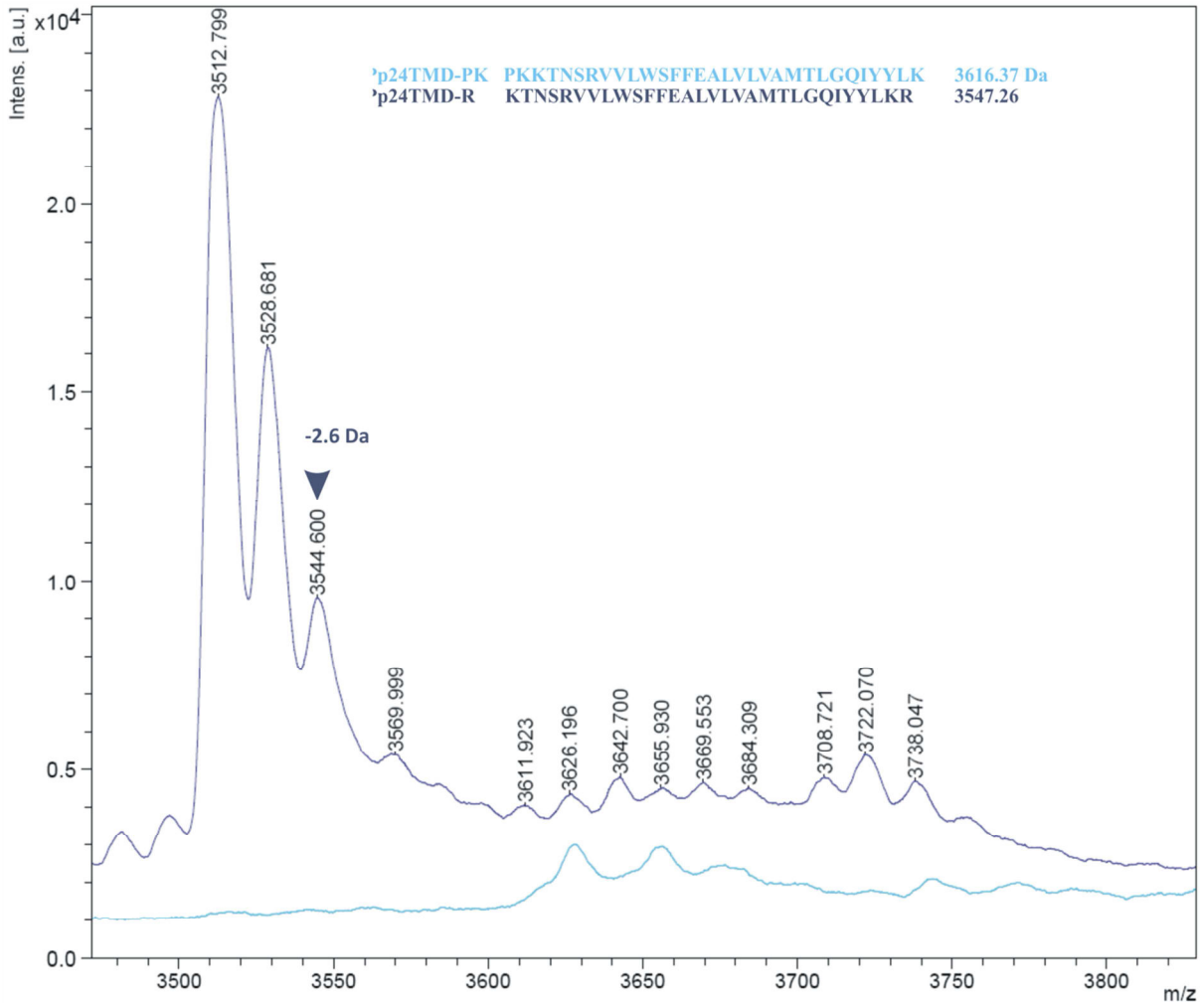

Figure 57: Chromatogram and mass spectrometry spectra after formic acid cleavage of HPLC fraction containing the fusion protein (A, B) or the insoluble fraction (C). (A) The TAF12-p24TMD was purified by HPLC under a 10-95% isopropanol/water gradient (red) during 60min from the injection of the equivalent of 2.8l and 500ml culture for the induced and non-induced conditions, respectively, resuspended in formic acid/water (75/25, v/v). The purification was performed on Gilson HPLC using a Jupiter C4 preparative column. The resulting chromatogram only shows the absorbance at 214nm as function of time (min) for the induced (blue) and non-induced (purple) conditions. The cyan and black boxes indicate the fractions in which peptides with close mass to the one we expected were identified. The fraction frame in cyan is recovered in the injection peak (PI). (B) MALDI-TOF spectra of the fractions frame in black for the induced (blue and cyan), non-induced (purple) conditions. (C) Mass spectra when cleavage was achieved directly on insoluble fraction after HPLC purification. 1µl of each eluted HPLC fraction was mixed with 1µl of SA matrix and analyzed MALDI-TOF using linear mode detection under 30% laser power. The calibration was performed with the protein calibration standard I. The red arrow pinpoints the peak with a close mass to that of p24TMD

However, as we did not identify the fusion protein in the purified fraction (Figure 56B), we deduced that this peptide results from the cleavage of a protein that is repressed in induced conditions. Moreover, this peptide is only presents in the non-induced and not in the induced condition. For all these peaks, a difference of few Dalton compared to the expected mass was observed. This difference could be explained by the low resolution of the peaks and the difficulty to get a good calibration for proteins. Indeed, among the three calibrants we used, the one with the highest molecular weight (16,952.30 Da) is already in the expected range of our protein and the two others are below (8,476.65 and 8,565.61Da). Based on these results, we could only speculate about the fact that the detected peptides can correspond to the p24TMD with some residues lacking as we should confirm by sequencing. In addition, as the cleavage was performed not on a pure fraction of the fusion protein (HPLC elution fraction or insoluble fraction), it is likely that these peptides come also from other proteins. Moreover, the detection of p24TMD is somehow tricky and the presence of others peptide did probably not help.

3.2.4. Conclusions

To summarize, here we set up the expression of the TAF12-p24TMD* fusion protein in BL AI bacteria strain. After solubilisation of the insoluble fraction in Guanidine 6M, this protein was localized as expected in inclusion bodies. Its purification by cobalt affinity chromatography and reverse phase HPLC did not yield pure fraction indicating that other proteins bind on cobalt resin either directly or indirectly via interaction with the TAF12-TMD*. The presence of these proteins make the quantification of the protein of interest difficult to achieve. Moreover, it impairs the purification and the detection of the peptide after cleavage of the fusion protein. This can be explained by the fact that the p24TMD* could interact with these proteins via hydrophobic interaction and thus, elute in the same fraction or it can also elute with peptides coming from other proteins that share the same hydrophobic feature. The later argument was confirmed by mass spectrometry spectra (not shown). Therefore, effort has to be put first on the best way to purify the fusion protein in order to improve peptide purification and detection after cleavage. In addition, mass spectrometry detection methods have to be also specifically adapted to the peptide.

General conclusion

In summary, to optimize our chance to obtain the p24TMD peptide we used two expression systems that allow its expression as a MBP (pMal c5X) and TAF12 (pTIPX4) fusion protein. Different bacteria strains and expression parameters (IPTG concentration, OD 600nm, temperatures) were tested in rich medium. In both cases, we set up the conditions of expression of these proteins. However, we encounter different problems with each system. Although we succeed to obtain pure MBP-p24TMDH, we have a lot of degradation and a considerable part of protein flowing through the column thus, significantly reduced the yield. After cleavage, compare to the total yield of protein, we have 12 times less amount of peptide due to the important proportion in size between the fusion partner and the peptide. In addition, as the truncated protein lacks residues in the C-

terminus, we then yield a short and full length peptide after the cleavage. These contribute to reduce the amount of the full peptide. Therefore, with the purpose to obtain enough among of peptide to perform for several NMR investigations, this system is limiting. Indeed, as shown we yield 3mg of total protein in minimum medium thus, 0.25mg of peptide (short and full length).

In contrast to MBP-p24TMDH, the purification of TAF12-p24TD was difficult as it always eluted with other proteins thus impairing its quantification and the purification of the peptide. In addition, a part of the protein also flows through the column (data not shown). In both cases, we hardly detect the peptide in a reproducible manner. Based on these observation, effort have to be put first to improve the purification of the fusion protein. This can be done by playing quantity of resin, the different concentrations of imidazole that are used to wash the column before the elution. However, the expression and optimisation in minimum medium still have to be achieved

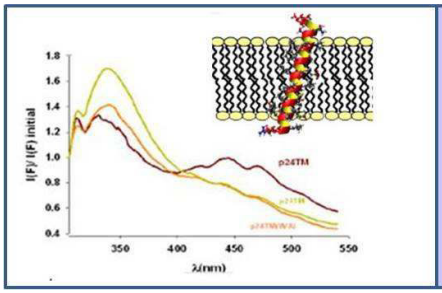

Chapter-4

EXPERIMENTAL RESULTS: BIOPHYSICAL INVESTIGATION OF PROTEIN-LIPID INTERACTIONS

Protein-lipid interactions play a key role in many cellular functions. With the goal to get insights in these functions, here we investigated two interactions: the p24TMD interaction with sphingomyelin and the CRAC motif with cholesterol. As the first one was proposed to be specific, biophysical investigations were performed to understand the mechanism of this specificity and thus, a better understanding of its function. In addition, membrane topology of CRAC in presence of cholesterol was investigated with the purpose to understand the role of the cholesterol in this interaction. This chapter will present and discussed the different results we obtained.

Chapter 4. Experimental results: Biophysical investigation of protein-lipid interactions

4.1. Biophysical and structural characterization of p24TMD-SM C18 interaction

4.1.1. Introduction

Cellular traffic of proteins and lipids is mostly ensured by vesicles along the secretory pathway. The COat Protein I and II (COPI and II) vesicles mediate this transport in the early secretory pathway between the ER and the Golgi apparatus (Brügger et al., 2000; Rothman and Wieland, 1996). A specific enrichment of one sphingomyelin species, SM C18, was found in the COPI transport vesicles (Brügger et al., 2000). In studies using Förster resonance energy transfer (FRET) and immunoprecipitation, Contreras et al were able to attribute this specific sorting to the p24 protein which is abundant in the COPI membrane (Contreras et al., 2012b). They showed that this interaction is achieved with an almost exclusive specificity for the SM C18. They identified a molecular recognition motif (VXXTLXXIY) within the p24 transmembrane domain (p24-TMD) which binds this lipid using mutagenisis studies. Strikingly, whereas many protein-lipid interactions involve either the lipid head group or acyl chain, this interaction seems to involve both the head group and the backbone of this sphingolipid. Interestingly, the p24-TMD seems to be sufficient for the interaction and a molecular dynamic (MD) model was proposed (Figure 12C). In addition, they suggest a role of SM C18 in regulating the equilibrium between an inactive monomeric and an active oligomeric state of the p24 protein, which in turn regulates COPI-dependent transport (Contreras et al., 2012; Popoff et al., 2011). In order to understand the mechanism of this specificity, we performed structural investigations to get more insights into this model.

With this purpose, we first carried out some preliminary CD and fluorescence spectroscopy experiments to define the best conditions to investigate this interaction, as these techniques require less peptide compared to NMR spectroscopy. In further studies, we investigated the p24TMD topology and dynamics in model membranes made of POPC or of a lipid composition similar to the one found in the Golgi apparatus in order to characterize its interaction with SM C18. In addition, side chains of residues that occur in the binding motif were specifically labelled with ^{2}H and investigated by solid-state NMR to characterize the effect of SM C18 on their dynamics. POPC is widely used as simplified biological membrane model as its structure and properties mimic that of the natural phospholipids. Thus, the peptide was first reconstituted into POPC and POPC/SM (95/5) and investigated by static solid-state NMR approaches. Deuterium and ^{15}N solid-state NMR spectroscopy of static oriented samples have been used to characterize membrane interactions of many polypeptides and provide valuable structural information (Bechinger et al., 2004, 2011; Weingarth and Baldus, 2013). The fundamental concept of this approach for the structure determination is based on the inherent anisotropy of NMR interactions. Typically, a ^{2}H and/or ^{15}N labelled peptide is reconstituted in oriented (with respect to the

magnetic field) phospholipid membranes. For such oriented samples, the alignment of helical peptides can be deduced from the measured ^{15}N chemical shift in a straightforward manner (Bechinger and Sizun, 2003). In addition, the dynamics of the labelled site and the angular restraints can be deduced from the ^{2}H NMR spectra line-shape and the measured deuterium quadrupolar splitting, respectively.
In combination this information allows for an accurate determination of the tilt and pitch angles of peptides reconstituted into oriented membranes and has already provided valuable information on a variety of synthetic membrane polypeptides (Aisenbrey and Bechinger, 2004; Aisenbrey et al., 2006; Michalek et al., 2013).
As lipids contribute to the final structural features of membrane-associated peptides, we investigated the conformation and the dynamics of the lipid bilayer in presence of the peptide using ^{31}P and ^{2}H solid-state NMR. With 100% natural abundance in phospholipids forming membranes and its high sensitivity, the ^{31}P nucleus is a good candidate to probe the structure and the dynamic of the phospholipid head groups. In contrast, with a very low natural abundance and low sensitivity, ^{2}H nuclei have to be enriched in lipids. Many deuterated lipids are commercially available thus allowing investigation of the fatty acyl chain packing and membrane dynamic (Bechinger and Salnikov, 2012; Henzler-Wildman et al., 2004; Kim et al., 2009).
In addition, as p24TMD proteins are enriched in the Golgi-derived COPI vesicles; we performed preliminary investigation of p24TMD peptide topology and dynamics in membranes with a complex Golgi-like lipid composition using the same solid-state NMR methods. The dynamics of the valine-19 side chain involved in the interaction with SM C18 was also investigated to understand the effect of SM C18 on the side chain.
This chapter will thus describe the physico-chemical approaches we used to establish a suitable protocol of p24TMD reconstitution in artificial membranes as well as the results of the investigation of p24TMD-SM C18 interaction. These results will be discussed with regard to the proposed model in order to shed light on this interaction and understand its function.

4.1.2. Preliminary biophysical studies of p24TMD in membrane

4.1.2.1. Experimental

Materials:
Organic solvents were purchased from Sigma Aldrich (Saint. Louis, MO) with a purity of 99%; and lipids from Avanti Polar Lipids (Birmingham AL, USA); F-moc amino acids from Bachem (Heidelberg, Germany) or Applied Biosystems (Weiterstadt, Germany); Isotope labeled amino acids from Cortecnet (Voisins les Bretonneux, France) or Aldrich (Saint Louis, MI, USA); TentaGel-R-RAM resin from Rapp Polymer (GmbH, Tubingen, Germany).

4.1.2.1.1. Peptides synthesis

Peptides were prepared by solid phase peptide synthesis SPPS using an automatic synthesizer (Millipore 9050) and Fmoc chemistry. They were synthetized on TentaGel-R-RAM resin (Rapp Polymer GmbH, Tubingen, Germany) using an excess of Fmoc protected amino acid (Merck, Darmstadt, Germany). Isotope labeled peptides were prepared using ^{15}N and ^{2}H amino acids (Cortecnet, Voisins les Bretonneux, France, or Aldrich, Saint Louis, MI, USA) incorporated at a chosen position. After synthesis, the resin was placed on a glass filter and washed with ethanol, acetic acid and ether. The cleavage of the peptide from resin and deprotection of amino acids side chains were performed in a solution containing 28 ml of tri-fluoro-acetic acid (TFA), 1.5 ml of water and 300 µl of triethylsilane under stirring for 4 hours at room temperature (RT). The peptide in solution is taken-up in toluene (50/50) (v / v) and the solvent evaporated using a rotary evaporator (Buchi R-200). The peptide was then precipitated and washed in cold ether to remove protecting groups by repeated cycles (3 times) of vortexing and centrifugation at 11000 g for 30 minutes at 4 ° C. The pellet containing the peptide was finally air dried to remove ether, solubilized in 4% acetic acid to exchange the counter ions, frozen in liquid nitrogen and lyophilized. The cleavage product was analyzed by MALDI-TOF to check the presence of the full peptide.

4.1.2.1.2. Purification by reverse phase HPLC

The peptides were dissolved in 90% of solvent A (acetonitrile/water/TFA, 10/90/0.1, v/v), 10% solvent B (acetonitrile/TFA, 100/ 0.1, v/v) at a final concentration of 10mg/ml or 1mg/ml for preparative and analytic HPLC respectively. They were then purified by reversed phase HPLC either with a semi-preparative HPLC (Bischoff Chromatography, Leonberg, Germany) or a preparative HPLC (Gilson Chromatography, Villiers-Le-Bel, France) on Prontosil 300-6-C4 5.0-µm (Bischoff, Leonberg, Germany) or Luna 100-C18 5.0-µm columns (Phenomenex, France) using an acetonitrile/water gradient. The gradient was established by increasing the percentage in volume of solvent B over solvent A and the peptides eluted at a given concentration of the solvent B. When using the Bischoff system, the flow rates were 1 ml/min or 10 ml/min for the analytic or preparative HPLC, respectively, and 20ml/min on the Gilson apparatus. The protein absorbance was monitored at 214, 254 and 280 nm using an UV detector. The purity of p24TMD was tested by analytical HPLC.

4.1.2.1.3. Identification of the peptide by MALDI

The identity of the peptides was verified by matrix-assisted laser desorption ionization mass (MALDI) spectrometry. The matrix α-cyano-4-hydroxycinnamic acid (α-cyano) was prepared at a final concentration of 10 mg / ml in acetonirile/H2O/TFA (30/70/0.1, v/v). The samples were prepared as a drop in on the target plate surface (05 174, Bruker) in a final volume of 1µl by mixing the peptide and the matrix (peptide/matrix, 50/50, v/v). Samples were dried at the ambient air, and analysed with the MALDI-TOF spectrometer (Bruker Daltonics Autoflex model). The mass axis was calibrated externally using polypeptides mixture with defined mass ranging from ~700 to 3200 Da (peptide standard

calibration II, Bruker Daltonics, Bremen, Germany). Mass spectra were analyzed by the FlexAnalysis software provided by Bruker Daltonics.

4.1.2.1.4. Reconstitution in liposomes

We first tested the solubility of the peptide in different solvents (water, dichloromethane (DCM), 2, 2, 2-tri-fluoro-ethanol (TFE), 1, 1, 1, 3, 3, 3-hexafluoro-2-propanol (HFIP)) at the concentration of 1mg/ml at room temperature (RT). The test of solubility/reconstitution was achieved by adding POPC (1-palmitoyl-2-oleoyl-sn-glycero-3-phosphocholine) or POPC/POPG (1-palmitoyl-2-oleoyl-sn-glycero-3-phospho-L-glycerol) (75/25 molar ratio) liposomes at different concentrations to 30 µM of peptide in phosphate buffer 10mM, pH7. The general protocol of liposome preparation is described in chapter 2. Briefly, lipids were dissolved in dichloromethane and the solvent evaporated under a nitrogen stream. Final traces of solvent were removed by lyophilization overnight and the resulting film hydrated in 10 mM phosphate buffer pH 7. The solution was tip sonicated to form unilamellar vesicles (SUV). The sonication was performed at 4°C on ice to prevent heating of the sample concomitant with hydrolysis. Aggregates and pieces of titanium coming from the tip sonicator (soniprep 150, MSE (SANYO), Tokyo, Japan) were removed by centrifugation for 30 min, 11 000 g at room temperature.
We also prepared proteoliposomes to test the reconstitution of the peptides in a membrane. Aliquots of 30µM peptide in water were prepared from 1 mg/ml stock solution, and the water removed by lyophilization. A stock solution of lipids was prepared at 10mM by dissolving the POPC either in TFE or HFIP. 100µl (1mM) of this stock solution were added to the lyophilized peptide and completed with the corresponding solvent to a final volume of 1 ml. After vortexing, the solvents were evaporated under a stream of nitrogen gas. The remaining traces of solvent were removed by vaccum overnight using the pump and cold trap of a lyophilizer and the resulting proteo-lipids hydrated in 10mM phosphate buffer pH7. As described above, from this solution, SUVs were obtained by sonication and centrifugation in the same conditions. The interaction of the peptide with the membrane and its structure was monitored by CD and fluorescence spectroscopy.

4.1.2.1.5. Reconstitution in detergent

A stock solution of peptide was prepared in water, samples diluted to a final concentration of 30µM, and the water removed by lyophylization overnight. The peptide was dissolved again in HFIP and the solvent was evaporated under a stream of nitrogen gas and under vacuum overnight. It was thereafter resuspended in 10mM phosphate buffer pH7. The detergent stock solutions of n-dodecylphosphocholine (DPC) and SDS were prepared at final concentrations of 10 mM and 100 mM, respectively and diluted to different concentrations ranging from 0.1mM to 16 mM to titrate the peptide. CD and fluorescence spectroscopy were used to follow physical property changes of the peptide adsorption to membrane lipids and to estimate its secondary structures content.

4.1.2.1.6. Circular Dichroism

CD spectra were recorded on a Jasco J-510 spectropolarimeter (Tokyo, Japan) with a 50 nm/min scan speed, a bandwidth of 3 nm, 5 scans were collected covering the range 250 to 190 nm using a quartz cell of 1mm path length, at 25 °C. The recorded spectra processed using the spectra manager software of the instrument, and the baseline corrected for the used solvent contribution by subtraction. Secondary structure analyses were performed with CDpro Web server using the CONTINLL algorithm (Sreerama and Woody, 2000).
Samples were all prepared with a final concentration of peptide and lipids at 30µM and 1mM, respectively, in a final volume of 300µl within the CD cuvette. A peptide stock solution at 1mg/ml was prepared in water and the OD 280nm measured to determine the concentration. The POPC lipid stock was prepared at 10 or 100mM. For the titration of the peptide with liposomes or detergents, the needed volume of the peptide stock solution to achieve 30µM final concentration was transferred into the cell and increasing volume of lipids stock solution was added to titrate the peptide. Lipid stocks were prepared at high concentration to allow the test of large range of concentrations by adding tiny volumes in order to prevent variation in the final peptide concentration.

4.1.2.1.7. **Tryptophan fluorescence**

The intrinsic fluorescence of p24TMD due to the presence of a tryptophan was measured using a FluoroLog spectrophotometer (HORIBA, Ltd., 522 Kyoto, Japan) with the polarization filters always at the magic angle. Fluorescence emission spectra were recorded from 295nm to 455 nm at an excitation wavelength of 280 nm. The excitation slit width was 1 nm; the emission slit width 4 nm. The peptide was prepared in 10mM phosphate buffer, pH 7.2 at a final concentration of 30µM and either reconstituted in liposomes (proteo-liposomes) or titrated in a step-wise manner using an increased amount of SUV phospholipids vesicles or increased detergent concentrations. When proteo-liposomes were used, the concentration of peptide was the same for the different lipids concentrations and their preparation as described above. A series of emission spectra was recorded at 25°C while stirring.

4.1.2.1.8. **Preparation of oriented samples for ssNMR**

Several conditions of sample preparation were tested to obtain the following final protocol as will be described later. Selectively labeled ^{15}N and/or ^{2}H p24TMD was first dissolved in HFIP, and the solvent was removed under a stream of nitrogen. The peptide was then dissolved in HFIP/water 50/50 (v/v) and added in a step-wise manner to POPC in HFIP. The solvent was evaporated between each step in such a manner that the water content remained low in order to avoid peptide aggregation. The peptide was mixed to lipid to achieve a final peptide-to-lipid (P/L) molar ratio of 1 %. Thereafter, the solvent was partially evaporated under a stream of nitrogen to reduce its total volume to about 0.5ml. We then obtained a clear and viscous sample that was deposited onto roughly 20 ultrathin (thickness 00, i.e. about 80 µm) glass plates (6 × 11mm or 8 x 22 mm, Paul Marienfeld, Lauda-Königshofen, Germany), slowly dried in air and the residual solvent evaporated

under high vacuum. Sample hydration was achieved at 93% humidity for 2 - 3 days at room temperature and the glass plates were stacked on top of each other. The stack was stabilized by wrapping with Teflon tape and the whole sample sealed in plastic to avoid dehydration.

4.1.2.1.9. Solid state NMR experiments: ^{31}P, ^{15}N, ^{2}H

Spectra were recorded on a Bruker Avance NMR spectrometer operating at 9.4 Tesla and equipped with a double resonance E-free flat coil probe (Bruker, Rheinstetten, Germany). The samples were prepared and inserted into the coil with the normal parallel to the magnetic field. All spectra were recorded at 295 K.
In addition, ^{31}P and ^{2}H ssNMR spectra of lipids in non-oriented samples provided information on the macroscopic order of the lipids.

The proton-decoupled ^{31}P solid-state NMR spectra were recorded at 161.937 MHz on a Bruker Avance 400 MHz NMR spectrometer using a Hahn echo pulse sequence (Rance and Byrd, 1983). The recording was carried out at room temperature with an echo time of 40 µs, a repetition time of 3 s, a ^{31}P B1 field of 60-80 kHz and a spectral width of 40-120 kHz. The spectra were referenced relative to 85% phosphoric acid (H_3PO_4) at 0 ppm. An exponential line broadening (LB) of 150 Hz was applied prior to Fourier transformation.

The proton-decoupled ^{15}N solid-state NMR spectra were recorded at 40.54 MHz on a Bruker Avance NMR 400 MHz spectrometer using a cross polarization (CP) pulse sequence (Pines et al., 1973). The recording was carried out with a CP contact time of 800 µs, a repetition time of 3 s, ^{1}H B_1 field of 31 kHz, a spectral with of 38 kHz and acquisition times ranging from 6 to 20 ms. The spectra were calibrated relative to external ammonium chloride ($^{15}NH_4Cl$) at 40 ppm (Bertani et al., 2014). An exponential apodization function with a line broadening of 100Hz was applied prior to Fourier transformation.

Deuterium solid-state NMR spectra of $^{2}H_3$–alanine labelled peptide reconstituted in lipid bilayers were recorded at 61.4 MHz on a Bruker Avance 400 MHz NMR spectrometer using a quadrupole echo sequence (Davis et al., 1976). The recording was done using a spectral window of 500 kHz, with a B_1 field of 40.3 kHz, an acquisition time of 8 ms and a recycling time of 1.5 s, respectively. After the acquisition, the FID was left-shifted to allow its transformed part to begin at the exact top of the echo. The spectra were calibrated on $^{2}H_2O$ at 0 ppm. Before Fourier transformation, an exponential multiplication with a LB of 500 Hz was applied.

To investigate also the effect of the peptide on membrane, deuterium solid-state NMR spectra of samples made of POPC labelled with 31 deuterium nuclei along the palmitoyl chain were measured on a Bruker Avance 400 MHz NMR spectrometer using a quadrupolar echo sequence (Davis et al., 1976). The spectra were recorded with a repetition delay of 0.3 s, an echo time of 100 µs, a B_1 field of 40 kHz. The FID was

measured in a spectral with of 100 kHz to allow a precise adjustment of the echo by a left-shift of the FID after the acquisition. The processing included an exponential apodization with line broadening of 200 Hz for the lipid and 500 Hz for the peptide spectra, respectively. The spectra were referenced relative to D_2O.

4.1.2.2. **Results and Discussion**

4.1.2.2.1. **Preparation of the synthetic peptides**

With the goal to investigate the p24 SM C18 structure and interaction, we designed two peptides starting from the membrane spanning residues of the natural p24 protein (21 aa, underlined in Table 8). Their sequences and the characteristics are listed in **Table 8**. The first peptide named p24TMD, has 31 amino acids, where the p24 transmembrane residues are flanked by additional amino acids (green) of the full length p24 protein including the proposed SM binding motif (red). In order to improve the solubility of this peptide, charged amino acids (brown) were added at the N-terminus (Nter) and C-terminus (Cter). The second peptide p24TMDH, has the same sequence than the one published by Contreras et al. It is made of 34 residues and has the same sequence than p24TMD except its Nter which encompasses more amino acids from the full length p24 protein.

The selectively labelled [^{15}N-A20]-p24TMD peptide was first synthesized using Fmoc SPPS. The crude synthetic peptide was purified by reverse phase HPLC using an acetonitrile/water gradient ranging from 30 to 95% solvent B during 30min. The peptide was eluted at 44% solvent B as indicated on the HPLC chromatogram (red star, Figure 58). **Table 9** summarizes yields that were obtained before and after purification of the peptide. Based on these data, we obtained 39 mg (10%) of peptide after the synthesis and purification with a loss of about 83% during the last step. Indeed, we encountered difficulties during the purification as the peptide sticks to the column and sometimes elutes only with difficulty. Its purity was estimated at 96% by analytic HPLC and the identity verified by MALDI spectrometry. The MALDI spectrum of the purified fraction (Figure 59) displays a single peak with mass (m/z 3671.684) that is close to the expected mass of the single label peptide (m/z 3675.44). This is indicative that the peptide is quite pure, with clear improvements when compared to the crude peptide (not shown). The slight mass difference could be explained by error during the calibration.
In contrast, p24TMDH synthesis was trickier than for p24TMD. Although it yields more crude peptide compared to p24TMD (Table 9), resuspension of the crude peptide prior to HPLC purification results in peptide aggregation. This is likely related to the absence of charged amino acids at the amino terminus of the peptide.

Table 8 : List of synthetic peptides with their amino acids sequences and biophysical properties. The transmembrane residues are highlight and contain the SM binding motif (red). It is flanked by the natural amino acids sequence (green) and added charged amino acids (brown)

SYNTHETIC PEPTIDES	SEQUENCES	PROPERTIES
p24TMD	NH_2-KKTNSRVVLWSFFEALVLVAMTLGQIYYLKR-$CONH_2$	Length: 31 residus pI: 10.17 Mw: 3674.44 g mol^{-1} ξ: 8250 cm^{-1} M^{-1}
p24TMDH	NH_2-GINDNTNSRVVLWSFFEALVLVAMTLGQIYYLKR-$CONH_2$	Length: 34 residus pI: 8.50 Mw: 3931.60 g mol^{-1} ξ: 8250 cm^{-1} M^{-1}

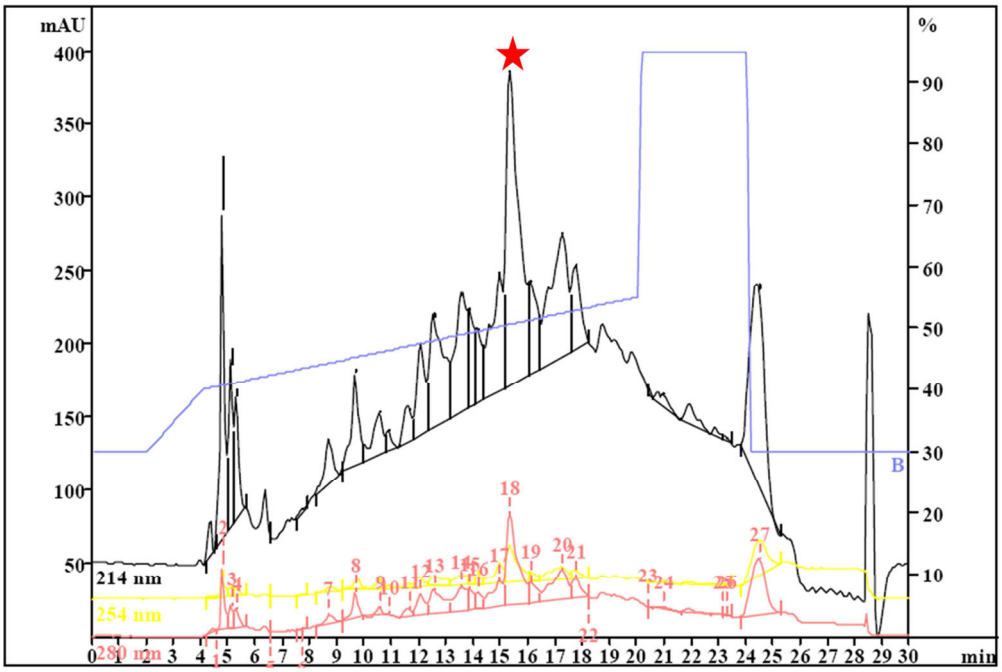

Figure 58: HPLC chromatogram of p24TMD purification. The black line represents protein absorbance at 214nm, the yellow line at 254nm and the red line at 280nm. The latter is essentially due to Trp. The star indicates the elution fraction in which the peptide was identified

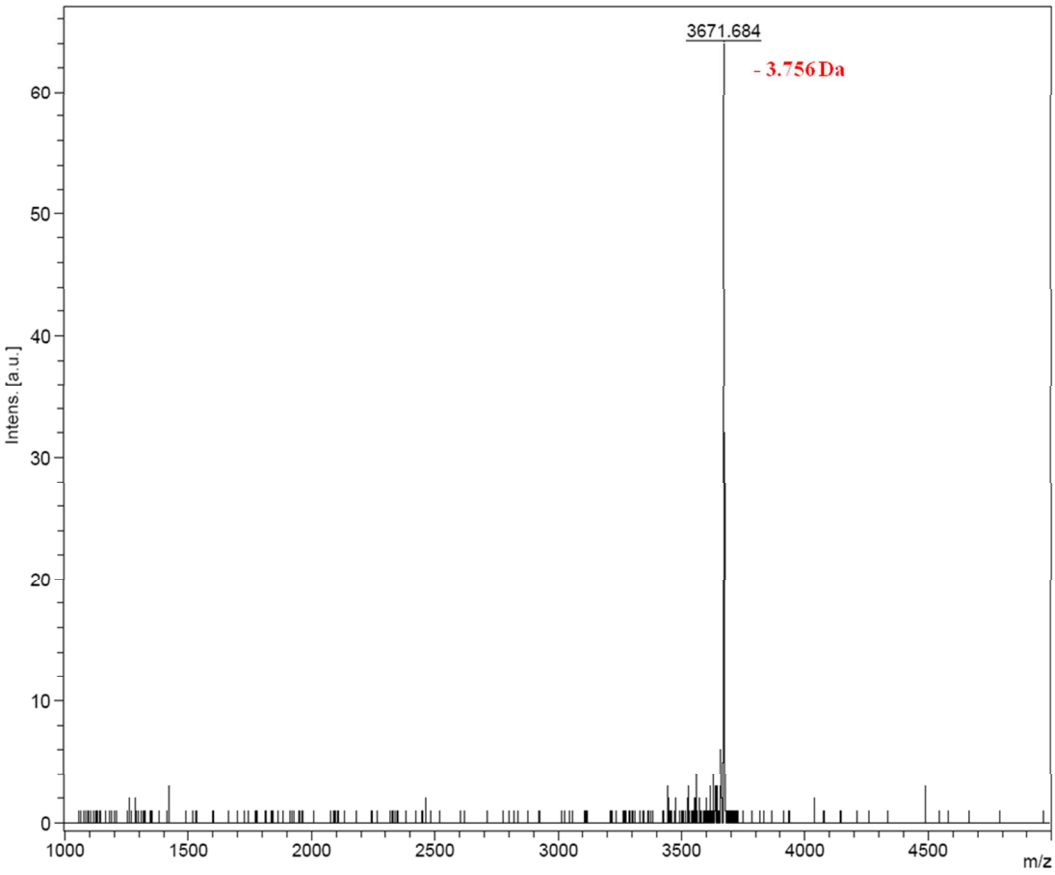

Figure 59: Identification of p24TMD after purification by MALDI spectrometry. 0.5µl of p24TMD HPLC fraction 44% solvent B (100% acetonitrile 0.1% TFA) was mixed with α-cyano matrix, dried at air and analyzed by MALDI-TOF mass spectrometry with a reflectron mode

Table 9: Summary of the different yields after peptide synthesis and purification. The synthesis of both peptides is difficult but was improved by using double coupling. From a p24TMD synthesis of 5.9 10-2 mmol about 39mg of peptide were obtained after the purification step while we didn't succeed the complete purification of p24TMDH because of aggregation

PEPTIDES	SOLID PHASE PEPTIDE SYNTHESIS			AFTER RP-HPLC	TOTAL YIELD (%)
	Theoric mass (mg)	Crude (mg)	Yield (%)	Pure (mg)	
p24TMD	367	218	59.4	39	10.6
p24TMDH	354	242	68.4	-	-

4.1.2.2.2. Investigation of p24TMD reconstitution in membranes

Membrane-associated peptides are difficult to study experimentally because they tend to aggregate during sample preparation. Thus, a large number of membrane mimetic systems have been developed to allow their biophysical investigation (Warschawski et al., 2011). With this purpose, we performed p24TMD reconstitution assays in liposomes and the success of these assays was checked using CD and fluorescence spectroscopy as these techniques are useful to investigate or follow changes in peptide secondary structure (Lees et al., 2006; Musse et al., 2006; Sreerama and Woody, 1993). Moreover, they are relatively fast and less material consuming thus, allowing the test of wide range of experimental conditions. We therefore took advantage of these techniques to set suitable experimental conditions for solid state NMR which required more time and material.

4.1.2.2.2.1. Investigation of p24TMD reconstitution using CD and fluorescence spectrometry

The solubility of the synthetic peptide alone was first tested in different solvents including dichloromethane (DCM), TFE, aqueous solutions (water or buffer) and water/HFIP mixtures. CD and fluorescence spectroscopy were performed only for the solvent that did not form visible aggregates. As shown of Figure 60A, for most of the solvents we tested, the peptide gives characteristic CD spectra of helical conformation except for the phosphate buffer. When dissolved initially in HFIP and in water after HFIP evaporation (water# in caption), the CD spectra are characterized by low intensities compared to water/HFIP (50/50, v/v) which displays the most pronounced intensities with a maximum at 193nm and minima at 208 and 222nm. These results suggest that the peptide adopts a helical conformation in water, water#, and water/HFIP (50/50, v/v) with a well-defined helical structure in the later. In contrast, the peptide is less helical in phosphate buffer and likely precipitate.

The natural occurrence of Trp within many proteins and peptides in combination with its fluorescence signal being dependent on its close environment makes fluorescence spectroscopy a good probe to follow conformation changes in proteins or peptides that harbour it in their sequences. (Lakey et al., 1993). In an apolar environment, Trp gives high blue-shifted (the maximum at the left corner) fluorescence intensities, whereas in a polar environment, a low (reduced or quenched) spectral intensities and a red shift are observed (Sun et al., 2010).

In good agreement with CD data, p24TMD in phosphate buffer gives no fluorescence signal as shown in Figure 60B; indicating that the peptide may form large aggregates which quench hide Trp that thus cannot emit. Trp fluorescence is increased and blue-shifted for p24TMD in water/HFIP (50/50, v/v) when compared to p24TMD in water; whereas it increased and red-shifted in water#. These results suggest that in water/HFIP; the peptide becomes more structured, as already observed by CD spectroscopy, thereby promoting a hydrophobic environment around the Trp. It had been shown that HFIP forms strong hydrogen bonds and structures at the same time some polypeptides by its hydrophobic properties (Bégué et al., 2004). In water and water#, the peptide may form large oligomers and small oligomers respectively.

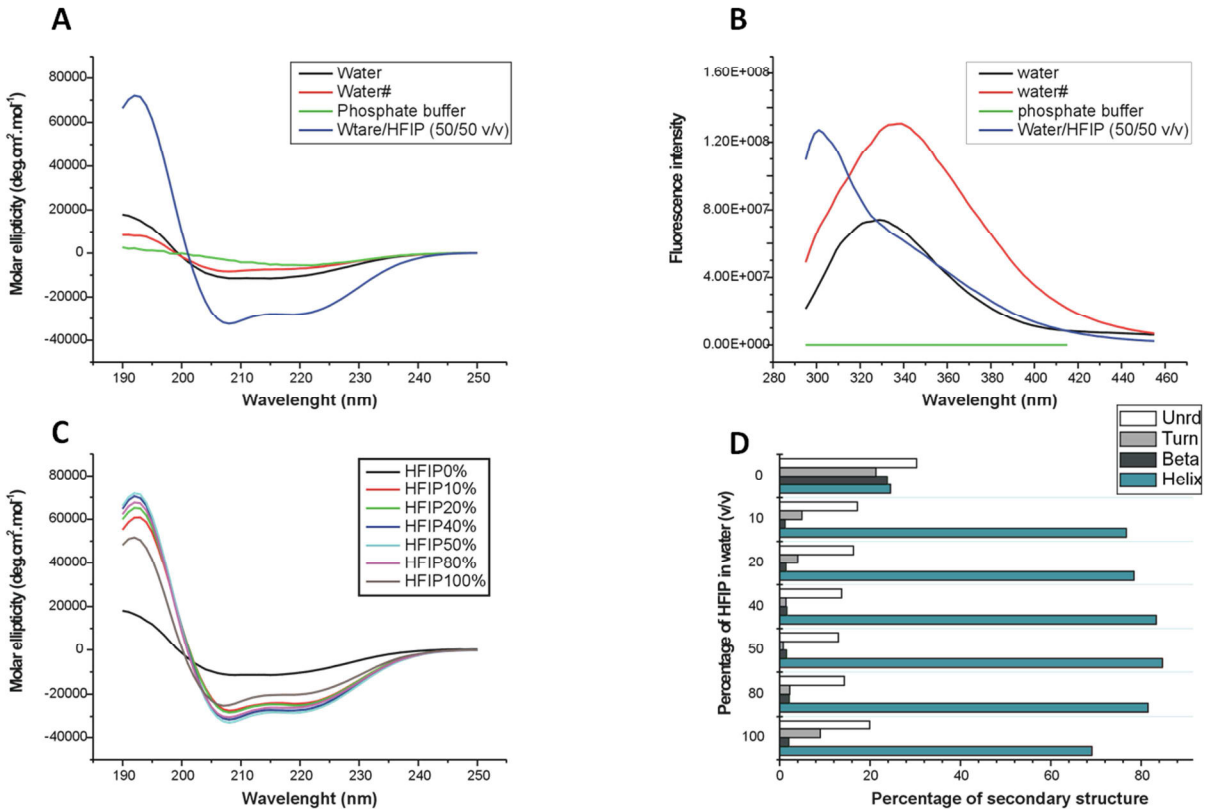

Figure 60: Characterization of p24TMD in different solvents to test its solubility. The peptide was prepared in different solvents at the final concentration of 30µM and its secondary structure and the Trp fluorescence were followed by CD (A) and fluorescence (B) respectively. In addition, the peptide secondary structure change was followed upon increasing volume of HFIP in a water/HFIP (v/v) mixture (C). A 1mg/ml stock solution of p24TMD was prepared in water and the concentration of peptide determined by absorbance at 280nm by use of the extinction coefficient. The necessary amount for 30µM final concentration of peptide was transferred into different tubes and the water was evaporated under vacuum. Thereafter, a giving volume of HFIP was added to the peptide, and completed with water to obtain the desired volume ratio of water/HFIP in 1ml and 300µl used for the CD measurement. The secondary structure composition of p24TMD was estimated from the raw CD data using the CDPro software (Sreerama and Woody, 2004). For the caption in (A) and (B): water# correspond to the peptide in water but that was dissolved first in HFIP and the solvent evaporated.

As the peptide seems to be most helical in water/HFIP (50/50, v/v), we then decided to follow the conformational changes in p24TMD relative to the increase volume of HFIP in order to determine the best water/HFIP ratio. With this purpose, a 1mg/ml p24TMD solution stock was prepared in water, its absorbance measured at 280nm and used to determine the peptide concentration. This stock solution was diluted into several tubes in order to obtain final concentrations of 30µM in 1ml and the solvent removed under vacuum. The lyophilised peptide was dissolved in different water/HFIP volume ratio in a final volume of 300µl with increase HFIP ranging from 0 to 100%.

As shown in figure 42C, the peptide adopts an α-helical secondary structure even in presence of small amounts of HFIP with more than 80% helix content in water/HFIP (50/50, v/v) (Figure 60D). This result also suggests that this helical conformation can be maintained during the reconstitution.

In order to define the reconstituted-competent state of the peptide, we first tested its interaction with POPC liposome using Trp fluorescence. POPC has properties that are quite close to the phospholipids found in biological membranes and was therefore a good candidate to start the experiments. We also tested POPC: POPG (2:1) liposomes in order to study the effect of the charge on p24TMD-lipid interaction as POPG carries a negatively charged head group.

The peptide was dissolved in 10 mM phosphate buffer pH7 at a final concentration of 30µM, titrated with different concentrations of POPC or POPC: POPG (2:1) liposomes ranging from 0 to 2mM prepared in the same buffer and the Trp fluorescence measured. As shown in Figure 61A, the changes in the fluorescence signal of p24TMD are significantly more pronounced in the presence of POPC liposomes when compared to the addition of POPC: POPG liposomes (Figure 61B). This indicates that the peptide interacted more with POPC, where alterations are observed even at low lipid concentrations, than with POPC: POPG liposomes. We further decided to check whether this interaction changes the structure of the peptide using CD spectroscopy. The CD data indicate that the peptide is in β-sheet/random coil conformation and that its structure is not affected upon increasing the concentration of POPC liposomes (Figure 61C and D). These results suggest that the peptide is not inserted as a transmembrane helix instead it interacts with the surface of POPC liposome and might form aggregates.

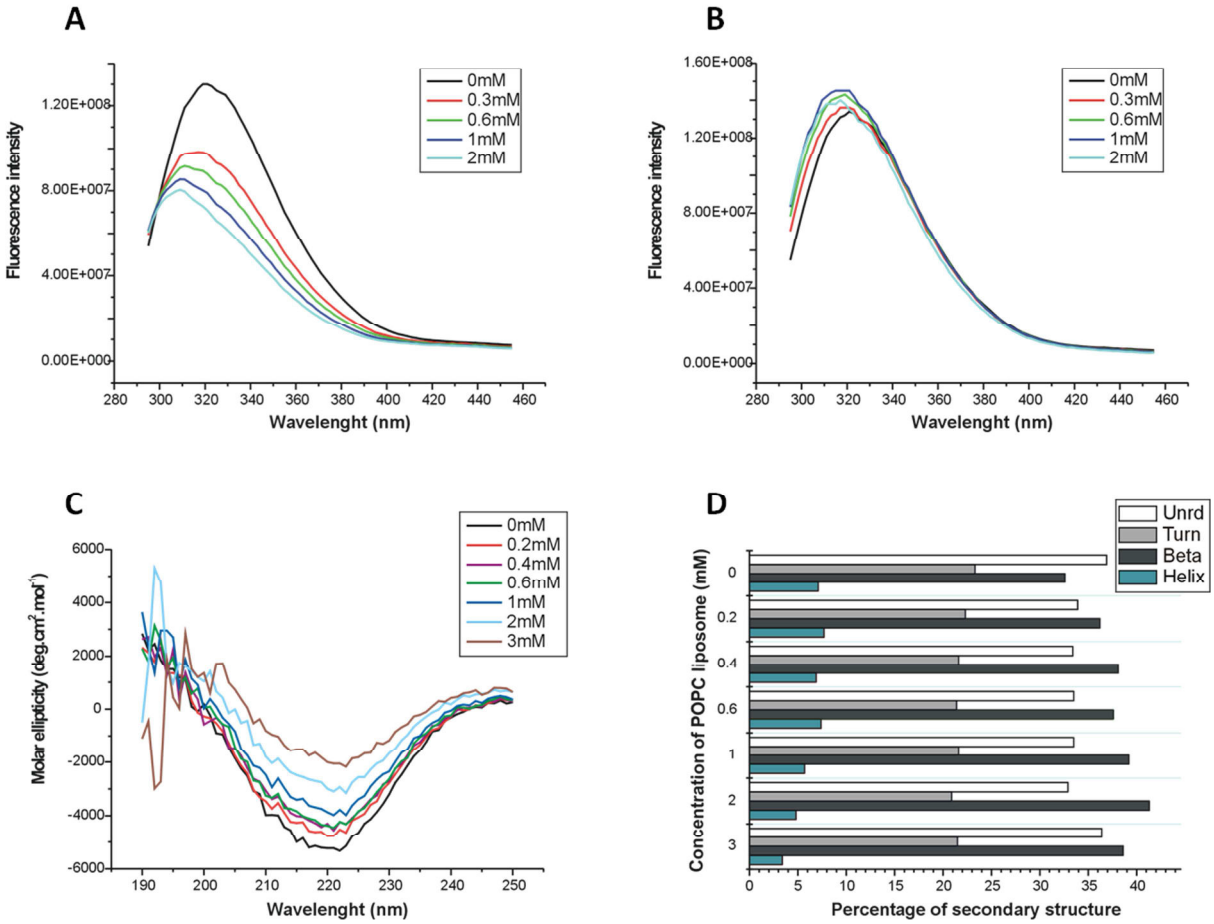

Figure 61: Characterization of p24TMD interactions with lipids using fluorescence spectrosocpy. The Trp fluorescence of 30 mM peptide in 10 mM phosphate buffer, pH7 is shown upon titration with POPC (A) or POPC: POPG (2:1) (B) at different lipid concentrations ranging from 0 to 2 mM, (C) CD spectra of p24TMD in presence of POPC liposomes and (D) the estimation of the secondary structure at different lipid concentration ranging from 0 to 3 mM

In order to force the insertion of p24TMD in liposome membranes, we prepared proteo-liposomes as described above. Briefly, p24TMD and POPC were both dissolved either in HFIP (p24/POPC# in caption) or TFE (p24/POPC* in caption), the solvents evaporated and the sample hydrated in 10 mM phosphate buffer, pH7. The final peptide-to-lipid (P/L) molar ratio is 3%. CD data (Figure 62A) indicated that the peptide adopts α-helical conformation when reconstituted into liposomes with a well-defined structure when first dissolved in HFIP. This result is in good agreement with Trp fluorescence (Figure 62B) and therefore suggests that p24TMD is inserted in POPC membranes as a transmembrane helix.

These results confirm that HFIP maintained the peptide in a reconstitution-competent state.

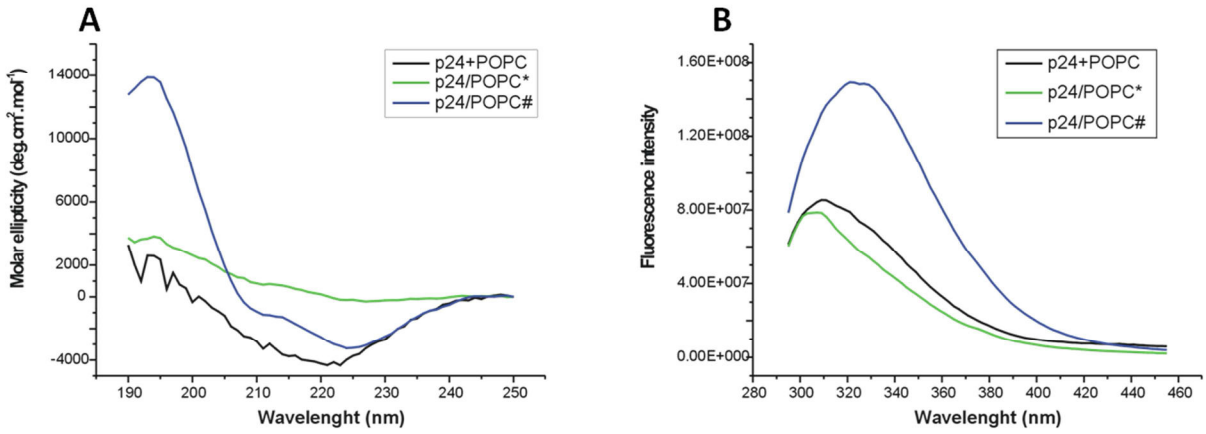

Figure 62: Test of p24TMD reconstitution-competent state in POPC. Circular dichroism (A) and Trp fluorescence (B). The table explains the captions

Caption	Description
P24+POPC	POPC liposome in phosphate buffer 10mM, pH7 added to p24 30µM in the same buffer at the final concentration of 1mM (P/L molar ratio, 3/100)
p24/POPC*	p24 /POPC proteoliposomes (P/L molar ratio, 3/100) in phosphate buffer 10mM, pH7 (peptide and lipid were dissolved in TFE and the solvent evaporated)
p24/POPC#	p24/POPC proteoliposomes (P/L molar ratio, 3/100) in phosphate buffer 10mM, pH7 (peptide and lipid were dissolved in HFIP and the solvent evaporated)

To define the best conditions for p24TMD reconstitution, we tested the peptide concentration, the buffer, and finally lipids with different head group and thickness as these parameters influence the insertion of the peptide into the membrane.

The effect of peptide concentration was tested by preparing proteo-liposomes in 10 mM phosphate buffer, pH7 with a fixed POPC concentration of 1 mM and peptide concentrations ranging from 10 to 60 µM. The CD data (Figure 63A) indicate that at 30 µM, the peptide adopts a well-defined α-helical structure whereas fluorescence spectroscopy (Figure 63B) shows that Trp is in a more hydrophobic environment.

In addition to phosphate buffer, we also tested the reconstitution of the peptide when lipids are hydrated in Hepes buffer pH 7, a zwitterionic buffer. The CD data (Figure 64A) show that the structure of the peptide doesn't change with buffer and this is confirmed with the estimation of the quantitative analysis of the secondary structure (Figure 64B). This is in good agreement with the fluorescence spectra which indicate that the Trp environment doesn't change. Based on these data, we decided to keep phosphate buffer for further reconstitution.

Finally, as the lipid's acyl chain and head group can both important determinants of the membrane properties and the interactions with transmembrane protein segment, we investigated the effect of these parameters on p24TMD reconstitution in different lipids. Their structures are summarized in Figure 65. Briefly, taking POPC as our reference, we

tested the effect of lipid's head group size and acyl chain length (membrane hydrophobic thickness) by using POPE and DMPC, respectively, with POPE having a small head group and DMPC a shorter acyl length when compared to POPC. Furthermore, DMPC carries two saturated fatty acyl chains whereas the oleoyl of POPC is monounsaturated. The interaction of p24TMD with SM was also investigated by preparing proteo-liposome with lipids mixture of POPC/SM (95/5) and POPC/POPE/SM (85/10/5).

CD spectra (Figure 66A) show that p24TMD adopts α-helical conformation when reconstituted with the different lipids except for POPE. Compared to POPC, in POPE proteo-liposome, the peptide is in β-sheet/random conformation indicating that the size of lipid head group affects the structure of the peptide. The conformation doesn't change significantly with the lipid thickness (DMPC) and in POPC/POPE/SM proteo-liposome. Interestingly, in POPC/SM proteo-liposomes, p24TMD is more structured when compared to POPC proteo-liposomes suggesting that there is an interaction with SM and this interaction affect its structure. The estimation of secondary structure shows indeed that POPC/SM proteo-liposomes have the highest helix content whereas POPE proteo-liposomes displayed the highest the β-sheet/random percentage (Figure 66B).

Fluorescence data (Figure 66C) are also in good agreement with CD as the fluorescence intensity recorded for POPC/SM proteo-liposome is highest while it decreases and left shifted with the other lipids. However, compared to CD spectra, the fluorescence signal show significant differences when the thickness (DMPC), the lipid head group (POPE), or the lipid composition change indicating that the Trp environment changes when compared to POPC bilayers. In addition to CD data, these results suggest a change of the oligomerization of the peptide.

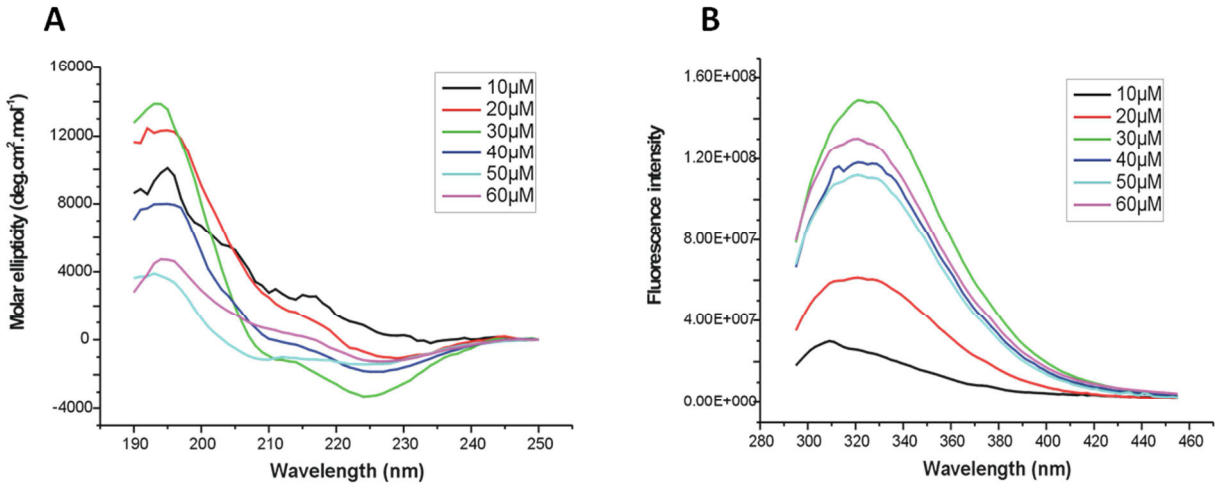

Figure 63: Test of p24TMD concentration for the reconstitution in POPC. (A) Circular dichroism of p24TMD reconstituted in POPC 1mM at different concentration ranging from 10 to 60µM and (B) the Trp fluorescence

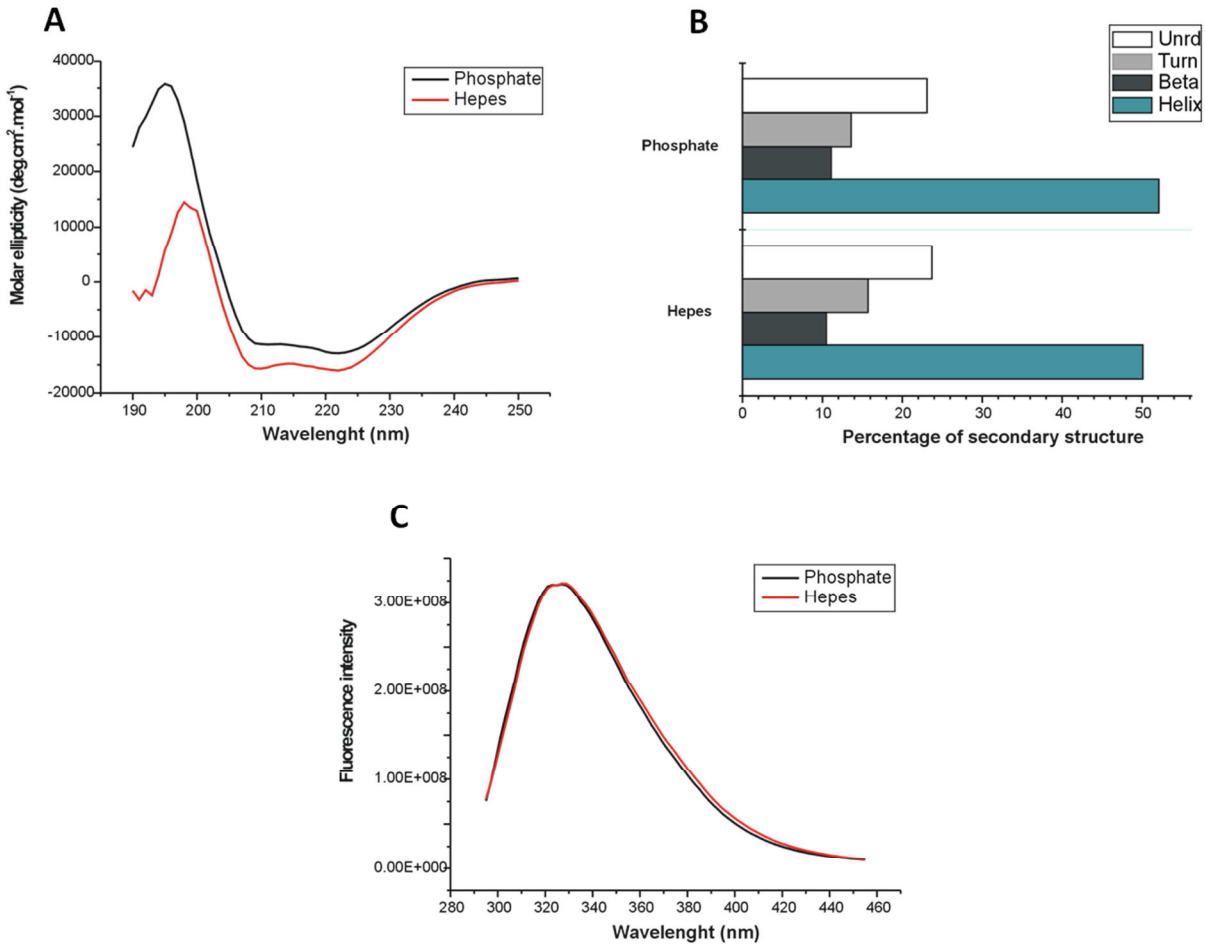

Figure 64: Test of the influence of buffer for p24TMD reconstitution in POPC. (A) Circular dichroism spectra of p24-POPC proteo-liposomes (P/L molar ratio, 3/100) prepared in phosphate or Hepes buffer and (B) the estimation of secondary structure. (C) Trp fluorescence of the same samples. All was measured at T=25°C

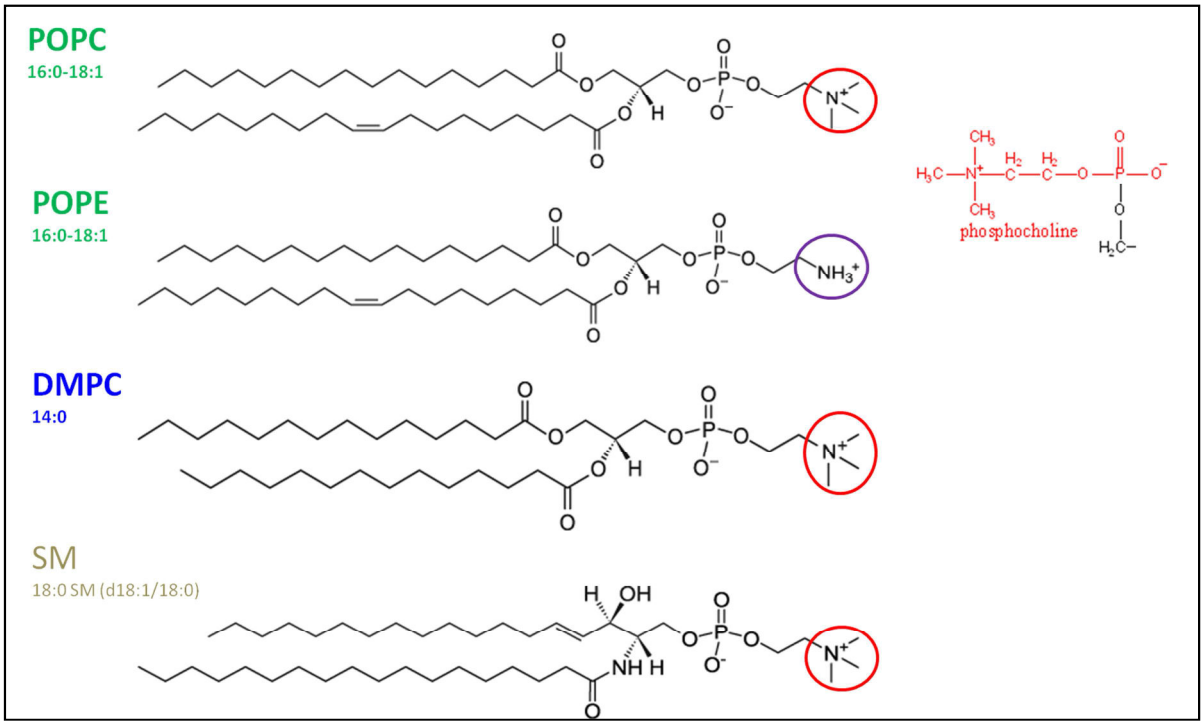

Figure 65: Structure of lipids with their different properties. The differences for the head group (size) are highlight by red and purple circles for large and small head group respectively; while for the acyl chain differences are highlight by lipid's names that are written in green and blue for the long and short acyl chain respectively. SM was used to investigate its interaction with p24TMD as it interacts with membrane and modified its properties

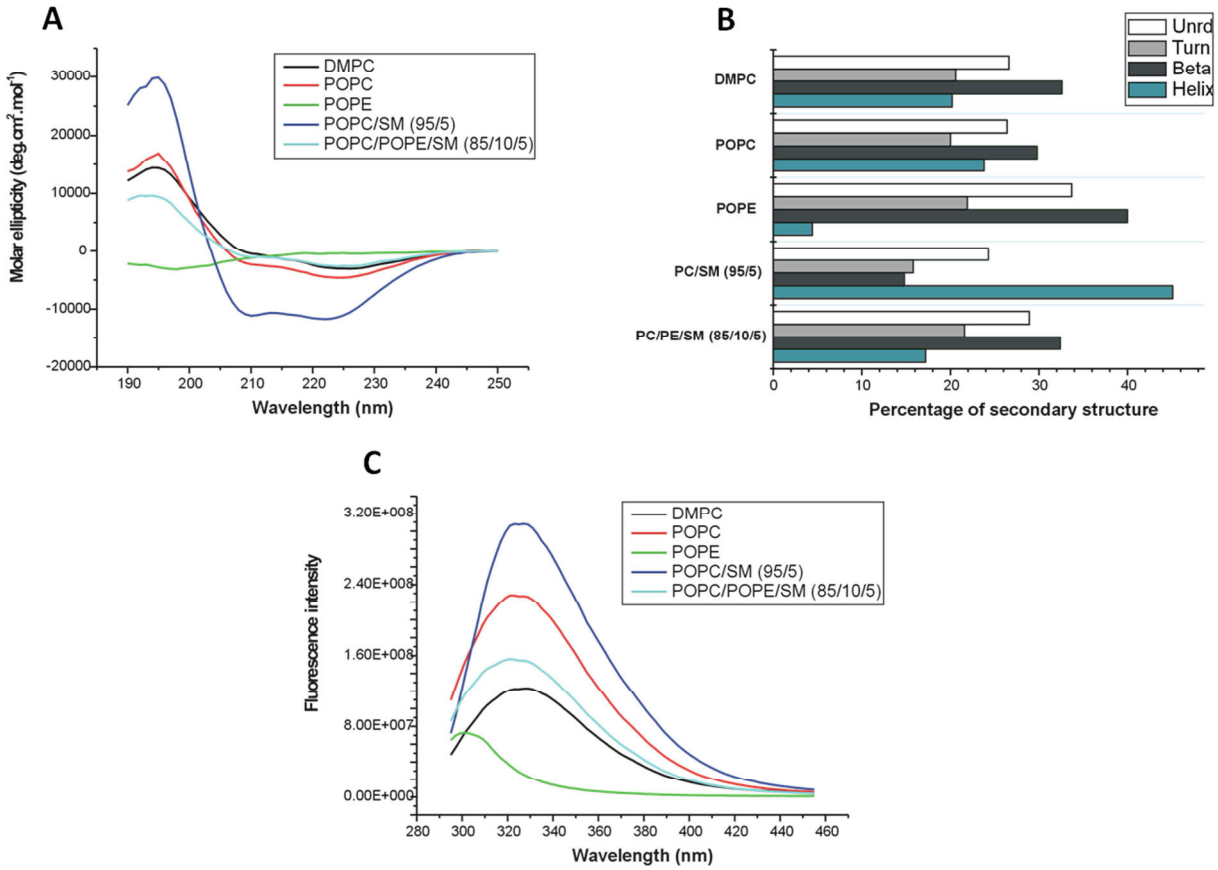

Figure 66: Effect of lipid's physical parameters and SM interaction with p24TMD. (A) Circular dichroism spectra of p24 in proteo-liposomes (P/L molar ratio, 3/100) prepared in phosphate buffer and with different lipids: DMPC, POPC, POPE, POPC/SM (95/5), POPC/PE/SM (85/10/5) and (B) estimation of secondary structure composition. (C) Trp fluorescence of the same samples. All was measured at T25°C except for DMPC (37°C)

Based on these results, we can conclude that the structure of the peptide is likely modulated by the lipid head group, the membrane thickness and the presence of SM. They also indicate that there is an interaction between p24TMDs and that the peptide is probably inserted in the POPC/SM (95/5) membrane.

In summary, we show that the lipid head group and the thickness affect p24TMD affinity for the membrane. Except for POPE, the peptide adopts a helical conformation with more helix content in POPC/SM (95/5) membranes suggesting an interaction with SM when compared to POPC membranes. We therefore kept this lipid mixture as well as the defined experimental conditions for the preliminary solid state NMR assays described in the next section.

4.1.2.2.2.2. Investigation of p24TMD reconstitution using solid-state NMR spectroscopy

Solid-state NMR spectroscopy is a well-established approach for the investigation of the topology of membrane-associated polypeptides (Aisenbrey and Bechinger, 2004a, 2004b; Bechinger and Sizun, 2003c; Bechinger et al., 1999, 2004; Cross, 1997b) in particular ^{15}N NMR spectroscopy of uniaxially oriented sample has proven to provide direct information on the membrane alignment of helical peptides (Bechinger and Sizun, 2003c; Salnikov and Bechinger, 2011). The sample preparation is very important in this technique and should therefore be performed carefully as it affects the quality of the resulting spectrum. Here we describe how we improved our protocol and thus yield good NMR spectra using ^{15}N NMR spectroscopy by varying different parameters (ratio of peptide/lipid, solvent...) during NMR sample preparation.

Our first sample test was achieved under conditions similar to the first CD experiments. Shortly, selectively labelled [^{15}N-A20]-p24TMD peptide and POPC were both dissolved in HFIP at a final molar ratio P/L of 1.9% and the solvent removed under a nitrogen stream. The mixture was applied on glass plates, dried to remove the solvent, hydrated at 98% humidity and sealed as described in the experimental protocol above. The sample was then oriented with the normal parallel to the magnetic field B_0 in a double resonance probe (e-free probe) and the ^{1}H-^{15}N decoupled NMR spectrum recorded on a 400 MHz spectrometer at room temperature (RT). In this condition, we obtained a broad peak (Figure 67A, left) indicating that the NH bond of the peptide does not adopt one but a wide range of orientations. As phosphates (^{31}P) are naturally abundant in the lipid head groups, they are used as a probe to check the lipid alignment relative to the magnetic field B_0. We therefore also recorded the ^{1}H decoupled ^{31}P NMR spectrum of this sample. The spectra indicate that membranes are not well aligned with respect to B_0 (Figure 67A, right). From these results, we hypothesize that the peptide aggregates at the surface of membrane bilayers.

We therefore took advantage of the CD results and first dissolved the peptide in HFIP, removed the solvent and then dissolved it in HFIP/water (50/50, v/v) which gives a high helix percentage (> 80%) as shown in Figure 60D. Thereafter, the peptide was mixed with POPC in HFIP not at a P/L molar ratio of 1.9% but at 1% final molar ratio and the solvent evaporated. The next steps of the sample preparation were done as described above and the NMR spectra recorded under the same conditions on a 300 MHz spectrometer. The ^{1}H decoupled ^{15}N NMR spectrum of this sample shows two peaks: a sharp peak at 224.8 ±5 ppm and a broad peak around 100 ppm (Figure 67B, left). This result indicates that one population of the p24TMD peptide adopts a well-defined transmembrane orientation whereas another fraction adopts an approximately in-plane orientation. Quite interesting, when compared to the previous NMR spectrum (Figure 67A, left), it seems that one part of the broad peak shifts and gives rise to this resolved peak. The integral of the area under these signals indicate that the transmembrane population represents 1/4 and the in-plane population 3/4. Under these conditions, we have thus converted a population of peptide in a transmembrane orientation. The ^{1}H decoupled ^{31}P NMR spectrum shows that membranes are better-aligned than previously. These results suggest that the broad peak might come indeed from peptide aggregation at the membrane. Considering that the peptide is not well structured in water as CD spectroscopy shows, we then decided to keep the water content as low as possible during solvent evaporation in order to avoid peptide aggregation.

With this purpose, the peptide was prepared in HFIP/water (50/50, v/v) as described above and added not directly but in a step-wise manner to POPC (P/L 1%). The solvent evaporation was also achieved in a step-wise manner avoiding high water content when compared to HFIP during each step. The next steps of the sample preparation were done as previously described and the spectra recorded in the same conditions on a 300 MHz spectrometer. The ^{1}H-^{15}N decoupled NMR spectrum gives rise to a sharp peak at 224±3 ppm (Figure 69C, left) indicating the presence of a single population of peptide with a well-defined transmembrane orientation. Interestingly, we obtained the same chemical shift value as in the previous experiment. This indicates that when prepared under the last conditions tested, the peptide is reconstituted in a stable manner into the membrane bilayer. This observation is supported by the results we obtained when the peptide is dissolved in HFIP/water (80/20, v/v) which also gave a high helix percentage (> 80%) Figure 60D) and added in a step-wise manner to POPC (P/L, 1%). Indeed, as shown on Figure 67D, a sharp peak is observed and the measured chemical shift (222 ±3ppm) is not significantly different from the previous results (considering the error from the calibration of the NMR scale). However, although the chemical shift has not changed significantly, CD and Trp fluorescence spectra indicate that p24TMD is more helical and might be inserted in the membrane when dissolved in HFIP/water (50/50, v/v) and added in a step-wise manner to POPC in order to form proteoliposomes (data not shown). The ^{1}H-^{31}P decoupled NMR spectrum shows that membranes are also well-aligned.

In order to set up and optimize the protocol of p24TMD reconstitution in membrane bilayers, we used ssNMR of a uniaxially oriented sample to investigate its topology in POPC. Here we defined the experimental conditions to prepare the peptide in oriented membranes and reconstitute it in a stable manner in membrane bilayer. All ssNMR samples were prepared with these conditions.

A part of the CD results were reported in an article published on june 2014 (Kemayo Koumkoua et al., 2014).

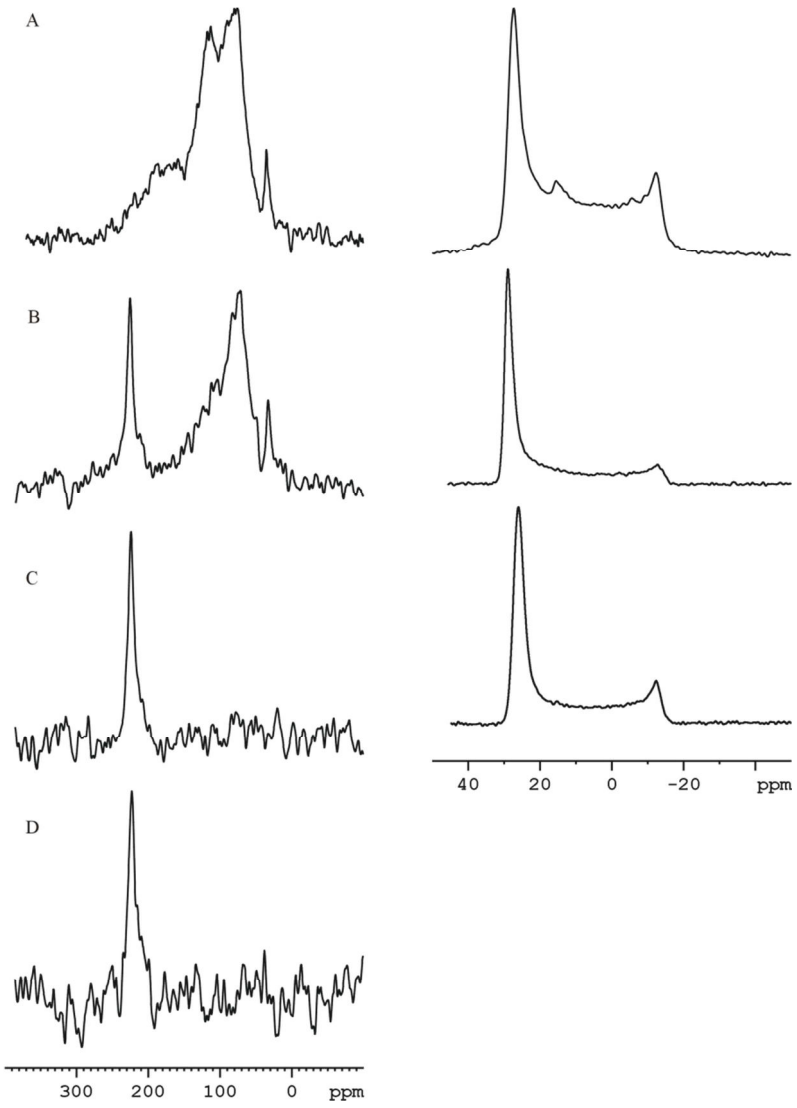

Figure 67: Proton-decoupled ^{15}N cross polarization ssNMR spectra (left) of [^{15}N-A20]-p24TMD reconstituted into oriented POPC membranes prepared in different conditions: A) when the peptide and lipids are both dissolved in HFIP (P/L, 1.9%), (B) the peptide is first dissolved in HFIP/water (50/50, v/v) before being mixed with lipids (P/L, 1%), (C) the peptide is first dissolved in HFIP/water (50/50, v/v) or (D) (80/20, v/v) and added to the lipids in a step-wise manner (P/L, 1%). The proton-decoupled ^{31}P ssNMR spectra of the POPC head group in membrane for each described conditions (right). The first spectrum (A) was recorded at 9.4 Tesla and the others on the 7.1 Tesla at RT

4.1.2.2.3. Investigation of p24TMD reconstitution in micelles

Bilayers membranes study by liquid state NMR pose difficulties as this technique is limited by the size of molecules or their complexes. Because of their relatively small size, micelles are commonly used for liquid state NMR as a minimalist system of a membrane to investigate membrane peptides in solution (Beswick et al., 1999; Campagna et al., 2007; Lauterwein et al., 1979). In order to set up a protocol of p24TMD reconstitution in

micelles, we performed some tests using DPC (n-dodecylphosphocholine) and SDS (sodium dodecyl sulfate), zwitterionic and anionic detergents, respectively. DPC micelles simulate eukaryotic cell membranes, which are generally rich in zwitterionic phospholipids while SDS has been chosen to mimic the negatively charged phospholipids found in membranes. Their structures are shown in Figure 68. Taking advantage of the previous results, we first dissolved the peptide in HFIP/H_20 (50/50, v/v), evaporated the solvents and resuspended it in 10 mM phosphate buffer, pH 7 at the final concentration of 30 µM. We then titrated the peptide with variable concentrations of DPC and SDS ranging from 0 to 5 mM and 16 mM, respectively, more or less two times the critical micellar concentration (CMC) and the conformational changes were followed by CD and fluorescence spectroscopy.

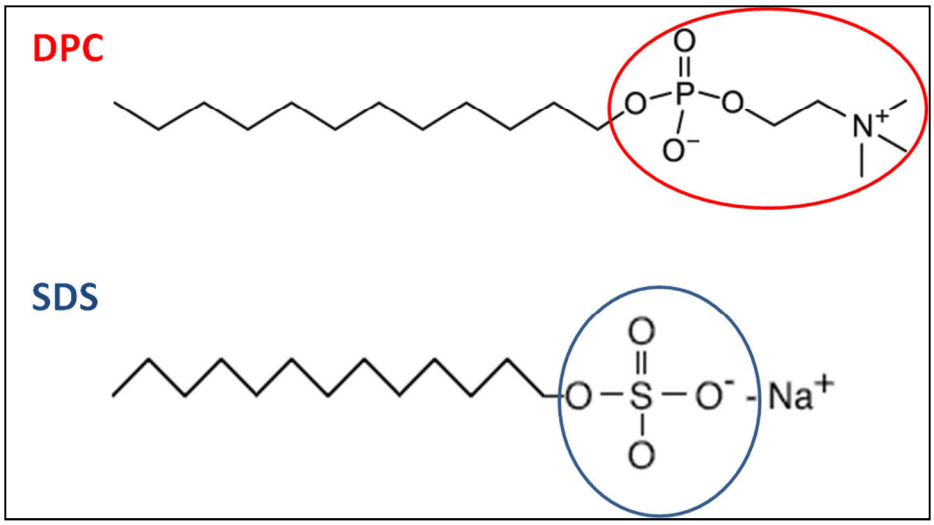

Figure 68: Molecular structure of SDS (anionic) and DPC (zwitterionic) detergents. Their respective CMC are 8 mM and 1.5 mM in water (Manzo et al., 2013)

As shown on Figure 69A and C, at low SDS concentration (< 2mM), the conformation of the peptide is not significantly affected with the increasing concentration of detergent. Above 2 mM, the p24TMD become more helical. This conformation change is proportional to the increased concentration of SDS below the CMC (6-8 mM) but slightly reduced α-helicity above. In contrast, the peptide adopts well-defined α-helix conformations with increased concentrations of DPC above the CMC (1.5 mM) (Figure 69 B and D). In addition, fluorescence signals give significant changes in DPC compared to SDS indicating an important interaction between the first detergent and the p24TMD (Figure 69 E and F). The intensities also increased (higher than SDS) proportionally with higher concentrations of DPC and stabilized above the CMC suggesting that the Trp became more deeply inserted in the hydrophobic core of the DPC micelle. These results suggest that DPC may promote stable helix formation. We therefore decided to investigate the structure of the peptide by liquid state NMR in DPC.

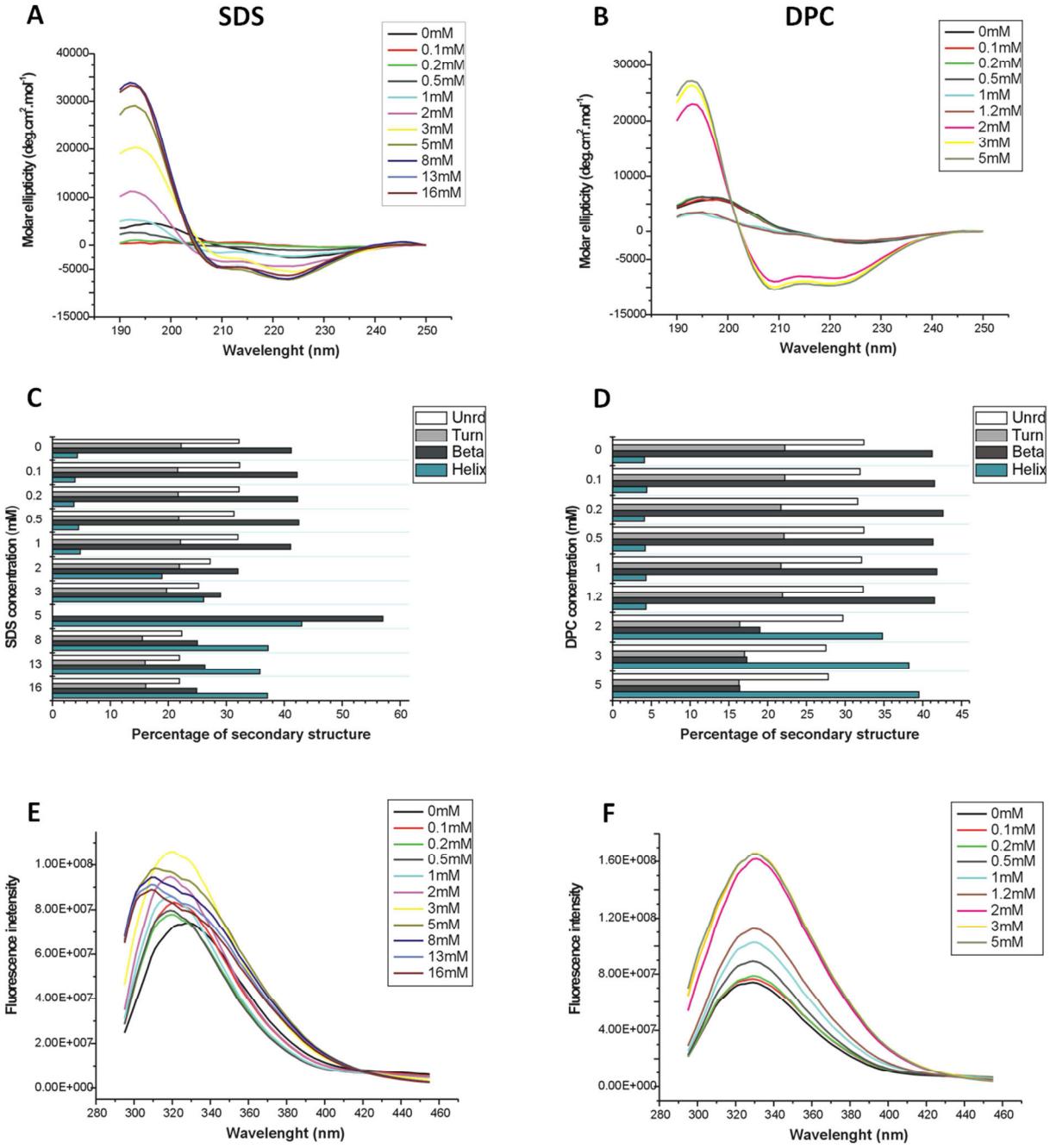

Figure 69: CD and fluorescence of p24TMD in detergents (SDS and DPC). 30µM of peptide was prepared in 10 mM phosphate buffer, pH7 and titrated with SDS and DPC at variable concentration ranging from 0 to 16 mM and 0 to 5mM respectively. The CD spectra of the peptide in SDS (A) and DPC (B) were recorded at 25°C. The secondary structure was extracted from raw CD data for the peptide in SDS (C) and in DPC (D) using CDPro software. Fluorescence experiences were achieved in the same conditions in SDS (E) and in DPC (F).

4.1.2.3. **Conclusions**

In summary, here we defined experimental conditions of p24TMD reconstitution in liposomes. We first tested the solubility of the peptide in different solvents and show that p24TMD in water is not well structured whereas it adopts a well-defined α-helix conformation in HFIP/water (50/50, v/v). We show that when the peptide is titrating with POPC liposomes, it does not insert in membrane but probably aggregates at the surface of liposome. We therefore decided to force them into membrane by preparing proteo-liposomes. We show that reconstitution is affected by the lipid head group and the thickness as they change the peptide affinity for the membrane. Indeed, when reconstituted in POPC/SM (95/5) membranes compared to POPC, it seems that SM interacts with p24TMD and that this interaction improved the peptide structure into a better-defined helical conformation. Therefore, we kept this lipid mixture and conditions in further NMR experiences. By playing on low water content during the preparation of solid state NMR, we were able to prevent peptide aggregation that thus results in well resolved spectra. In addition, as we plan to perform liquid state NMR, we also investigate p24TMD feature in presence of detergent. Our results suggest that DPC promote stable helix formation compare to SDS detergent.

4.1.3. Investigation of p24TMD-SMC18 interaction by solid-state NMR

4.1.3.1. Experimental

Static solid-state NMR spectroscopy was performed on oriented and non-oriented samples in order to provide structural information of p24TMD and macroscopic order of lipids in presence of the peptide respectively. All lipids, including deuterated POPC-d31 were purchased from Avanti Polar Lipids (Birmingham AL, USA).

4.1.3.1.1. Preparation of oriented samples

Peptides (Table 10) were obtained by solid phase peptide synthesis as described in the previous experimental section (4.1.2.1). The solid-state NMR samples were prepared by dissolving first separately 150mg lipids in total and 7mg of peptide. Pure POPC was dissolved in 1ml HFIP and for the lipid mixture sphingomyelin (SM), POPE, POPS, cholesterol (chol) and POPC were separately dissolved in HFIP and mixed to satisfy the desired mass ratio. Binary and more complex lipid compositions were prepared by mixing SM/POPC, POPC/POPE/POPS/chol/SM, and POPC/POPE/POPS/chol in the respective final mass ratios 95/5, 52/19/5/16/8 and 60/19/5/16. In parallel, selectively labeled peptide was first dissolved in HFIP, and the solvent removed under a stream of nitrogen. Thereafter, it was resuspended in HFIP/water 50/50 (v/v) and added in a step-wise manner to lipids in HFIP with a final peptide-to-lipid (P/L) molar ratio of 1 %. This was performed in such a manner that the water content remained low in order to avoid peptide aggregation. The solvent was gently evaporated under a stream of nitrogen gas until the samples became viscous. The mixtures were spread on 15 to 20 ultra-thin cover glasses

(thickness 00 = 80µm; 6 × 11mm or 8 x 22 mm, Paul Marienfeld, Lauda-Königshofen, Germany), dried first in air and thereafter under high vacuum over night to remove residual traces of organic solvent. The samples were hydrated for 2-3 days at 93% relative humidity achieved by a saturated salt solution of KNO_3 in ^{2}H-depleted water at room temperature (~25°C). Thereafter, the glass plates were stacked on top of each other, physically stabilized by wrapping with Teflon tape and the whole sample sealed in plastic to avoid dehydration. The solid-state NMR experiments were then carried out at room temperature. When different temperatures were applied for example for the investigation of the dynamics this is specifically indicated.

4.1.3.1.2. Preparation of non-oriented samples

Non-oriented samples were prepared by dissolving 0.13 mg of p24TMD and 2mg of deuterated POPC (POPC-*d*31) in HFIP. The solvent was evaporated under a stream of nitrogen thus a film forms on the walls of the glass tube. The sample was then resuspended in 200µl of 10mM phosphate buffer by vortexing and sonication in a water bath followed by 10 freeze/thaw cycles. The resulting suspension was transferred into a plastic tube for micro centrifuges (VVR Radnor, PA, USA) and the vesicles were pelleted using a bench-top centrifuge (Biofuge Pico, Hearaeus Instruments, Hanau, Germany) at 13 000 rpm for 1min. The NMR measurements were directly performed on this sample.

4.1.3.1.3. ^{31}P, ^{15}N, ^{2}H solid-state NMR measurements

Solid-state NMR spectra were acquired on a Bruker Avance wide-bore NMR spectrometer operating at 9.4 or 7.05 Tesla. Both using commercial triple-resonance probes equipped with a flat coil (Bruker Biospin Rheinstetten, Germany). The spectra of oriented samples were recorded with the membrane normal in a parallel or perpendicular (turned by 90°) orientation relative to the magnetic field direction, respectively.

Proton-decoupled ^{31}P solid-state NMR spectra of oriented samples were recorded at 161.937 MHz using a Hahn echo pulse sequence (Rance and Byrd, 1983) with the following parameters: ^{31}P B_1 field ~50 kHz, echo time 40 µs, spectral width 40-120 kHz, typically 30-128 scans, and repetition time 3 s. The spectra were referenced relative to 85% phosphoric acid (0 ppm). An exponential apodization function corresponding to a line broadening of 100 Hz was applied before Fourier transformation.

Proton-decoupled ^{15}N solid-state NMR spectra were recorded at 40.54 MHz using a cross polarization (CP) pulse sequence (Pines et al., 1973). The recording was carried out with the following parameters: ^{1}H B_1 field of 31 kHz, CP contact time of 800 µs, acquisition times ranging from 6 to 20 ms, spectral with 38 kHz, and repetition time of 3 s. The spectra were calibrated relative to external ammonium chloride ($^{15}NH_4Cl$) at 40 ppm (Bertani et al., 2014). An exponential apodization function with a line broadening of 200Hz was applied prior to Fourier transformation.

Deuterium solid-state NMR spectra of $^{2}H_3$–alanine labelled peptide reconstituted in oriented lipid bilayers were recorded at 61.4 MHz using a quadrupolar echo pulse sequence (Davis et al., 1976) and the following parameters: ^{2}H B_1 field 40.3 kHz, acquisition time 8 ms, spectral window 500 kHz and recycling time 1.5 s. After the acquisition, the FID was left-shifted to start the FID with the top of the echo. The spectra were calibrated with $^{2}H_2O$ at 0 ppm. Before Fourier transformation, an exponential multiplication with a LB of 500 Hz was applied.

Deuterium solid-state NMR spectra of liposomes made of $^{2}H_{31}$–POPC or of $^{2}H_{31}$–POPC / SM C18 in presence or in the absence of p24TMD were recorded on a Bruker Avance 300 MHz NMR spectrometer using a quadrupolar echo sequence. The recording was done using the following parameters: ^{2}H B_1 field 40 kHz, echo time 100 µs, repetition delay 0.3 s. The FID was measured in a spectral with of 100 kHz to allow a precise adjustment of the echo by a left-shift of the FID after the acquisition. The processing included an exponential apodization with line broadening of 200 Hz for the lipid and 500 Hz for the peptide spectra, respectively. The spectra were referenced relative to D_2O.

4.1.3.1.4. Calculation of angular restraints from experimental solid-state NMR spectra

To determine the peptide orientation that agrees with the experimental spectra, a coordinate system was defined where the α-helical tilt and pitch angle are the angle between the long axis of the helix and the membrane normal, and between the membrane normal and the line within an arbitrary plane of the peptide helical wheel projection, respectively. Assuming an ideal α-helix conformation, the Protein Data Bank (PDB) file of the oriented helix was generated in MOLMOL. The coordinates of the labelled ^{15}N atom, the corresponding amide proton and the C atom of the previous residue were extracted from this file and used to calculate the ^{15}N chemical shift tensor in the same reference frame using the main ^{15}N chemical shift tensors (55.8, 81.4, 228.6 ppm) as reported by (Salnikov et al., 2009). By successively rotating the peptide molecule around the pitch and the tilt angle the three-dimensional orientational space was systematically screened in 50 × 50 steps using a program (Aisenbrey and Bechinger, 2004a; Aisenbrey et al., 2006) written in MATHEMATICA 3.0 (Wolfram Research, Champaign, IL). Contour plots mark the angular pairs that agree with the experimental results. The simulation of the ^{2}H solid-state NMR spectra was performed using its atomic coordinates. Both contour plots (^{15}N and ^{2}H) were superimposed and the tilt and pitch angles were read at the cross line section respectively on the Z and the X axis.

4.1.3.2. Results

4.1.3.2.1. Investigation of p24TMD in simple membranes

This section presents the results that were obtained in simple POPC and binary POPC/SM C18 (95/5) membranes. Here we investigated the effect of SM C18 on the p24TMD topology and the dynamics of the Leu23 side chain.

a) Effect of SM C18 on p24TMD topology and dynamics

To analyse the topology of p24TMD in presence of SM C18, selectively ^{15}N labelled p24TMDs was prepared by solid phase peptide synthesis (Table 10) and purified by reverse phase HPLC (~96% purity). Each peptide was reconstituted in POPC and POPC/SM (95/5) membranes and the whole sample oriented with the normal parallel to the magnetic field B_0 as described above. The topology of the helix within the membranes and the alignment of the lipid bilayers relative to the magnetic field was investigated by ^{15}N and ^{31}P solid-state NMR spectroscopy respectively.

When the ^{15}N ssNMR spectrum of p24TMD labelled at position 19 ([^{15}N V19-^{2}H L23]-p24TMD) was recorded, a peak was obtained at 217.3 ± 6ppm (Figure 70A, black) indicating that the peptide spans the membrane in a transmembrane fashion. The ^{1}H-decoupled ^{31}P spectrum of the hydrated POPC membrane bilayers (93% humidity) (Figure 70A, black, right) give a main intensity around 25-30ppm indicating that membranes are in a liquid crystalline phase and aligned with their normal predominantly parallel to the to the magnetic field B_0 (Harzer and Bechinger, 2000). Interestingly when we test the reproducibility with the same peptide reconstituted in POPC in the same conditions, we obtained a chemical shift at 220.6±5ppm which is identical within the experimental error.
In further investigation, several others positions were labelled (16, 18, 20 and 23) and reconstituted in POPC bilayers. The resulting ^{15}N spectra gave quite well-defined peak with chemical shift > 200ppm as summarized in Table 10 confirming that p24TMD adopts a transmembrane orientation (Figure 70B, black and Figure 71A, B, C black). They all gave quite similar chemical shifts within the experimental error except for position 18 (Table 11) suggesting that this residue (Leucine) is in a different environment. The ^{1}H-decoupled ^{31}P spectra indicate that POPC membrane are aligned with the normal parallel to B_0. These results confirm the reproducibility of the experiences and thus the orientation of the peptide in POPC bilayers.
When the different peptides were reconstituted in POPC/SM (95/5), the values of the chemical shift indicate that the peptide adopts a transmembrane orientation as for all the positions they were > 200ppm (Table 11). These values are quite similar except for position 18, again confirming that this residue is in a different environment. When these values were compared to those obtained in POPC membranes, we did not observe a significant

difference. The width of peaks is similar as shown Figure 54. These results indicate that the SM C18 does not affect the topology of p24TMD. The ^{1}H-decoupled ^{31}P spectra indicate that POPC membranes are aligned parallel with respect to B_0 (Figure 70,B and Figure 71A, B, C, grey) .

Table 10: Summary of synthetic ^{15}N and/or ^{2}H isotope labelled p24TMD peptides. The transmembrane amino acids are in bold with the residues involved in the binding with SM C18 highlight. The labelled amino acids are highlight in red for ^{2}H, in green for ^{15}N and their position indicates.

Names	Labelled Sequences
[^{2}HV19-^{15}NL23]-p24TMD	NH_2-KKTNSR**VVLWSFFEALVL**^{2}H**V**^{15}N**AMT**^{15}N**L**^{2}H**GQIY**YLKR-$CONH_2$ (19, 23)
[^{15}NV19-^{2}HL23]-p24TMD	NH_2-KKTNSR**VVLWSFFEALVL**^{15}N**V**^{2}H**AMT**^{2}H**L**^{15}N**GQIY**YLKR-$CONH_2$ (19, 23)
[^{15}NL23-^{2}HA20]-p24TMD	NH_2-KKTNSR**VVLWSFFEALVL**^{2}H**V**^{15}N**A**^{2}H**MT**^{15}N**L**^{2}H**GQIY**YLKR-$CONH_2$ (20, 23)
[^{15}NA20]-p24TMD	NH_2-KKTNSR**VVLWSFFEALVL**^{15}N**V**^{15}N**A**^{2}H**MT**^{2}H**LGQIY**YLKR-$CONH_2$ (20)
[^{15}NL18-^{2}HA20]-p24TMD	NH_2-KKTNSR**VVLWSFFEALV**^{15}N**L**^{2}H**V**^{15}N**A**^{2}H**MT**^{2}H**LGQIY**YLKR-$CONH_2$ (18, 20)
[^{15}NV19-^{2}HA15]-p24TMD	NH_2-KKTNSR**VVLWSFFEA**^{2}H**LVL**^{15}N**V**^{15}N**AMT**^{2}H**L**^{15}N**GQIY**YLKR-$CONH_2$ (15, 19)
[^{15}NL18-^{2}HA15]-p24TMD	NH_2-KKTNSR**VVLWSFFEA**^{2}H**LVL**^{15}N**V**^{15}N**AMT**^{2}H**L**^{15}N**GQIY**YLKR-$CONH_2$ (15, 18)
[^{15}NL16-^{2}HA15]-p24TMD	NH_2-KKTNSR**VVLWSFFEA**^{2}H**L**^{15}N**VL**^{15}N**V**^{15}N**AMT**^{2}H**L**^{15}N**GQIY**YLKR-$CONH_2$ (15, 16)

19 20

NH_2-KKTNSR**VVLWSFFEALVL<u>V</u>AM<u>TL</u>GQ<u>IY</u>**YLKR-$CONH_2$

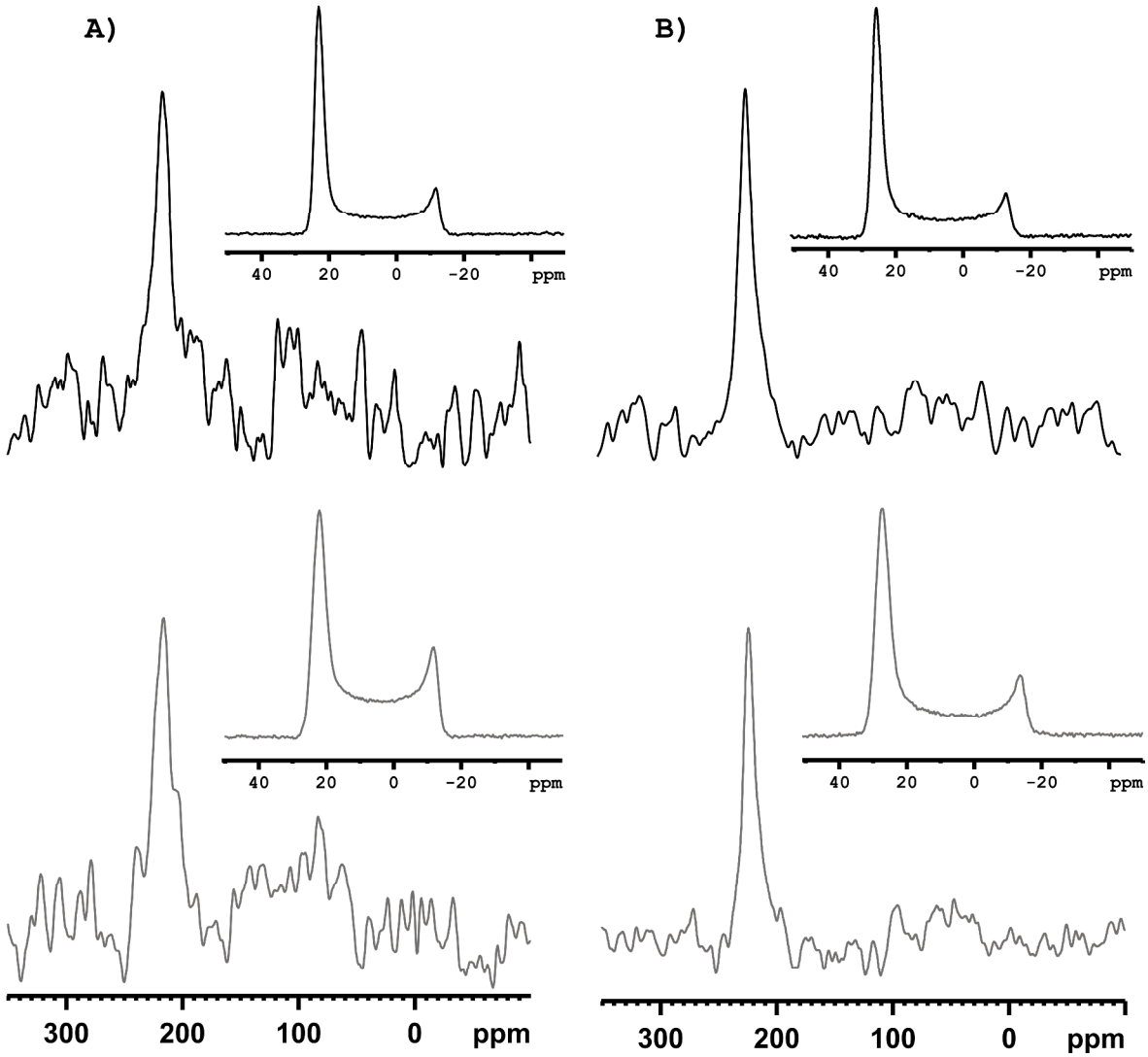

Figure 70: Proton-decoupled ^{15}N cross polarization ssNMR spectra of 7mg of A) [^{15}N<u>V19</u>-^{2}HL23]-p24TMD and (B) [^{15}N-A20]-p24TMD reconstituted in oriented 150mg POPC (black) or POPC/SM (95/5) (grey) membranes. The spectra were recorded on the 400MHz at RT. Their respective superimposition is presented on the bottom. The p24TMD sequence is represented with the TMD in bold, the ^{15}N labelled position are indicated by residue numbers and the amino acids involved in the binding with SM C18 are underlined. All the spectra were acquired with 42000 scans except for the spectra of [^{15}N <u>V19</u>-^{2}H L23]-p24TMD in POPC/ SM (95/5) membranes (panel A, grey) which was acquired during 5 days (153000 scans)

This result could explain the low signal-to-noise of the peptide ^{15}N spectrum in POPC (Figure 72A, black) as the non-aligned lipids could contribute the small but broad signal around 100 ppm.

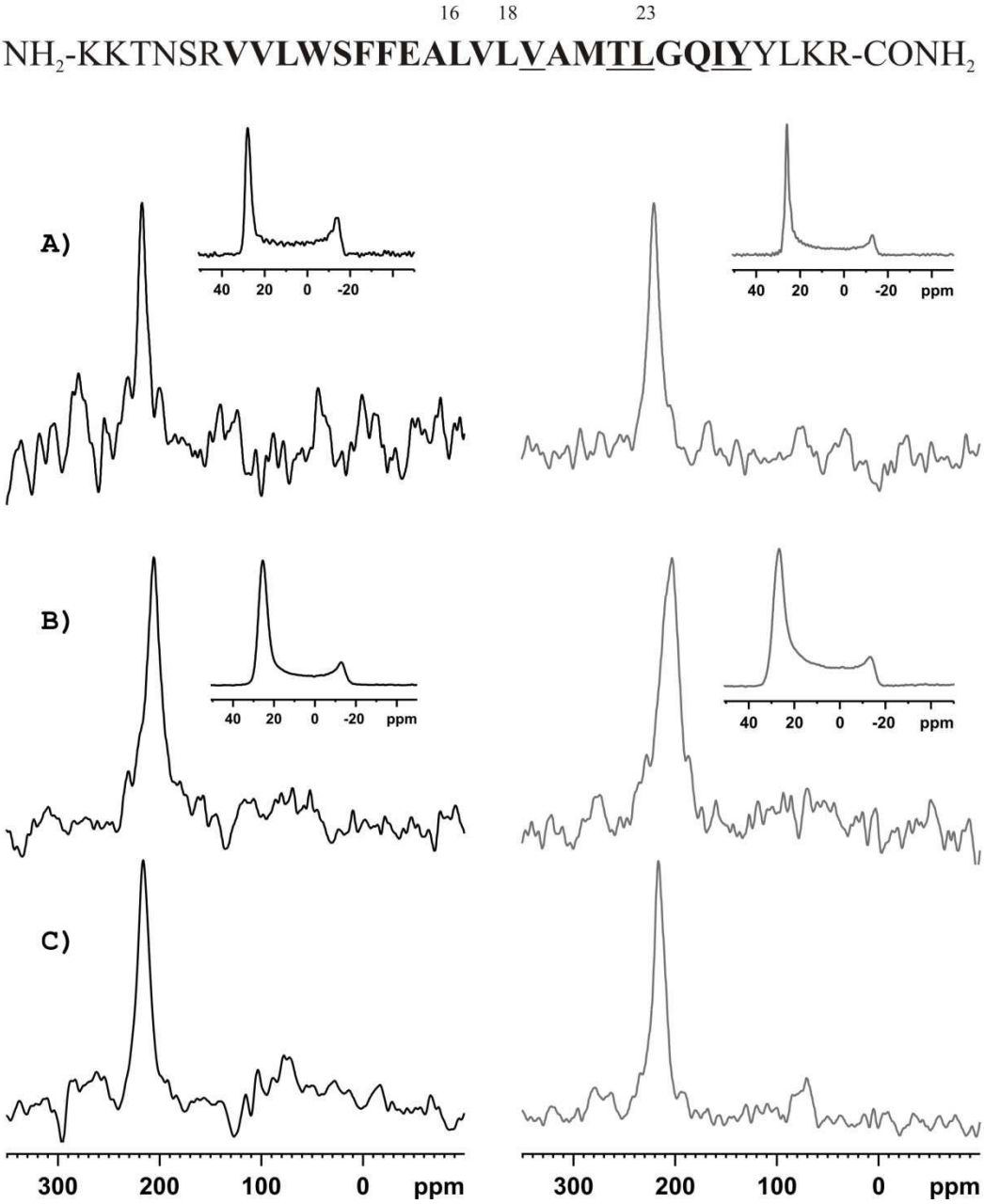

Figure 71: Proton-decoupled ^{15}N ssNMR spectra of A) [^{15}N L23-^{2}H A20]-p24TMD, B) [^{15}N L18-^{2}H A15]-p24TMD and C) [^{15}N L16-^{2}H A15]-p24TMD in oriented POPC (black) or POPC/SM (95/5) (grey) membranes. All the spectra were recorded on the 400MHz at RT except for (C) that was recorded on the 300MHz spectrometer. The corresponding ^{31}P spectra are represented on the top left and were all calibrated to 0ppm. The ^{15}N labeled position are indicated on the p24TMD sequence.

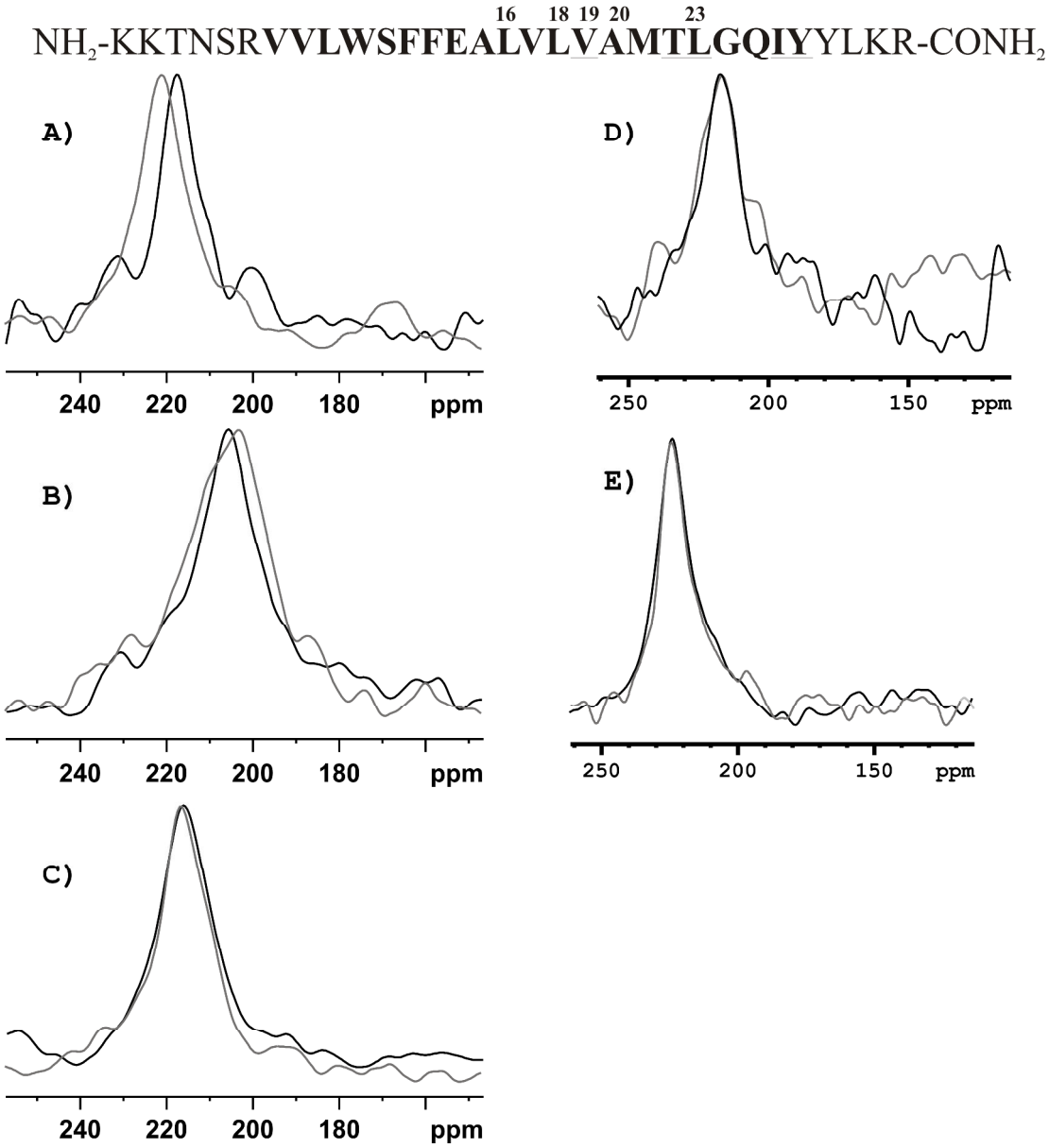

Figure 72: Superimposition of the ^{15}N ssNMR spectra (left) of A) [^{15}N L23-^{2}H A20]-p24TMD, B) [^{15}N L18-^{2}H A15]-p24TMD, C) [^{15}N L16-^{2}H A15]-p24TMD), [^{15}NV19-^{2}HL23]-p24TMD and [^{15}N-A20]-p24TMD in oriented POPC (black) or POPC/SM (95/5) (grey) membranes. The ^{15}N chemical shift values of the different label residues are summarized in the table below

Table 11: Summary of chemical shift values of p24TMD labelled at different position reconstituted in POPC and POPC/SM (95/5) membranes

	^{15}N label position	Chemical shift (ppm)		Spectrometer
		POPC	POPC/SM (95/5)	
A)	L23	217.5±3	220.4±2	400MHz
B)	L18	205.6±2	203±3	400MHz
C)	L16	216.3±2	216.6±2	300MHz
D)	V19	217.3±6	216.4±3	400MHz
E)	A20	223.6±4	224.1±3	400MHz

In order to further challenge this observation, the p24-TMD was incorporated into membranes where the content of SM C18 was increased to 10 mole%. With this purpose, [^{15}N L18-^{2}H A20]-p24TMD was first dissolved in 80%HFIP, and reconstituted at a peptide to lipid ratio of 1/100 into oriented membranes of POPC, POPC/ SM (95/5) or POPC/ SM (90/10). The chemical shift values were, respectively 203.5±5 ppm, 201.5±5 ppm and 207.8±6 ppm confirming the previous results (Table 11). However, increased concentration of SM C18 led to line-broadening (Figure 73A, blue) suggesting a small change in topology. This line-broadening could also arise from less membrane fluidity but this should correlate with the ^{31}P spectrum; which is not the case as it did not appear broader (Figure 73B, blue). Thus, this result supports the change in the peptide topology. Interestingly when we test the reproducibility, we obtained a quite similar chemical shift value (205.9 ±7ppm) with a similarly broad peak (data not shown), thus confirming this result.

The ^{31}P spectra of the different membranes show that lipid head groups are aligned with the magnetic field (Figure 73B). However, the ^{31}P spectrum of the POPC membrane shows a broader line-shape compare to the other membranes. This could come from the sample preparation or hydration.

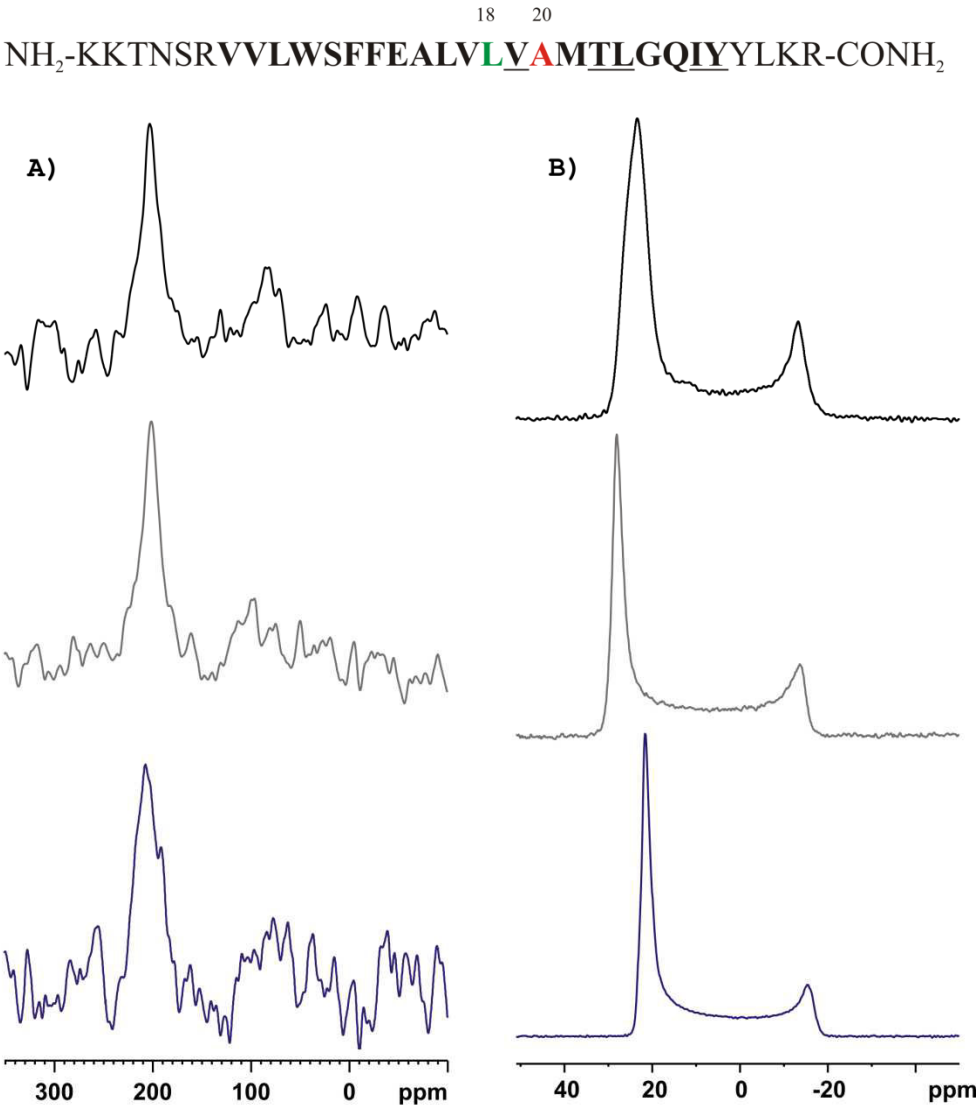

Figure 73: Effect of the increased proportion of SM C18. (A) The ^{15}N ssNMR spectra of [^{15}N L18-^{2}H A20]-p24TMD in oriented POPC (black), POPC/SM (95/5) (grey) and POPC/SM (90/10) (purple) membranes and B) the ^{31}P spectra of each membrane calibrated to 0ppm. All spectra were recorded 9.4 Tesla RT. The ^{15}N label residue within p24TMD sequence above is highlight in green and the ^{2}H residue in red

In addition, we also investigated p24TMD orientation and dynamics in membranes using ^{2}H quadrupolar splitting of the alanine ^{2}H-methyl group. Indeed, the alanine methyl group is directly attached to the peptide backbone thus, the Cα–Cβ bond exhibits a well-defined alignment relative to the helix long axis (Vostrikov et al., 2010). Furthermore, due to the fast exchange around this Cα–Cβ bond, the deuterons are equivalent resulting in identical NMR spectra. Thus the spectrum of $^{2}H_3$-labelled alanine in oriented samples relative to the magnetic field exhibits a characteristic quadrupolar splitting spectrum with the value and the shape depending on the dynamics of the ^{2}H site (see simulated $^{2}H_3$-labelled alanine spectrum Figure 74A). Moreover, the quadrupolar splitting is correlated to the relative

alignment of the Cα–Cβ bond thus, the relative alignment of the helix axis (see Equation 17).

With this purpose, several single $^{2}H_{3}$- alanine labeled p24TMDs were synthetized (see Table 10) and ^{2}H spectra of the oriented samples were recorded at 9.4 Tesla spectrometer different temperatures. When reconstituted in POPC membranes, the ^{2}H spectrum of the p24TMD sequence labelled at position Ala-15 shows a broad quadrupolar lineshape (Figure 74B) indicating that the Cα-Cβ bond does not have a well-defined orientation but rather displays a mosaic spread. In POPC/SM (95/5) the ^{2}H quadrupolar lineshape was also broader (Figure 74C, right) with no significant difference compared to POPC (Figure 74C, left). However, as the quadrupolar splitting maxima obtained in POPC/SM (95/5) look well-defined, we can therefore determine the quadrupolar splitting value by measuring directly the frequency difference between the two maxima. While for POPC, it was estimated by measuring the left half frequency (ν) multiplied by 2 as shown on Figure 74C (left). We respectively obtained ± (21.6 ±2.6) kHz and ± (20.1 ±1.5) kHz for the peptide in POPC and POPC/SM (95/5). In good agreement with the ^{15}N NMR spectroscopy, these results confirm that SM C18 does not affect the peptide orientation. Angles between the Cα-Cβ bond and the magnetic field B_0 were estimated to 43.4° or 68.1° and 44.2° or 67.0° for the peptide in POPC and POPC/SM (95/5) respectively.

In order to investigate p24TMD dynamic in POPC and POPC/SM (95/5), ^{2}H spectra of the reconstituted peptide labelled at position 15 were recorded at -20°C. The resulting spectra display characteristic quadrupolar powder pattern spectra for both membranes (Figure 75A). However, when the ^{15}N solid-state NMR spectrum is recorded at -20°C for the same peptide labelled at position 16 ([$^{2}H_{3}$ Ala15- ^{15}N Leu16]-p24TMD) and reconstituted in POPC, the resulting spectrum exhibits a predominant peak at 220 ppm and a broad distribution of intensities between 100 and 40ppm indicating that the majority of peptide adopts a transmembrane orientation (Figure 75A, Top). Notably, the ^{15}N nucleus is more robust compared to ^{2}H in the sense that its line-shape is less sensitive to tiny movement. This suggests that at room temperature the peptide scans a distribution of orientations fast enough to partially average the anisotropy on the time scale of the ^{2}H quadrupolar splitting. In addition, the ^{2}H spectrum of [$^{2}H_{3}$Ala15- ^{15}NVal19]-p24TMD in POPC/SM (95/5) at 4°C resulted in larger more broad quadrupolar splittings with low intensity compared to that at room temperature (Figure 75B) indicating that the peptide is in an intermediate exchange in membrane.

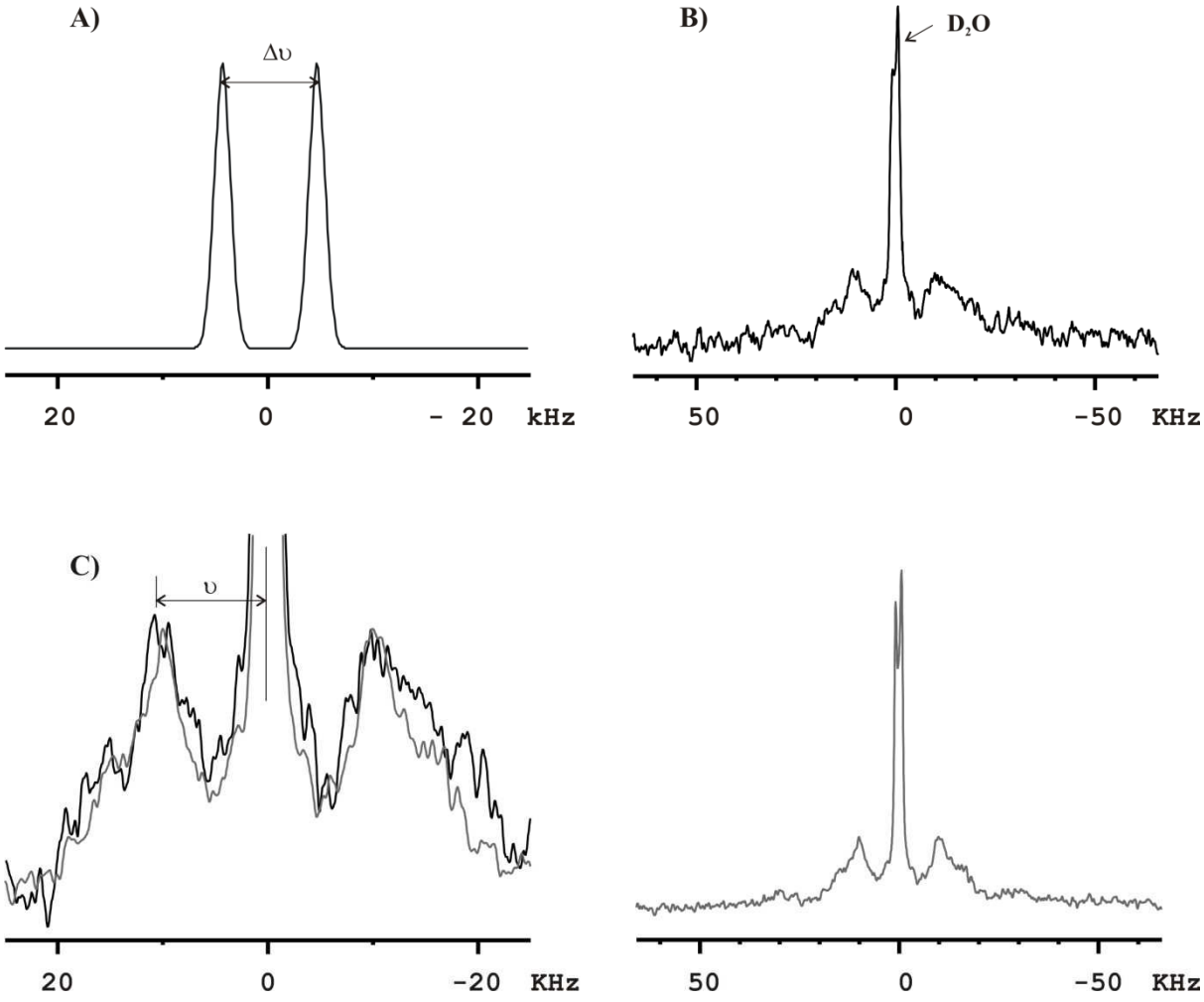

Figure 74: (A) Simulated spectrum of $^{2}H_{3}$-alanine with an angle of 48°±1° between the Cα-Cβ bond and the magnetic field when a static quadrupolar coupling constant of 72 kHz is assumed. (B) Experimental ^{2}H solid-state NMR spectra of [$^{2}H_{3}$Ala15- ^{15}N Leu18]-p24TMD reconstituted into oriented POPC (black) and POPC/SM (95/5) (gray) bilayers. Spectra were recorded on a 400MHz spectrometer at RT and LB of 500Hz applied for each spectrum. The DHO peak in the middle of each spectrum was calibrated to zero. (C) The zoom of the experimental spectra superimposition. For the spectrum obtained in POPC, Δν was determined by 2-fold multiplication of the measured ν as indicated.

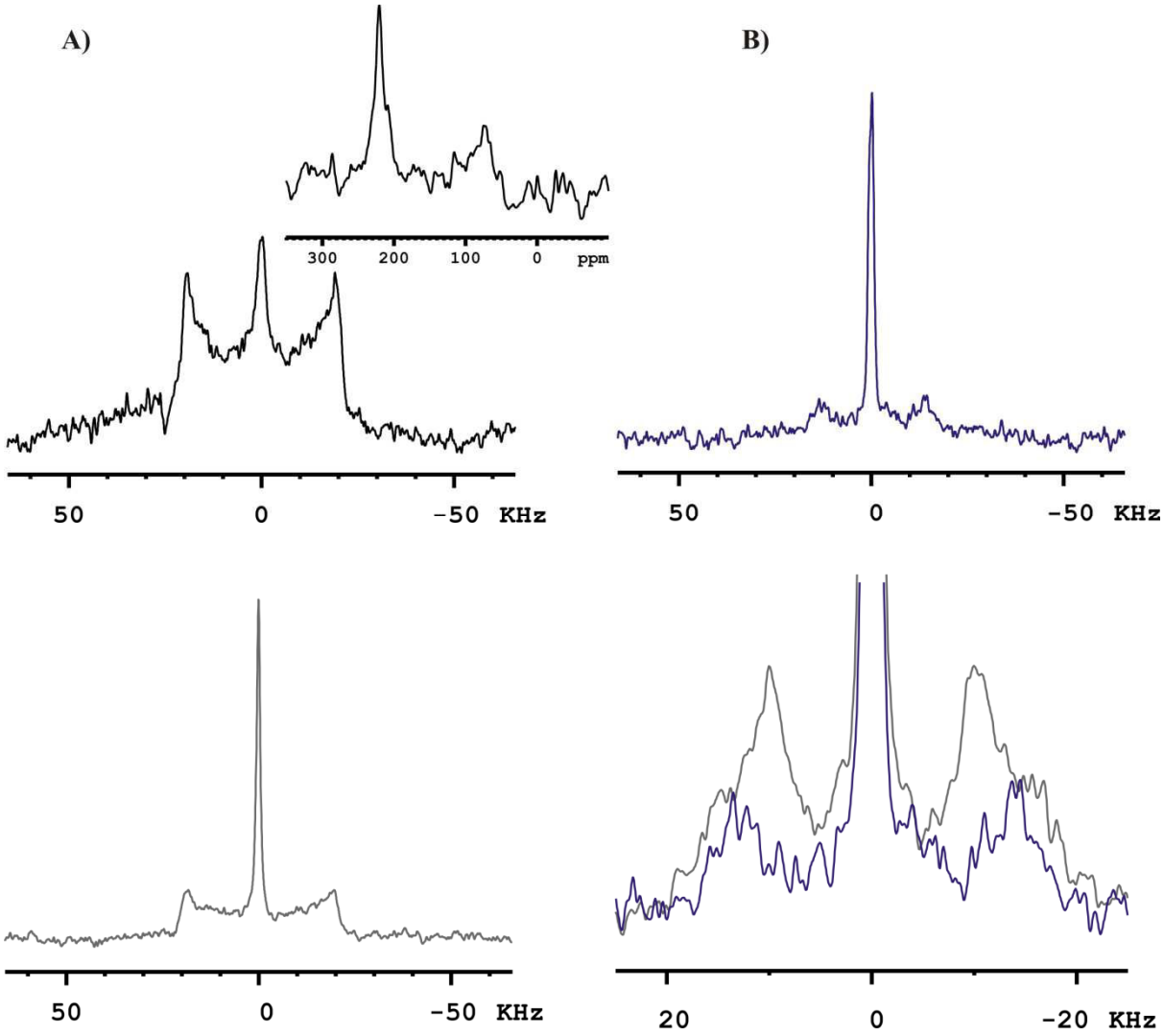

Figure 75: (A) ^{2}H solid-state NMR spectra of [$^{2}H_3$ Ala15- ^{15}N Leu16]-p24TMD and [$^{2}H_3$Ala15- ^{15}N Val19]-p24TMD reconstituted respectively into oriented POPC (black) and POPC/SM (95/5) (grey) bilayers, at -20°C. ^{15}N spectrum of [$^{2}H_3$ Ala15- ^{15}N Leu16]-p24TMD in POPC (black) at -20°C is shown on top of the ^{2}H spectrum. (B) ^{2}H solid-state NMR spectrum of [$^{2}H_3$Ala15- ^{15}NVal19]-p24TMD into oriented POPC/SM (95/5) (purple) at 4°C. The spectra below represent the superimposition of this spectrum with the one recorded in POPC/SM (95/5) bilayers at room temperature (grey). All spectra were recorded on a 400MHz Advance Bruker NMR spectrometer and a line-broadening of 500Hz was applied.

We also investigated the effect of increased concentration of SM C18 on p24TMD dynamics. The peptide labelled at position 20 (Ala-20) was reconstituted into oriented POPC, POPC/SM (95/5), or POPC/SM (90/10) and measured on the 400MHz spectrometer at RT.

As shown on Figure 76, the recorded ^{2}H spectra display broad line-shape with high D_2O peak that thus reduced the signal intensities. The observed differences of HDO intensities suggests that the samples were not hydrated to the same degree. However, we emphasized the region with the signal of the peptide in order to see if there is any difference. None of the spectra display a well-defined splitting but rather a mosaic spread pattern indicating that there might be several orientations of the Ala20 side chain within the different membranes. Although there is no difference in width, the maxima of ^{2}H spectra obtained for the peptide in POPC/SM (95/5) is more defined (Figure 76B, superimposition, see arrows) as compared to those in POPC/SM (90/10) (Figure 76B, superimposition, bottom) which is consistent with what we previously observed with the position A-15 (Figure 76C, right). Thus, increasing concentration of SM C18 may slightly affect the orientation of the peptide (Figure 58B, blue). Thus suggesting less mosaicity in presence of SM C18 (5%). However, we could not determine the quadrupolar splitting at the maxima which are less well resolved.

In addition, by tilting the coil as shown Figure 76A (middle), the sample became aligned perpendicular relative to the magnetic field and provided information on the rotational diffusion of the peptide within the membrane. When the ^{2}H spectrum of p24TMD was recorded in POPC oriented perpendicular to B_0, the resulting spectrum was not different from the one recorded with the coil oriented parallel (Figure 76A pink and spectra superimposition). Thus indicating that the deuterium atoms of the alanine methyl group are not aligned with the lipids. We did not do the same with POPC/SM (95/5).

In summary, to characterize p24TMD-SM C18 interaction we investigated the effect of SM C18 on the alignment and dynamics of p24TM helix using ^{15}N and ^{2}H ssNMR spectroscopy. Although the ^{15}N chemical shift shows that the peptide adopts quite well-defined transmembrane alignment in POPC and POPC/ SM C18 (95/5) membranes, ^{2}H spectra which are more sensitive to motion, indicated that the peptide adopts several orientations. In POPC/ SM C18 (95/5) membranes, we did not observe any significant change in peptide topology when compared to POPC suggesting that SM C18 does not change the orientation of the peptide. However, we show that it affects the peptide orientation in a concentration dependant manner (increase concentration). ^{2}H spectra of the Alanine 20 methyl group and Alanine 15 respectively indicate that this residue does not aligne with the lipids, and the peptides are in intermediate exchange in membrane.

As the orientation of the peptide does not change in POPC/SM (95/5), the contour plot show in Figure 77A was generated in Mathematica using the experimental ^{15}N chemical shift and ^{2}H quadrupolar splitting (Table 12) we obtained in these membranes. The contour plot of all residues cross at one point except for the alanine-20. This residue was shown to not be aligned with lipids thus probably not aligned with the other residues. Therefore, the topology of the peptide represented in Figure 77B was obtained with angles that agree with both the ^{2}H quadrupolar splitting of Ala-15 and the ^{15}N chemical shift of the other labeled

residues (circle zone on the contour plot). The tilt and pitch angles were respectively estimated to 19 and 235°.

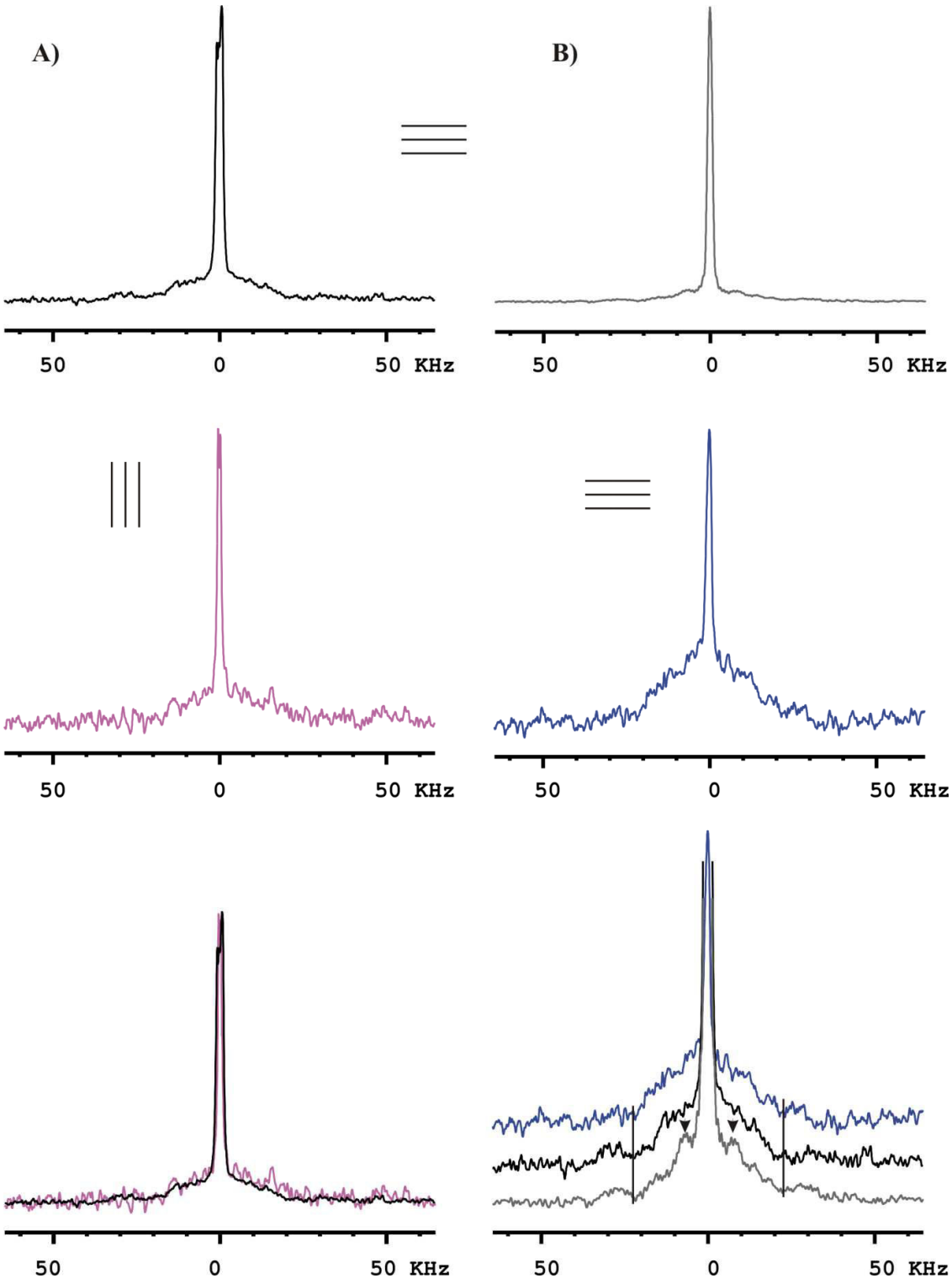

Figure 76: (A) ^{2}H solid-state NMR spectra of [$^{2}H_3$Ala20- ^{15}N Leu18]-p24TMD and [$^{2}H_3$Ala20- ^{15}N Leu23]-p24TMD reconstituted into POPC bilayers with the lipids oriented parallel (black) and perpendicular (pink) to the magnetic field respectively. (B) ^{2}H solid-state NMR spectrum of [$^{2}H_3$ Ala20- ^{15}N Leu18]-p24TMD into POPC/SM (95/5) (gray) and POPC/SM (90/10) (blue) bilayers,

with the normal oriented parallel to B_0. The spectra below represent the superimposition of the different spectra. Spectra were recorded at 9.4 Tesla on the Advance Bruker NMR spectrometer except the one POPC/SM (95/5) (gray) which was recorded at 11.7 RT. A LB of 500Hz was applied to all spectra.

Table 12: Summary of ^{15}N chemical shift and ^{2}H quadrupolar splitting values in POPC and POPC/SM (95/5) membranes. The values that were used for calculation of the peptide orientation are highlight in light grey

Labelled positions	^{15}N chemical shift (ppm)		^{2}H quadrupolar splitting (kHz)	
	POPC	POPC/SM (95/5)	POPC	POPC/SM (95/5)
A15	-	-	21.6±2.6	20.1±1.5
L16	215.5±4.5	216±3.8	-	-
L18	206.13±9.32	205.15±8.45	-	-
	202.50±6.26	201.35±6.65	-	-
V19	216.64±4.04	218.05±6.65	-	-
	220.25±5.24	219±6	-	-
A20	223.55±4.15	224.1±3.7	-	-
L23	217.50±4	220.83±4	-	-

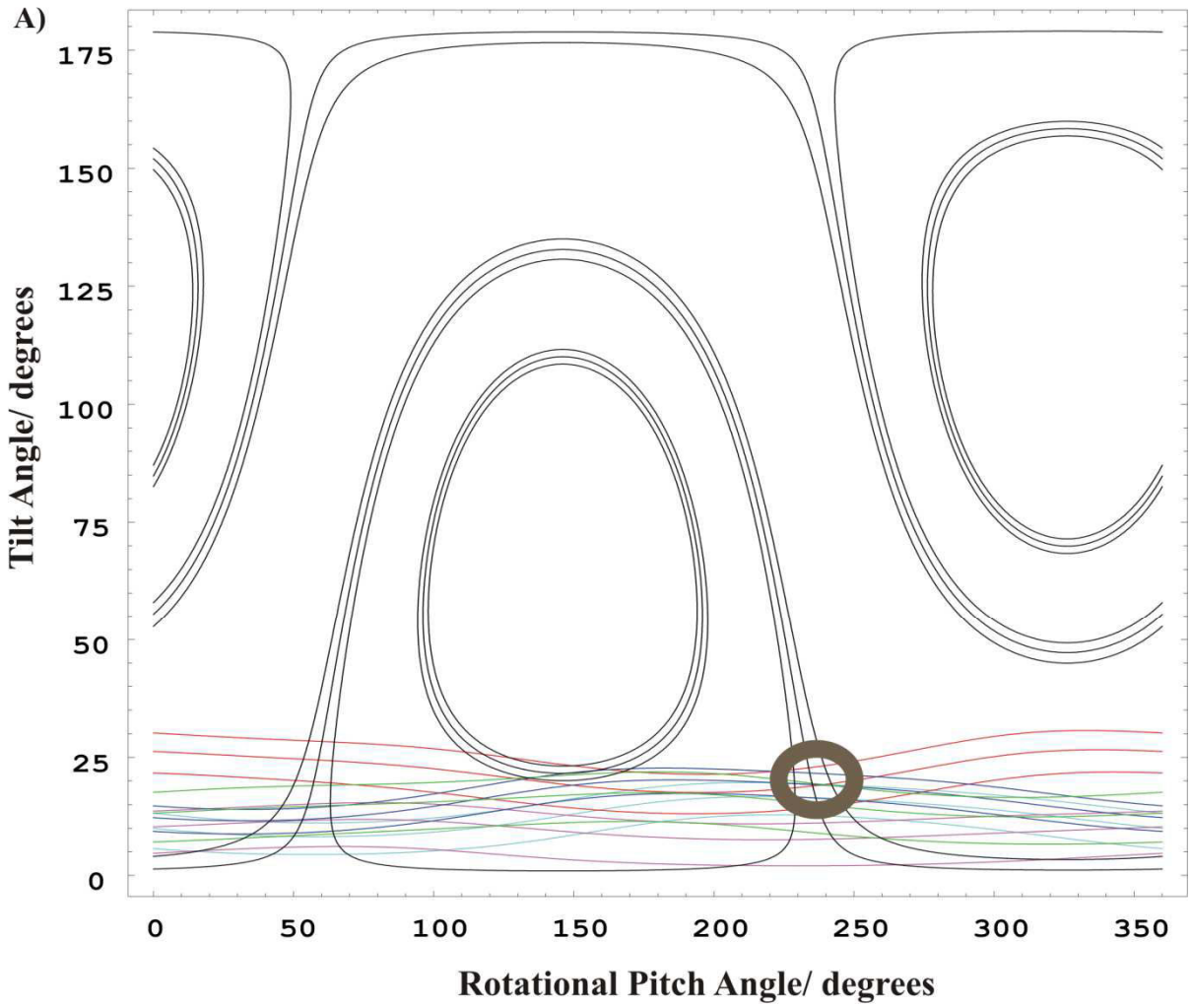
A)
Tilt Angle/ degrees
175
150
125
100
75
50
25
0
0
50
100
150
200
250
300
350
Rotational Pitch Angle/ degrees

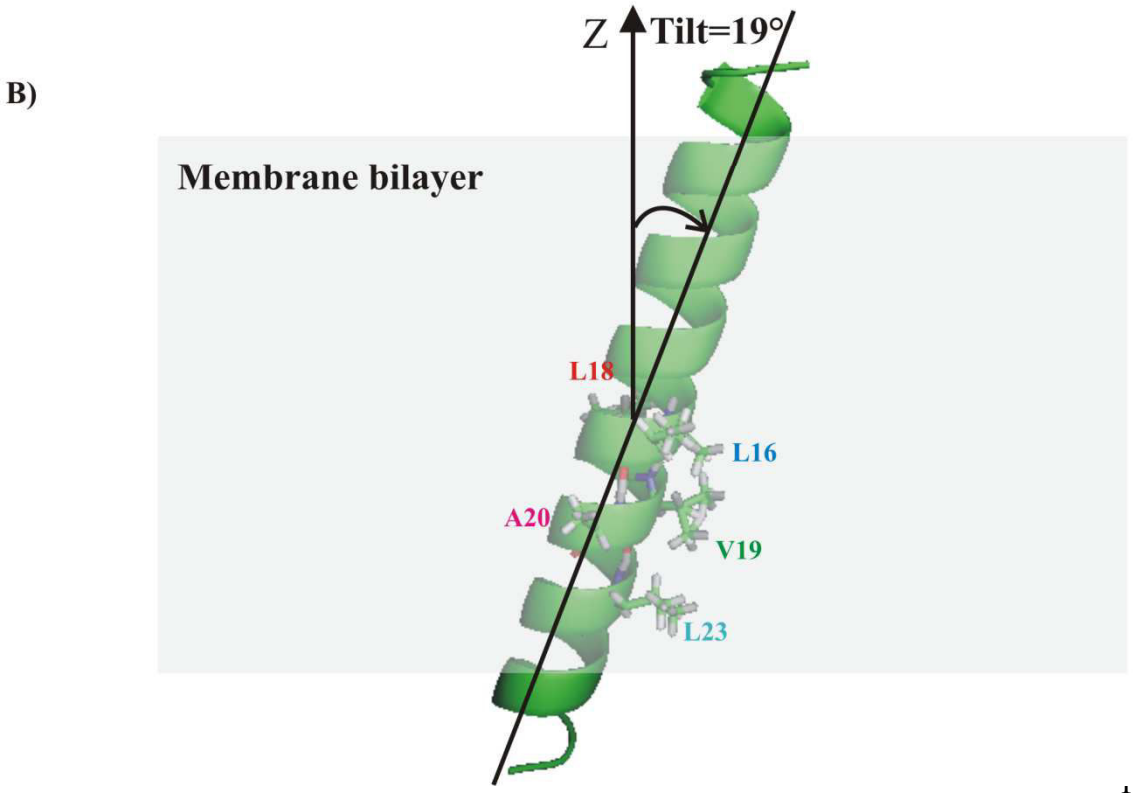
B)
Z
Tilt=19°
Membrane bilayer
L18
L16
A20
V19
L23

Figure 77: (A) The contour plot that results from experimental measurements of the ^{2}H quadrupolar splitting of Ala-15 (20±3) kHz in black, the ^{15}N chemical shift are represented for Leu-16 (216±4) ppm in blue, Leu-18 (205.15±8.45) ppm in red, Val-19 (218.05±6.65) ppm in green, Ala-20 (224±4) ppm in pink, Leu-23 (220±4) ppm in turquoise. These restraints were all obtained for thr p24TMD into POPC/SM (95/5). The angular pairs that agree with both the ^{2}H quadrupolar splitting of Ala-15 and the ^{15}N chemical shift are circled and (B) the corresponding topology relative to the membrane illustrated.

b) Effect of SM C18 on the Leucine-23 side-chain

The leucine-23 was identified as one of the residues involved in interaction with SM C18 (Contreras et al., 2012). In order to characterize this interaction, we investigated the effect of SM C18 on the dynamics of this side chain residue. With this purpose, the synthetic peptide with $^{2}H_3$-leucine-d_{10} at position 23 was synthesized, reconstituted into oriented POPC or POPC/SM (95/5). The ^{2}H quadrupolar spectra were recorded at RT (~ 25°C) and -20°C with the membrane normal parallel or perpendicular to the magnetic field (respectively Figure 78 and Figure 79).

When [$^{2}H_3$-leucine-d_{10}]-p24 in POPC and POPC/SM (95/5) membrane bilayers were aligned with the normal parallel to the magnetic field, the resulting ^{2}H spectra look quite similar and did not give much signal at room temperature (see Figure 78A and B, left) suggesting that the leucine-23 side chains explored intermediate exchange in both membranes. This results also indicate that SM C18 doesn't affect the dynamics of these side chains. At -20°C, the movements are reduced enough to be neglected as the membrane is in a gel phase thus, the resulting ^{2}H spectra displayed broad line widths corresponding to all the orientations. Consequently, the recorded ^{2}H spectra at -20°C are broader and give more signal confirming in membranes (Figure 78A and B, right) at RT. The superimposition of these spectra at -20°C (see Figure 78C, right) show a tiny increase of the line width in presence of SM C18 when compared to spectra at RT (see Figure 78C, left). Thus, suggesting that it may induce small changes in the leucine-23 side chain order which are not detectable at RT. Unfortunately, the spectra did not give resolved deuterium signals from the different labelled segments for order parameters analysis.

The ^{2}H spectra were also recorded in both membranes with the lipid bilayers normal aligned perpendicular to the magnetic field at RT and -20°C and superimposed onto the previous ones, as shown on Figure 79 (pink). At RT, ^{2}H spectra again did not give much signal and no significant difference when compared to the previous ones, suggesting that the side chain of leucine-23 is not aligned with the lipid bilayer. At -20°C, the signal intensity is also increased and the spectrum became broad thus confirming that leucine-23 side chains are in intermediate exchange at RT. However, the superimposition with the spectra we obtained at -20°C with the lipids normal parallel to B_0, show no difference and half intensity signal in presence and absence of SM C18 respectively (see Figure 79B). This difference in the spectra for the two sample alignments (Figure 79right) indicates that the

side chains of this residue are characterized by some degree of alignment in absence of SM C18 but not in presence thus, that it may affect the alignment these side chains. However, we could not characterize this alignment in more detail because of the broad quadrupolar splitting of the labelled segments.

In conclusion, SM C18 may induce small changes in the leucine-23 sidechainalignment. Although we did not observe much signal at RT, we can only speculate about the fact that the results at -20°C may reflect those at RT as the faster dynamics at RT make it more difficult to detect.

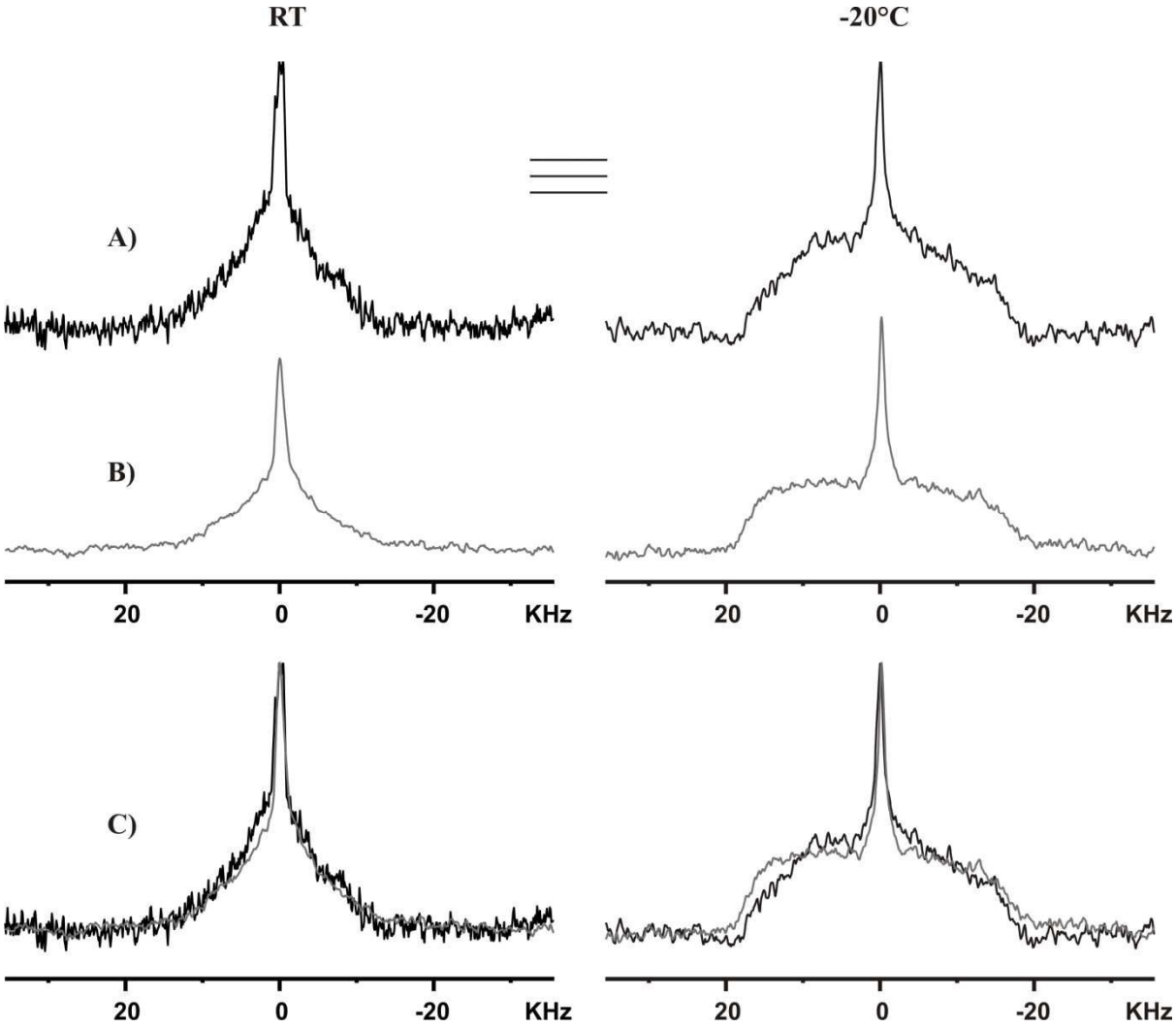

Figure 78: ^{2}H quadrupolar spectra of the $^{2}H_{3}$-leucine-23 (d10) side chain at RT (left) and -20°C (right) in POPC (A) and POPC/ SM (95/5) (B) membranes when the lipid bilayers are oriented with the lipids normal parallel to the magnetic field. All the spectra were recorded on the 400MHz ssNMR spectrometer. (C) Superimposition of spectra.

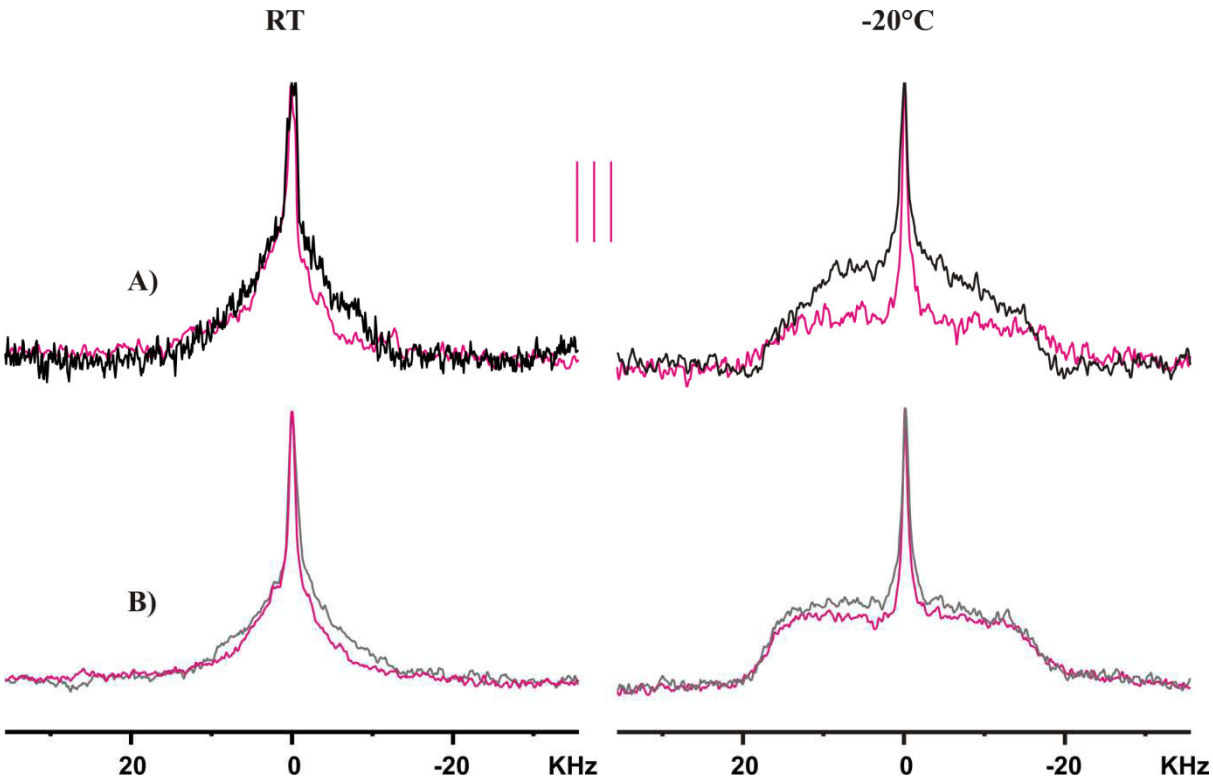

Figure 79: ^{2}H quadrupolar spectra of the $^{2}H_3$-leucine-23 (d10) side chain at RT (left) and -20°C (right) in POPC (A) and POPC/ SM (95/5) (B) membranes when the lipid bilayers are oriented with the lipids normal parallel (black and gray) or perpendicular to the magnetic field. All the spectra were recorded on the 400MHz ssNMR spectrometer

4.1.3.2.2. Investigation of p24TMD in Golgi like membrane

As the sorting of SM C18 in the COPI vesicles transport which are active in the Golgi cell compartment was exclusively pinpointed to the p24TMD protein (Brügger et al., 2000), we therefore decided to investigate the peptide interaction in a lipid composition close to their natural environment. With this purpose, the [$^{2}H_3$ Val19- ^{15}N Leu23]-p24TMD was reconstituted in a complex lipid mixture mimicking that of the Golgi membrane and investigated by ^{2}H and ^{15}N ssNMR spectroscopy. The results we obtained and reported here are those of the first test we achieved in such complex lipid system. These experiments should therefore be repeated.

When the ^{15}N ssNMR spectra of the peptide labelled at position 23 and reconstituted into POPC/POPE/POPS/Chol/SM (52/19/5/16/8) bilayer were recorded at different temperatures ranging from -3 to 37°C, we obtained broad spectra with low signal (see Figure 80A). However, for all the spectra, we observe a peak with a chemical shift >200ppm, but also a peak between 50 and 100ppm that became broad at low temperature. These results indicate that there are two populations of peptide: one that adopts a transmembrane orientation and the other in an in plane orientation. We integrated the

surface under each peak and the ratio was plotted versus the temperature as represented on the graph Figure 80A (bottom). The ratio is mostly > 1 for the different temperatures except at 17°C, indicating that the peptide mostly adopts a transmembrane orientation.
We also investigated the effect of SM C18 on deuterated valine-19, a residue of the binding motif. As shown on Figure 62B, in oriented POPC/POPE/POPS/Chol/SM (52/19/5/16/8) and POPC/POPE/POPS/Chol (60/19/5/16) membranes at 20°C, ^{2}H quadrupolar spectra give low signal intensity compared to other temperatures (-20, 0 and 40°C). Thus, indicating that these side chains are in intermediate exchange. At 40°C as the dynamics are more important, we observed small change in ^{2}H quadrupolar line width which slightly increases in presence of SM C18 thus, indicating that valine-19 side chains order is affected. Again the ^{2}H quadrupolar splitting of the deuterated segments gave a broader peak, therefore we could not distinguish the different deuterium labels and analyse how the SM C18 affect them. However, in order to estimate the quadrupolar splitting changes, we measured the quadrupolar splitting at half of the signal without the water peak (see Figure 62B) and plot versus the temperature as shown Figure 80B (see bottom). At -20°C and 40°C we noticed small change in presence of SM C18 indicating that this lipid affects Valine-19 side chain.

In conclusion, we investigated p24TMD-SM C18 interactions in Golgi-like membranes and have shown that the peptide is mostly reconstituted in a transmembrane manner. We did not investigate the dynamics of the whole peptide and this should be done in our perspective in order to understand if it is affected by SM C18. However, we showed that SM C18 induces a small change in the order of the valine-19 side chain.

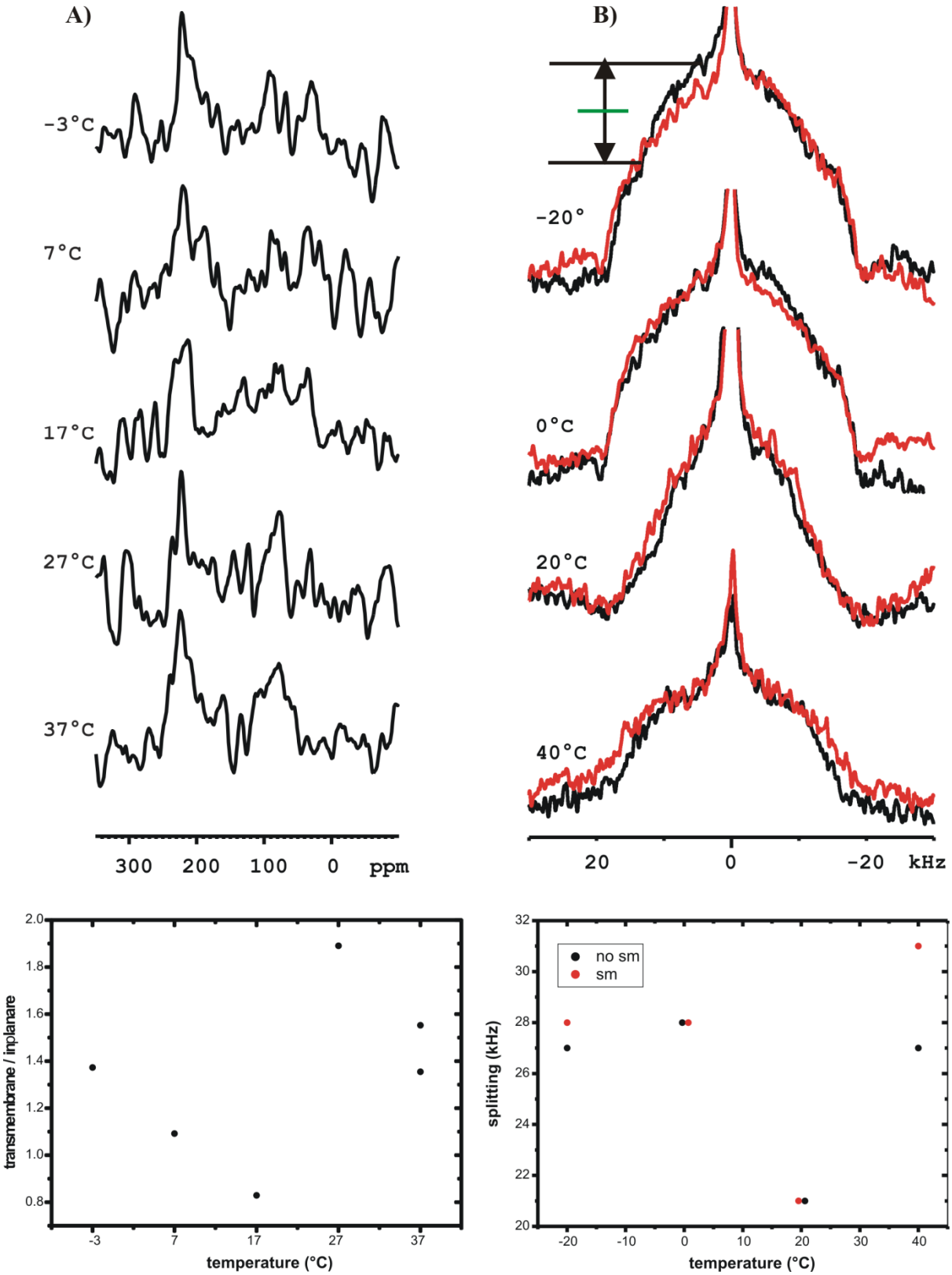

Figure 80: (A) ^{1}H-^{15}N ssNMR spectra of [$^{2}H_3$ Val19- ^{15}N Leu23]-p24TMD in POPC/POPE/POPS/Chol/SM (52/19/5/16/8) membrane bilayer, recorded at different temperatures on the 400MHz. The air under each peak was integrated and plot with temperature. A ratio of 1 corresponds to half of transmembrane and half in plane peptide orientation. (B) ^{2}H quadrupolar

spectra were recorded at different temperature in POPC/POPE/POPS/Chol/SM (52/19/5/16/8) and POPC/POPE/POPS/Chol (60/19/5/16) membranes and the quadrupolar splitting was estimated at the half maximum without the water peak (define as shown) and plot with the temperature

4.1.3.2.3. Investigation of p24TMD effect on membranes

The lipid fatty acyl chains packing can be analysed by ^{2}H solid-state NMR spectroscopy on non-oriented samples. To this end, liposomes are prepared with deuterated lipids (throughout their acyl chain). Deuterium is a spin 1 nucleus thus characterized by three energy levels among which two allowed transitions. When ^{2}H solid-state NMR spectrum of a single oriented deuterated site is measured, a characteristic well-defined doublet is observed from which the quadrupolar splitting ($\Delta\nu_Q$) can be determined by measuring the frequency separation of the maxima forming the doublet (Figure 81A, left). In contrast, a single non-oriented deuterated site results in a characteristic quadrupolar powder pattern (Figure 81A, right). When many sites are labelled, the different quadrupolar splittings overlap as shown on the simulated ^{2}H solid-state NMR spectrum of POPC-d_{31} (Figure 81B, left). The quadrupolar splitting of each deuterated CD_2 and CD_3 segment is then measured from the ^{2}H NMR spectra and the deuterium order parameters (S_{CD}) of each C-D bond extracted according to the formula:

$$\Delta^i \nu = \frac{3}{4}\left(\frac{e^2 qQ}{h}\right) S^i_{C-D} \qquad (17)$$

where (e^2qQ/h) is the static quadrupole coupling constant (167 kHz) for a C–D bond (Davis, 1983). The representation of these order parameters in a position-dependant manner (Figure 81B, right) gives information on the alignment and dynamics of the lipid acyl chains (Gottler and Ramamoorthy, 2009; Salnikov et al., 2009b; Sathiah Thennarasu, 2010; Seelig, 1977). The highest degree of order is giving by the segment close to the phospholipid headgroup due to the low degree of freedom, while it decrease towards the ends of the lipid acyl chains that would be located in the hydrophobic core of the membranes (Figure 81B, right).

To investigate the effect of p24TMD on the lipid fatty acyl chains packing, deuterated POPC (POPC-*d*31) and POPC-*d*31/SM (95/5) liposomes were prepared in presence or absence of peptide at 1/15 P/L molar ratio and measured by ^{2}H solid-state NMR spectroscopy at 7.04 Tesla RT.

The ^{2}H spectra of POPC-*d*31 and POPC-*d*31/SM (95/5) lipid vesicles in absence of peptides are shown on Figure 81C (left). POPC-*d*31/SM (95/5) ^{2}H spectrum exhibit many well resolved splitting duplets when compared to POPC-*d*31 indicating that POPC acyl chains exhibit less motion. In addition, the largest quadrupolar splitting which is assigned to the relatively rigid CD_2 groups closest to the glycerol backbone increase from 24.8 kHz to 26.4 kHz in presence of SM while the smallest quadrupolar splitting assigned to the

methyl group at the end of the acyl chains within the bilayer core slightly change from 2.2 to 2.7 kHz. The order parameters were obtained as described above and the profiles represented assuming that the segmental order follows a plateau from segment 2 to 8 and thereafter varies along the acyl chain as shown on Figure 81C (right). The POPC S_{CD} profiles slightly increase in the presence of 5% SM along the acyl chain starting from C9 to the C15 with the highest value at 0.21 indicating the SM induce a slight order of acyl chain.

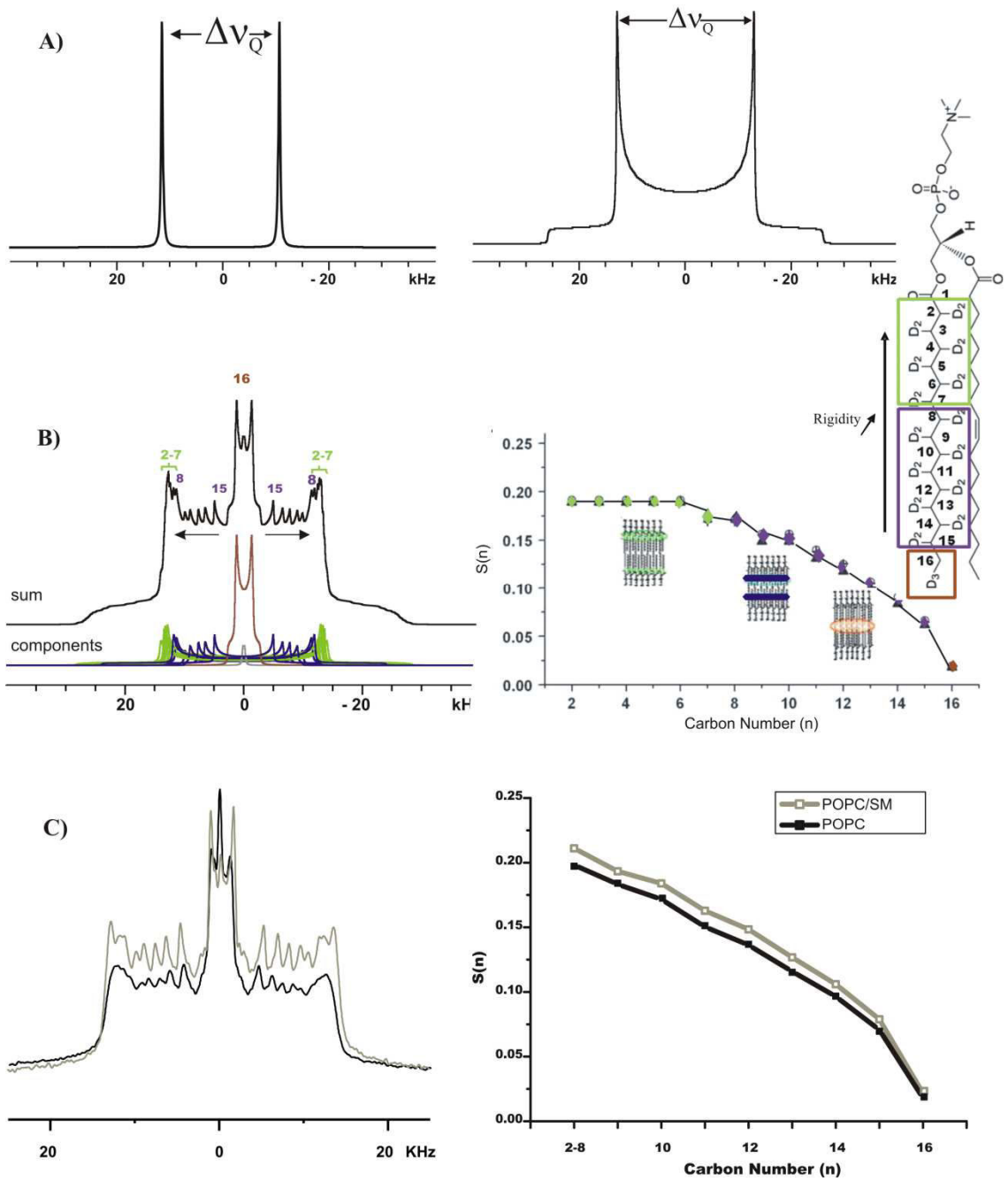

Figure 81: (A) Simulated ^2H solid-state NMR spectrum of oriented (left) and non-oriented (right) sample carrying a single deuterated site. The frequency separation between the two main intensities gives the deuterium quadrupolar splitting ($\Delta\nu_Q$). (B) Simulated ^2H solid-state NMR

spectrum of non-oriented POPC-d_{31} with the different quadrupolar powder pattern of ^2H labelled CD_2 and CD_3 segments add up (left). The comparison of the measured quadrupolar splitting with that of static sample allows the determination of the different order parameters (S_{CD}) which is plotted in a position-dependant manner (right). The structure of POPC-d_{31} with the corresponding deuterated CH_2 and CH_3 segments are represented. S_{CD} increases with the packing (rigidity) of the lipid acyl chain. (C) The experimental quadrupolar echo spectra of POPC-d_{31} (black) and POPC-d_{31}/SM C18 (kaki) recorded at RT, on a Bruker Advance 300MHz spectrometer (left). The order parameters were obtained from the $\Delta\nu_Q$ extracted from ^2H echo spectra (left) divided by a constant (167 kHz) and plot in a position dependent-manner

When 1 mol% of p24TMD was added to POPC-*d*31 membranes, it causes a slight increase of the ^2H quadrupolar splittings with better resolved peaks compared to that of POPC (Figure 82A, left). The largest and the smallest quadrupolar splitting are 25.6 and 2.6 kHz, which corresponds to an order parameter of 0.20 and 0.02 respectively. The analysis of the spectrum yields an increase of the order parameters of 0.01 units for the CH_2/CH_3 groups which are located most deeply in the core of the membrane bilayer (positions > 9) (Figure 82 A, right). In contrast the addition of p24TMD to POPC-*d*31/SM (95/5) membranes at 1mol% has hardly any influence on the ^2H quadrupolar splittings compared to POPC-*d*31/SM (95/5) membranes (Figure 82B, left). Analysis of the spectra yielded similar order parameters for the entire lipid chain length in presence or absence of the peptide (Figure 82B, right). These results suggest that the SM C18 neutralize the effect of the peptide on POPC.

The respective effect of the peptide and SM C18 on the POPC acyl chain can be easily identify with the superimposition of all these results (Figure 82C). They indicate that the peptide affects the order of POPC acyl chain in absence but not in presence of SM thus, SM C18 decrease their flexibility. The POPC phase diagram shown that at low SM percentage (5%) and up to the melting temperature (Tm= -2.9±1.3°C), POPC membrane are in liquid disorder phase (ld) (de Almeida et al., 2003; Curatolo et al., 1985). We can therefore conclude that the peptide and SM C18 affect the POPC acyl chain flexibility but not the phase.

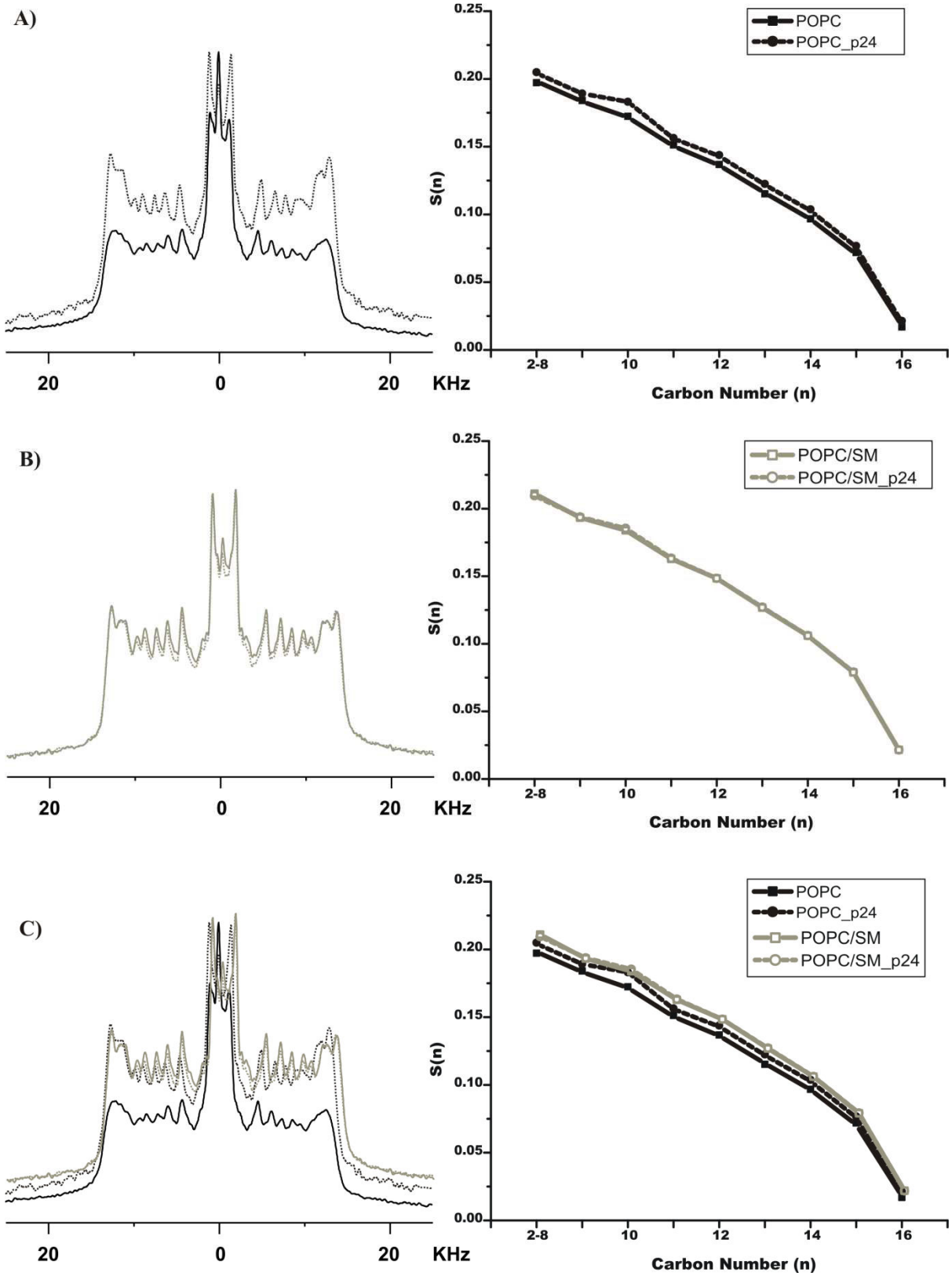

Figure 82: Comparison of ^{2}H echo spectra acquired for lipid vesicles of (A) POPC-d31, (B) POPC-d31 /SM (95:5) either alone (full line) or in the presence of 1 mol% peptide (dash line) at 37°C, (C) The superimposition of all the spectra. The respective smoothed order parameter (SCD) profiles are shown to the right of the spectra

4.1.3.3. **Conclusion:**

We showed here that SM C18 at 5% does not affect the whole p24TMD orientation but change the order of leucine-23 side chain which was identified in the binding motif. Consistently when the peptide is reconstituted in Golgi-like membrane, we show that the side chain order of another residue of this motif, the valine-19 is also affect bilayer. However, we could not determine how these order parameters change. These results indicate that the peptide interacts with the SM C18 via the residue side chains of the binding motif. Therefore, we tried REDOR ssNMR experiment to determine the distance between the side chain of the Tyrosine 27 ([^{13}CTyr27]-p24TMD) and SM C18 at the atomic level. Indeed in the simulate model proposed by Contreras and al, the polar head group of sphingomyelin 'wraps around' this residue side chain (Contreras et al., 2012a). Unfortunately, we did not yield workable spectra as we only obtained lipid signal. When dynamics was investigated, we showed that the whole peptide and the side chains are in intermediate exchange. SM C18 does not affect this dynamic. The peptide and SM C18 perturb the POPC fatty acyl chain order but not the phase.
In perspective, effort have to focus on REDOR experiment in order to obtain atomic distances and refine the proposed model.

4.2. Biophysical study of the CRAC motif and cholesterol interaction

4.2.1. Introduction

Cholesterol is the major sterol of membrane eukaryotic cells. Here we investigated its interaction with a consensus amino acid sequence -L / V-X1-5 X1-5-Y-R / K- called CRAC (Cholesterol Recognition/interaction Amino acid Consensus). This motif was first identified by Li and Papadopoulos in the peripheral-type benzodiazepine receptor (PBR)(Li and Papadopoulos, 1998b), an outer mitochondrial membrane protein involved in the regulation of cholesterol transport in this organelle membrane. The CRAC motif was shown to interact with cholesterol and was identified in various proteins that bind this sterol such as some members of the G-proteins coupled receptors (serotonine) or some viral membrane proteins (Jafurulla et al., 2011; Schroeder, 2010; Vincent et al., 2002).
This motif was identified in the pre transmembrane or membrane proximal region (MPR) of the HIV membrane fusion protein gp41(Vincent et al., 2002). This protein derived from proteolysis cleavage of a precursor, the envelope glycol-protein 160. It forms heterotrimeric complex or "spike" with the gp120 which derived also from gp160 cleavage. The gp41 and gp120 proteins are both involved in the early stage of HIV infection and respectively acts in the fusion of cellular/viral membranes and presents the receptor binding sites for the CD4. The gp41 is a type I trans- membrane protein composed of three domains as represent on Figure 83: the extracellular domain or ectodomain involved in membranes fusion, the transmembrane domain (TM) and the cytoplasmic domain (CT). The pre-transmembrane region or external MPER (membrane proximal

external area) is a tryptophan-rich region. Although the three dimensional structure of native gp41 is not yet known, some structures have been solved for the truncated gp41. These structures are highly conserved particularly the MPER (Coutant et al., 2008; Merk and Subramaniam, 2013). This region of the gp41 ectodomain was shown to play a crucial role in the fusion of viral and cellular membranes (Muñoz-Barroso et al., 1999). The LWIYK motif was identified at the C-terminus of this region and modulate membranes fusion (Abad et al., 2009; Chen et al., 2009).

Although the gp41 LWIKY interaction with cholesterol have been extensively investigated for instance by mutagenesis, many questions remain on the mechanism of this interaction. In order to understand this mechanism, Dr Omar Rifi investigated the interaction of this motif with cholesterol by solid state NMR during his thesis work in our laboratory (Rifi, 2014). With this purpose, he designed several peptides of 33 amino acids with the CRAC motif including the CRAC_1. This peptide contains the L-W-Y-I-K sequence flanked at the N-terminus with few amino acids of the gp41 and at C-terminus with repetition of Ala-Leu residues (alanine-leucine) which replace the natural transmembrane sequence (KKNITNW**LWYIK**LFIMIALALALALALALALKK). Two lysines were added at both ends (N and C-terminus) to enhance the solubility. When the orientation of the CRAC_1 ^{15}N labelled within the LWYIK motif (Leu 8) reconstituted in oriented POPC and POPC/Chol (70/30) was investigated by ^{15}N solid state NMR spectroscopy, the giving chemical shift indicated a transmembrane orientation and that cholesterol (30%) affects this orientation (Rifi, 2014). Based on these results together with CD and FITR data which suggested that the CRAC_1 is mostly structure in helix, he proposed two membrane models of this peptide in which the NH vector of the Leu8 within the CRAC motif is aligned with that of the transmembrane domain or not as shown Figure 84A. However, membrane topology model of the gp41 that was proposed shows the MPER with the CRAC motif lying on membrane surface as represents on Figure 84B (Abad et al., 2009) thus, promoting the interaction with cholesterol. Therefore, we proposed here to investigate the topology of the transmembrane segment in order to determine the alignment of its axis relative to the membrane bilayer normal aligned parallel to the magnetic field.

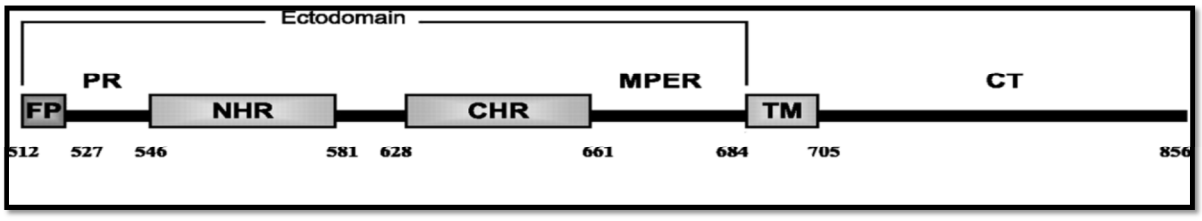

Figure 83: Schematic representation of the domains of gp41 (Montero et al., 2008). Abbreviations: fusion peptide (FP), Nt Heptades Repeat (NHR), Ct Heptades Repeats (CHR), Membrane Proximal External Region (MPER), Transmembrane (TM) and Cytoplasmic (CT)

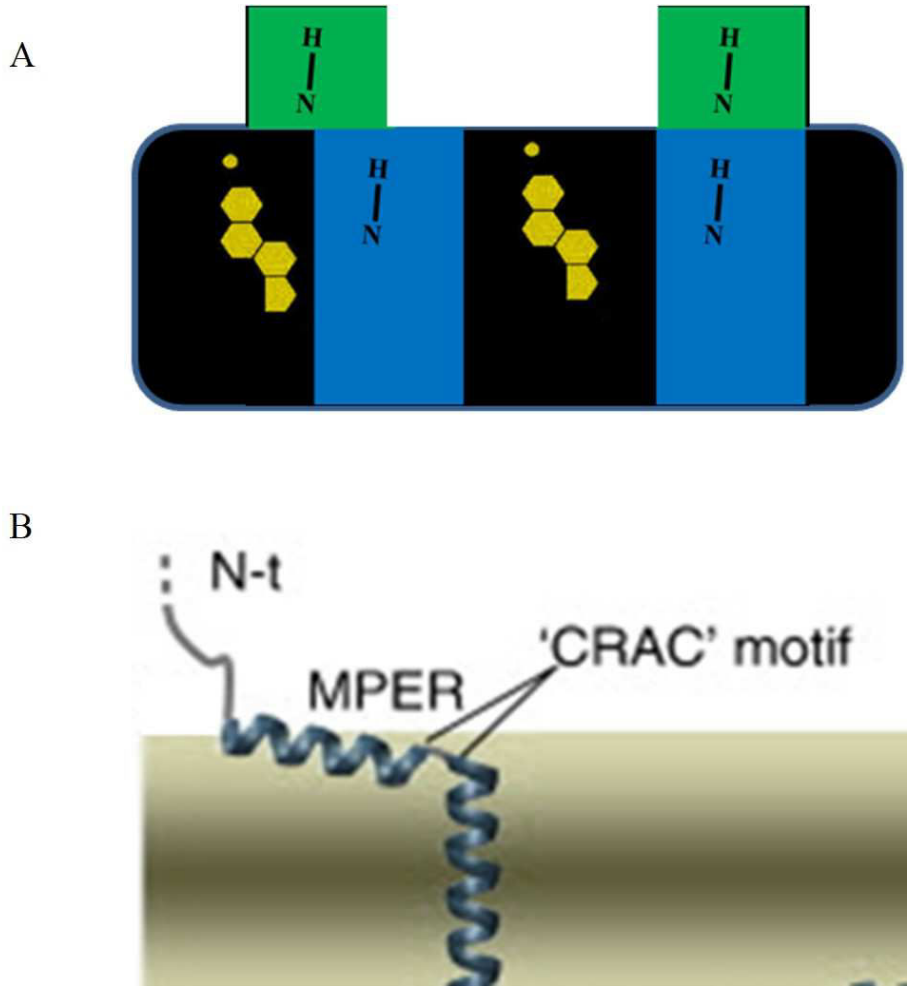

Figure 84: Membrane topology model of (A) CRAC_1 and (B) HIV-1 gp41 MPER with the CRAC motif (Abad et al., 2009). The CRAC motif and the TM of the CRAC_1 peptide are highlight in green and blue respectively

4.2.1.1. **Experimental**

The materials are the same than previously (see experimental section in 4.1.2.1). The solid phase peptide synthesis was achieved as described in the experimental section above (see experimental section in 4.1.2.1).

4.2.1.1.1. **Purification by reverse phase HPLC**

The peptide was dissolved in 90% of solvent A (acetonitrile/water/TFA, 10/90/0.1, v/v), 10% solvent B (acetonitrile/TFA, 100/ 0.1, v/v) at a final concentration of 10mg/ml and purified by RP-HPLC under acetonitrile/water/TFA using a C18 column (Luna 100-C18 5.0-µm columns, Phenomenex, France). The purification was performed on a preparative HPLC (Gilson Chromatography, Villiers-Le-Bel, France). The identity of the peptides was verified by MALDI-TOF spectrometry using matrix α-cyano-4-hydroxycinnamic acid (α-cyano).

4.2.1.1.2. Preparation of oriented samples

The CRAC_1 and the lipids (POPC and POPC/Chol 70/30) were first separately dissolved in chloroform / methanol (v / v, 2/1). Thereafter, they were mixed in other to achieve the molar ratio peptide / lipids of 2%. The solvents were evaporated under nitrogen stream until the solution turns viscous (to about 200µl). Equal quantities of the sample were applied as small elongated droplets on the surface of individual ultra-thin cover glass plates (thickness 00 = 80µm; 6 × 11mm or 8 x 22 mm, Paul Marienfeld, Lauda-Königshofen, Germany). The trace of solvents was evaporated at air and under vacuum. The sample was thereafter hydrated in a closed chamber at 93% relative humidity and left to equilibrate for typically about 2 to 3 days at room temperature. The glasses were stacked on top of each other and wrapped in Teflon tape and a plastic film to prevent dehydration of the sample.

4.2.1.1.3. ^{31}P, ^{15}N, ^{2}H solid-state NMR acquisition

Solid-state NMR spectra were acquired on a Bruker Avance wide-bore NMR spectrometer operating at 9.4 or 7.05 Tesla. Both using commercial triple-resonance probes equipped with flat coil (Bruker Biospin Rheinstetten, Germany). The spectra of oriented samples were recorded with the membrane normal parallel or perpendicular (turned by 90°) orientation relative to the magnetic field direction, respectively.
Proton-decoupled ^{31}P solid-state NMR spectra of oriented samples were recorded at 161.937 MHz using a Hahn echo pulse sequence (Rance and Byrd, 1983) with the following parameters: ^{31}P B_1 field ~50 kHz, echo time 40 µs, spectral width 40-120 kHz, typically 30-128 scans, and repetition time 3 s. The spectra were referenced relative to 85% phosphoric acid (0 ppm). An exponential apodization function corresponding to a line broadening of 100 Hz was applied before Fourier transformation.
Proton-decoupled ^{15}N solid-state NMR spectra were recorded at 40.54 MHz using a cross polarization (CP) pulse sequence (Pines et al., 1973). The recording was achieved with the following parameters: ^{1}H B_1 field of 31 kHz, CP contact time of 800 µs, acquisition times ranging from 6 to 20 ms, spectral with 38 kHz, and repetition time of 3 s. The spectra were calibrated relative to external ammonium chloride ($^{15}NH_4Cl$) at 41.5 ppm (Bertani et al., 2014). An exponential apodization function with a line broadening of 200Hz was applied prior to Fourier transformation.

4.2.1.2. Results: Influence of the cholesterol on the topology of CRAC_1 transmembrane domain:

In order to investigate the topology of CRAC_1 transmembrane domain, this peptide was ^{15}N single labelled at different positions (18 and 24) and reconstituted in POPC and POPC/Chol (70/30) at the final ratio peptide/lipid 2%. The whole samples were oriented with the membrane normal parallel to B_0 and investigated by ^{15}N solid-state NMR. When [^{15}NAla18]–CRAC_1 was reconstituted in POPC/Chol (70/30), the ^{1}H-^{31}P decoupled

spectrum recorded indicates that lipids are quite well aligned (Figure 85A, left). All ^{1}H decoupled ^{31}P spectra show a good alignment of lipids for the other samples (data not shown). The ^{15}N spectra of this peptide in POPC membrane gives a quite broad peak with a chemical shift value of 205.7±8.5ppm (Figure 85A, left, red). In presence of Chol 30%, the peak became broader with an increased chemical shift at 220.3±16.2ppm (Figure 85A, left, black). This result indicates that the peptide does not adopts a well-defined transmembrane orientation but shows a mosaic spread and confirmed that cholesterol affects the topology of this peptide (Rifi, 2014). Interestingly, the difference of the ^{15}N chemical shift obtained in both membranes for this position was quite similar to the one we obtained for the peptide labelled at position 24 (Figure 85A). Indeed, in POPC and POPC/Chol (70/30) membranes, the 15N spectra respectively give peaks at 176.4 ±4.2and 189.5±6.5 ppm (Figure 85A, right, red and black respectively). However, peaks are well-defined compared to those we obtained for the position 18 and give values <200ppm indicating that the NH of Ala 24 amide bond display a defined orientation approximately parallel to the membrane normal in both membranes. These results suggest that the NH vector of Ala 18 which is close to the membrane surface is likely not aligned perfectly with the NH of Ala 24 deeply insert in the membrane. As the chemical shifts that were obtained for the CRAC motif were >200ppm (Rifi, 2014), together with these results we deduced that the NH of the CRAC motif (^{15}N Leu8) may likely aligned with that of the transmembrane part close to the membrane surface (^{15}N Ala18) and with that of the deep transmembrane segment (^{15}N Ala24). We therefore propose the model represented Figure 85B.

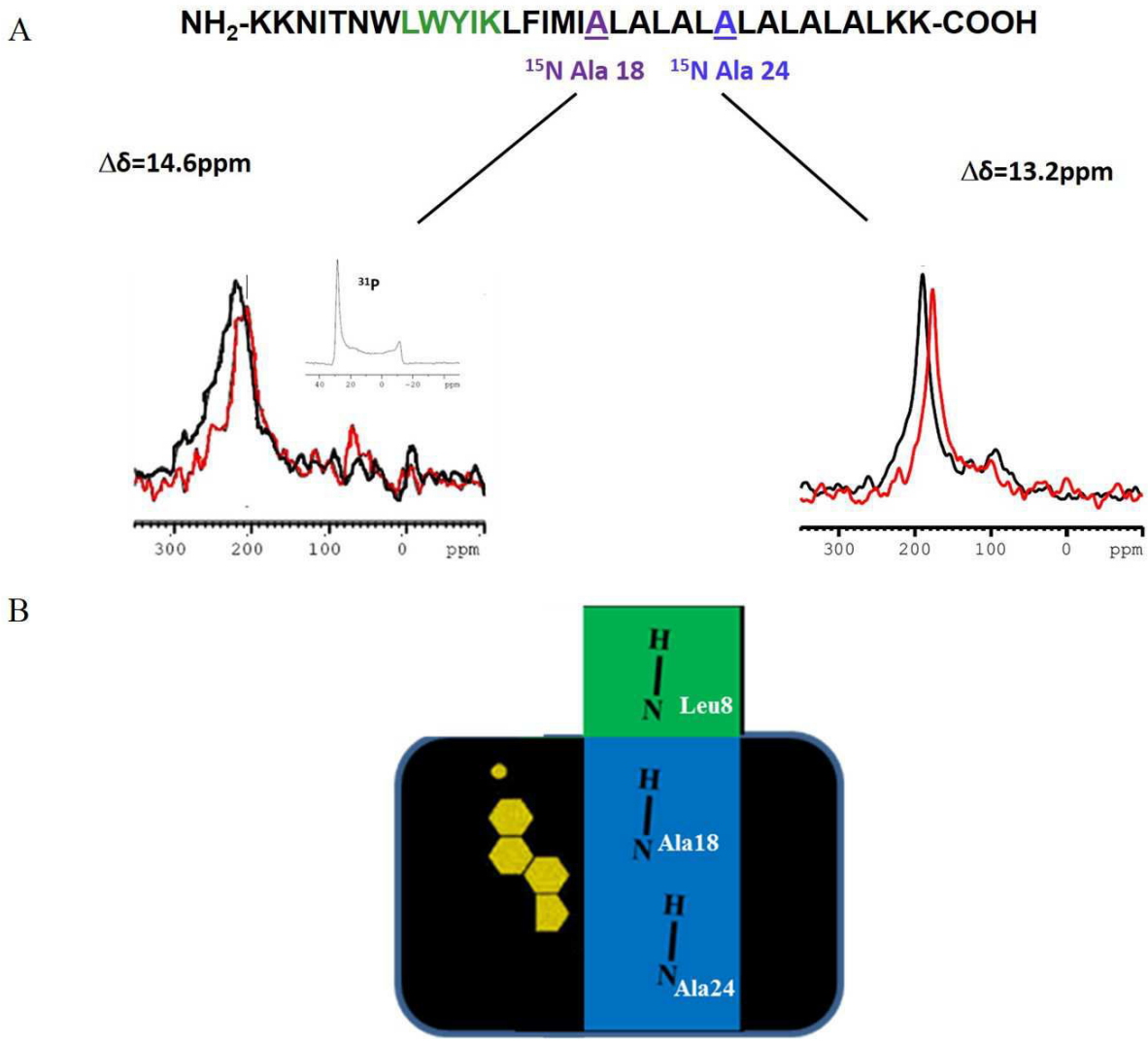

Figure 85: Proposed model of the potential orientation of NH bond within the CRAC_1. The CRAC motif and the TM of the CRAC_1 peptide are highlight in green and blue respectively, the membrane in black and the cholesterol in yellow

4.2.2. Conclusion

In summary, our result confirm that the cholesterol induced other orientation of the CRAC_1. In the previous model, Dr Rifi proposed two membrane models of this peptide as represented Figure 84A. Our investigation of the CRAC_1 transmembrane topology propose an alternative model to the previous ones. Indeed, this model suggest that the HN vector of the Leu8 is likely not well-aligned with all the HN of the transmembrane segment except the one of the segment close to the membrane (Ala18). However, this model does not help to explain the interaction of the CRAC motif with the cholesterol as this region should be close to the membrane surface. Thus we have undertaken other investigations particularly with the CRAC motif and truncated version of the CRAC_1 lacking the transmembrane part or the MPER with the CRAC motif. We started to investigate the interaction of the LWYIK motif with cholesterol using CD spectrometry (data not shown

here). In perspective, the topology and the dynamics of these peptides have to be study in order to refine the proposed model.

GENERAL CONCLUSION AND PERSPECTIVES

This chapter gives an overview on the concluding remarks on the work presented in this thesis and some future perspectives.

Chapter 5. General conclusion and perspectives

Here we investigate interaction of p24TMD with SM C18 and CRAC with cholesterol which are respectively involved in cellular traffic and mechanism of HIV infection. With this purpose, we proposed to use a number of biophysical approaches, including solid-state NMR spectroscopy, to study these interaction details. The different conclusions are summarize in the following sections.

5.1. Expression of p24TMD and structural characterization of p24TMD-SM C18 interaction

Brügger et al found the sorting of a specific sphingolipid specie, the SM C18 in the COPI vesicles. Further investigation pinpoints this sorting to the p24 protein suggesting an interaction between these molecules. More this interaction was proposed to regulate the COPI biogenesis and thus its role in the cellular traffic. A simulated model of this interaction was proposed. Therefore, to shed light on this model in order to establish the structure the protein-lipid complex in membrane bilayer, we proposed to study p24TMD topology and dynamics in membrane using solid-state NMR spectroscopy. With this purpose in mind, we undertake the bacterial expression of the peptide which ensure a low cost production of relatively large amounts of labelled material required for NMR spectrometry. Here we presented the conclusions on p24TMD expression and the structural investigation that were achieved to characterize its interaction with SM C18.

5.1.1. Conclusions on p24TMD bacterial expression

As the expression of membrane protein can be difficult, we strategically used two recombinant vectors (pMal c5X-p24TMDH and pTIPX4-p24TMD) in order to optimize our chances to obtain the peptide.

We set up the conditions of expression for both constructions but encountered some difficulties with the purification. The MBP-p24TMDH and TAF12-p24TMD fusion proteins were respectively identified as expected in the soluble protein fraction and the insoluble fraction particularly in inclusion bodies. However, in both case, important part of proteins was lost through the column suggesting that the peptide likely induced conformational changes of the fusion protein partner thus reducing it affinity with the resin during affinity chromatography. In addition, in the case of TAF12-p24TMD as it co-eluted with other proteins, we suggest that the peptide may interact with other protein likely through hydrophobic interactions.

We set the conditions of cleavage for both protein using TEV-protease for MBP-p24TMDH and formic acid 75% for TAF12-p24TMD fusion protein. We hardly identified the peptide in a reproducible manner in both cases after cleavage. In the case of MBP-p24TMDH we suspected that the difficulty to detect the peptide is related to the important proteolysis and the bigger difference in size between the fusion protein partner and the peptide. When came to TAF12-p24TMD, this problem was mainly related to the presence of additional proteins that co-eluted with our protein. Indeed, the presence of other proteins probably interfere with the peptide since it is hydrophobic thus, may interact with these

proteins or other peptides. However, despite these difficulties to detect the peptide, mass spectrometry on a relatively pure peptide sample send by our collaborator in Heidelberg also indicated that the method of detection does not systematically work. Thus effort has to focus on both the purification step but suitable method that allow reproducible detection of the peptide have also to be developed.

In conclusion, considering that we expected at the end to recover few milligrams of the peptide for NMR investigation, the PTIPX4-p24TMD seems to be more suitable to achieve this goal as we did not observe important proteolysis. This recombinant vector also presents the advantage that the fusion partner is not very big in size compare to the peptide. However, the purification step need to be improve in other to recover the pure fusion protein and facilitate the purification and characterization of the peptide. In addition, as these results were obtained in rich medium, the expression in minimum medium have to be achieve for the protein isotope labelling.

5.1.2. Conclusions on biophysical and structural characterization of p24TMD-SM C18 interaction

In parallel to the bacterial expression, the peptide was obtained by solid phase peptide synthesis and characterized by MALDI-TOF spectrometry. It secondary structure was investigated by CD and Trp fluorescence spectrometry in presence of liposomes or when prepared into proteo-liposomes in order to set suitable conditions to investigate p24TMD-SM C18 interaction. The peptide is almost structured with 20% helix in water. When prepared in proteo-liposomes, its structure does not change but became more helical in presence of SM C18 compared POPC confirming the peptide interact with membrane. We showed that this interaction is modulate by the lipid head group and acyl chain. The best p24TMD reconstitution-competent state among the conditions we tested was obtained in HFIP/Water (50/50, v/v) with more that 80% helix.

In further studies to characterize p24TMD-SM C18 interaction we investigate the effect of SM C18 on the alignment and dynamic of p24TM helix using ^{15}N and ^{2}H solid-state NMR spectroscopy. When reconstituted in POPC membrane bilayers, ^{15}N spectra indicates that the peptide adopts transmembrane orientation that does not change in presence of 5% SM C18. ^{2}H spectra indicate that the peptide may adopts more than one transmembrane orientations and does not significantly change in POPC/SM C18 (95/5). When compared to the SM C18 concentration that was used by Contreras et al, it is already five times more. However, our data indicate that SM C18 (10%) promote mosaicity.

Although SM C18 does not affect the whole p24TMD orientation, we showed that it changes the side chain order of residues that were previously defined as involved in this interaction. Interestingly, this result was confirmed in complex membrane with Golgi-like lipid composition. Despite the fact we could not measure these changes, this result suggest that SM C18 interact with side chain. As the simulated model of the complex proposed that polar head group of sphingomyelin ‘wraps around’ the Tyrosine 27 side chain (Contreras et al., 2012a), we performed REDOR to determine the molecular distance of this interaction. Unfortunately, we did not yield workable spectra as we only obtained lipid signal. However, based on the angular restraints (19 and 235° for the tilt and pitch angles

respectively) we obtained from our experimental NMR spectra, we proposed a model of the peptide within POPC/SM C18 (95/5) as the orientation in these membranes is the same than in POPC membranes. In order to refine this experimental model, further studies have to focus on REDOR experiences to define the distances between the different interaction sites.

In addition, we investigate the dynamics of the peptide and side chains residues in POPC and POPC/SM C18 (95/5). Our data indicate that the whole peptide and the side chains are in intermediate exchange and SM C18 does not affect this dynamic.

In order to investigate the effect of the peptide on membrane, it was reconstituted in POPC membrane with deuterated acyl chain (POPC-*d31*) and ^{2}H spectra recorded. We showed that when 1 mol% of p24TMD was added to POPC-*d*31 membranes, it causes a slight increase of the acyl chain order whereas in POPC-*d*31/SM (95/5) membranes it hardly affects the order. As we observed that the peptide and SM C18 individually perturb the POPC fatty acyl chain, these results suggest that the SM C18 likely neutralized the effect of p24TMD on POPC.

5.2. Biophysical study of the CRAC motif and cholesterol interaction

With the purpose to get more insights on the mechanism of interaction between the CRAC motif and the cholesterol, Dr Omar Rifi investigated the topology of a peptide model CRAC_1 that was designed with the consensus LWYIK motif. When the ^{15}N-^{2}H labelled peptide (within this motif and the transmembrane segment respectively) was reconstituted in oriented POPC and POPC/Chol (70/30) and investigated by ^{15}N solid state NMR spectroscopy, he observed that it adopts a well-defined transmembrane orientation in POPC that is affects in presence of cholesterol (30%) (Rifi, 2014). Based on these results and those obtained with CD and FITR, he proposed two membrane models of this peptide in which the NH vector of the Leu8 within the CRAC motif is aligned with that of the transmembrane domain or not. We proposed to investigate the topology of the transmembrane segment in order to refine this model.

With this purpose, ^{15}N CRAC_1 peptides labelled within the transmembrane domain at positon 18 (close to membrane surface) and 24 (deep in the membrane) were synthetized. These peptides were reconstituted in POPC and POPC/cholesterol (70/30) at 2% peptide/lipid molar ratio and investigated with ^{15}N NMR spectroscopy. ^{15}N spectra indicated that the NH vector of Ala18 is oriented in a transmembrane fashion in oriented POPC and cholesterol (30%) induced other transmembrane population of CRAC_1 thus, suggesting that this vector is aligned with that of the Leu8 within the CRAC motif. The ^{15}N spectra of the peptide labelled at position 24 indicated that the NH vector is not aligned parallel with the POPC membrane normal suggesting that this vector is not perfectly transmembrane. Thus based on these results, we proposed a model in which the HN vector of the Leu8 is aligned with that of the Ala 18 but likely not with HN of Ala 24 that is deeply inserted in the membrane. However, other investigations particularly of the CRAC motif and truncated version of the CRAC_1 lacking the transmembrane part or the MPER

with the CRAC motif have to be done. In perspective, the topology and the dynamics of these peptides have to be study in order to refine the proposed model.

References

Abad, C., Martínez-Gil, L., Tamborero, S., and Mingarro, I. (2009). Membrane topology of gp41 and amyloid precursor protein: Interfering transmembrane interactions as potential targets for HIV and Alzheimer treatment. Biochim. Biophys. Acta BBA - Biomembr. *1788*, 2132–2141.

Abragam A (1961). The principles of nuclear magnetism. Claredon Press Oxf.

Ahram, M., Litou, Z.I., Fang, R., and Al-Tawallbeh, G. (2006). Estimation of membrane proteins in the human proteome. In Silico Biol. *6*, 379–386.

Aisenbrey, C., and Bechinger, B. (2004a). Tilt and rotational pitch angle of membrane-inserted polypeptides from combined 15N and 2H solid-state NMR spectroscopy. Biochemistry (Mosc.) *43*, 10502–10512.

Aisenbrey, C., and Bechinger, B. (2004b). Investigations of polypeptide rotational diffusion in aligned membranes by 2H and 15N solid-state NMR spectroscopy. J. Am. Chem. Soc. *126*, 16676–16683.

Aisenbrey, C., Sizun, C., Koch, J., Herget, M., Abele, R., Bechinger, B., and Tampé, R. (2006). Structure and Dynamics of Membrane-associated ICP47, a Viral Inhibitor of the MHC I Antigen-processing Machinery. J. Biol. Chem. *281*, 30365–30372.

Aisenbrey, C., Bertani, P., and Bechinger, B. (2010a). Solid-state NMR investigations of membrane-associated antimicrobial peptides. Methods Mol. Biol. Clifton NJ *618*, 209–233.

Aisenbrey, C., Bertani, P., and Bechinger, B. (2010b). Solid-state NMR investigations of membrane-associated antimicrobial peptides. Methods Mol. Biol. Clifton NJ *618*, 209–233.

Alberts, B., Johnson, A., Lewis, J., Raff, M., Roberts, K., and Walter, P. (2002). Membrane Proteins.

Anantharaman, V., and Aravind, L. (2002). The GOLD domain, a novel protein module involved in Golgi function and secretion. Genome Biol. *3*, research0023.

Anderson, R.G. (1998). The caveolae membrane system. Annu. Rev. Biochem. *67*, 199–225.

Andronesi, O.C., Becker, S., Seidel, K., Heise, H., Young, H.S., and Baldus, M. (2005). Determination of membrane protein structure and dynamics by magic-angle-spinning solid-state NMR spectroscopy. J. Am. Chem. Soc. *127*, 12965–12974.

D'Angelo, G., Polishchuk, E., Di Tullio, G., Santoro, M., Di Campli, A., Godi, A., West, G., Bielawski, J., Chuang, C.-C., van der Spoel, A.C., et al. (2007). Glycosphingolipid synthesis requires FAPP2 transfer of glucosylceramide. Nature *449*, 62–67.

Antonny, B., Beraud-Dufour, S., Chardin, P., and Chabre, M. (1997). N-terminal hydrophobic residues of the G-protein ADP-ribosylation factor-1 insert into membrane phospholipids upon GDP to GTP exchange. Biochemistry (Mosc.) *36*, 4675–4684.

Baneyx, F. (1999). Recombinant protein expression in Escherichia coli. Curr. Opin. Biotechnol. *10*, 411–421.

Baumann, N.A., Sullivan, D.P., Ohvo-Rekilä, H., Simonot, C., Pottekat, A., Klaassen, Z., Beh, C.T., and Menon, A.K. (2005). Transport of newly synthesized sterol to the sterol-enriched plasma membrane occurs via nonvesicular equilibration. Biochemistry (Mosc.) *44*, 5816–5826.

Bechinger, B., and Sizun, C. (2003a). Alignment and structural analysis of membrane polypeptides by 15N and 31P solid-state NMR spectroscopy. Concepts Magn. Reson. Part A *18A*, 130–145.

Bechinger, B., and Sizun, C. (2003b). Alignment and structural analysis of membrane polypeptides by 15N and 31P solid-state NMR spectroscopy. Concepts Magn. Reson. Part A *18A*, 130–145.

Bechinger, B., and Sizun, C. (2003c). Alignment and structural analysis of membrane polypeptides by 15N and 31P solid-state NMR spectroscopy. Concepts Magn. Reson. Part A *18A*, 130–145.

Bechinger, B., Kinder, R., Helmle, M., Vogt, T.C., Harzer, U., and Schinzel, S. (1999). Peptide structural analysis by solid-state NMR spectroscopy. Biopolymers *51*, 174–190.

Bechinger, B., Aisenbrey, C., and Bertani, P. (2004). The alignment, structure and dynamics of membrane-associated polypeptides by solid-state NMR spectroscopy. Biochim. Biophys. Acta BBA - Biomembr. *1666*, 190–204.

Bechinger, B., Resende, J.M., and Aisenbrey, C. (2011). The structural and topological analysis of membrane-associated polypeptides by oriented solid-state NMR spectroscopy: established concepts and novel developments. Biophys. Chem. *153*, 115–125.

Bégué, J.-P., Bonnet-Delpon, D., and Crousse, B. (2004). Fluorinated Alcohols: A New Medium for Selective and Clean Reaction. Synlett 18–29.

Bertani, P., Raya, J., and Bechinger, B. (2014). 15N chemical shift referencing in solid state NMR. Solid State Nucl. Magn. Reson. *61-62*, 15–18.

Beswick, V., Guerois, R., Cordier-Ochsenbein, F., Coïc, Y.M., Tam, H.D., Tostain, J., Noël, J.P., Sanson, A., and Neumann, J.M. (1999). Dodecylphosphocholine micelles as a membrane-like environment: new results from NMR relaxation and paramagnetic relaxation enhancement analysis. Eur. Biophys. J. EBJ *28*, 48–58.

Béthune, J., Wieland, F., and Moelleken, J. (2006a). COPI-mediated transport. J. Membr. Biol. *211*, 65–79.

Béthune, J., Kol, M., Hoffmann, J., Reckmann, I., Brügger, B., and Wieland, F. (2006b). Coatomer, the coat protein of COPI transport vesicles, discriminates endoplasmic reticulum residents from p24 proteins. Mol. Cell. Biol. *26*, 8011–8021.

Béthune, J., Kol, M., Hoffmann, J., Reckmann, I., Brügger, B., and Wieland, F. (2006c). Coatomer, the coat protein of COPI transport vesicles, discriminates endoplasmic reticulum residents from p24 proteins. Mol. Cell. Biol. *26*, 8011–8021.

Blom, T., Somerharju, P., and Ikonen, E. (2011). Synthesis and biosynthetic trafficking of membrane lipids. Cold Spring Harb. Perspect. Biol. *3*, a004713.

Blum, R., and Lepier, A. (2008). The luminal domain of p23 (Tmp21) plays a critical role in p23 cell surface trafficking. Traffic Cph. Den. *9*, 1530–1550.

Brown, D.A., and London, E. (1997). Structure of detergent-resistant membrane domains: does phase separation occur in biological membranes? Biochem. Biophys. Res. Commun. *240*, 1–7.

Brown, D.A., and London, E. (1998). Functions of lipid rafts in biological membranes. Annu. Rev. Cell Dev. Biol. *14*, 111–136.

Brügger, B., Erben, G., Sandhoff, R., Wieland, F.T., and Lehmann, W.D. (1997). Quantitative analysis of biological membrane lipids at the low picomole level by nano-electrospray ionization tandem mass spectrometry. Proc. Natl. Acad. Sci. U. S. A. *94*, 2339–2344.

Brügger, B., Sandhoff, R., Wegehingel, S., Gorgas, K., Malsam, J., Helms, J.B., Lehmann, W.D., Nickel, W., and Wieland, F.T. (2000). Evidence for segregation of sphingomyelin and cholesterol during formation of COPI-coated vesicles. J. Cell Biol. *151*, 507–518.

by Biomembranes: Molecular Structure and Function.

Campagna, S., Saint, N., Molle, G., and Aumelas, A. (2007). Structure and mechanism of action of the antimicrobial peptide piscidin. Biochemistry (Mosc.) *46*, 1771–1778.

Chen, R. (2012). Bacterial expression systems for recombinant protein production: E. coli and beyond. Biotechnol. Adv. *30*, 1102–1107.

Chen, S.S.-L., Yang, P., Ke, P.-Y., Li, H.-F., Chan, W.-E., Chang, D.-K., Chuang, C.-K., Tsai, Y., and Huang, S.-C. (2009). Identification of the LWYIK Motif Located in the Human Immunodeficiency Virus Type 1 Transmembrane gp41 Protein as a Distinct Determinant for Viral Infection. J. Virol. *83*, 870–883.

Ciufo, L.F., and Boyd, A. (2000). Identification of a lumenal sequence specifying the assembly of Emp24p into p24 complexes in the yeast secretory pathway. J. Biol. Chem. *275*, 8382–8388.

Clark, L.A., Wahl, J.M., Steiner, J.M., Zhou, W., Ji, W., Famula, T.R., Williams, D.A., and Murphy, K.E. (2005). Linkage analysis and gene expression profile of pancreatic acinar atrophy in the German Shepherd Dog. Mamm. Genome Off. J. Int. Mamm. Genome Soc. *16*, 955–962.

Cohen, S.N., Chang, A.C., Boyer, H.W., and Helling, R.B. (1973). Construction of biologically functional bacterial plasmids in vitro. Proc. Natl. Acad. Sci. U. S. A. *70*, 3240–3244.

Contreras, F.-X., Ernst, A.M., Wieland, F., and Brügger, B. (2011). Specificity of intramembrane protein-lipid interactions. Cold Spring Harb. Perspect. Biol. *3*.

Contreras, F.-X., Ernst, A.M., Haberkant, P., Björkholm, P., Lindahl, E., Gönen, B., Tischer, C., Elofsson, A., von Heijne, G., Thiele, C., et al. (2012a). Molecular recognition of a single sphingolipid species by a protein's transmembrane domain. Nature *481*, 525–529.

Contreras, F.-X., Ernst, A.M., Haberkant, P., Björkholm, P., Lindahl, E., Gönen, B., Tischer, C., Elofsson, A., von Heijne, G., Thiele, C., et al. (2012b). Molecular recognition of a single sphingolipid species by a protein's transmembrane domain. Nature *481*, 525–529.

Coskun, U., and Simons, K. (2010). Membrane rafting: from apical sorting to phase segregation. FEBS Lett. *584*, 1685–1693.

Coskun, U., and Simons, K. (2011). Cell membranes: the lipid perspective. Struct. Lond. Engl. 1993 *19*, 1543–1548.

Cosson, P., and Letourneur, F. (1994). Coatomer interaction with di-lysine endoplasmic reticulum retention motifs. Science *263*, 1629–1631.

Costa, S., Almeida, A., Castro, A., and Domingues, L. (2014). Fusion tags for protein solubility, purification and immunogenicity in Escherichia coli: the novel Fh8 system. Front. Microbiol. *5*.

Cotman, M., Jezek, D., Fon Tacer, K., Frangez, R., and Rozman, D. (2004). A functional cytochrome P450 lanosterol 14 alpha-demethylase CYP51 enzyme in the acrosome: transport through the Golgi and synthesis of meiosis-activating sterols. Endocrinology *145*, 1419–1426.

Coutant, J., Yu, H., Clément, M.-J., Alfsen, A., Toma, F., Curmi, P.A., and Bomsel, M. (2008). Both lipid environment and pH are critical for determining physiological solution structure of 3-D-conserved epitopes of the HIV-1 gp41-MPER peptide P1. FASEB J. Off. Publ. Fed. Am. Soc. Exp. Biol. *22*, 4338–4351.

Cross, T.A. (1997a). Solid-state nuclear magnetic resonance characterization of gramicidin channel structure. Methods Enzymol. *289*, 672–696.

Cross, T.A. (1997b). Solid-state nuclear magnetic resonance characterization of gramicidin channel structure. Methods Enzymol. *289*, 672–696.

Daleke, D.L. (2003). Regulation of transbilayer plasma membrane phospholipid asymmetry. J. Lipid Res. *44*, 233–242.

Daleke, D.L. (2007). Phospholipid flippases. J. Biol. Chem. *282*, 821–825.

D'Angelo, G., Vicinanza, M., and De Matteis, M.A. (2008). Lipid-transfer proteins in biosynthetic pathways. Curr. Opin. Cell Biol. *20*, 360–370.

Davis, J.H., Jeffrey, K.R., Bloom, M., Valic, M.I., and Higgs, T.P. (1976). Quadrupolar echo deuteron magnetic resonance spectroscopy in ordered hydrocarbon chains. Chem. Phys. Lett. *42*, 390–394.

Denzel, A., Otto, F., Girod, A., Pepperkok, R., Watson, R., Rosewell, I., Bergeron, J.J., Solari, R.C., and Owen, M.J. (2000). The p24 family member p23 is required for early embryonic development. Curr. Biol. CB *10*, 55–58.

Devaux, P.F., and Morris, R. (2004). Transmembrane asymmetry and lateral domains in biological membranes. Traffic Cph. Den. *5*, 241–246.

Dominguez, M., Dejgaard, K., Füllekrug, J., Dahan, S., Fazel, A., Paccaud, J.P., Thomas, D.Y., Bergeron, J.J., and Nilsson, T. (1998). gp25L/emp24/p24 protein family members of the cis-Golgi network bind both COP I and II coatomer. J. Cell Biol. *140*, 751–765.

Donaldson, J., and Segev, N. (2000). Regulation and Coordination of Intracellular Trafficking: An Overview.

Dowhan, W., and Bogdanov, M. (2009). Lipid-dependent membrane protein topogenesis. Annu. Rev. Biochem. *78*, 515–540.

Dufourc, E.J. (2008). Sterols and membrane dynamics. J. Chem. Biol. *1*, 63–77.

Edidin, M. (2003). The state of lipid rafts: from model membranes to cells. Annu. Rev. Biophys. Biomol. Struct. *32*, 257–283.

Emery, G., Gruenberg, J., and Rojo, M. (1999). The p24 family of transmembrane proteins at the interface between endoplasmic reticulum and Golgi apparatus. Protoplasma *207*, 24–30.

Emery, G., Rojo, M., and Gruenberg, J. (2000). Coupled transport of p24 family members. J. Cell Sci. *113 (Pt 13)*, 2507–2516.

Eugster, A., Frigerio, G., Dale, M., and Duden, R. (2004). The alpha- and beta'-COP WD40 domains mediate cargo-selective interactions with distinct di-lysine motifs. Mol. Biol. Cell *15*, 1011–1023.

Fadok, V.A., Voelker, D.R., Campbell, P.A., Cohen, J.J., Bratton, D.L., and Henson, P.M. (1992). Exposure of phosphatidylserine on the surface of apoptotic lymphocytes triggers specific recognition and removal by macrophages. J. Immunol. Baltim. Md 1950 *148*, 2207–2216.

Fagone, P., and Jackowski, S. (2009). Membrane phospholipid synthesis and endoplasmic reticulum function. J. Lipid Res. *50 Suppl*, S311–S316.

Franco, M., Chardin, P., Chabre, M., and Paris, S. (1996). Myristoylation-facilitated binding of the G protein ARF1GDP to membrane phospholipids is required for its activation by a soluble nucleotide exchange factor. J. Biol. Chem. *271*, 1573–1578.

Futatsumori, M., Kasai, K., Takatsu, H., Shin, H.W., and Nakayama, K. (2000). Identification and characterization of novel isoforms of COP I subunits. J. Biochem. (Tokyo) *128*, 793–801.

García-Fruitós, E., Sabate, R., de Groot, N.S., Villaverde, A., and Ventura, S. (2011). Biological role of bacterial inclusion bodies: a model for amyloid aggregation. FEBS J. *278*, 2419–2427.

García-Sáez, A.J., and Schwille, P. (2010). Stability of lipid domains. FEBS Lett. *584*, 1653–1658.

Gommel, D., Orci, L., Emig, E.M., Hannah, M.J., Ravazzola, M., Nickel, W., Helms, J.B., Wieland, F.T., and Sohn, K. (1999). p24 and p23, the major transmembrane proteins of COPI-coated transport vesicles, form hetero-oligomeric complexes and cycle between the organelles of the early secretory pathway. FEBS Lett. *447*, 179–185.

Gommel, D.U., Memon, A.R., Heiss, A., Lottspeich, F., Pfannstiel, J., Lechner, J., Reinhard, C., Helms, J.B., Nickel, W., and Wieland, F.T. (2001). Recruitment to Golgi membranes of ADP-ribosylation factor 1 is mediated by the cytoplasmic domain of p23. EMBO J. *20*, 6751–6760.

Gross, R.W. (1985). Identification of plasmalogen as the major phospholipid constituent of cardiac sarcoplasmic reticulum. Biochemistry (Mosc.) *24*, 1662–1668.

Haberkant, P., Schmitt, O., Contreras, F.-X., Thiele, C., Hanada, K., Sprong, H., Reinhard, C., Wieland, F.T., and Brügger, B. (2008). Protein-sphingolipid interactions within cellular membranes. J. Lipid Res. *49*, 251–262.

Halter, D., Neumann, S., van Dijk, S.M., Wolthoorn, J., de Mazière, A.M., Vieira, O.V., Mattjus, P., Klumperman, J., van Meer, G., and Sprong, H. (2007). Pre- and post-Golgi translocation of glucosylceramide in glycosphingolipid synthesis. J. Cell Biol. *179*, 101–115.

Hanada, K., Kumagai, K., Yasuda, S., Miura, Y., Kawano, M., Fukasawa, M., and Nishijima, M. (2003). Molecular machinery for non-vesicular trafficking of ceramide. Nature *426*, 803–809.

Hannig, G., and Makrides, S.C. (1998). Strategies for optimizing heterologous protein expression in Escherichia coli. Trends Biotechnol. *16*, 54–60.

Hara-Kuge, S., Kuge, O., Orci, L., Amherdt, M., Ravazzola, M., Wieland, F.T., and Rothman, J.E. (1994). En bloc incorporation of coatomer subunits during the assembly of COP-coated vesicles. J. Cell Biol. *124*, 883–892.

Harter, C., and Wieland, F.T. (1998). A single binding site for dilysine retrieval motifs and p23 within the gamma subunit of coatomer. Proc. Natl. Acad. Sci. U. S. A. *95*, 11649–11654.

von Heijne, G. (2006). Membrane-protein topology. Nat. Rev. Mol. Cell Biol. *7*, 909–918.

Heikinheimo, L., and Somerharju, P. (2002). Translocation of Phosphatidylthreonine and -serine to Mitochondria Diminishes Exponentially with Increasing Molecular Hydrophobicity. Traffic *3*, 367–377.

Heimburg, T. (2009). Physical Properties of Biological Membranes. ArXiv09022454 Phys.

Hermansson, M., Hokynar, K., and Somerharju, P. (2011). Mechanisms of glycerophospholipid homeostasis in mammalian cells. Prog. Lipid Res. *50*, 240–257.

Hishikawa, D., Hashidate, T., Shimizu, T., and Shindou, H. (2014). Diversity and function of membrane glycerophospholipids generated by the remodeling pathway in mammalian cells. J. Lipid Res. *55*, 799–807.

Holthuis, J.C.M., and Levine, T.P. (2005). Lipid traffic: floppy drives and a superhighway. Nat. Rev. Mol. Cell Biol. *6*, 209–220.

Hong, M. (2006). Solid-state NMR studies of the structure, dynamics, and assembly of beta-sheet membrane peptides and alpha-helical membrane proteins with antibiotic activities. Acc. Chem. Res. *39*, 176–183.

Hughes, H., and Stephens, D.J. (2008). Assembly, organization, and function of the COPII coat. Histochem. Cell Biol. *129*, 129–151.

Hwang, P.M., Pan, J.S., and Sykes, B.D. (2014a). Targeted expression, purification, and cleavage of fusion proteins from inclusion bodies in Escherichia coli. FEBS Lett. *588*, 247–252.

Hwang, P.M., Pan, J.S., and Sykes, B.D. (2014b). Targeted expression, purification, and cleavage of fusion proteins from inclusion bodies in Escherichia coli. FEBS Lett. *588*, 247–252.

Hynynen, R., Laitinen, S., Käkelä, R., Tanhuanpää, K., Lusa, S., Ehnholm, C., Somerharju, P., Ikonen, E., and Olkkonen, V.M. (2005). Overexpression of OSBP-related protein 2 (ORP2) induces changes in cellular cholesterol metabolism and enhances endocytosis. Biochem. J. *390*, 273–283.

Jafurulla, M., Tiwari, S., and Chattopadhyay, A. (2011). Identification of cholesterol recognition amino acid consensus (CRAC) motif in G-protein coupled receptors. Biochem. Biophys. Res. Commun. *404*, 569–573.

Janmey, P.A., and Kinnunen, P.K.J. (2006a). Biophysical properties of lipids and dynamic membranes. Trends Cell Biol. *16*, 538–546.

Janmey, P.A., and Kinnunen, P.K.J. (2006b). Biophysical properties of lipids and dynamic membranes. Trends Cell Biol. *16*, 538–546.

Jansen, M., Ohsaki, Y., Rita Rega, L., Bittman, R., Olkkonen, V.M., and Ikonen, E. (2011). Role of ORPs in sterol transport from plasma membrane to ER and lipid droplets in mammalian cells. Traffic Cph. Den. *12*, 218–231.

Jasińska, R., Zborowski, J., and Somerharju, P. (1993). Intramitochondrial distribution and transport of phosphatidylserine and its decarboxylation product, phosphatidylethanolamine. Application of pyrene-labeled species. Biochim. Biophys. Acta *1152*, 161–170.

Jean-François, F., Castano, S., Desbat, B., Odaert, B., Roux, M., Metz-Boutigue, M.-H., and Dufourc, E.J. (2008). Aggregation of cateslytin beta-sheets on negatively charged

lipids promotes rigid membrane domains. A new mode of action for antimicrobial peptides? Biochemistry (Mosc.) *47*, 6394–6402.

Jenne, N., Frey, K., Brugger, B., and Wieland, F.T. (2002). Oligomeric state and stoichiometry of p24 proteins in the early secretory pathway. J. Biol. Chem. *277*, 46504–46511.

Kaiser, H.-J., Orłowski, A., Róg, T., Nyholm, T.K.M., Chai, W., Feizi, T., Lingwood, D., Vattulainen, I., and Simons, K. (2011). Lateral sorting in model membranes by cholesterol-mediated hydrophobic matching. Proc. Natl. Acad. Sci. U. S. A. *108*, 16628–16633.

Kang, H.W., Wei, J., and Cohen, D.E. (2010). PC-TP/StARD2: Of membranes and metabolism. Trends Endocrinol. Metab. TEM *21*, 449–456.

Kaplan, M.R., and Simoni, R.D. (1985). Intracellular transport of phosphatidylcholine to the plasma membrane. J. Cell Biol. *101*, 441–445.

Kawano, M., Kumagai, K., Nishijima, M., and Hanada, K. (2006). Efficient trafficking of ceramide from the endoplasmic reticulum to the Golgi apparatus requires a VAMP-associated protein-interacting FFAT motif of CERT. J. Biol. Chem. *281*, 30279–30288.

Kemayo Koumkoua, P., Aisenbrey, C., Salnikov, E., Rifi, O., and Bechinger, B. (2014). On the design of supramolecular assemblies made of peptides and lipid bilayers. J. Pept. Sci. Off. Publ. Eur. Pept. Soc. *20*, 526–536.

Kiessling, V., Wan, C., and Tamm, L.K. (2009). Domain Coupling in Asymmetric Lipid Bilayers. Biochim. Biophys. Acta *1788*, 64–71.

Killian, J.A. (1998). Hydrophobic mismatch between proteins and lipids in membranes. Biochim. Biophys. Acta *1376*, 401–415.

Kim, Y.J., Guzman-Hernandez, M.L., and Balla, T. (2011). A highly dynamic ER-derived phosphatidylinositol-synthesizing organelle supplies phosphoinositides to cellular membranes. Dev. Cell *21*, 813–824.

Kirchhausen, T. (2000). Three ways to make a vesicle. Nat. Rev. Mol. Cell Biol. *1*, 187–198.

Krogh, A., Larsson, B., von Heijne, G., and Sonnhammer, E.L. (2001). Predicting transmembrane protein topology with a hidden Markov model: application to complete genomes. J. Mol. Biol. *305*, 567–580.

Kuznetsov, G., and Nigam, S.K. (1998). Folding of secretory and membrane proteins. N. Engl. J. Med. *339*, 1688–1695.

Lakey, J.H., Duché, D., González-Mañas, J.M., Baty, D., and Pattus, F. (1993). Fluorescence energy transfer distance measurements. The hydrophobic helical hairpin of colicin A in the membrane bound state. J. Mol. Biol. *230*, 1055–1067.

Lalanne, F., and Ponsin, G. (2000). Mechanism of the phospholipid transfer protein-mediated transfer of phospholipids from model lipid vesicles to high density lipoproteins. Biochim. Biophys. Acta *1487*, 82–91.

Lauterwein, J., Bösch, C., Brown, L.R., and Wüthrich, K. (1979). Physicochemical studies of the protein-lipid interactions in melittin-containing micelles. Biochim. Biophys. Acta *556*, 244–264.

Laws, D.D., Bitter, H.-M.L., and Jerschow, A. (2002). Solid-state NMR spectroscopic methods in chemistry. Angew. Chem. Int. Ed Engl. *41*, 3096–3129.

Lebiedzinska, M., Szabadkai, G., Jones, A.W.E., Duszynski, J., and Wieckowski, M.R. (2009). Interactions between the endoplasmic reticulum, mitochondria, plasma membrane and other subcellular organelles. Int. J. Biochem. Cell Biol. *41*, 1805–1816.

Lee, A.G. (2003). Lipid-protein interactions in biological membranes: a structural perspective. Biochim. Biophys. Acta *1612*, 1–40.

Lee, M.C.S., Miller, E.A., Goldberg, J., Orci, L., and Schekman, R. (2004). Bi-directional protein transport between the ER and Golgi. Annu. Rev. Cell Dev. Biol. *20*, 87–123.

Lees, J.G., Miles, A.J., Wien, F., and Wallace, B.A. (2006). A reference database for circular dichroism spectroscopy covering fold and secondary structure space. Bioinforma. Oxf. Engl. *22*, 1955–1962.

Letourneur, F., Gaynor, E.C., Hennecke, S., Démollière, C., Duden, R., Emr, S.D., Riezman, H., and Cosson, P. (1994). Coatomer is essential for retrieval of dilysine-tagged proteins to the endoplasmic reticulum. Cell *79*, 1199–1207.

Lev, S. (2010). Non-vesicular lipid transport by lipid-transfer proteins and beyond. Nat. Rev. Mol. Cell Biol. *11*, 739–750.

Li, H., and Papadopoulos, V. (1998a). Peripheral-type benzodiazepine receptor function in cholesterol transport. Identification of a putative cholesterol recognition/interaction amino acid sequence and consensus pattern. Endocrinology *139*, 4991–4997.

Li, H., and Papadopoulos, V. (1998b). Peripheral-type benzodiazepine receptor function in cholesterol transport. Identification of a putative cholesterol recognition/interaction amino acid sequence and consensus pattern. Endocrinology *139*, 4991–4997.

Lilie, H., Schwarz, E., and Rudolph, R. (1998). Advances in refolding of proteins produced in E. coli. Curr. Opin. Biotechnol. *9*, 497–501.

Lindmo, K., and Stenmark, H. (2006). Regulation of membrane traffic by phosphoinositide 3-kinases. J. Cell Sci. *119*, 605–614.

Lingwood, D., and Simons, K. (2010). Lipid rafts as a membrane-organizing principle. Science *327*, 46–50.

London, E. (2002). Insights into lipid raft structure and formation from experiments in model membranes. Curr. Opin. Struct. Biol. *12*, 480–486.

Lowe, M., and Kreis, T.E. (1998). Regulation of membrane traffic in animal cells by COPI. Biochim. Biophys. Acta BBA - Mol. Cell Res. *1404*, 53–66.

Makrides, S.C. (1996). Strategies for achieving high-level expression of genes in Escherichia coli. Microbiol. Rev. *60*, 512–538.

Marzioch, M., Henthorn, D.C., Herrmann, J.M., Wilson, R., Thomas, D.Y., Bergeron, J.J., Solari, R.C., and Rowley, A. (1999). Erp1p and Erp2p, partners for Emp24p and Erv25p in a yeast p24 complex. Mol. Biol. Cell *10*, 1923–1938.

McConnell, H.M., and Kornberg, R.D. (1971). Inside-outside transitions of phospholipids in vesicle membranes. Biochemistry (Mosc.) *10*, 1111–1120.

McMahon, H.T., and Gallop, J.L. (2005). Membrane curvature and mechanisms of dynamic cell membrane remodelling. Nature *438*, 590–596.

van Meer, G., Voelker, D.R., and Feigenson, G.W. (2008a). Membrane lipids: where they are and how they behave. Nat. Rev. Mol. Cell Biol. *9*, 112–124.

Merk, A., and Subramaniam, S. (2013). HIV-1 envelope glycoprotein structure. Curr. Opin. Struct. Biol. *23*, 268–276.

Merrifield, R.B. (1963). Solid Phase Peptide Synthesis. I. The Synthesis of a Tetrapeptide. J. Am. Chem. Soc. *85*, 2149–2154.

Merrill, A.H. (2002). De novo sphingolipid biosynthesis: a necessary, but dangerous, pathway. J. Biol. Chem. *277*, 25843–25846.

Mesmin, B., and Maxfield, F.R. (2009). Intracellular sterol dynamics. Biochim. Biophys. Acta *1791*, 636–645.

Milhas, D., Clarke, C.J., and Hannun, Y.A. (2010). Sphingomyelin metabolism at the plasma membrane: implications for bioactive sphingolipids. FEBS Lett. *584*, 1887–1894.

Montero, M., van Houten, N.E., Wang, X., and Scott, J.K. (2008). The membrane-proximal external region of the human immunodeficiency virus type 1 envelope: dominant site of antibody neutralization and target for vaccine design. Microbiol. Mol. Biol. Rev. MMBR *72*, 54–84, table of contents.

Mouritsen, O.G., and Bloom, M. (1984). Mattress model of lipid-protein interactions in membranes. Biophys. J. *46*, 141–153.

Muñoz-Barroso, I., Salzwedel, K., Hunter, E., and Blumenthal, R. (1999). Role of the Membrane-Proximal Domain in the Initial Stages of Human Immunodeficiency Virus Type 1 Envelope Glycoprotein-Mediated Membrane Fusion. J. Virol. *73*, 6089–6092.

Murata, T., Yamato, I., Kakinuma, Y., Leslie, A.G.W., and Walker, J.E. (2005). Structure of the rotor of the V-Type Na+-ATPase from Enterococcus hirae. Science *308*, 654–659.

Musse, A.A., Wang, J., Deleon, G.P., Prentice, G.A., London, E., and Merrill, A.R. (2006). Scanning the membrane-bound conformation of helix 1 in the colicin E1 channel domain by site-directed fluorescence labeling. J. Biol. Chem. *281*, 885–895.

Ngo, M.H., Colbourne, T.R., and Ridgway, N.D. (2010). Functional implications of sterol transport by the oxysterol-binding protein gene family. Biochem. J. *429*, 13–24.

Nilsson, I., Ohvo-Rekilä, H., Slotte, J.P., Johnson, A.E., and von Heijne, G. (2001). Inhibition of protein translocation across the endoplasmic reticulum membrane by sterols. J. Biol. Chem. *276*, 41748–41754.

Nilsson, T., Jackson, M., and Peterson, P.A. (1989). Short cytoplasmic sequences serve as retention signals for transmembrane proteins in the endoplasmic reticulum. Cell *58*, 707–718.

Odorizzi, G., Babst, M., and Emr, S.D. (2000). Phosphoinositide signaling and the regulation of membrane trafficking in yeast. Trends Biochem. Sci. *25*, 229–235.

Opella, S.J., Ma, C., and Marassi, F.M. (2001). Nuclear magnetic resonance of membrane-associated peptides and proteins. Methods Enzymol. *339*, 285–313.

Orci, L., Stamnes, M., Ravazzola, M., Amherdt, M., Perrelet, A., Söllner, T.H., and Rothman, J.E. (1997). Bidirectional transport by distinct populations of COPI-coated vesicles. Cell *90*, 335–349.

Ouzzine, M., Boyd, A., and Hulmes, D.J.S. (1996). Expression of active, human lysyl oxidase in Escherichia coli. FEBS Lett. *399*, 215–219.

Pagano, R.E. (1990). Lipid traffic in eukaryotic cells: mechanisms for intracellular transport and organelle-specific enrichment of lipids. Curr. Opin. Cell Biol. *2*, 652–663.

Palade, G.E., and Siekevitz, P. (1956). Pancreatic microsomes; an integrated morphological and biochemical study. J. Biophys. Biochem. Cytol. *2*, 671–690.

Perozo, E., Kloda, A., Cortes, D.M., and Martinac, B. (2002). Physical principles underlying the transduction of bilayer deformation forces during mechanosensitive channel gating. Nat. Struct. Biol. *9*, 696–703.

Pines, A., Gibby, M.G., and Waugh, J.S. (1973). Proton-enhanced NMR of dilute spins in solids. J. Chem. Phys. *59*, 569–590.

Pomorski, T., and Menon, A.K. (2006). Lipid flippases and their biological functions. Cell. Mol. Life Sci. CMLS *63*, 2908–2921.

Popoff, V., Adolf, F., Brügger, B., and Wieland, F. (2011). COPI budding within the Golgi stack. Cold Spring Harb. Perspect. Biol. *3*, a005231.

Prinz, W.A. (2010). Lipid trafficking sans vesicles: where, why, how? Cell *143*, 870–874.

Rajendran, L., and Simons, K. (2005). Lipid rafts and membrane dynamics. J. Cell Sci. *118*, 1099–1102.

Rance, M., and Byrd, R.A. (1983). Obtaining high-fidelity spin- {1}/{2} powder spectra in anisotropic media: Phase-cycled Hahn echo spectroscopy. J. Magn. Reson. *52*, 221–240.

Randazzo, P.A., Yang, Y.C., Rulka, C., and Kahn, R.A. (1993). Activation of ADP-ribosylation factor by Golgi membranes. Evidence for a brefeldin A- and protease-sensitive activating factor on Golgi membranes. J. Biol. Chem. *268*, 9555–9563.

Reinhard, C., Harter, C., Bremser, M., Brügger, B., Sohn, K., Helms, J.B., and Wieland, F. (1999). Receptor-induced polymerization of coatomer. Proc. Natl. Acad. Sci. U. S. A. *96*, 1224–1228.

Rifi, O. (2014). Production des polypeptides issus des glycoprotéines d'enveloppe du VIH-1 pour des études biophysique et structurale par RMN et DC. University of Strasbourg.

Robinson, M.S. (2004). Adaptable adaptors for coated vesicles. Trends Cell Biol. *14*, 167–174.

Rothman, J.E., and Kennedy, E.P. (1977). Asymmetrical distribution of phospholipids in the membrane of Bacillus megaterium. J. Mol. Biol. *110*, 603–618.

Rothman, J.E., and Lenard, J. (1977). Membrane asymmetry. Science *195*, 743–753.

Rothman, J.E., and Wieland, F.T. (1996). Protein sorting by transport vesicles. Science *272*, 227–234.

Salnikov, E.S., and Bechinger, B. (2011). Lipid-Controlled Peptide Topology and Interactions in Bilayers: Structural Insights into the Synergistic Enhancement of the Antimicrobial Activities of PGLa and Magainin 2. Biophys. J. *100*, 1473–1480.

Salnikov, E., Bertani, P., Raap, J., and Bechinger, B. (2009). Analysis of the amide (15)N chemical shift tensor of the C(alpha) tetrasubstituted constituent of membrane-active peptaibols, the alpha-aminoisobutyric acid residue, compared to those of di- and tri-substituted proteinogenic amino acid residues. J. Biomol. NMR *45*, 373–387.

Samuelson, J. (2011). Bacterial Systems. In Production of Membrane Proteins, A.S. Robinson, ed. (Wiley-VCH Verlag GmbH & Co. KGaA), pp. 11–35.

Sato, H., and Feix, J.B. (2006). Peptide-membrane interactions and mechanisms of membrane destruction by amphipathic alpha-helical antimicrobial peptides. Biochim. Biophys. Acta *1758*, 1245–1256.

Scales, S.J., Pepperkok, R., and Kreis, T.E. (1997). Visualization of ER-to-Golgi transport in living cells reveals a sequential mode of action for COPII and COPI. Cell *90*, 1137–1148.

Schröder-Köhne, S., Letourneur, F., and Riezman, H. (1998). Alpha-COP can discriminate between distinct, functional di-lysine signals in vitro and regulates access into retrograde transport. J. Cell Sci. *111 (Pt 23)*, 3459–3470.

Schroeder, C. (2010). Cholesterol-binding viral proteins in virus entry and morphogenesis. Subcell. Biochem. *51*, 77–108.

Sharpe, H.J., Stevens, T.J., and Munro, S. (2010). A comprehensive comparison of transmembrane domains reveals organelle-specific properties. Cell *142*, 158–169.

Siekevitz, P., and Palade, G.E. (1958). A cyto-chemical study on the pancreas of the guinea pig. III. In vivo incorporation of leucine-1-C14 into the proteins of cell fractions. J. Biophys. Biochem. Cytol. *4*, 557–566.

Simons, K., and Ikonen, E. (1997). Functional rafts in cell membranes. Nature *387*, 569–572.

Simons, K., and van Meer, G. (1988). Lipid sorting in epithelial cells. Biochemistry (Mosc.) *27*, 6197–6202.

Simons, K., and Vaz, W.L.C. (2004). Model systems, lipid rafts, and cell membranes. Annu. Rev. Biophys. Biomol. Struct. *33*, 269–295.

Sleight, R.G., and Pagano, R.E. (1983). Rapid appearance of newly synthesized phosphatidylethanolamine at the plasma membrane. J. Biol. Chem. *258*, 9050–9058.

Sørensen, H.P., and Mortensen, K.K. (2005a). Advanced genetic strategies for recombinant protein expression in Escherichia coli. J. Biotechnol. *115*, 113–128.

Sørensen, H.P., and Mortensen, K.K. (2005b). Soluble expression of recombinant proteins in the cytoplasm of Escherichia coli. Microb. Cell Factories *4*, 1.

Sprong, H., van der Sluijs, P., and van Meer, G. (2001). How proteins move lipids and lipids move proteins. Nat. Rev. Mol. Cell Biol. *2*, 504–513.

Sreerama, N., and Woody, R.W. (1993). A self-consistent method for the analysis of protein secondary structure from circular dichroism. Anal. Biochem. *209*, 32–44.

Sreerama, N., and Woody, R.W. (2000). Estimation of protein secondary structure from circular dichroism spectra: comparison of CONTIN, SELCON, and CDSSTR methods with an expanded reference set. Anal. Biochem. *287*, 252–260.

Sreerama, N., and Woody, R.W. (2004). On the analysis of membrane protein circular dichroism spectra. Protein Sci. Publ. Protein Soc. *13*, 100–112.

Stamnes, M.A., Craighead, M.W., Hoe, M.H., Lampen, N., Geromanos, S., Tempst, P., and Rothman, J.E. (1995). An integral membrane component of coatomer-coated transport vesicles defines a family of proteins involved in budding. Proc. Natl. Acad. Sci. U. S. A. *92*, 8011–8015.

Stone, S.J., and Vance, J.E. (2000). Phosphatidylserine synthase-1 and -2 are localized to mitochondria-associated membranes. J. Biol. Chem. *275*, 34534–34540.

Strating, J.R.P.M., and Martens, G.J.M. (2009). The p24 family and selective transport processes at the ER-Golgi interface. Biol. Cell Auspices Eur. Cell Biol. Organ. *101*, 495–509.

Strating, J.R.P.M., van Bakel, N.H.M., Leunissen, J.A.M., and Martens, G.J.M. (2009). A comprehensive overview of the vertebrate p24 family: identification of a novel tissue-specifically expressed member. Mol. Biol. Evol. *26*, 1707–1714.

Studier, F.W., Rosenberg, A.H., Dunn, J.J., and Dubendorff, J.W. (1990). Use of T7 RNA polymerase to direct expression of cloned genes. Methods Enzymol. *185*, 60–89.

Sud, M., Fahy, E., Cotter, D., Brown, A., Dennis, E.A., Glass, C.K., Merrill, A.H., Murphy, R.C., Raetz, C.R.H., Russell, D.W., et al. (2007). LMSD: LIPID MAPS structure database. Nucleic Acids Res. *35*, D527–D532.

Sun, F., Zong, W., Liu, R., Chai, J., and Liu, Y. (2010). Micro-environmental influences on the fluorescence of tryptophan. Spectrochim. Acta. A. Mol. Biomol. Spectrosc. *76*, 142–145.

Tafesse, F.G., Ternes, P., and Holthuis, J.C.M. (2006). The multigenic sphingomyelin synthase family. J. Biol. Chem. *281*, 29421–29425.

Taylor, T.C., Kahn, R.A., and Melançon, P. (1992). Two distinct members of the ADP-ribosylation factor family of GTP-binding proteins regulate cell-free intra-Golgi transport. Cell *70*, 69–79.

Trotter, P.J., and Voelker, D.R. (1994). Lipid transport processes in eukaryotic cells. Biochim. Biophys. Acta *1213*, 241–262.

Vance, J.E. (2008). Phosphatidylserine and phosphatidylethanolamine in mammalian cells: two metabolically related aminophospholipids. J. Lipid Res. *49*, 1377–1387.

Vance, J.E., and Steenbergen, R. (2005). Metabolism and functions of phosphatidylserine. Prog. Lipid Res. *44*, 207–234.

van Meer, G., and Lisman, Q. (2002). Sphingolipid transport: rafts and translocators. J. Biol. Chem. *277*, 25855–25858.

van Meer, G., Voelker, D.R., and Feigenson, G.W. (2008b). Membrane lipids: where they are and how they behave. Nat. Rev. Mol. Cell Biol. *9*, 112–124.

Vidovic, V., Prongidi-Fix, L., Bechinger, B., and Werten, S. (2009a). Production and isotope labeling of antimicrobial peptides in Escherichia coli by means of a novel fusion partner that enables high-yield insoluble expression and fast purification. J. Pept. Sci. Off. Publ. Eur. Pept. Soc. *15*, 278–284.

Vidovic, V., Prongidi-Fix, L., Bechinger, B., and Werten, S. (2009b). Production and isotope labeling of antimicrobial peptides in Escherichia coli by means of a novel fusion partner that enables high-yield insoluble expression and fast purification. J. Pept. Sci. *15*, 278–284.

Vincent, N., Genin, C., and Malvoisin, E. (2002). Identification of a conserved domain of the HIV-1 transmembrane protein gp41 which interacts with cholesteryl groups. Biochim. Biophys. Acta *1567*, 157–164.

Voelker, D.R. (2009). Genetic and biochemical analysis of non-vesicular lipid traffic. Annu. Rev. Biochem. *78*, 827–856.

Wada, I., Rindress, D., Cameron, P.H., Ou, W.J., Doherty, J.J., Louvard, D., Bell, A.W., Dignard, D., Thomas, D.Y., and Bergeron, J.J. (1991). SSR alpha and associated calnexin are major calcium binding proteins of the endoplasmic reticulum membrane. J. Biol. Chem. *266*, 19599–19610.

Wakabayashi, M., Okada, T., Kozutsumi, Y., and Matsuzaki, K. (2005). GM1 ganglioside-mediated accumulation of amyloid beta-protein on cell membranes. Biochem. Biophys. Res. Commun. *328*, 1019–1023.

Warnock, D.E., Lutz, M.S., Blackburn, W.A., Young, W.W., and Baenziger, J.U. (1994). Transport of newly synthesized glucosylceramide to the plasma membrane by a non-Golgi pathway. Proc. Natl. Acad. Sci. U. S. A. *91*, 2708–2712.

Warschawski, D.E., Arnold, A.A., Beaugrand, M., Gravel, A., Chartrand, É., and Marcotte, I. (2011). Choosing membrane mimetics for NMR structural studies of transmembrane proteins. Biochim. Biophys. Acta BBA - Biomembr. *1808*, 1957–1974.

Waters, M.G., Serafini, T., and Rothman, J.E. (1991). "Coatomer": a cytosolic protein complex containing subunits of non-clathrin-coated Golgi transport vesicles. Nature *349*, 248–251.

Wegmann, D., Hess, P., Baier, C., Wieland, F.T., and Reinhard, C. (2004). Novel isotypic gamma/zeta subunits reveal three coatomer complexes in mammals. Mol. Cell. Biol. *24*, 1070–1080.

Weidler, M., Reinhard, C., Friedrich, G., Wieland, F.T., and Rösch, P. (2000). Structure of the cytoplasmic domain of p23 in solution: implications for the formation of COPI vesicles. Biochem. Biophys. Res. Commun. *271*, 401–408.

Wen, C., and Greenwald, I. (1999). p24 proteins and quality control of LIN-12 and GLP-1 trafficking in Caenorhabditis elegans. J. Cell Biol. *145*, 1165–1175.

Wirtz, K.W., and Zilversmit, D.B. (1969). Participation of soluble liver proteins in the exchange of membrane phospholipids. Biochim. Biophys. Acta *193*, 105–116.

Yang, X.-Y., Ren, C.-P., Wang, L., Li, H., Jiang, C.-J., Zhang, H.-B., Zhao, M., and Yao, K.-T. (2005). Identification of differentially expressed genes in metastatic and non-metastatic nasopharyngeal carcinoma cells by suppression subtractive hybridization. Cell. Oncol. Off. J. Int. Soc. Cell. Oncol. *27*, 215–223.

Ye, J., and DeBose-Boyd, R.A. (2011). Regulation of cholesterol and fatty acid synthesis. Cold Spring Harb. Perspect. Biol. *3*.

Yin, J., Li, G., Ren, X., and Herrler, G. (2007). Select what you need: a comparative evaluation of the advantages and limitations of frequently used expression systems for foreign genes. J. Biotechnol. *127*, 335–347.

Zachowski, A. (1993). Phospholipids in animal eukaryotic membranes: transverse asymmetry and movement. Biochem. J. *294 (Pt 1)*, 1–14.

Zimmerberg, J., and Kozlov, M.M. (2006). How proteins produce cellular membrane curvature. Nat. Rev. Mol. Cell Biol. *7*, 9–19.

Zwerger, M., Kolb, T., Richter, K., Karakesisoglou, I., and Herrmann, H. (2010). Induction of a massive endoplasmic reticulum and perinuclear space expansion by expression of lamin B receptor mutants and the related sterol reductases TM7SF2 and DHCR7. Mol. Biol. Cell *21*, 354–368.

Publications

Special Issue Article

Journal of PeptideScience

Received: 7 March 2014 Revised: 29 April 2014 Accepted: 29 April 2014 Published online in Wiley Online Library: 7 June 2014

(wileyonlinelibrary.com) DOI 10.1002/psc.2656

On the design of supramolecular assemblies made of peptides and lipid bilayers‡

Patricia Kemayo Koumkoua, Christopher Aisenbrey, Evgeniy Salnikov, Omar Rifi and Burkhard Bechinger*

Peptides confer interesting properties to materials, supramolecular assemblies and to lipid membranes and are used in analytical devices or within delivery vehicles. Their relative ease of production combined with a high degree of versatility make them attractive candidates to design new such products. Here, we review and demonstrate how CD- and solid-state NMR spectroscopic approaches can be used to follow the reconstitution of peptides into membranes and to describe some of their fundamental characteristics. Whereas CD spectroscopy is used to monitor secondary structure in different solvent systems and thereby aggregation properties of the highly hydrophobic domain of p24, a protein involved in vesicle trafficking, solid-state NMR spectroscopy was used to deduce structural information and the membrane topology of a variety of peptide sequences found in nature or designed. ^{15}N chemical shift solid-state NMR spectroscopy indicates that the hydrophobic domain of p24 as well as a designed sequence of 19 hydrophobic amino acid residues adopt transmembrane alignments in phosphatidylcholine membranes. In contrast, the amphipathic antimicrobial peptide magainin 2 and the designed sequence LK15 align parallel to the bilayer surface. Additional angular information is obtained from deuterium solid-state NMR spectra of peptide sites labelled with $^{2}H_3$-alanine, whereas ^{31}P and ^{2}H solid-state NMR spectra of the lipids furnish valuable information on the macroscopic order and phase properties of the lipid matrix. Using these approaches, peptides and reconstitution protocols can be elaborated in a rational manner, and the analysis of a great number of peptide sequences is reviewed. Finally, a number of polypeptides with membrane topologies that are sensitive to a variety of environmental conditions such as pH, lipid composition and peptide-to-lipid ratio will be presented. Copyright © 2014 European Peptide Society and John Wiley & Sons, Ltd.

Keywords: oriented solid-state NMR spectroscopy; circular dichroism (CD) spectroscopy; p24; magainin; LAH4; CRAC domain; designed model peptide; supported lipid bilayers; membrane topology; peptide-membrane interactions; transmembrane domain

Introduction

Peptides are used to design new materials, drug delivery systems and analytical devices [1–4]. They can be prepared in quantitative amounts in a reproducible manner and under stringent conditions of quality control. With the advent and development of solid-phase peptide synthesis as well as methods for bacterial over expression, it has become feasible to prepare peptide libraries where the characteristics of the resulting sequences can be easily modulated by amino acid exchange using not only the 20 common amino acids but also non-natural, chiral and even non-peptidic building blocks almost at will [5–7]. Furthermore, labels can be included or added for fluorescence, EPR or NMR spectroscopic measurements, which provide a convenient means to investigate and modulate the design features, or to be used as sensors for practical applications. Consequently, as can be seen by the diverse contributions to this Special Issue, the practical applications of peptides are wide spread, and in this paper, we will focus on their use in lipid membrane environments.

Apart from their relative ease in preparation and their versatility, peptides have the added advantage that when designed in the appropriate manner, they form or can be included into self-associating systems [1–4,8]. Biological or model membranes are such supramolecular complexes that self-assemble into bimolecular layers of high Ohmic resistance, and these can be doped with sensors, linked to solid supports, and connected to electrodes just to mention a few examples [9–11]. In particular, lipid vesicles or supported lipid bilayers have found their way into a number of applications such as drug delivery or sensor devices [12,13]. A virus or a vesicle for drug delivery that at the same time carries a receptor-recognition sequence represents a setting where the barrier forming properties of lipid membranes and the selective recognition of targets have successfully been combined with each other [13,14].

During the design and assembly of such supramolecular assemblies, a number of methods are required that allows one to monitor and control if the desired structural elements fold and behave as anticipated. Therefore, in this paper, we will present

* Correspondence to: Burkhard Bechinger, Université de Strasbourg / CNRS, UMR7177, Institut de Chimie, 1, rue Blaise Pascal, 67070 Strasbourg, France. E-mail: bechinge@unistra.fr

‡ This article is published in Journal of Peptide Science as part of the Special Issue devoted to contributions presented at the 1st International Conference on Peptide Materials for Biomedicine and Nanotechnology, Sorrento, October 28-31, 2013, edited by Professor Giancarlo Morelli, Professor Claudio Toniolo and Professor Mariano Venanzi.

Université de Strasbourg / CNRS, UMR7177, Institut de Chimie, 1, rue Blaise Pascal, 67070 Strasbourg, France

Abbreviations: *CD, circular dichroism; DPC, dodecyl phosphocholine; CP, cross polarization; CRAC, cholesterol recognition/interaction amino acid consensus; di-C12:0-PC, 1,2-dilauroyl-sn-glycero-3-phosphocholine; di-C20:1-PC, 1,2-dieicosenoyl-sn-glycero-3-phosphocholine; EPR, electron paramagnetic resonance; FID, free induction decay; HFIP, 1,1,1,3,3,3-hexafluoroisopropanol; MAS, magic angle spinning; NMR, nuclear magnetic resonance; POPC, 1-palmitoyl-2-oleoyl-sn-glycero-3-phosphocholine; SM, sphingomyelin; SUV, small unilamellar vesicles; TFE, 2,2,2-trifluoroethanol; TMD, transmembrane domain.*

a few examples how biophysical approaches have helped us to follow the membrane reconstitution process and which information can be obtained from such measurements from the final assembly. In particular, we will demonstrate how the reconstitution process was optimized for a highly hydrophobic membrane anchor using CD spectroscopy and how solid-state NMR spectroscopy can be used to determine the topology and alignment of the membrane constituents.

Materials and Methods

Materials

Organic solvents were from Sigma Aldrich (Saint Louis, MO, USA). The lipids were from Avanti Polar Lipids (Alabaster, AL, USA). Fmoc-amino acids were from NovaBiochem Merck-Millipore (Darmstadt Germany).

Peptide Synthesis

The peptides were prepared by solid-phase peptide synthesis using a Millipore 9050 automatic synthesizer and the Fmoc-chemistry. The [^{15}N-Leu23, $^{2}H_3$-Ala20]-p24TMD peptide has the sequence KKTNS RVVLW SFFEA LVLV**A** MT**L**GQ IYYLK R-CONH2 where a ^{15}N-labelled leucine and $^{2}H_3$-alanine (Cortecnet, Voisins les Bretonneux, France, or Aldrich, Saint Louis, MI, USA) were incorporated at the positions shown in bold. Another transmembrane model sequence, which was extended by a CRAC motif was designed carrying a $^{2}H_3$-alanine at position 24 (KKNIT NWLWY LKLFI MIALA LAL**A**L ALALA LKK-$CONH_2$). The magainin 2 (GIGKF LHSAK KFGKA FVGEI MNS-$CONH_2$), hΦ19W (KKKAL LALLA LAWAL ALLAL LAKKK) and KL15 (KKLLK ALKKL LKKLK) sequences have been presented previously [15,16]. Table 1 provides an overview of the peptide sequences discussed in this paper.

The peptides were purified by reversed phase high-performance liquid chromatography (HPLC) (Bischoff Chromatography, Leonberg, Germany) or (Gilson Chromatography, Villiers-Le-Bel, France) on Prontosil 300-6-C4 5.0-μm (Bischoff, Leonberg, Germany) or Luna 100-C18 5.0-μm columns (Phenomenex, France) using an acetonitrile/water gradient. The gradient was established with solvent A (acetonitrile/water/TFA, 10/90/0.1, v/v) and B (acetonitrile/TFA, 100/0.1, v/v), and the peptides eluted at the solvent B concentration as indicated in the succeeding text. When tested by analytical HPLC, the purity of p24TMD was 96%. This being the most difficult to dissolve and resolve, it can be safely estimated that all peptides are > 90% pure. The identity of the peptides was verified by matrix-assisted laser desorption ionization mass spectrometry. For the peptides used here, the theoretical masses and the elution (in % B) from the HPLC columns are the following: CRAC-TM (MW 3769.8, 65% B), hΦ19W (2673.5, 40%), KL15 (1793.4, 19%), magainin 2 (2465.9, 26%) and p24TM (3674.4, 44%). The measured experimental masses are in general within 1–2 units of the expected values when taking into consideration that ^{15}N and $^{2}H_3$ labels increase the mass by +1 and +3 units, respectively.

Circular Dichroism Spectroscopy

A 1 mg/mL stock solution of the p24TMD sequence was prepared in water. The concentration of peptide was determined by absorbance at 280 nm by use of an extinction coefficient calculated from the content of tryptophan, tyrosine and cysteine residues [17] (cf. http://www.basic.northwestern.edu/biotools/proteincalc.html). This stock solution was dried and dissolved in 300 μL of the respective solvents to give a 30 μM concentration.

In another set of experiments, the p24TMD peptide was reconstituted into membranes by dissolving the peptide and POPC in HFIP/water 50/50 (v/v). The solvent was removed first under a stream of nitrogen to form a thin film and then by exposure to high vacuum. Thereafter, the sample was hydrated with 10 mM phosphate buffer and tip sonicated to form small unilamellar vesicles.

The CD spectra were recorded on a Jasco J-510 spectropolarimeter (Tokyo, Japan) with a 50 nm/min scan speed, and data points were collected from 250 to 190 nm at 25°C using a quartz cell of 1 mm path length. The spectra were processed using the spectra manager software of the instrument, and the baseline corrected for solvent contributions (H_2O) by subtraction. Secondary structure analyses were performed with the CDpro Web server using the CONTINLL algorithm [18].

Sample Preparation for Solid-State NMR Spectroscopy

The preparation steps for the reconstitution of peptides into uniaxially oriented samples are documented in detail and illustrated in references [19,20]. In short, selectively labelled [^{15}N-Leu23, $^{2}H_3$-Ala20]-p24TMD was first dissolved in HFIP, and the solvent was removed under a stream of nitrogen. The

Table 1. Amino acid sequences of the peptides discussed in this paper

Alamethicin[a]	Ac-Aib-Pro-Aib-Ala-Aib-Aib-Gln-Aib-Val-Aib-Gly-Leu-Aib-Pro-Val-Aib-Aib-Gln-Gln-Phl						
CRAC-TM	KKNIT	NWLWY	LKLFI	MIALA	LALAL	ALALA	LKK-$CONH_2$
hΦ19W	KKKAL	LALLA	LAWAL	ALLAL	LAKKK		
Htt17[b]	MATLE	KLMKA	FESLK	SF			
ICP47[c]	SWALE	MADTF	LDNMR	VGPRT	YADVR	DEINK	RGR
KL15	KKLLK	ALKKL	LKKLK				
LAH4	KKALL	ALALH	HLAHL	ALHLA	LALKK	A-$CONH_2$	
Magainin 2	GIGKF	LHSAK	KFGKA	FVGEI	MNS-$CONH_2$		
PGLa	GMASK	AGAIA	GKIAK	VALKA	L-$CONH_2$		
p24TMD	KKTNS	RVVLW	SFFEA	LVLVA	MTLGQ	IYYLK	R-$CONH_2$

The one-letter code is used except for the peptaibol alamethicin, which caries a considerable number of unusual amino acids.

[a]The F50/7 isomorph is shown.′ Aib: α-aminoisobutyric acid, Phl: L-phenylalaninol.

[b]Htt17 represents the most amino-terminal residues of the huntingtin protein.

[c]Residues 2-34 of this 88 residue early gene product of Herpes simplex virus.

peptide was then dissolved in HFIP/water 50/50 (v/v), which had been shown to result in stable helix formation (Figure 1B). Thereafter, the peptide was added in a step-wise manner to POPC in HFIP. This was performed in such a manner that the water content remained low, and peptide aggregation was avoided.

Thereafter, the solvent was partially evaporated under a stream of nitrogen to reduce its total volume to about 0.5 mL. At this point, the clear and viscous sample was deposited onto 20 ultrathin glass plates (thickness 00 (about 80 μm), 6 × 11 mm or 8 x 22 mm for some of the other peptides, Paul Marienfeld, Lauda-Königshofen, Germany), slowly dried in air and the residual of solvent evaporated under high vacuum. Sample hydration was achieved at 98% humidity and the glass plates stacked on top of each other. The sample was stabilized by Teflon tape and sealed in plastic wrapping to avoid dehydration. The final peptide-to-lipid (P/L) molar ratio is 1%.

The oriented samples made of 5 mole% [^{15}NLeu17]-hΦ19W in POPC, 2 mole% [^{15}N-Ala15]-magainin2 in di-C12:0-PC, 2 mole% [^{15}N-Leu7]-KL15 in di-C20:1-PC and 2 mole% [$^{2}H_3$-Ala24]-CRAC-TM in POPC were prepared in an analogous manner by initially co-dissolving the peptide and lipid in TFE (hΦ19W, KL15), methanol/chloroform 2:1 (v/v, CRAC-TM) or methanol/chloroform 1:1 (v/v; magainin 2).

Non-oriented samples were prepared in an analogous manner except that a film of 0.13 mg peptide and 2 mg of deuterated lipid was formed in a glass tube, which was then resuspended in 200 μL of 10 mM phosphate buffer by vortexing and sonication in a water bath followed by 10 of freeze/thaw cycles. The resulting vesicle suspension was pelleted in a bench-top centrifuge (Biofuge Pico, Hearaeus Instruments, Hanau, Germany) at 13 000 rpm for 1 min directly into a tube for microcentrifuges (VWR Radnor, PA, USA), which was directly used for the NMR measurements.

Solid-State NMR Spectroscopy

The samples were inserted with the normal parallel to the magnetic field of a Bruker Avance NMR spectrometer operating at 9.4 Tesla (Rheinstetten, Germany) and the NMR spectral acquisitions calibrated as described in detail in reference [19]. All spectra were recorded at 295 K.

Proton-decoupled ^{31}P solid-state NMR spectra were recorded using a Hahn echo pulse sequence [21] with an echo time of 40 μs, a repetition time of 3 s, a ^{31}P B_1 field of 80 kHz and a spectral width of 40 kHz. An exponential line broadening of 150 Hz was applied prior to Fourier transformation. The spectra were referenced relative to 85% H_3PO_4.

Proton-decoupled ^{15}N solid-state NMR spectra were recorded using a CP pulse sequence [22] with a CP time of 800 μs, a repetition time of 3 s, a B_1 field of 31 kHz (^{15}N and ^{1}H channel) and a spectral with of 38 kHz. The FIDs were subject to an exponential apodization with line broadening of 100 Hz prior to Fourier transformation. The spectra were calibrated relative to external ammonium chloride (40 ppm), which places NH_3 at 0 ppm [23].

Deuterium solid-state NMR spectra of samples made of POPC labelled with d_{31} along the palmitoyl chain were measured using a quadrupolar echo sequence [24] with a repetition delay of 0.3 s for the lipid and 0.6 s for the peptide spectra, an echo time of 100 μs, a B_1 field of 40 or 62 kHz for the lipid and peptide spectra, respectively. The FID was oversampled with a spectral with of 100 kHz enabling the precise adjustment of the echo by left-shifts after the acquisition. The processing included an exponential apodization with line broadening of 200 Hz for the lipid and 500 Hz for the peptide spectra, respectively. The spectra were referenced relative to D_2O.

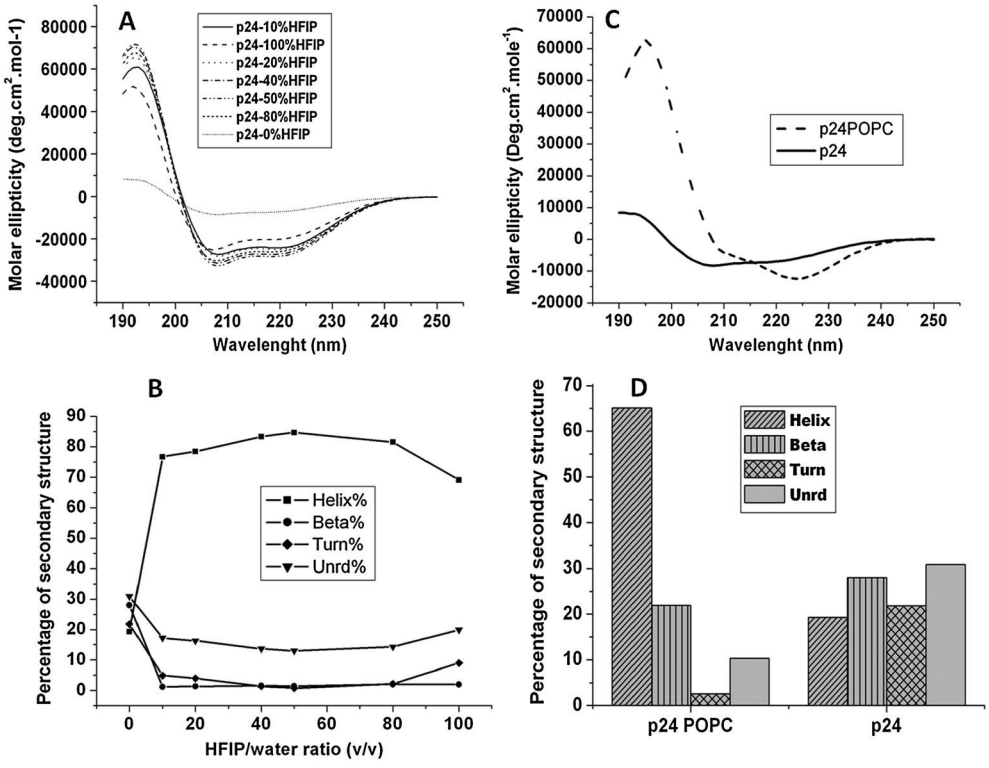

Figure 1. Circular dichroism data to optimize p24TMD reconstitution. (A) p24TMD folding in solvents of different HFIP/water composition. (B) The secondary structure preferences of p24TMD as a function of HFIP concentration. (C) CD spectra of p24TMD in POPC liposomes (dashed line) or in aqueous buffer (solid line). The spectra were recorded in 10 mM phosphate buffer, pH 7 at 25°C. (D) The secondary structure composition of p24TMD in the presence or absence of POPC as obtained from the CD spectra using the CDPro software.

Journal of PeptideScience

Results and Discussion

Developing a Membrane Reconstitution Protocol for Hydrophobic Peptides

Cellular membranes consist of a wide variety of lipid species varying in head group and fatty acyl chain composition. The lipid composition not only varies between organelles, but they are also distributed unevenly between the inner and outer leaflets of the cellular or organelle membranes [25,26].

Whereas many membrane lipids and/or their precursors are synthesized in the endoplasmic reticulum of eukaryotic cells, they are then transported either monomolecularily by lipid transport proteins, or with the membrane in intracellular transport vesicles [27]. There is a continuous flow of lipids between the endoplasmic reticulum the Golgi, the plasma membrane and the endomembrane system, and during the transport the lipids are processed and sorted to assure the differing lipid compositions of individual subcellular membranes. In this context, a highly specific interaction of a SM lipid carrying a C18 fatty acyl chain with the (predicted) transmembrane domain of p24, a protein of the COPI transport vesicles has been described [28–30]. Such observations are strongly suggestive that the lipids provide more than merely the 'solvent' for the proteins and the 'bricks' of the membrane barrier; however, when compared to protein or nucleic acid interactions, little is known about specific protein–lipid interactions [31].

In order to analyse this interaction of p24 with membranes of different composition, a 31 amino acid polypeptide, which includes the hydrophobic domain of the p24 protein, was designed. The sequence of the peptide is KKTNS RVVLW SFFEA LVLV**A** MT**L**GQ IYYLK R-CONH2 , where the underlined residues make up a domain of high hydrophobicity. The doubly underlined positions have been identified as being of high relevance for the specificity of interactions with SM C18 [30], and charged amino acids were added at the N-terminus and C-terminus to act as anchor sequences and to improve peptide solubility and handling. Alanine-20 and leucine-23 (in bold) were labelled with stable ^{2}H and ^{15}N isotopes, respectively, for NMR spectroscopic investigations. It should be noted that the study of membrane-associated peptides can be a difficult task as they tend to aggregate, and their preparation and purification are often difficult.

In order to investigate the interaction of different lipids with p24TMD (Table 1), a reconstitution assay was performed where, in a first step, the synthetic peptide was dissolved in a variety of solvents including TFE, dichloromethane, HFIP and aqueous solutions as well as in the presence of detergents and investigated by CD spectroscopy.

Interestingly, for most of the solvents used to initially dissolve the peptides and lipids, the CD spectra are either characterized by low intensities and/or characteristic of high β-sheet/random coil conformations (not shown) suggesting aggregated structures during the reconstitution process [32,33]. Depending on the peptide finding a good solvent where both the lipids and the peptides are dissolved can be difficult, but in our and others hands, but HFIP has proven a versatile solvent for this purpose [20,34–36]. HFIP exhibits a combination of strong hydrogen bonding and at the same time hydrophobic properties with structurating capabilities on some polypeptides [37]. As a consequence, it has been shown to dissolve hydrogen bond acceptors such as organic polyamides, polyacrylonitriles, polyesters and even β-sheet aggregated polypeptides [38,39].

Indeed, when the secondary structure was tested upon exposure to HFIP/water mixtures, for which the composition was varied in a systematic manner, the peptide adopts a largely α-helical secondary structure in the presence of even small amounts of HFIP suggesting that, under these conditions, it can be maintained in a reconstitution-competent state (Figure 1A). A more detailed analysis indicates that p24TMD is ≥80% helical in HFIP/water 50/50 (v/v) (Figure 1B).

Therefore, the peptide was reconstituted into liposomes starting from such an HFIP/water mixture, which is also suitable to dissolve many phospholipids. After co-dissolving peptides and POPC, the solvents were evaporated in such a manner to form a film along the glass walls of the test tube, resuspended in buffer, vortexted, sonicated, and the thus prepared sample analysed by CD spectroscopy (Figure 1C). The CD spectrum of 3 mole% p24TMD reconstituted in POPC SUV is shown in Figure 1C and compared with the spectrum of 30 μM p24TMD in aqueous buffer. Whereas the high helix-forming propensity is maintained in the membrane environment, much of the spectral intensity is lost in the absence of lipids (Figure 1D).

This example illustrates how optical spectroscopy can help to scan a large number of solvents and experimental conditions with the goal to develop a protocol for efficient membrane reconstitution. Optical techniques such as CD- and fluorescence spectroscopy require orders of magnitude less peptide than, for example, NMR spectroscopy. The semi-quantitative information that they provide about the global secondary structure of the peptide in a wide variety of conditions provides a good screening opportunity to test a large number of sample conditions in a single or a few days. Similar approaches can be used in order to find a suitable detergent for concentration for multidimensional solution NMR investigations [40–42].

Investigating the Membrane Interactions of Polypeptides by Solid-State NMR

In a next step, the p24TMD was investigated by solid-state NMR spectroscopy, a technique which can provide quite detailed information about the structure, topology and interactions of membrane-associated peptides [43,44]. The method requires several milligrammes of isotopically labelled peptides per sample and many hours of spectrometer time. It is therefore advantageous that essential steps of the membrane reconstitution protocol were already established using CD spectroscopy (Figure 1). In solid or semi solid samples, the NMR parameters are anisotropic, that is, the chemical shifts and dipolar and quadrupolar couplings all depend on the molecular alignment relative to the magnetic field of the spectrometer [44]. In samples where all spatial orientations are present, this results in very broad spectral line shapes with little or no spectral resolution [45]. In order to re-introduce high-resolution into these spectra either very fast sample spinning around the MAS can be applied and results in spectral averaging and narrow lines [43], or static oriented samples are investigated that reveal the NMR parameters of just one molecular orientation in space [44]. The latter approach has been applied to membrane-associated peptides, which have been labelled with ^{13}C, ^{15}N and/or ^{2}H [44,46].

Whereas MAS solid-state NMR follows similar concept as multidimensional NMR in solution by providing isotropic chemical shift spectra and correlations representative of distance or intra-molecular angles [43], uniaxially oriented samples reveal valuable highly complementary information about the alignment

of bonds and consequently whole molecules relative to the magnetic field direction [44]. These data can be used to reconstruct the structure of biomacromolecules and/or the relative alignment of molecules within supramolecular complexes [41,47]. A successful approach consists in labelling a peptide bond with ^{15}N and reconstituting the peptide into lipid bilayers that are oriented with the normal parallel to the magnetic field direction. From such samples, alignment information of the ^{15}N-H vector and thus the helical domain are obtained in a straightforward manner [44,45]. Notably, the natural abundance of ^{15}N is only 0.4% of all nitrogen atoms, therefore, in general, only the signal from the isotopically enriched sites (typically >95%) is observed. For helical domains labelled with ^{15}N at their backbone chemical shifts around 200 ppm correlate with transmembrane helices, whereas values <100 ppm are indicative of domains oriented parallel to the bilayer surface [45]. The tilt and azimuthal angles of the helices can be determined quite accurately when it is possible to combine the ^{15}N chemical shift information with angular restraints that are obtained from $^{2}H_3$-labelled alanines, where the resulting deuterium quadrupolar splitting is correlated to the relative alignment of the Cα–Cβ bond, and this combination has provided valuable information on a variety of polypeptides that were prepared by solid-phase peptide synthesis [15,48–50].

When the ^{15}N solid-state NMR spectrum of p24TMD labelled at the leucine-23 position was investigated, a chemical shift of 217 ppm was recorded (Figure 2A). This measurement, together with the high helical content measured by CD spectroscopy, is indicative that the peptide spans the membrane in a transmembrane helical fashion.

Whereas natural transmembrane helical sequences are of complex compositions, they all share a high hydrophobicity and a length of typically 16–20 residues. Several of these have been investigated by ^{15}N solid-state NMR spectroscopy and a transmembrane alignment confirmed (e.g. [34,51–54]). These general features can be used to design much simpler domains such as sequences made solely of leucines or of mixtures of alanines and leucines [55–61]. One such reductionist peptide, hΦ19W (Table 1), has been designed in our laboratory, with an additional tryptophan for fluorescence studies [15,16]. For [^{15}N-Leu17]-hΦ19W, a ^{15}N chemical shift is observed at 202 ± 2.5 ppm when reconstituted into oriented POPC bilayers thereby confirming the transmembrane helical design of the sequence (Figure 2B). Notably, dimerisation or higher order oligomerisation of such transmembrane sequences can be controlled by small modifications of their primary sequences [62–64].

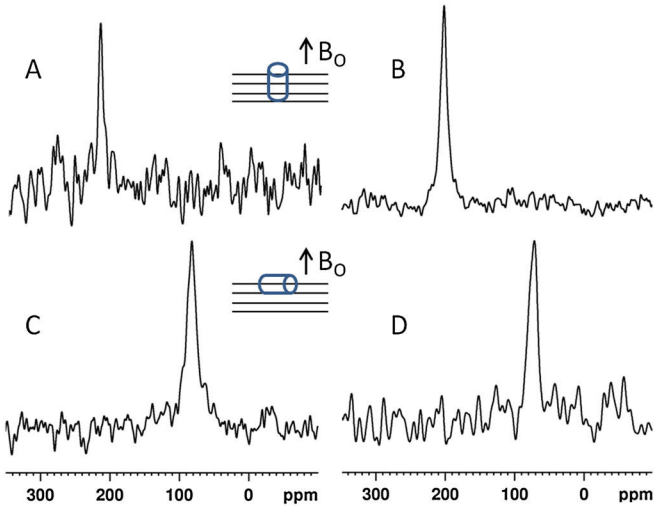

Figure 2. Proton-decoupled ^{15}N cross polarization NMR spectra of peptides labelled with ^{15}N at a specific position and reconstituted into oriented phosphatidylcholine membranes: (A) 1 mole % [^{15}N-Leu23]-p24TMD in POPC, (B) 5 mole% [^{15}N-Leu17]-hΦ19W in POPC, (C) 2 mole % [^{15}N-Ala15]-Magainin2 in di-C12:0-PC and (D) 2 mole % [^{15}N-Leu7]-KL15 in di-C20:1-PC. The corresponding helix orientation for each row is sketched in the inserts.

The solid-state NMR spectrum of another designed transmembrane helical domain is shown in Figure 3A. Here, the peptide was prepared with an alanine carrying a deuterated methyl group, reconstituted into oriented phospholipid membranes and investigated by ^{2}H solid-state NMR spectroscopy. Due to fast rotation around the Cα–Cβ bond, all three deuterons are equivalent and exhibit identical NMR spectra. The deuterium nucleus is quadropolar (spin 1), characterized by three energy levels with two allowed transitions. Therefore, the spectrum of the deuterated alanine methyl group is characterized by two lines, which can be separated by up to 72 kHz, its exact value depending on the dynamics of the deuterated site and its alignment relative to the magnetic field of the NMR spectrometer (for additional details cf. reference [44]). For the transmembrane model sequence labelled at position Ala-24, the frequency difference between the two peaks is 12 ± 1 kHz and represents the quadrupolar splitting, which is directly correlated to the average angle of the Cα–Cβ bond relative to the magnetic field direction/membrane normal (Figure 3B).

In contrast, many amphipathic sequences exhibit a high hydrophobic moment and consequently they align at the membrane interface parallel to the surface. One of the early examples investigated by the ^{15}N solid-state NMR technique is magainin 2, which orients parallel to the membrane surface under many different conditions so far investigated [65]. This observation is confirmed by the experiment shown in Figure 2C, where the peptide was reconstituted into a very thin membrane made of di-C12:0-PC and a chemical shift of 82 ± 4 ppm is measured. Notably, membranes of small hydrophobic thickness have been shown to promote a transmembrane alignment of other peptide sequences [55,66,67], and this experiment thereby provides a stringent test for the propensity of a sequence to traverse the bilayer. In-plane alignments have also been observed for many other sequences found in nature including antimicrobial peptides [40,49,68–76], signal sequences [52], surfactant peptides [77], the amino-terminal membrane anchor of huntingtin [41] or a domain of the Herpes virus protein ICP47 [48] (Table 1). Furthermore, peptide sequences have been designed to orient along the membrane surface [78–81], and this design has been confirmed by solid-state NMR spectroscopy, for example, for [^{15}N-Leu7]-KL15 [15] (Table 1), which exhibits a chemical shift of 71 ± 5 ppm in di-20:1-PC lipid bilayers (Figure 2D).

Furthermore, some polypeptides exhibit a more dynamic behaviour where transitions from the in-planar configuration to more inserted and even transmembrane alignments can be triggered by environmental changes such as pH [61,82–85], lipid fatty acyl [67,72,86,87] or head group composition [72,88,89], hydration [34,90], buffer [89], peptide concentration [87,91] or the presence of other peptides. Notably, domain realignment in the presence of other polypeptides could be of importance for the regulation of membrane proteins [67,86]. Even alamethicin (Table 1), a long-standing paradigm for the formation of pores by transmembrane helical bundles [92] has been found

Journal of PeptideScience

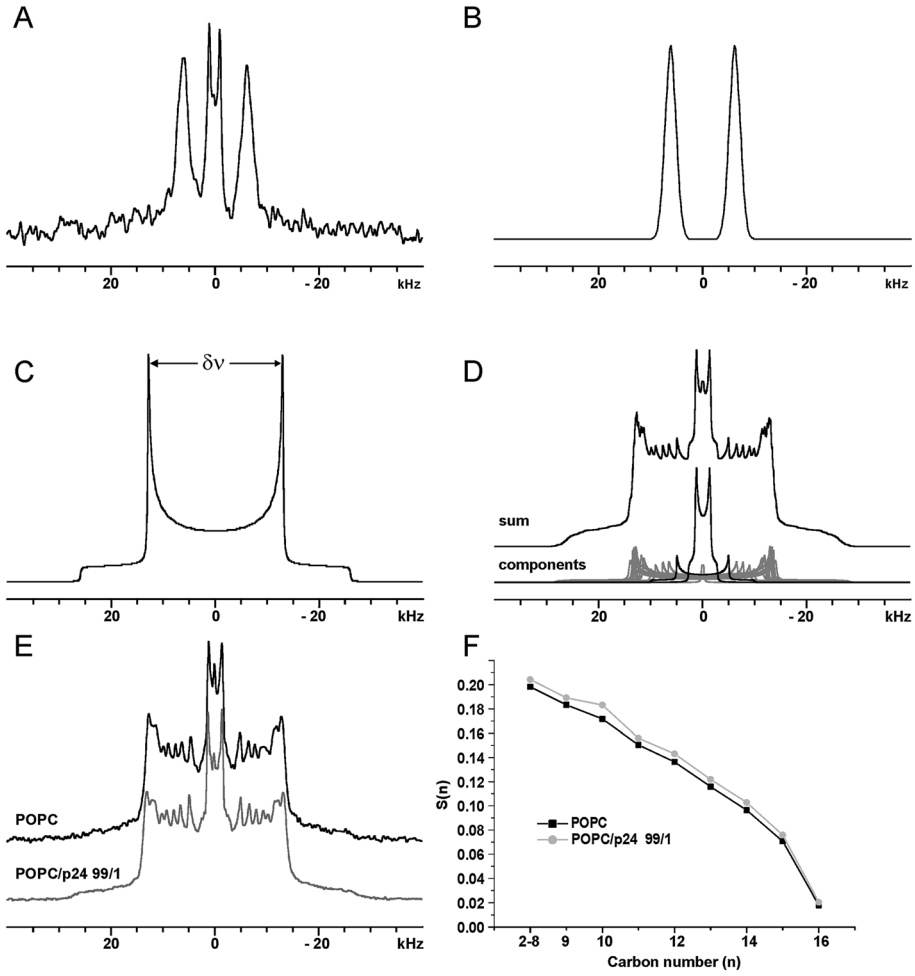

Figure 3. (A) ^{2}H spectrum of the [$^{2}H_3$-Ala24] CRAC-TM model sequence reconstituted into oriented POPC bilayers. The central doublet corresponds to water molecules interacting with the oriented membrane. (B) Simulated spectrum of $^{2}H_3$-alanine with an angle of 48° ± 1° between the Cα–Cβ bond and the magnetic field when a static quadrupolar coupling constant of 72 kHz is taken into a consideration. (C) Simulated spectrum of a ^{2}H solid-state NMR spectrum obtained from a non-oriented sample carrying a single site labelled with ^{2}H (powder pattern of a quadrupolar nucleus). (D) Simulated ^{2}H solid-state NMR spectrum of POPC-d_{31} where the signals from many sites with different quadrupolar splitting add up. (E) Experimental ^{2}H solid-state NMR spectra of POPC-d_{31} in the presence (grey) or absence (black) of [^{15}N-Leu23]-p24TMD. (F) Deconvolution of the spectra shown in E provides position-dependent quadrupolar splittings and the corresponding deuterium order parameters S_{CD}. The p24TMD peptide causes a small increase in several of the POPC-d_{31} order parameters. The estimated error bar is <0.004 for S_{CD}, which fits within the outline of the symbols used in panel E.

to switch between transmembrane and in-planar alignments under certain conditions [87,88]. In a similar manner, magainin 2 and PGLa (Table 1) have been considered to exhibit stable in-planar alignment. Interestingly, whereas magainin 2 has shown in-planar orientations under all conditions so far investigated [65], this is not the case for PGLa. The latter has been found to be able to adopt a multitude of topologies in a manner that depends on environmental factors such as lipid composition, peptide-to-lipid-ratio and the presence of magainin 2 [67,86].

The question remains which structural features cause the different physico-chemical behaviour of PGLa and magainin 2, both being linear cationic amphipathic peptides found in the skin of the African clawed frog. At the present time, we can only speculate, as to our knowledge, no experimental data have been accumulated to answer this question. However, the structures of a number of amphipathic helical peptides have been determined in DPC micelles, and their alignments tested in oriented lipid bilayers. On the one hand, these include magainin 2 [93,94] and the 17-residue N-terminal membrane anchor of huntingtin, Htt17 [41,50], both exhibiting stable orientations along the membrane surface. On the other hand, PGLa [95,96] and LAH4 [84,89,97] undergo transitions in more tilted and even transmembrane alignments more easily (Table 1). When the Edmundson wheels are constructed of the domains that are found to be helical in micellar environments, the following differences become apparent (Figure 4). First, the helical domain of LAH4 PGLa ends with a lysine, and including this residue in the analysis enlarges considerably the hydrophilic face of the α-helices. It seems well possible that this residue at the very end of the helical structure is in dynamic exchange between helical and non-helical conformations, while in the latter conformation, it can interact more easily with the aqueous phase. Whereas the occurrence of lysine in the helical domain may be stabilized by its possibility to snorkel to the membrane surface, it should also be mentioned that, in a highly curved micelle, the energetic penalty of keeping a lysine at the C-terminus of the helix is less pronounced than in a planar lipid bilayer. Second, when the helical wheel is analysed by assuming that this C-terminal lysine is in a non-helical conformation and exposed to the water face the hydrophobic angles of LAH4 and PGLa are much increased and considerably larger

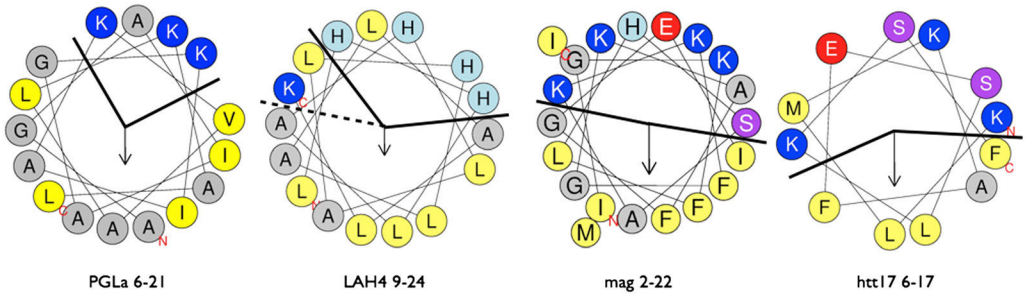

Figure 4. Helical wheel representations of PGLa, LAH4 at acidic pH, magainin 2 and Htt17. The outlines of the helices are taken from NMR structures that have been determined in DPC micelles [41,93,95,97]. The charged residues are shown in red (negative), dark and light blue (positive), the polar ones in magenta, hydrophobic residues in yellow and the glycines and alanines which exhibit little preference for the interface or the hydrophobic interior in grey [82]. The very N-terminal and C-terminal residues of the helix domains are marked by red letters. The black lines indicate the separation of predominantly charged/polar face from the hydrophobic side, where the dotted lines include the most C-terminal lysine of LAH4 whereas the continuous lines exclude this residue. The arrows represent the calculated hydrophobic moments. The helices were created using http://heliquest.ipmc.cnrs.fr [131].

when compared with Htt17 or magainin 2 (Figure 4). Third, the hydrophobic moments of the helical domains with less stable topologies are considerably smaller than those of magainin 2 or Htt17 (Table 1). Whereas a strong hydrophobic moment combined with a large hydrophobic angle suggest that the helices that penetrate more deeply into the membrane hydrophobic core exhibit less stable alignments, the resulting topological changes may be coupled to conformational rearrangements. In this context, it is noteworthy that small energetic differences can tip the balance between different topologies, and the exchange of a single amino acid can cause a shift from an in-planar to a transmembrane propensity [56,57].

Peptide domains that monitor specific environmental conditions, including, for example, a different membrane composition or pH in cancerous tissues, or that accumulate in the presence of specific receptor molecules have a high potential to be useful in materials developed for biomedical applications [8,98,99]. Other environmental factors that have been suggested or experimentally proven to influence the membrane topology of polypeptides are transmembrane electric fields [92,100], peptide-peptide interactions [67,101] and/or membrane hydration [34,67,87].

Figure 2 shows the NMR spectra of two sequences isolated first from natural sources and two peptides designed to adopt a particular topology. Clearly, with our present knowledge, it is possible to design peptides that interact with a lipid matrix in a defined manner [84,102] and to use oriented solid-state NMR spectroscopy (Figure 2), ATR FTIR [103,104] or oriented CD spectroscopy [105,106] to validate such design features. Whereas the latter two techniques can follow the topology in a semi-quantitative manner, the analysis by solid-state NMR spectroscopy in combination with isotopic labelling can be applied in a residue-specific and/or domain-specific manner. When required, the NMR approach has the potential for a full structure determination using larger sets of isotopic labels and/or more elaborate NMR experiments [107–109]. Importantly, the aforementioned examples and the published data also illustrate that the technique can be applied to membranes of very different fatty acyl chain (Figure 2) or lipid head group composition [65] and to a wide variety of peptides and proteins [107–111]. Therefore, when a material or a devise is to be developed, the NMR methods described are by far not limited to systems that closely resemble the aforementioned examples. Notably, more recent developments in the field of solid-state NMR even allow a topological analysis for peptides in non-oriented membrane systems [112], and the characterization of the dynamics and thereby the oligomerization of membrane-associated peptides using the same samples that helped in the topological analysis [41,113]. Such experiments provide additional useful information to fine-tune the design and preparation of peptide-based materials and devices.

So far, the discussion of the design features of the peptide-lipid supramolecular assemblies focused on particular characteristics and functionalities of the peptides as well as methods to analyse their structure, topology and dynamics in membranes. However, the lipid membranes are soft and adapt to the environment, therefore, the lipids can much contribute to the properties of the final result and need to be taken into consideration. As the ^{31}P nucleus is one of the more sensitive NMR nuclei and the only isotope of the phosphorous atom, no isotopic enrichment is necessary to record quite sensitive ^{31}P solid-state spectra of the phospholipids, which in addition are typically present in tenfold to 1000-fold molar excess when compared with peptides. The ^{31}P solid-state NMR spectra of the oriented phosphatidylcholine sample containing 2 mole% KL15 is shown in Figure 5A. This is the same sample for which the ^{15}N solid-state NMR spectra are shown in Figure 2D. The spectrum exhibits a broad spectral line shape between 30 and −15 ppm with its major intensity around 30 ppm. Thereby, the ^{31}P chemical shift of the phosphatidylcholine headgroup in the liquid crystalline bilayer shows an anisotropy of 45 ppm in a related manner as outlined for the ^{15}N chemical shift of the peptide bond (cf. above). Whereas the phospholipids that are aligned with their long axis parallel to the magnetic field direction resonate at 30 ppm (Figure 5B), those perpendicular exhibit a chemical shift at −15 ppm. A spectrum with all lipid alignments present at random is shown in Figure 5C. In Figure 5A, the sample has been aligned in such a manner that the glass plate normal coincides with the magnetic field of the spectrometer, and the spectrum is therefore indicative that a large proportion of the lipids are aligned parallel to the membrane normal. The spectrum shown in Figure 5A can be explained by the addition of contributions such as the ones represented in Figure 5B and C, where the smaller intensities <30 ppm are due to misaligned sample. However, phospholipids where the molecular orientation is rearranged in the vicinity of the p24 domain or a range of head group conformations, which may, for example, be a result of electrostatic interactions [114] should also be considered.

Notably, macroscopic alignment of pure POPC lipid bilayers has been achieved in the past where only a 30 ppm signal intensity becomes visible suggesting that a high degree of sample alignment can be obtained by orienting pure phospholipid bilayers between glass plates [19,40,115]. In contrast, the ^{31}P line shapes observed in the presence of antimicrobial peptides are

Journal of PeptideScience

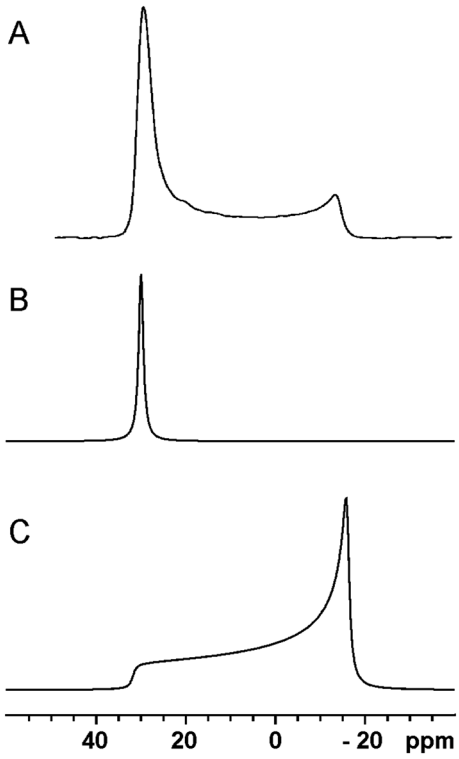

Figure 5. (A) Proton-decoupled ^{31}P solid-state NMR spectrum of di-C20:1-PC in the presence of 2 mole% [^{15}N-Leu7]-KL15. Simulated ^{31}P solid-state NMR spectra of liquid crystalline phosphatidylcholine bilayers (B) oriented with the lipid long axis parallel relative to the magnetic field direction and (C) exhibiting a random distribution of alignments.

suggestive for membrane thinning or regions of high local curvature [116]. Such membrane deformations may ultimately result in membrane pore formation and lysis [117]. Therefore, the ^{31}P-NMR spectra provide additional valuable information with regard to the interactions and/or mechanisms of action of the polypeptides. Importantly, antimicrobial peptides or peptide-derived mimetics have been included into the design of materials, for example, to confer antibacterial resistance to implants and surfaces [118–120]. Notably, for the design of novel, more efficient or cheaper to produce compounds or for the correct insertion into a new material, knowing the peptides' membrane insertion properties and their mechanism of action makes a considerable difference. For example, in the case of antimicrobial peptides, realizing that they interact in an interfacial fashion has resulted in the design of short peptides, alkylated tripeptides or amphipathic polymers that are unsuitable to span the membrane [121–123]. Their properties would be difficult to explain without the knowledge that the antimicrobial action of a number of peptides is better when aligned parallel to the membrane surface, rather than in the configuration of a transmembrane helical bundle as was initially suggested (reviewed in [100]).

Whereas the ^{31}P solid-state NMR spectra monitor the conformational and dynamic properties at the level of the headgroup of the phospholipids including local conformational rearrangements [114] and macroscopic phase transitions [124,125], the packing of the lipid fatty acyl chains can be analysed by ^{2}H solid-state NMR spectroscopy of liposomes prepared with deuterated lipids [126]. Many of those are available commercially and have been used to follow the effects of the peptides on the lipid fatty acyl chain order parameters [73,116,127].

The ^{2}H solid-state NMR spectrum of a single non-oriented deuterated site is represented in Figure 3C and the corresponding quadrupolar splitting $\Delta\nu_Q$ indicated. When many sites with different quadrupolar splittings overlap, spectra as the ones simulated in Figure 3D are obtained. Finally, Figure 3E compares the ^{2}H solid-state NMR spectra of pure POPC (deuterated throughout the palmitoyl chain) with that in the presence of p24TMD. Each deuterated CH_2 and CH_3 segment results in a deuterium quadrupolar powder pattern from which the frequency separation of the two main intensities, that is, the deuterium quadrupolar splitting $\Delta\nu_Q$, can be extracted (Figure 3C). The comparison of the measured segment-specific deuterium quadropolar splitting with that of a static sample can be directly represented by the deuterium order parameters, and these are shown in Figure 3F in a position-dependent manner. Whereas the intercalation of in-plane aligned helices has in many cases resulted in a significant decrease of the order parameter [128–130], the transmembrane p24 has only a small effect on the palmitoyl chain packing (Figure 3E and F). Whereas here the modifications of the membrane packing occur on a more local level changes in the overall morphology, macroscopic phase properties, membrane thickness and curvature are also reflected in the ^{2}H NMR line shapes [116] and in combination with the corresponding ^{31}P spectra provide a valuable global view on the lipid system. Together with the spectra recorded from the peptides, a comprehensive analysis of the supramolecular assembly is thereby obtained (Figures 1, 2 and 3A).

In conclusion, here, CD spectroscopy has been used to test solubility, secondary structure preferences and to refine the membrane reconstitution protocol for peptides into membranes. Solid-state NMR spectroscopy provides a valuable tool to analyse the topology of membrane-associated peptides, the packing and morphology of the lipid membranes and thereby control of the design of the peptide sequences. A considerable number of peptides have been analysed using these techniques and some exhibit interesting features for applications in materials in particular those that 'sense' the environmental conditions.

Acknowledgements

We are most grateful to Jesus Raya for help with the NMR spectrometers as well as Britta Brügger and Felix Wieland for valuable discussion. The financial contributions of the Agence Nationale de la Recherche (projects TRANSPEP, ProLipIn, membraneDNP and the LabEx Chemistry of Complex Systems), the University of Strasbourg, the CNRS, the Région Alsace and the RTRA International Center of Frontier Research in Chemistry, the French Foundation for Medical Research (FRM), the American Foundation for Research on Huntington's Disease (CHDI) are gratefully acknowledged.

References

1 Nune M, Kumaraswamy P, Krishnan UM, Sethuraman S. Self-assembling peptide nanofibrous scaffolds for tissue engineering: novel approaches and strategies for effective functional regeneration. *Curr. Protein. Pept. Sci.* 2013; **14**: 70–84.
2 Iwabata K, Sugai U, Seki Y, Furue H, Sakaguchi K. Applications of biomaterials to liquid crystals. *Molecules* 2013; **18**: 4703–17.
3 Chaturvedi K, Ganguly K, Nadagouda MN, Aminabhavi TM. Polymeric hydrogels for oral insulin delivery. *J. Control. Release* 2013; **165**: 129–38.
4 Liu J, Huang Y, Kumar A, Tan A, Jin S, Mozhi A, Liang X-J. pH-Sensitive nano-systems for drug delivery in cancer therapy. *Biotech. Adv.* 2013; 11.

5 Kimmerlin T, Seebach D. '100 years of peptide synthesis': ligation methods for peptide and protein synthesis with applications to beta-peptide assemblies. *J. Pept. Sci.* 2005; **65**: 229–60.
6 Vidovic V, Prongidi-Fix L, Bechinger B, Werten S. Production and isotope labeling of antimicrobial peptides in Escherichia coli by means of a novel fusion partner that enables high-yield insoluble expression and fast purification. *J. Pept. Sci.* 2009; **15**: 278–84.
7 Ramakers BE, van Hest JC, Löwik DW. Molecular tools for the construction of peptide-based materials. *Chem. Soc. Rev.* 2014; **43**: 2743–56.
8 Bechinger B, Vidovic V, Bertani P Kichler A A new family of peptide-nucleic acid nanostructures with potent transfection activities. *J. Pept. Sci.* 2011; **17**: 88–93.
9 Anrather D, Smetazko M, Saba M, Alguel YTS. Supported membrane nanodevices. *J. Nanosci. Nanotechnol.* 2004; **4**: 1–22.
10 Kocer A, Tauk L Dejardin P Nanopore sensors: from hybrid to abiotic systems. *Biosens. Bioelectron.* 2012; **38**: 1–10.
11 Reimhult E, Baumann M, Kaufmann S, Kumar K, Spycher P. Advances in nanopatterned and nanostructured supported lipid membranes and their applications. *Biotechnol. Genet. Eng. Rev.* 2010; **27**: 185–216.
12 Tanaka M Sackmann E Polymer-supported membranes as models of the cell surface. *Nature* 2005; **437**: 656–63.
13 Hatakeyama H, Akita H, Harashima H. A multifunctional envelope type nano device (MEND) for gene delivery to tumours based on the EPR effect: a strategy for overcoming the PEG dilemma. *Adv. Drug. Deliver. Rev.* 2011; **63**: 152–60.
14 Mickler FM, Möckl L, Ruthardt N, Ogris M, Wagner E, Bräuchle C. Tuning nanoparticle uptake: live-cell imaging reveals two distinct endocytosis mechanisms mediated by natural and artificial EGFR targeting ligand. *Nano Lett.* 2012; **112**: 3417–23.
15 Aisenbrey C, Bechinger B. Tilt and rotational pitch angles of membrane-inserted polypeptides from combined 15N and 2H solid-state NMR spectroscopy. *Biochemistry-Us* 2004; **43**: 10502–12.
16 Prongidi-Fix L, Bertani P, Bechinger B. The membrane alignment of helical peptides from non-oriented 15 N chemical shift solid-state NMR spectroscopy. *J. Am. Chem. Soc.* 2007; **129**: 8430–1.
17 Gill SC, Vonhippel PH. Calculation of protein extinction coefficients from amino-acid sequence data. *Anal. Biochem.* 1989; **182**: 319–26.
18 Sreerama N, Woody RW. Estimation of protein secondary structure from circular dichroism spectra: comparison of CONTIN, SELCON, and CDSSTR methods with an expanded reference set. *Anal. Biochem.* 2000; 252–60.
19 Aisenbrey C, Bertani P, Bechinger B. Solid-state NMR investigations of membrane-associated antimicrobial peptides. In Guiliani A, Rinaldi AC (ed.). Humana Press, Springer: Antimicrobial Peptides N.Y., 2010; 209–33.
20 Bechinger B, Bertani P, Werten S, Mendonca de Moraes C, Aisenbrey C, Mason AJ, Perrone B, Prudhon M, Sudheendra US, Vidovic V. The structural and topological analysis of membrane polypeptides by oriented solid-state NMR spectroscopy: sample preparation and theory. In Miguel C (ed.). *Membrane-Active Peptides: Methods and Results on Structure and Function*. International University Line: La Jolla, California, USA, 2010; 196–215.
21 Rance M, Byrd RA. Obtaining high-fidelity spin-1/2 powder spectra in anisotropic media: phase-cycled Hahn echo spectroscopy. *J. Magn. Reson.* 1983; **52**: 221–40.
22 Pines A, Gibby MG, Waugh JS. Proton-enhanced NMR of dilute spins in solids. *J. Chem. Phys.* 1973; **59**: 569–90.
23 Bertani P, Raya J, Bechinger B. 15N chemical shift referencing in solid state NMR. 2014, submitted.
24 Davis JH, Jeffrey KR, Bloom M, Valic MI, Higgs TP. Quadrupolar echo deuteron magnetic resonance spectroscopy in ordered hydrocarbon Chains. *Chem. Phys. Lett.* 1976; **42**: 390–4.
25 Gennis RB. *Biomembranes, Molecular Structure and Function*, Springer: New York,1989.
26 van Meer G, Voelker DR, Feigenson GW. Membrane lipids: where they are and how they behave. *Nat. Rev. Mol. Cell Biol.* 2008; **9**: 112–24.
27 Brugger B, Sandhoff R, Wegehingel S, Gorgas K, Malsam J, Helms JB, Lehmann WD, Nickel W, Wieland FT. Evidence for segregation of sphingomyelin and cholesterol during formation of COPI-coated vesicles. *J. Cell Biol.* 2000; **151**: 507–18.
28 Stamnes MA, Craighead MW, Hoe MH, Lampen N, Geromanos S, Tempst P, Rothman JE. An integral membrane component of coatomer-coated transport vesicles defines a family of proteins involved in budding. *Proc. Natl. Acad. Sci. U. S. A.* 1995; **92**: 8011–5.
29 Emery G, Rojo M, Gruenberg J. Coupled transport of p24 family members. *J. Cell Sci.* 2000; **113**: 2507–16.
30 Contreras FX, Ernst AM, Haberkant P, Björkholm P, Lindahl E, Gönen B, Tischer C, Elofsson A, von Heijne G, Thiele C, Pepperkok R, Wieland F, Brügger B. Molecular recognition of a single sphingolipid species by a protein's transmembrane domain. *Nature* 2012; **481**: 525–9.
31 Hunte C, Richers S. Lipids and membrane protein structures. *Curr. Opin. Struct. Biol.* 2008; **18**: 406–11.
32 Jean-Francois F, Castano S, Desbat B, Odaert B, Roux M, Metz-Boutigue MH, Dufourc EJ. Aggregation of cateslytin beta-sheets on negatively charged lipids promotes rigid membrane domains. A new mode of action for antimicrobial peptides? *Biochemistry-Us* 2008; **47**: 6394–402.
33 Toyama BH, Weissman JS. Amyloid structure: conformational diversity and consequences. *Annu. Rev. Biochem.* 2011; **80**: 557–85.
34 Aisenbrey C, Sudheendra US, Ridley H, Bertani P, Marquette A, Nedelkina S, Lakey JH, Bechinger B. Helix orientations in membrane-associated Bcl-X L determined by 15 N solid-state NMR spectroscopy. *Eur. Biophys. J.* 2007; **36**: 451–60.
35 Zagorski MG, Yang J, Shao HY, Ma K, Zeng H, Hong A. Methodological and chemical factors affecting amyloid beta peptide amyloidogenicity. *Amyloid, Prions, and Other Protein Aggregates* 1999; **309**: 189–204.
36 Kundu A, Kishore N. 1,1,1,3,3,3-hexafluoroisopropanol induced thermal unfolding and molten globule state of bovine alpha-lactalbumin: calorimetric and spectroscopic studies. *Biopolymers* 2004; **73**: 405–20.
37 Bégué J-P, Bonnet-Delpon D, Crousse B. Fluorinated alcohols: a new medium for selective and clean reaction Jean-Pierre Bégué, Danièle Bonnet-Delpon*, Benoit Crousse. *Synlett* 2004; **1**: 18–29.
38 Broersen K, Jonckheere W, Rozenski J, Vandersteen A, Pauwels K, Pastore A, Rousseau F, Schymkowitz J. A standardized and biocompatible preparation of aggregate-free amyloid beta peptide for biophysical and biological studies of Alzheimer's disease. *Protein Eng. Des. Sel.* 2011; **24**: 743–50.
39 Kuroda H, Chen YN, Kimura T, Sakakibara S. Powerful solvent systems useful for synthesis of sparingly-soluble peptides in solution. *Int. J. Pept. Protein Res.* 1992; **40**: 294–9.
40 Verly RM, de Moraes CM, Resende JM, Aisenbrey C, Bemquemer MP, Pilo-Veloso D, Valente AP, Alemida FC, Bechinger B. Structure and membrane interactions of the antibiotic peptide dermadistinctin k by solution and oriented 15 N and 31 P solid-state NMR spectroscopy. *Biophys. J.* 2009; **96**: 2194–203.
41 Michalek M, Salnikov E, Werten S, Bechinger B. Refined structure and topology of a huntingtin membrane anchor. *Biophys. J.* 2013; **105**: 699–710.
42 Marcotte I, Wegener KL, Lam YH, Chia BC, de Planque MR, Bowie JH, Auger M, Separovic F. Interaction of antimicrobial peptides from Australian amphibians with lipid membranes. *Chem. Phys. Lipids* 2003; **122**: 107–20.
43 Weingarth M, Baldus M. Solid-state NMR-based approaches for supramolecular structure elucidation. *Acc. Chem. Res.* 2013; **46**: 2037–46.
44 Bechinger B, Resende JM, Aisenbrey C. The structural and topological analysis of membrane-associated polypeptides by oriented solid-state NMR spectroscopy: established concepts and novel developments. *Biophys. Chem.* 2011; **153**: 115–25.
45 Bechinger B, Sizun C. Alignment and structural analysis of membrane polypeptides by 15N and 31P solid-state NMR spectroscopy. *Concepts Magn. Reson.* 2003; **18A**: 130–45.
46 Smith R, Separovic F, Milne TJ, Whittaker A, Bennett FM, Cornell BA, Makriyannis A. Structure and orientation of the pore-forming peptide, melittin, in lipid bilayers. *J. Mol. Biol.* 1994; **241**: 456–66.
47 Cross TA, Opella SJ. Solid-state NMR structural studies of peptides and proteins in membranes. *Curr. Opin. Struc. Biol.* 1994; **4**: 574–81.
48 Aisenbrey C, Sizun C, Koch J, Herget M, Abele U, Bechinger B Tampe R. Structure and dynamics of membrane-associated ICP47, a viral inhibitor of the MHC I antigen-processing machinery. *J. Biol. Chem.* 2006; **281**: 30365–72.
49 Resende JM, Moraes CM, Munhoz VHDO, Aisenbrey C, Verly RM, Bertani P, Cesar A, Pilo-Veloso D, Bechinger B. Membrane structure and conformational changes during bilayer-association of the antibiotic heterodimeric peptide distinction by oriented solid-state NMR spectroscopy. *Proc. Natl. Acad. Sci. U. S. A.* 2009; **106**: 16639–44.
50 Michalek M, Salnikov ES, Werten S, Bechinger B. Membrane interactions of the amphipathic amino-terminus of huntingtin. *Biochemistry-Us* 2013; **52**: 847–58.
51 Gustavsson M, Verardi R, Mullen DG, Mote KR, Traaseth NJ, Gopinath T, Veglia G. Allosteric regulation of SERCA by phosphorylation-

mediated conformational shift of phospholamban. *Proc. Natl. Acad. Sci. U. S. A.* 2013; **110**: 17338–43.
52 Aisenbrey C, Harzer U, Bauer-Manz G, Bär G, Husmal Chotimah IN, Bertani P, Sizun C, Kuhn A, Bechinger B. Proton-decoupled 15N and 31P solid-state NMR investigations of the Pf3 coat protein in oriented phospholipid bilayers. *FEBS J.* 2006; **273**: 817–28.
53 Vosegaard T, Kamihira-Ishijima M, Watts A, Nielsen NC. Helix conformations in 7TM membrane proteins determined using oriented-sample solid-state NMR with multiple residue-specific 15N labeling. *Biophys. J.* 2008; **94**: 241–50.
54 Salnikov ES, Friedrich H, Li X, Bertani P, Reissmann S, Hertweck C, O'Neil JD, Raap J, Bechinger B. Structure and alignment of the membrane-associated peptaibols ampullosporin A and alamethicin by oriented 15 N and 31 P solid-state NMR spectroscopy. *Biophys. J.* 2009; **96**: 86–100.
55 Harzer U, Bechinger B. The alignment of lysine-anchored membrane peptides under conditions of hydrophobic mismatch: a CD, 15 N and 31 P solid-state NMR spectroscopy investigation. *Biochemistry-Us* 2000; **39**: 13106–14.
56 Vogt TCB, Ducarme P, Schinzel S, Brasseur R, Bechinger B. The topology of lysine-containing amphipathic peptides in bilayers by CD, solid-state NMR and molecular modelling. *Biophys. J.* 2000; **79**: 2644–56.
57 Bechinger B, Membrane insertion and orientation of polyalanine peptides: a 15 N solid-state NMR spectroscopy investigation. *Biophys. J.* 2001; **82**: 2251–6.
58 Deber CM, Liu LP, Wang C. Perspective: peptides as mimics of transmembrane segments in proteins. *J. Pept. Res.* 1999; **54**: 200–5.
59 Holt A Killian JA Orientation and dynamics of transmembrane peptides: the power of simple models. *Eur. Biophys. J. Biophy.* 2010; **39**: 609–21.
60 Lewis RN, Zhang YP, Hodges RS, Subczynski WK, Kusumi A, Flach CR, Mendelsohn R, McElhaney RN. A polyalanine-based peptide cannot form a stable transmembrane alpha-helix in fully hydrated phospholipid bilayers. *Biochemistry-Us* 2001; **40**: 12103–11.
61 Gleason NJ, Vostrikov VV, Greathouse DV, Koeppe RE. Buried lysine, but not arginine, titrates and alters transmembrane helix tilt. *Proc. Natl. Acad. Sci. U. S. A.* 2013; **110**: 1692–5.
62 Choma C, Gratkowski H, Lear JD DeGrado WF. Asparagine-mediated self-association of a model transmembrane helix. *Nat. Struct. Biol.* 2000; **7**: 161–6.
63 Melnyk RA, Kim S, Curran AR, Engelman DM, Bowie JU, Deber CM. The affinity of GXXXG motifs in transmembrane helix-helix interactions is modulated by long-range communication. *J. Biol. Chem.* 2004; **279**: 16591–7.
64 Smith SO, Eilers M, Song D, Crocker E, Ying W, Groesbeek M, Metz G, Ziliox M, Aimoto S. Implications of threonine hydrogen bonding in the glycophorin A transmembrane helix dimer. *Biophys. J.* 2002; **82**: 2476–86.
65 Bechinger B. Insights into the mechanisms of action of host defence peptides from biophysical and structural investigations. *J. Pept. Sci.* 2011; **17**: 306–14.
66 Bechinger B, Skladnev DA, Ogrel A, Li X, Swischewa NV, Ovchinnikova TV, O'Neil JDJ, Raap J. 15 N and 31 P solid-state NMR investigations on the orientation of zervamicin II and alamethicin in phosphatidylcholine membranes. *Biochemistry-Us* 2001; **40**: 9428–37.
67 Salnikov E, Bechinger B. Lipid-mediated peptide-peptide interactions in bilayers: structural insights into the synergistic enhancement of the antimicrobial activities of PGLa and magainin 2. *Biophysical. J.* 2011; **100**: 1473–80.
68 Mason AJ, Bertani P, Moulay G, Marquette A, Perrone B, Drake AF, Kichler A, Bechinger B. Membrane interaction of chrysophsin-1, a histidine-rich antimicrobial peptide from red sea bream. *Biochemistry-Us* 2007; **46**: 15175–87.
69 Cotten M, Wieczorek WE, Sharma M, Truong M, Vollmar BS, Gordon ED, Venable RM, Pastor RW, Fu RQ. Atomic-Resolution three dimensional structures and membrane locations of antimicrobial piscidin 1 and piscidin 3 in aligned lipid bilayers: a solid-state nmr and molecular dynamics investigation. *Biophys. J.* 2011; **100**: 496.
70 Fernandez DI, Gehman JD, Separovic F. Membrane interactions of antimicrobial peptides from Australian frogs. *Biochim. Biophys. Acta* 2009; **1788**: 1630–8.
71 Cheng JTJ, Hale JD, Elliott M, Hancock REW, Straus SK. The importance of bacterial membrane composition in the structure and function of aurein 2.2 and selected variants. *Bba-Biomembranes* 2011; **1808**: 622–33.
72 Hallock KJ, Lee DK, Omnaas J, Mosberg HI, Ramamoorthy A. Membrane composition determines pardaxin's mechanism of lipid bilayer disruption. *Biophys. J.* 2002; **83**: 1004–13.
73 Henzler-Wildman KA, Martinez GV, Brown MF, Ramamoorthy A. Perturbation of the hydrophobic core of lipid bilayers by the human antimicrobial peptide LL-37. *Biochemistry-Us* 2004; **43**: 8459–69.
74 Gottler LM, Ramamoorthy A. Structure, membrane orientation, mechanism, and function of pexiganan--a highly potent antimicrobial peptide designed from magainin. *Biochim. Biophys. Acta* 2009; **1788**: 1680–6.
75 Thennarasu S, Tan A, Penumatchu R, Shelburne CE, Heyl DL Ramamoorthy A. Antimicrobial and membrane disrupting activities of a peptide derived from the human cathelicidin antimicrobial peptide LL37. *Biophys. J.* 2010; **98**: 248–57.
76 Durr UH, Sudheendra US Ramamoorthy A LL-37, the only human member of the cathelicidin family of antimicrobial peptides. *Biochim. Biophys. Acta* 2006; **1758**: 1408–25.
77 Bertani P, Vidovic V, Yang TC, Rendell J, Gordon LM, Waring AJ, Bechinger B, Booth V. Orientation and depth of surfactant protein B C-terminal helix in lung surfactant bilayers. *Bba-Biomembranes* 2012; **1818**: 1165–72.
78 Fernandez DI, Sani MA, Gehman JD, Hahm KS Separovic F Interactions of a synthetic Leu-Lys-rich antimicrobial peptide with phospholipid bilayers. *Eur. Biophys. J. Biophy.* 2011; **40**: 471–80.
79 Sudheendra US, Bechinger B. Topological equilibria of ion channel peptides in oriented lipid bilayers revealed by 15N solid-state NMR spectroscopy. *Biochemistry-Us* 2005; **44**: 12120–7.
80 Castano S, Desbat B, Laguerre M, Dufourcq J. Structure, orientation and affinity for interfaces and lipids of ideally amphipathic lytic LiKj (i = 2j) peptides. *Biochim. Biophys. Acta* 1999; **1416**: 176–94.
81 Ouellet M, Doucet JD, Voyer N, Auger M. Membrane topology of a 14-mer model amphipathic peptide: a solid-state NMR spectroscopy study. *Biochemistry-Us* 2007; **46**: 6597–606.
82 Aisenbrey C, Goormaghtigh E, Ruysschaert JM, Bechinger B. Translocation of amino acyl residues from the membrane interface to the hydrophobic core: thermodynamic model and experimental analysis using ATR-FTIR spectroscopy. *Mol. Membr. Biol.* 2006; **23**: 363–74.
83 Aisenbrey C, Kinder R, Goormaghtigh E, Ruysschaert JM, Bechinger B. Interactions involved in the realignment of membrane-associated helices: an investigation using oriented solid-state NMR and ATR-FTIR spectroscopies topologies. *J. Biol. Chem.* 2006; **281**: 7708–16.
84 Bechinger B. Towards membrane protein design: pH dependent topology of histidine-containing polypeptides. *J. Mol. Biol.* 1996; **263**: 768–75.
85 Hunt JF, Rath P, Rothschild KJ, Engelman DM. Spontaneous, pH-dependent membrane insertion of a transbilayer alpha-helix. *Biochemistry-Us* 1997; **36**: 15177–92.
86 Strandberg E, Zerweck J, Wadhwani P, Ulrich AS. Synergistic insertion of antimicrobial magainin-family peptides in membranes depends on the lipid spontaneous curvature. *Biophys. J.* 2013; **104**: L09–L11.
87 Huang HW, Wu Y. Lipid-alamethicin interactions influence alamethicin orientation. *Biophys. J.* 1991; **60**: 1079–87.
88 Salnikov E, Aisenbrey C, Vidovic V Bechinger B Solid-state NMR approaches to measure topological equilibria and dynamics of membrane polypeptides. *Biochim. Biophys. Acta* 2010; **1798**: 258–65.
89 Perrone B. *New methodologies of solid-state NMR and biophysical studies of antimicrobial and synthetic peptides in model and natural membranes*, University of Strasbourg, France: Strasbourg,2011.
90 He K, Ludtke SJ, Heller WT, Huang HW. Mechnaism of alamethicin insertion into lipid bilayers. *Biophys. J.* 1996; **71**: 2669–79.
91 Aisenbrey C, Bechinger B, Grobner G. Macromolecular crowding at membrane interfaces: adsorption and alignment of membrane peptides. *J. Mol. Biol.* 2008; **375**: 376–85.
92 Sansom MSP, The biophysics of peptide models of ion channels. *Prog. Biophysmolec. Biol.* 1991; **55**: 139–235.
93 Gesell J, Zasloff M, Opella SJ. Two-dimensional 1 H NMR experiments show that the 23-residue magainin antibiotic peptide is an a-helix in dodecylphosphocholine micelles, sodium dodecylsulfate micelles, and trifluoroethanol/water solution. *J. Biomol. NMR* 1997; 127–35.
94 Bechinger B, Salnikov ES, Aisenbrey C, Balandin SV, Zhmak MN, Ovchinnikova TV. Structure and alignment of the membrane-associated antimicrobial peptide arenicin by oriented solid-state NMR spectroscopy. *Biochemistry-Us* 2011; **50**: 3784–95.
95 Bechinger B, Zasloff M, Opella SJ. Structure and dynamics of the antibiotic peptide PGLa in membranes by multidimensional solution and solid-state NMR spectroscopy. *Biophys. J.* 1998; **74**: 981–7.

96 Tremouilhac P, Strandberg E, Wadhwani P, Ulrich AS. Conditions affecting the re-alignment of the antimicrobial peptide PGLa in membranes as monitored by solid state 2H-NMR. *Biochim. Biophys. Acta* 2006; **1758**: 1330–42.
97 Georgescu J, Verly RM, Bechinger B. NMR structures of the histidine-rich peptide LAH4 in micellar environments: membrane insertion, pH-dependent mode of antimicrobial action and DNA transfection. *Biophys. J.* 2010; **99**: 2507–15.
98 Andreev OA, Engelman DM, Reshetnyak YK. Novel concept of delivery of diagnostic and therapeutic agents to cells in acidic diseased tissue using energy of membrane-associated folding. *Biophys. J.* 2013; 104: 362A–A.
99 Mason AJ, Martinez A, Glaubitz C, Danos O, Kichler A, Bechinger B. The antibiotic and DNA-transfecting peptide LAH4 selectively associates with, and disorders, anionic lipids in mixed membranes. *FASEB J.* 2006; **20**: 320–2.
100 Bechinger B. The structure, dynamics and orientation of antimicrobial peptides in membranes by solid-state NMR spectroscopy. *Biochim. Biophys. Acta* 1999; **1462**: 157–83.
101 Tremouilhac P, Strandberg E, Wadhwani P, Ulrich AS. Synergistic transmembrane alignment of the antimicrobial heterodimer PGLa/magainin. *J. Biol. Chem.* 2006; **281**: 32089–94.
102 Bechinger B. Understanding peptide interactions with lipid bilayers: a guide to membrane protein engineering. *Curr. Opin. Chem. SS Biol.* 2000; **4**: 639–44.
103 Goormaghtigh E, Raussens V, Ruysschaert JM. Attenuated total reflection infrared spectroscopy of proteins and lipids in biological membranes [Review]. *Biochim. Biophys. Acta - Rev. Biomembr.* 1999; **1422**: 105–85.
104 Bechinger B, Ruysschaert JM, Goormaghtigh E. Membrane helix orientation from linear dichroism of infrared attenuated total reflection spectra. *Biophys. J.* 1999; **76**: 552–63.
105 Wu Y, Huang HW, Olah GA. Method of oriented circular dichroism. *Biophys. J.* 1990; **57**: 797–806.
106 Cheng JTJ, Hale JD, Elliot M, Hancock REW, Straus SK. Effect of membrane composition on antimicrobial peptides aurein 2.2 and 2.3 from Australian southern bell frogs. *Biophys. J.* 2009; **96**: 552–65.
107 Mroue KH, MacKinnon N, Xu JD, Zhu PZ, McNerny E, Kohn DH, Morris MD, Ramamoorthy A. High-resolution structural insights into bone: a solid-state NMR relaxation study utilizing paramagnetic doping. *J. Phys. Chem. B.* 2012; **116**: 11656–61.
108 Chu S, Coey AT, Lorigan GA. Solid-state (2)H and (15)N NMR studies of side-chain and backbone dynamics of phospholamban in lipid bilayers: investigation of the N27A mutation. *Biochim. Biophys. Acta* 2010; **1798**: 210–5.
109 Traaseth NJ, Shi L, Verardi R, Muller D, Barany G, Veglia G. Structure and topology of monomeric phospholamban in lipid membranes determined by a hybrid solution and solid-state NMR approach. *Proc. Natl. Acad. Sci. U. S. A.* 2009; **106**: 10165–70.
110 Chenal A, Prongidi-Fix L, Perier A, Aisenbrey C, Vernier G, Lambotte S, Fragneto G, Bechinger B, Gillet D, Forge V, Ferrand M. Deciphering membrane insertion of the diphtheria toxin translocation domain. *Eur. Biophys. J. Biophy.* 2011; **40**: 155.
111 Aisenbrey C, Prongidi-Fix L, Chenal A, Gillet D, Bechinger B. Side chain resonances in static oriented proton-decoupled 15N solid-state NMR spectra of membrane proteins. *J. Am. Chem. Soc.* 2009; **131**: 6340–1.
112 Hirschinger J, Raya J, Perrone B, Bechinger B. Chemical shift powder spectra obtained by using rotor-directed exchange of orientations cross-polarization (RODEO-CP). *Chem. Phys. Lett.* 2011; **508**: 155–64.
113 Aisenbrey C, Bechinger B. Investigations of peptide rotational diffusion in aligned membranes by 2H and 15N solid-state NMR spectroscopy. *J. Am. Chem. Soc.* 2004; **126**: 16676–83.
114 Scherer PG, Seelig J. Electric charge effects on phospholipid headgroups. phosphatidycholine in mixtures with cationic and anionic amphiles. *Biochemistry-Us* 1989; **28**: 7720–7.
115 Salnikov E, Aisenbrey C, Raya J, Bechinger B. Investigations of the structure, topology and dynamics of membrane-associated polypeptides by solid-state NMR spectroscopy. In Separovic F, Naito A (ed.). *New Developments in NMR: Advances in Biological Solid-State NMR*, Proteins and Membrane-Active Peptides: Royal Society of Chemistry, 2014; 214–34.
116 Kim C, Spano J, Park EK, Wi S. Evidence of pores and thinned lipid bilayers induced in oriented lipid membranes interacting with the antimicrobial peptides, magainin-2 and aurein-3.3. *Bba-Biomembranes* 2009; **1788**: 1482–96.
117 Bechinger B, Lohner K. Detergent-like action of linear cationic membrane-active antibiotic peptides. *Biochim. Biophys. Acta* 2006; **1758**: 1529–39.
118 Costa F, Carvalho IF, Montelaro RC, Gomes P, Martins MCL. Covalent immobilization of antimicrobial peptides (AMPs) onto biomaterial surfaces. *Acta Biomater.* 2011; **7**: 1431–40.
119 Siedenbiedel F, Tiller JC. Antimicrobial polymers in solution and on surfaces: overview and functional principles. *Polymers-Basel* 2012; **4**: 46–71.
120 Munoz-Bonilla A Fernandez-Garcia M Polymeric materials with antimicrobial activity. *Prog. Polym. Sci.* 2012; **37**: 281–339.
121 Al-Ahmad A, Laird D, Zou P, Tomakidi P, Steinberg T, Lienkamp K. Nature-inspired antimicrobial polymers - assessment of their potential for biomedical applications. *PLoS One* 2013; **8**: e73812.
122 Arnusch CJ, Albada HB, van Vaardegem M, Liskamp RMJ, Sahl HG, Shadkchan Y, Osherov N, Shai Y. Trivalent ultrashort lipopeptides are potent pH dependent antifungal agents. *J. Med. Chem.* 2012; **55**: 1296–302.
123 Dohm MT, Kapoor R, Barron AE. Peptoids: bio-inspired polymers as potential pharmaceuticals. *Curr. Pharm. Design.* 2011; **17**: 2732–47.
124 Seelig J 31P nuclear magnetic resonance and the head group structure of phospholipids in membranes. *Biochim. Biophys. Acta* 1978; **515**: 105–40.
125 Cullis PR, De Kruijff B. Lipid polymorphism and the functional roles of lipids in biological membranes. *Biochim. Biophys. Acta* 1979; **559**: 399–420.
126 Seelig J. Deuterium magnetic resonance: theory and application to lipid membranes. *Q. Rev. Biophys.* 1977; **10**: 353–418.
127 Bechinger B, Salnikov ES. The membrane interactions of antimicrobial peptides revealed by solid-state NMR spectroscopy. *Chem. Phys. Lipids* 2012; **165**: 282–301.
128 Salnikov ES, Mason AJ, Bechinger B. Membrane order perturbation in the presence of antimicrobial peptides by 2 H solid-state NMR spectroscopy. *Biochimie* 2009; **91**: 743.
129 Thennarasu S, Huang R, Lee DK, Yang P, Maloy L, Chen Z, Ramamoorthy A. Limiting an antimicrobial peptide to the lipid-water interface enhances its bacterial membrane selectivity: a case study of MSI-367. *Biochemistry-Us* 2010; **49**: 10595–605.
130 Gottler LM, Ramamoorthy A. Structure, membrane orientation, mechanism, and function of pexiganan - a highly potent antimicrobial peptide designed from magainin. *Bba-Biomembranes* 2009; **1788**: 1680–6.
131 Gautier R, Douguet D, Antonny B, Drin G. HELIQUEST: a Web server to screen sequences with specific alpha-helical properties. *Bioinformatics* 2008; **24**: 2101–2.

UNIVERSITÉ DE STRASBOURG

EDSC
Ecole Doctorale des
Sciences Chimiques

UNIVERSITE DE STRASBOURG

ECOLE DOCTORALE DES SCIENCES CHIMIQUES

RESUME DE LA THESE DE DOCTORAT

Discipline : Chimie/Physique

Spécialité (facultative) : Biophysique

Présentée par : Kemayo Koumkoua Patricia

Titre : **Caractérisation structurale d'une interaction protéine-lipide hautement spécifique**

Unité de Recherche : UMR7177, Institut de chimie de Strasbourg

Directeur de Thèse : Professeur Burkhard Bechinger

Co-Directeur de Thèse (s'il y a lieu) :

Localisation : Strasbourg/France

Thèse confidentielle : ☒NON ☐ OUI

A) Introduction et Objectif de la thèse :

Les membranes biologiques sont des systèmes organisés très complexes et dynamiques (**Figure1**) qui délimitent et maintiennent l'intégrité des cellules. Bien que son organisation ait été pendant longtemps été un sujet a débat, aujourd'hui le modèle le plus communément accepté est celui de « mosaïque fluide ». Il a été proposé en 1972 par Singer & Nicolson et décrit la membrane comme étant majoritairement constituée de lipides organisés en bicouches dans lesquelles sont insérées des protéines (Singer and Nicolson, 1972). Elle est composée de trois classes de lipides non uniformément repartis entre les feuillets d'une même membrane : les phospholipides, les sphingolipides et les stérols principalement le cholestérol. Ils diffèrent en fonction de la nature de leurs têtes polaires et de leurs chaines carbonées hydrophobes. Leurs répartitions diffèrent également entre les organelles d'une même cellule (**Figure2**) et suivant les types cellulaires créant ainsi une grande diversité membranaire (Coskun and Simons, 2011; Sud et al., 2007., 2003; van Meer et al., 2008) . C'est par exemple le cas de la sphingomyéline (SM) qui est spécifiquement présente dans la membrane plasmique (MP), l'appareil de Golgi et les endosomes et sa répartition dans les feuillets de ces différentes organelles varie. Cette diversité est également générée par les mouvements des lipides qui peuvent se déplacer d'un feuillet membranaire à un autre (flip-flop) ou par diffusion latérale et souvent s'organiser en micro domaine membranaire, connu sous le nom de domaine raft (Coskun and Simons, 2010).

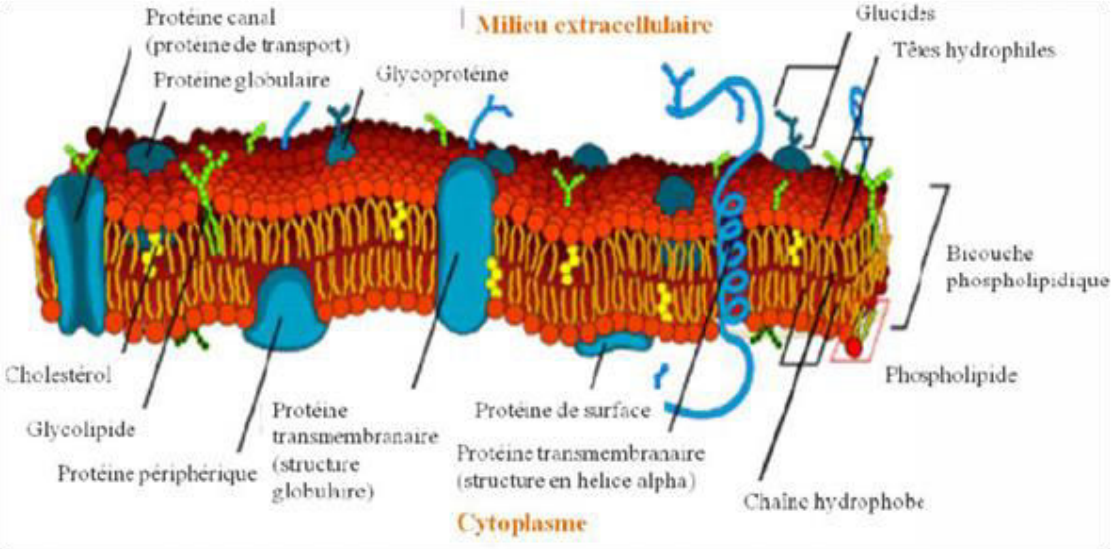

Figure1 : Architecture moléculaire d'une membrane biologique selon le modèle mosaïque fluide (adaptée de Singer et Nicolson, 1972).

La plupart des lipides membranaires et leurs précurseurs sont synthétisés dans le réticulum endoplasmique (RE). La sphingomyéline à l'exception est synthétisée dans l'appareil de Golgi à partir de la céramide provenant du RE. Après synthèse, les lipides sont transportés vers les différents compartiments cellulaires au travers de la voie de sécrétion principalement via les vésicules spécialisées COP I et II (COat Protein complex I et II) mais également via des protéines au travers d'interaction protéine-lipide. La vésicule COP I assure le transport rétrograde du compartiment golgien au RE et dans les deux entre citernes golgiennes, tandis que la COP II assure le transport antérograde. Elles sont responsables du transport des protéines et des lipides dans la cellule et leur formation semble dépendre de l'organisation des lipides dans les membranes (Brügger et al., 2000; Popoff et al., 2011).

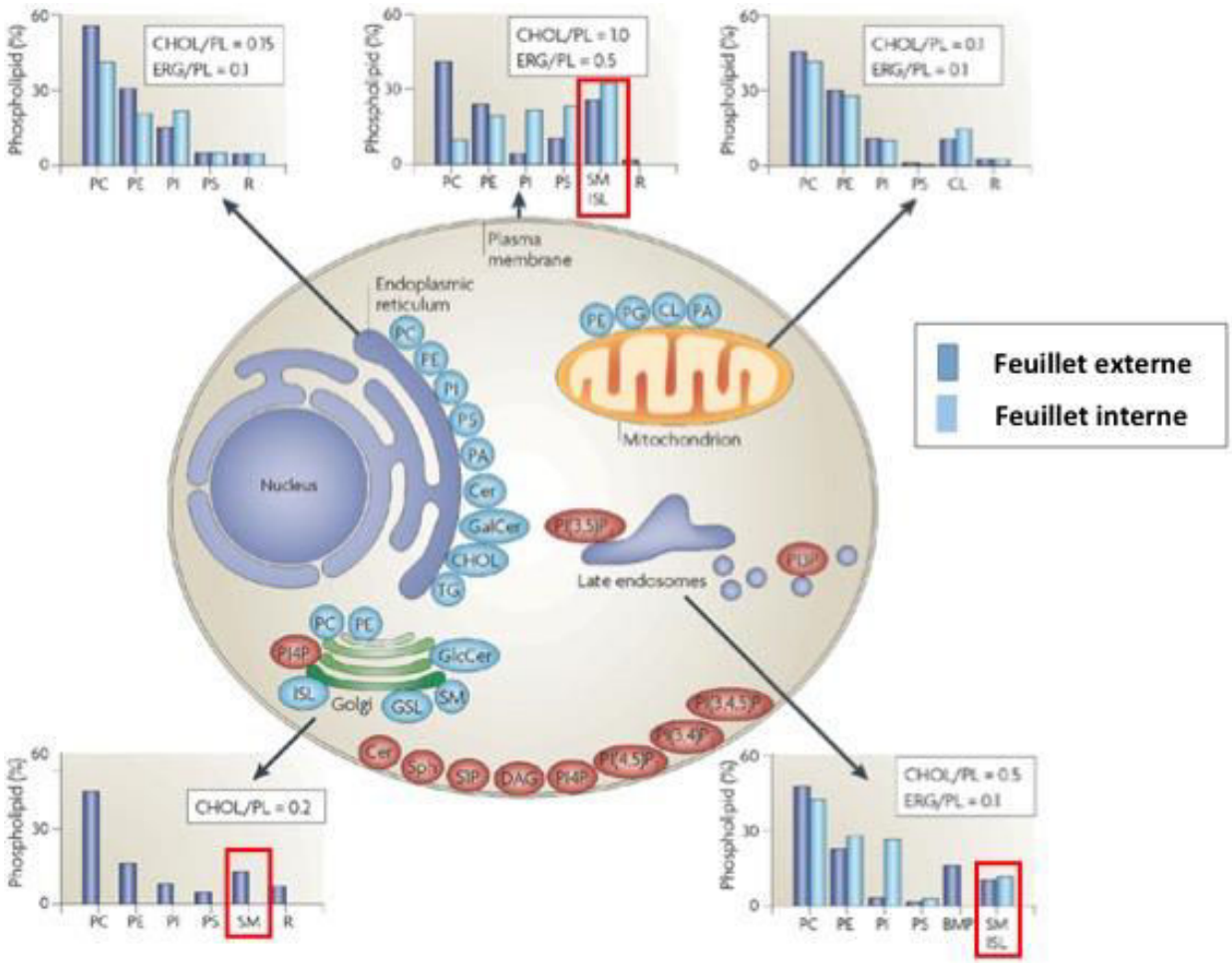

Figure 2: Compositions membranaires en lipide type d'une cellule eucaryote. Extrait de Van Meer G et al, 2008.

Ces vésicules sont recouvertes d'un complexe protéique formé de 7 sous-unités appelé Cotaomer et leurs membranes enrichis en protéines de la famille p24. Ce sont des protéines transmembranaires de type I avec une masse moléculaire de 24 kDa dont font partie les protéines p25, p23, p24, etc. Les protéines de cette famille partagent la même structure avec un grand domaine luminal appelé « Gold domain » formé de pont disulfure et servant de récepteur pour les molécules cargo, une région coil-coil, une partie transmembranaire et une petite partie cytoplasmique qui contient en général des motifs très conservés qui vont jouer un rôle dans le control de qualité des molécules transportées. Elles sont conservées dans différentes espèces à savoir, les plantes, les champignons, les mammifères ; suggérant qu'elles jouent un rôle très important. Bien que leurs fonctions ne soient pas clairement définit, plusieurs études ont montré l'implication de la protéine p24 dans la formation des vésicules COPI ainsi que dans le transport des molécules cargo (Kamińska et al., 2010).
Les travaux de *Brügger et al* ont mis en évidence la ségrégation de la sphingomyèline et du cholestérol durant la formation des vésicules COPI (Brügger et al., 2000). L'étude poussée de cette ségrégation a révélé la protéine p24 comme principal acteur. En effet, il a été montré par FRET et immuno-précipitation, que cette protéine interagit parmi les différentes espèces de SM spécifiquement avec la SM C18 (Contreras et al., 2012). L'interaction entre le p24 et la SM C18 est très spécifique et unique car elle est basée sur une affinité entre protéine-lipide impliquant à la fois la tête lipidique et leurs chaînes aliphatiques ce qui est assez rare. De plus, parmi les différentes espèces moléculaires de SM, il a été montré que seule la courbure de la tête polaire de la SM C 18 s'adapte et s'imbrique dans la structure de p24 (Contreras et al., 2012). Les travaux de *Contreras et al* ont également montré que cette interaction est conservée même lorsque la protéine est réduite

à son domaine transmembranaire (21 résidus). Ils ont également identifié dans ce domaine, le motif **V**XX**TL**XX**IY** responsable de l'interaction avec la SM. Leurs travaux ont permis de proposer un modèle moléculaire simulé (**Figure 3)**.
Cette interaction est potentiellement impliquée dans la régulation du mécanisme de formation des vésicules COP I. En effet, il a été suggéré que la protéine p24 est normalement dans un état monomérique mais dimèrise lorsqu'elle fixe la SM C18. Cette dimèrisation va provoquer un changement de conformation des protéines coatomèriques déclenchant ainsi leur polymérisation. Cette polymérisation va entrainer la courbure de la membrane du RE et donc la formation des vésicules COP I (Béthune et al., 2006; Contreras et al., 2012; Reinhard et al., 1999).

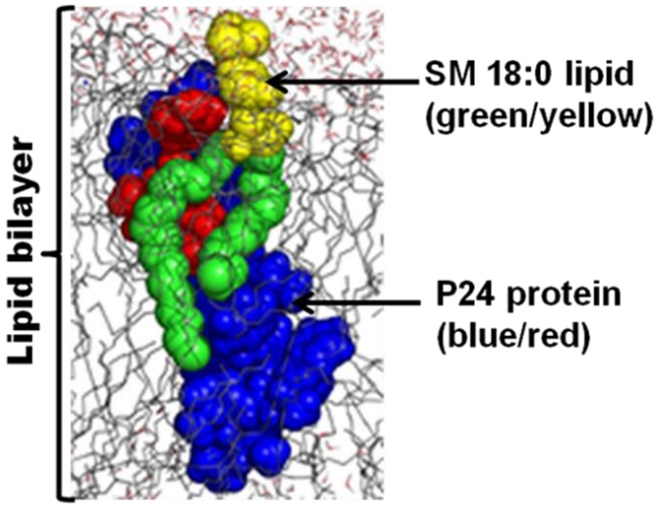

Figure 3 **:** Modèle d'interaction simulé de l'interaction entre p24TMD et la SM C18 (*Contreras et al, 2012).*

L'objectif durant ma thèse a été de caractériser la structure du site d'interaction entre le domaine transmembranaire de la protéine p24 (p24TMD) et la SM C18 dans un environnement membranaire, afin de valider ou non le modèle proposé. Mon travail s'est articulé sur deux volets principaux à savoir : l'obtention dans un premier temps du domaine transmembranaire de la protéine p24 appelé p24TMD par synthèse chimique et par expression en système bactérien. Ces deux techniques complémentaires ont permis d'obtenir le peptide spécifiquement marqué à une position ou uniformément marqué respectivement. En effet, l'un des prérequis pour l'étude des protéines par Résonnance Magnétique Nucléaire (RMN) c'est d'avoir une protéiné enrichit en isotope marqué. Nous avons dans un deuxième temps caractérisé le peptide dans des membranes artificielles en présence ou non de SM C18 utilisant des techniques de spectroscopie optique tels que le dichroïsme circulaire (CD), la fluorescence et la RMN. Les deux premières techniques ont permis d'étudier le repliement du peptide dans les membranes ; tandis que sa caractérisation structurale a principalement été réalisée par spectroscopie RMN.

B) Obtention du peptide p24TMD

Les travaux de *Contreras et al* ont montré que l'interaction du p24 avec la SM C18 était conservée même lorsque la protéine est réduite à sa partie transmembranaire. Partant de cette observation, nous avons conçu un peptide de 31 acides aminés (aa) appelé p24TMD composé du domaine transmembranaire de la protéine p24 (21 acides aminés, en gras), entouré de part et d'autre de quelques acides aminés de la séquence naturelle du p24, et de deux lysines (K) ajoutées en N terminal (Nter) de la séquence peptidique (Table1, en bleu) pour améliorer la solubilité du peptide. Un deuxième peptide de 36 acides aminés appelé p24TMDH (H pour Heidelberg) conçu par nos collaborateurs de l'université de Heidelberg a également été utilisé pour l'étude de cette interaction. Ce peptide a la même séquence que le p24TMD excepté son extrémité Nter qui comporte quelques acides aminés de la séquence naturelle du p24 (Table 1, en bleu).

Table1 : Séquences peptidique des peptides p24TMD et p24TMDH et représentation des protéines recombinantes MBP-p24TMDH et TAF12-p24TMD.

Noms	Séquences	Poids moléculaire
p24TMD	KKTNSR**VVLWSFFEALVLVAMTLGQIY**YLKR	3,675 kDa
p24TMDH	GINDNTNSR**VVLWSFFEALVLVAMTLGQIY**YLKR	3,932 kDa

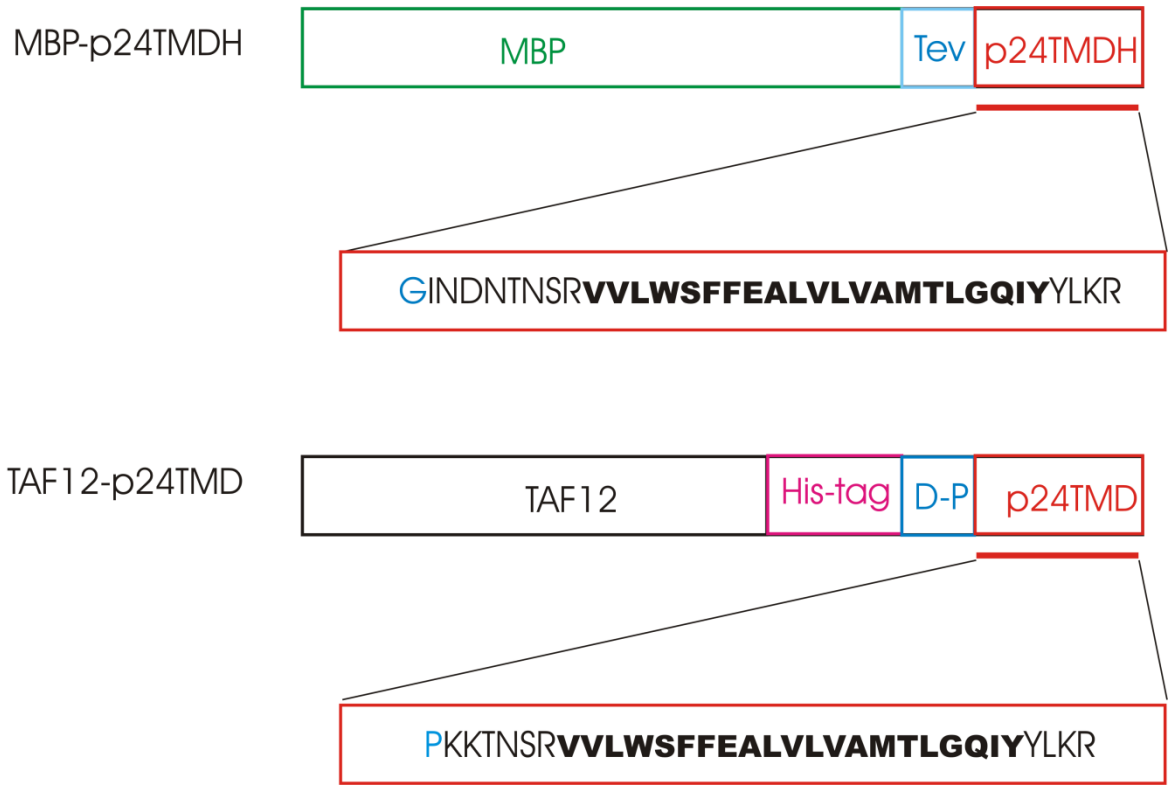

1) Expression en système bactérien

Dans l'objectif d'étudier cette interaction par spectroscopie de RMN afin d'obtenir des détails structuraux, il a été nécessaire de produire des peptides uniformément marqués. Pour cela, nous avons eu recours à l'expression en système bactérien qui est une technique communément utilisée à cet effet et qui comparée à la synthèse peptidique présente l'avantage de permettre un marquage uniforme des protéines à moindre coup.

1.1 Expression de la MBP-p24TMDH :

Nous avons dans un premier temps utilisé le vecteur d'expression pMal c 5X-p24TMDH conçu par nos collaborateurs pour permettre l'expression du peptide p24TMD fusionné à la Maltose Binding Protein (MBP). La protéine de fusion MBP permet l'expression de la protéine recombinante MBP-p24TMDH sous forme soluble et facilite également sa purification. En effet, elle possède une affinité pour l'amylose et peut de ce fait être isolée par chromatographie d'affinité à l'amylose. Un site de clivage enzymatique à la TEV protéase (protéase du virus de la gravure du tabac) permettant de séparer le peptide de la MBP après purification a également été introduit dans ce vecteur (**Table1**).
Afin de mettre en place un protocole, des tests d'expression en milieu riche ont été réalisés dans deux souches de *E.coli* : BL21 DE3 and BL21 DE3 pLysS. Ces souches ont tout d'abord été séparément transformées avec le vecteur pMal c 5X-p24TMDH. Une colonie de chaque souche bactérienne transformée a ensuite été ensemencé dans 50ml de milieu puis incubé toute la nuit a 37°C. Les différentes pré cultures ont ensuite été diluées dans un volume plus important de milieu riche afin de favorise de nouveau leur croissance. L'expression protéique a été induite lorsque la densité optique à 600nm (DO) des bactéries était autour de 1 avec 1mM d'IPTG. Après 4 heures d'induction, la culture bactérienne est arrêtée et les bactéries centrifugées. Les différents culots bactériens resuspendus et les cellules lysées par sonication. Après purification de notre protéine d'intérêt par chromatographie d'affinité et séparation en condition dénaturante par électrophorèse (SDS-PAGE), nous avons montré que le taux d'expression de la protéine MBP-p24TMDH était plus important avec la souche BL21 DE3 pLysS (**Figure4A et B**). La quantité effective de protéine obtenue a été estimée à 15mg/litre de culture.

Par ailleurs afin de marquer uniformément notre protéine d'intérêt, nous avons exprimé la protéine MBP-p24TMDH en milieu minimum (M9) en utilisant la souche BL21 DE3 pLysS et les mêmes conditions expérimentales décrites ci-dessus. La croissance bactérienne étant plus lente en milieu minimum qu'en milieu riche, nous avons testé différentes températures d'expression après induction (37, 30, 18°C). Parmi les différentes températures, nous avons observé que l'expression était plus importante à basse température (18°C) compare aux autres températures. Après purification, la quantité effective de protéine obtenue a été estimée à 3mg/litre de culture.

En résumé, nous avons pu mettre en place le protocole d'expression de notre protéine d'intérêt. Cependant, nous avons rencontré quelques problèmes à savoir que nous avons observé une perte importante de protéine durant l'étape de purification. De plus, le profil électrophorétique révèle également deux bandes : l'une migrant à la taille attendue (48 kDa) et une autre migrant en-dessous (42 kDa) (**Figure4C**). Cette dernière correspond vraisemblablement à la protéine tronquée. Cette forme dégradée étant plus importante en proportion par rapport à la forme entière (environ 3 fois plus), ne permet pas une quantification réelle de la protéine entière.

Afin d'obtenir le peptide p24TMD, nous avons réalisé le clivage de la MBP-p24TMD avec la TEV protéase à différents ratios enzyme/protéine (1/20 à 1/150) et températures (température ambiante (RT) et 4°C). Une cinétique de clivage a été également réalisée afin de déterminer les meilleures

conditions de clivage. Les résultats obtenus montrent qu'à 4°C pendant 24h, la Tev protéase semble être plus efficace que les autres conditions (**Figure 5**).

Cependant, après purification par HPLC ou par extraction au butanol, nous n'avons pas pu identifier le peptide d'intérêt par SDS-PAGE ou par spectrométrie de masse MALDI (Matrix-Assisted Laser Desorption/Ionisation).

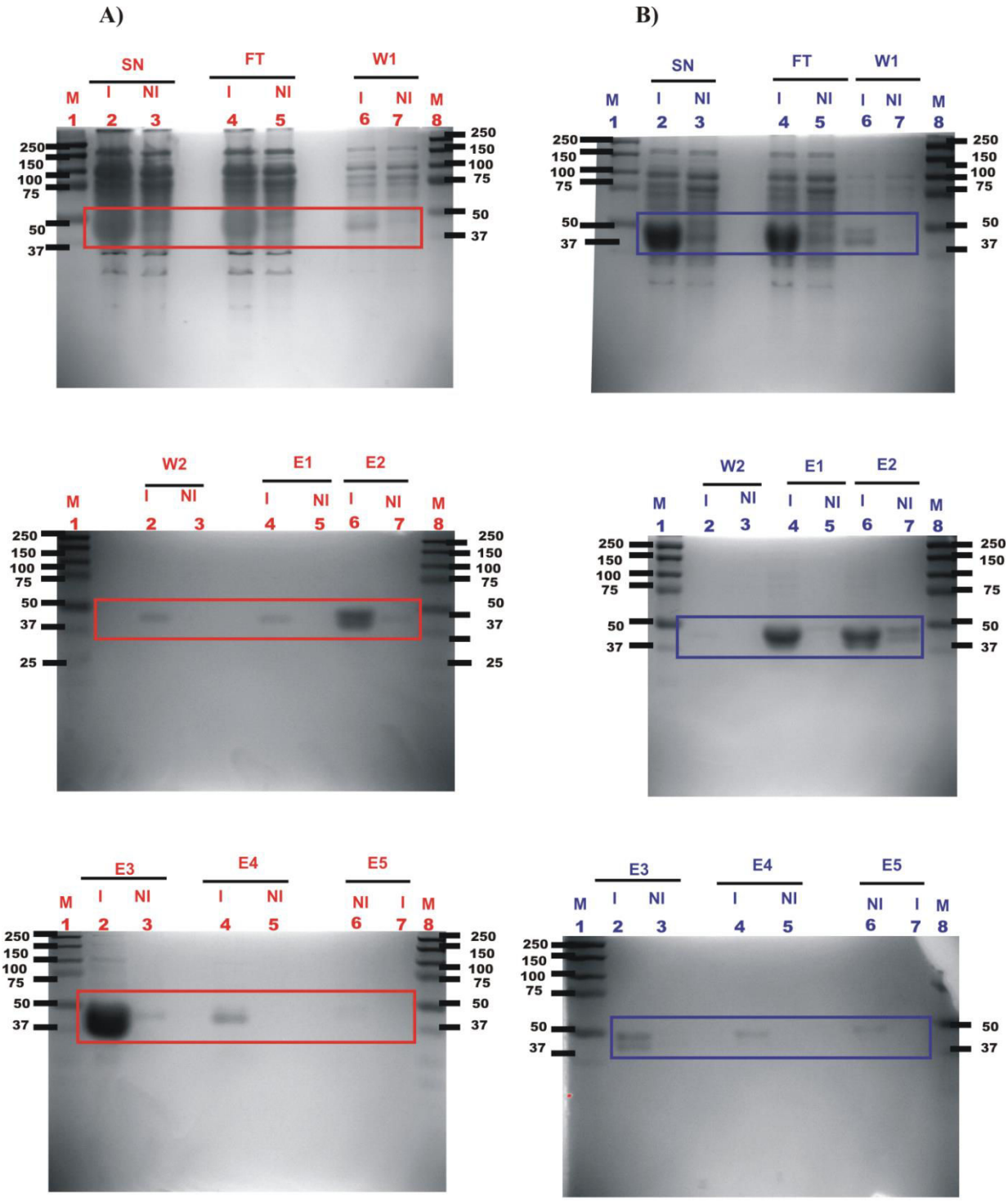

	MBP-p24TMDH	MBP5
Monomer (Da)	48176.62	42500
Dimer (Da)	9635.24	85000

C)

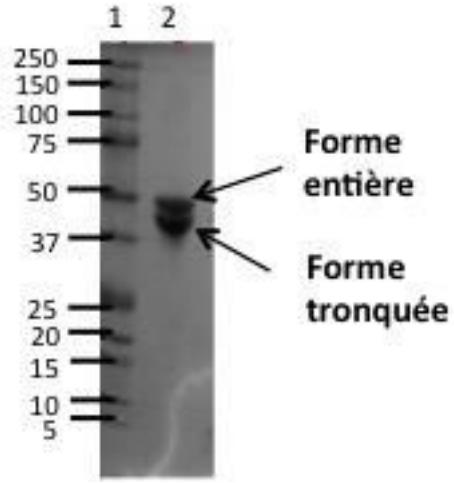

Figure 4 : Gels SDS PAGE obtenus après expression de la protéine dans les bactérie (A) BL21 DE3 pLysS et (B) BL21 DE3. Les fractions aliquotées durant les différentes étapes d'extraction pour les cultures induites (I) et non-induites (NI) ont été séparées sur gel 12% polyacrylamide en condition dénaturante (equivalent 500µl de culture). Après 1h de migration à 150V, les gels ont été colorés au bleu de Coomassie. Les différentes abréviations sont en anglais et se décrivent de façon suivante : SN: supernageant après la lyse cellulaire , FT: flowthrough, Surnageant après incubation de l'extrait cellulaire avec les billes d'amylose, W_n: étapes de lavage des billes d'amylose avec le n correspondant aux différentes étapes, E_n correspond aux étapes d'élutions avec les n correspondant aux différentes étapes, M: Marqueur de poids moléculaire. La table en dessous des gels contient les masses théoriques des différentes formes de la MBP-p24TMDH obtenues en utilisant leurs séquences en utilisant le logiciel ProtParam via le site ExPASy (http://web.expasy.org/protparam/). (C) Identification des formes tronquées et entières de la MBP-p24TMDH.

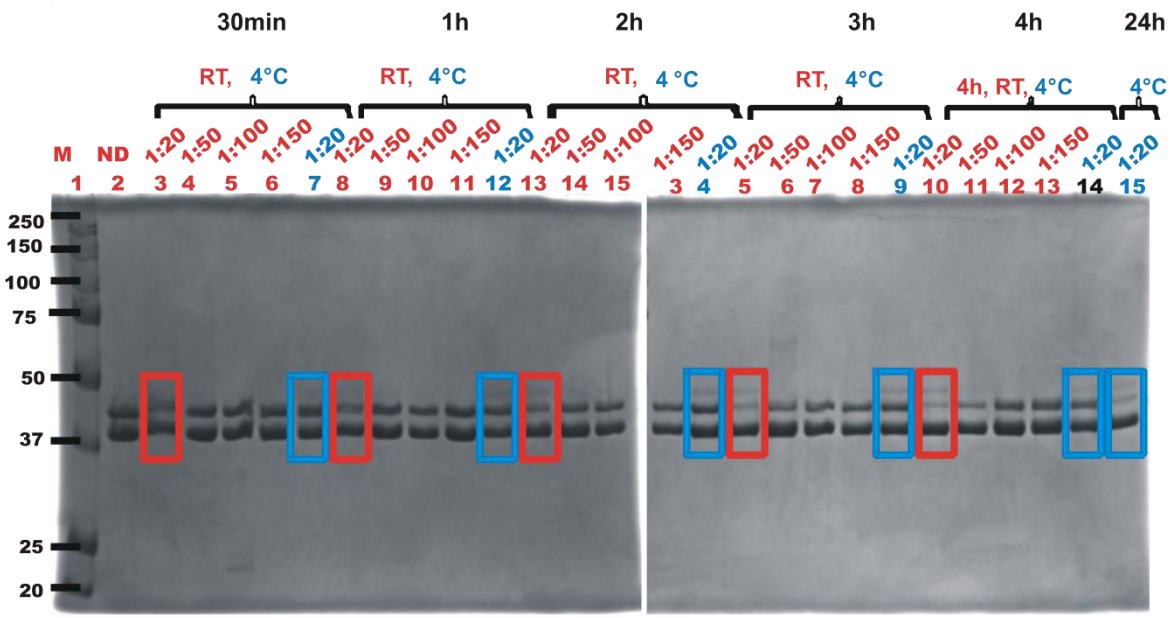

Figure 5 : Cinétique de clivage de la MBP-p24TMD à température ambiante (RT) et à 4°C.

1.2 Expression du TAF12-p24TMD :

Nous avons par la suite conçu un autre vecteur dans notre laboratoire appelé pTIXP4-p24TMD* et qui permet d'exprimer le peptide p24TMD fusionné au TAF12 (TATA box binding protein (TBP)-Associated Factor 12 Histone fold Domain), un facteur de transcription utilisé ici comme protéine de fusion. Il favorise l'accumulation de la protéine de fusion dans les corps d'inclusion limitant ainsi sa toxicité pour les bactéries (Vidovic et al., 2009). Afin de faciliter la purification de la protéine recombinante TAF12-p24TMD, une série de six histidines (His tag) a été introduite à la suite du TAF12 suivi d'un site Aspartate-Proline (DP) de clivage à l'acide formique afin de permettre le clivage de TAF12 et la purification du p24TMD (**Table1**).

Afin de mettre en place le protocole d'expression de ce nouveau vecteur, différentes souches bactériennes (BL21 DE3, BL21 DE3 pLys S, BL21 AI) ont d'abord été testés. Les résultats obtenus ont montré que l'expression du TAF12-p24TMD est plus importante dans BL21AI (données non présentées). Cette souche par rapport aux autres, a spécifiquement été conçue pour permettre l'expression de protéine toxique. Elle contient une copie chromosomique du gène de l'ARN polymerase de T7 sous le contrôle étroit de la araBAD promoteur permettant l'induction de l'expression protéique par l'arabinose en plus de l'IPTG pour les vecteurs pETs comme le pTIXP4. Par la suite, différents paramètres (inducteur, OD de l'induction et de la température) ont été testés suivant les étapes d'expression décrites précédemment. Les différents tes ont montrés que la meilleure expression se fait lorsque l'induction est faite à la DO (600nm) ≈ 1, par ajout de 0,8mM d'IPTG et 1% d'arabinose à 37°C durant 3h (**Figure 6**). Après l'expression, les cellules sont lysées par sonication et centrifugées à 111000 g, pendant 30 min à 4 °C. Le culot correspondant à la partie insoluble (Mbe+CI) est ensuite récupéré et solubilisé avec de la guinidine 6M afin de séparer la fraction membranaire (Mbe) des corps d'inclusion (CI). Cette séparation est réalisée par centrifugation à 12900 g pendant 20 min à 20 °C et le surnageant correspondant aux corps d'inclusion est incubé pendant 1h avec de la résine de cobalt afin de purifier notre protéine d'intérêt. Après incubation la résine de cobalt est lavée et la protéine TAF12-p24TMD purifié. Afin d'identifier cette protéine, un aliquot de chaque fraction des différentes étapes de purification a été préparé et séparé par électrophorèse sur un gel de polyacrylamide 16% en condition dénaturante (**Figure 6**).

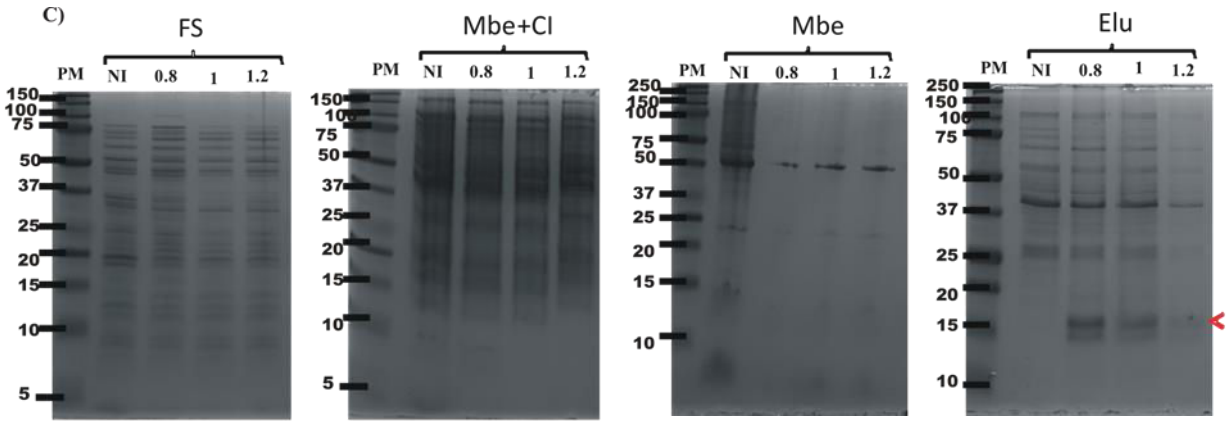

	Weight (kDa)
TAF12-p24TMD monomer	15.623
TAF12-p24TMD dimer	31.247

Figure 6 : SDS-PAGE des différentes fractions durant l'étape de purification du TAF12-p24TMD.
Des aliquotes différentes fractions obtenues durant l'étape de purification pour les cultures induites (I) à différentes concentrations d'IPTG (0,8 ; 1, 1,2 mM) et constante arabinose (1%) ou non-induites (NI) ont été préparés et séparés par électrophorèse sur gel 16% en conditions dénaturantes durant 1h à 150V. Les quantités déposées pour chaque fraction ainsi que leurs abréviations sont les suivantes : 24µl (équivalent 120µl de culture) de fractions soluble (FS) et insoluble (Mbe+CI), 12µl (équivalent 1,2ml de culture) e fraction membranaire (Mbe), 25µl (équivalent 1,2ml de culture) d'élution et 12µl de marqueur de poids moléculaire (PM). La flèche rouge indique la protéine d'intérêt et le tableau les masses théoriques attendues.

Les résultats obtenus montrent notre protéine d'intérêt est présente dans les élutions confirmant qu'elle accumule bien dans les corps d'inclusions (**Figure 6**). Cependant, il a été difficile de la quantifier à cause de la présence d'autres protéines qui sont éluées en même temps. Ces protéines peuvent soient avoir une affinité pour la résine de cobalt ou se liées à au TAF12-p24TMD via des interactions hydrophobes ; ce qui explique leur présence dans les élutions.
De plus, en purifiant par chromatographie liquide en phase inverse ces élutions ou directement la fraction insoluble solubilisé préalablement par la guanidine 6M (Mbe+CI), nous nous n'avons pas pu obtenir une fraction pure de notre protéine d'intérêt. En effet, après purification de la fraction (Mbe+CI) par chromatographie inverse et analyse par spectrométrie de masse MALDI des fractions élutions, les spectres obtenus montrent qu'elles ne sont pas pures y compris la fraction dans laquelle nous avons identifié un pic de masse proche de celle attendu pour le TAF12-p24TMD (**Figure 7**).

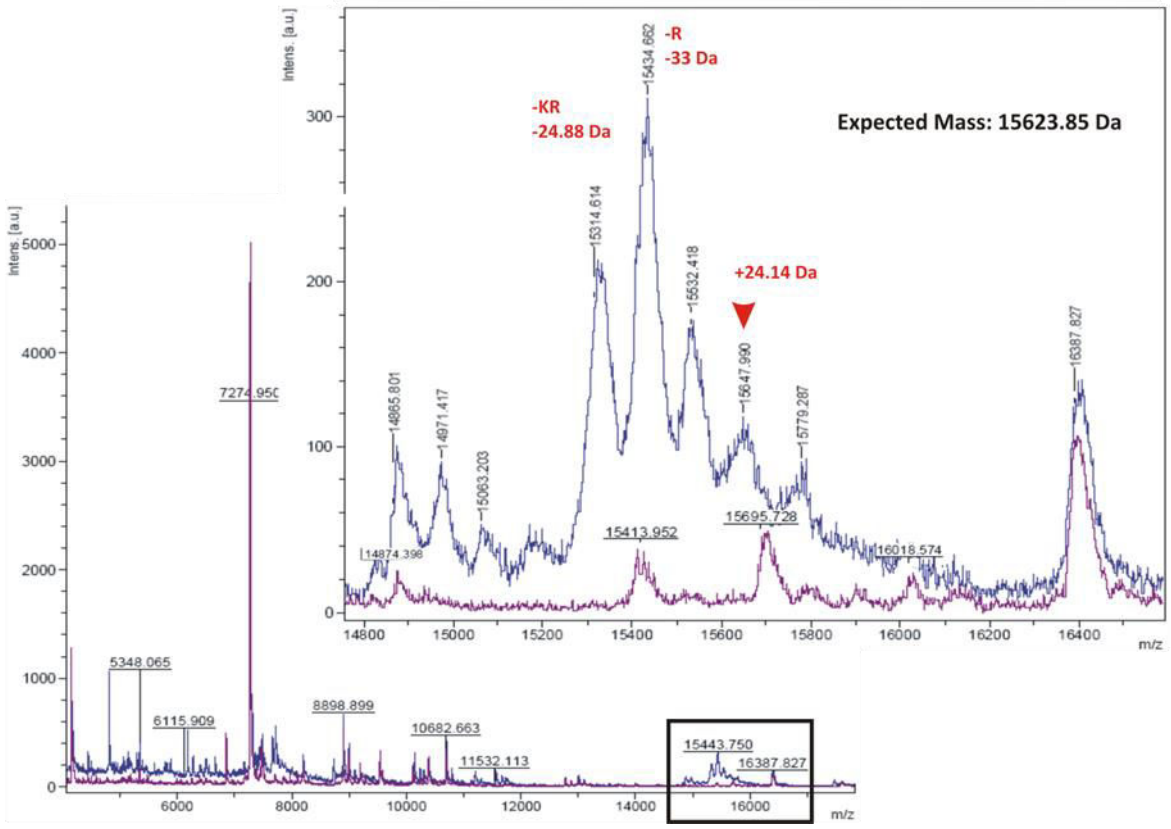

Figure 7 : Spectre de masse MALDI après purification de la fraction insoluble solubilisée dans le guanidine 6M et purification par chromatographie en phase inverse. 1µl de chaque elution a été mélangée à 1µl de matrice SA (Sinapinic Acid) puis analysé par spectrométrie de masse MALDI-TOF en mode linéaire avec 30% de laser. La calibration a été réalisée au préalable avec un mélange de protéine de masse connues (protein calibration standard I). Nous avons montré ici la superposition des spectres entiers (à gauche) des fractions d'élution obtenues en condition induite (bleu) et non-induite (violet) dans laquelle nous avons identifié le pic avec une masse proche de celle attendue (zone encadrée). A droite, un agrandissement de cette region. La flèche rouge indique le pic correspondant potentiellement au TAF12-p24TMD. Les abréviations –KR et –R indiquent les pics correspondant potentiellement à la protéine d'intérêt sans les résidus KR (Lysine et Arginine) et R (Arginine)situés en C-terminal de sa séquence.

Nous avons ensuite mélangé cette fraction à 75% d'acide formique et incubé à 50°C pendant 24h afin de cliver le peptide p24TMD du TAF12. Ce clivage se fait avec ajout d'une proline (P) en Nter du peptide (voir séquence **Table1**). Après purification par chromatographie en phase inverse et analyse des fractions d'élution par spectrométrie de masse MALDI, nous avons identifié dans une des fractions un pic pouvant potentiellement correspondre au peptide p24TMD mais tronqué en Nter (**Figure 8**). Nous ne pouvons néanmoins que spéculer sur ce résultat car ce peptide pourrait bien être le résultat de la protéolyse d'autres protéines présentent dans l'élution de départ. Une façon de s'en assurer aurait été de faire un séquençage peptidique pour en connaître la séquence.

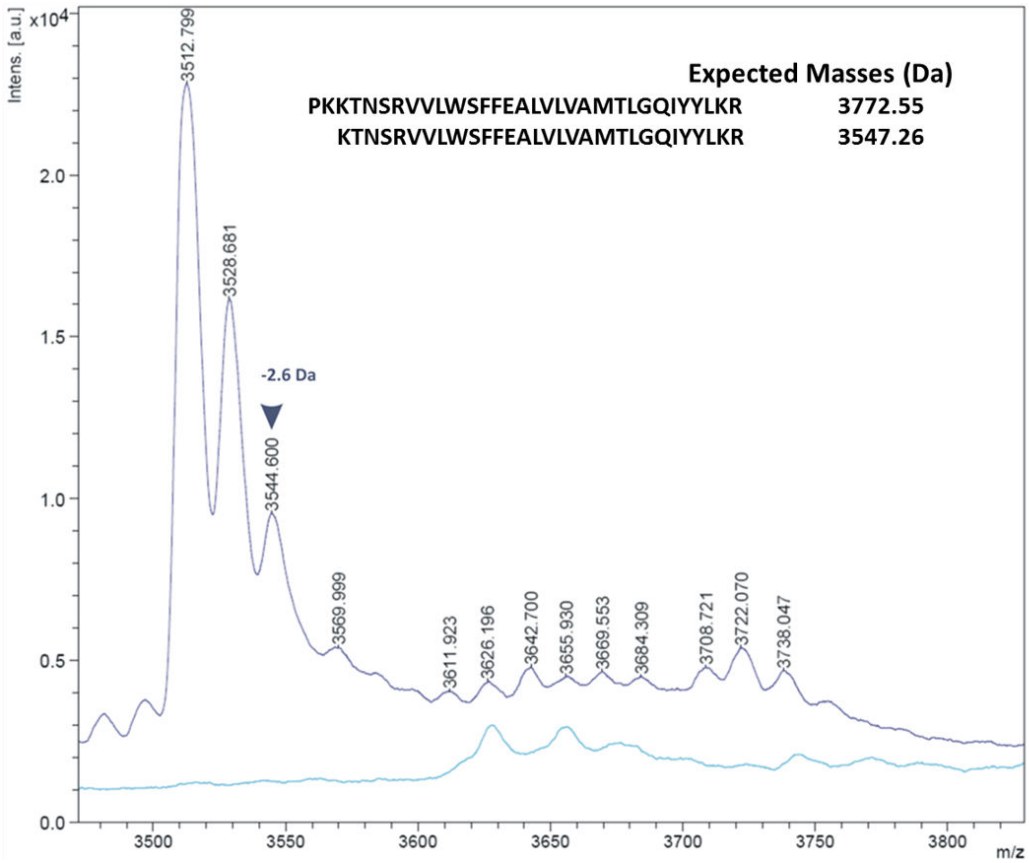

Figure 8 : Spectre de masse MALDI après clivage du p24TMD et purification en phase inverse. Les spectres des fractions obtenues en condition induite (violet) et non induite (turquoise) sont présentés ici. La calibration a été réalisée avec un mélange de protéine de masse connues (protein calibration standard I). La flèche bleue indique potentiellement le p24TMD tronqué.

En résumé, dans le but d'obtenir le peptide p24TMD uniformément marqué, nous avons mis au point les protocoles d'expression des protéines de fusion MBP-p24TMDH et TAF12-p24TMD en milieu riche. Dans les deux cas, nous avons pu identifier les protéines de fusion respectivement dans la fraction soluble et les corps d'inclusion comme attendu. Cependant, après l'étape de purification nous n'avons pas pu quantifier la protéine TAF12-p24TMD à cause de la présence d'autres protéines éluées simultanément. Nous n'avons pas pu obtenir de fraction pure de cette protéine même en la séparant d'autres protéines par chromatographie en phase inverse. En revanche, bien que nous avons pu quantifier la MBP-p24TMDH, la présence d'une forme tronquée présente en proportion plus importante constitue un problème majeur avec ce système d'expression parceque cette observation affecte le rendement final du peptide. Dans les deux cas, nous avons pu mettre en place un protocol de clivage dans le cas de MBP-p24TMDH après purification par chromatographie d'affinité à l'amylose et directement à partir de la fraction insoluble pour le TAF12-p24TMD. Afin de purifier les peptides, nous avons utilisé l'extraction au butanol et la chromatographie en phase inverse. Dans les deux cas nous n'avons pas pu identifier le peptide entier. En effet, après clivage du TAF12-p24TMD, nous avons caractériser par spectrométrie de masse un peptide qui pourrait potentiellement correspondre au p24TMD tronqué de 2 acides aminé en Nter. Dans le cas de la MBP-p24TMDH, nous n'avons pas pu caractériser le peptide ni par électrophorèse ou par spectrométrie de masse. La difficulté à identifier le peptide p24TMDH peut s'expliquer par la différence de taille importante entre la protéine de fusion MBP (42.5 kDa) et le peptide (3.9 kDa). De plus, ce peptide est très hydrophobe et agrège probablement avec d'autres peptides ou protéines en solution. En considérant les difficultés majeures rencontrées avec les deux systèmes d'expression, nous avons proposé de continuer à travailler avec le pTIXP4-p24TMD (TAF12-p24TMD). En effet ce système présent moins de dégradation et comparé au pMal c 5X-p24TMDH. De plus, la protéine de fusion TAF12 (11,8 kDa) ne représente que 4 fois la taille du peptide

p24TMD (3,7 kDa). Cependant, des efforts considérables sont à mettre en place en ce qui concerne l'étape de purification de la protéine de fusion TAF12-p24TMD car elle est importante pour le rendement final et la caractérisation du peptide. Des méthodes adéquates de détection du peptide par spectrométrie de masse doivent également être développé plus spécifiquement. La **Table 2** ci-dessous récapitule tous les résultats obtenus en ce qui concerne l'expression des deux peptides.

Table2 : Résumé des résultats obtenus avec les différents vecteurs d'expression.

		pMal c 5X-p24TMDH	pTIPX4-p24TMD
Protéines de fusion	Expression	Mis en place	Mis en palce
	Purification	Forme tronquée et perte	Pas de fraction pure et perte
	Quantification	15.6mg/litre de culture	Difficile
Clivage	Protocol	Mis en place	Mis en place
Peptides	Purification	Difficile	Difficile
	Quantification	Non	Non
	Charactérisation	Non	Pepdide tronqué?

N'ayant pas pu obtenir le peptide entier par expression en système bactérien, nous avons utilisé la synthèse chimique qui présente l'avantage de permettre l'obtention de rendement important de peptide pure dans un temps relativement court comparé à l'expression en système bactérien. Cependant, le marquage homogène d'un peptide revient extrêmement plus cher en terme de coût. Cette technique est néanmoins adaptée au marquage spécifique d'une position dans une séquence peptidique. De plus, le rendement dépend de la taille et de la séquence du peptide. Une autre limite majeure concerne le fait que tous les acides aminés marqués ne sont pas toujours disponibles sur le marché.

Nous avons testé la synthèse chimique en phase solide (Fmoc) des deux peptides. La synthèse du p24TMDH était beaucoup plus difficile et les rendements obtenus très faible voir sans peptide. Nous avons utilisé le double couplage pour améliorer ce rendement. Après synthèse, celui-ci était respectivement de 59,4 et 68,4% pour le p24TMD et le p24TMDH par rapport à la masse théorique attendue. Cependant, nous n'avons pas pu purifier le p24TMDH parce qu'il agrégeait même en le solubilisant dans différents solvants (eau/isopropanol ou eau/HFIP). En revanche nous avons pu purifier le p24TMD par chromatographie en phase reverse en utilisant un gradient d'acétonitrile / eau allant de 30 à 95% de solvant B (acétonitrile/TFA 100/0.1, v/v). Bien que le rendement après purification était seulement de 10%, les quantités de peptide obtenues étaient néanmoins suffisante pour faire 2 à trois échantillons pour la RMN (entre 20 et 30mg). En plus, la pureté des échantillons obtenus a été estimée à 96%, ce qui montre qu'ils sont relativement purs et ce critère est indispensable à l'analyse par RMN. Nous avons par la suite caractérisé le peptide par spectrométrie de masse MALDI (**Figure 9**).

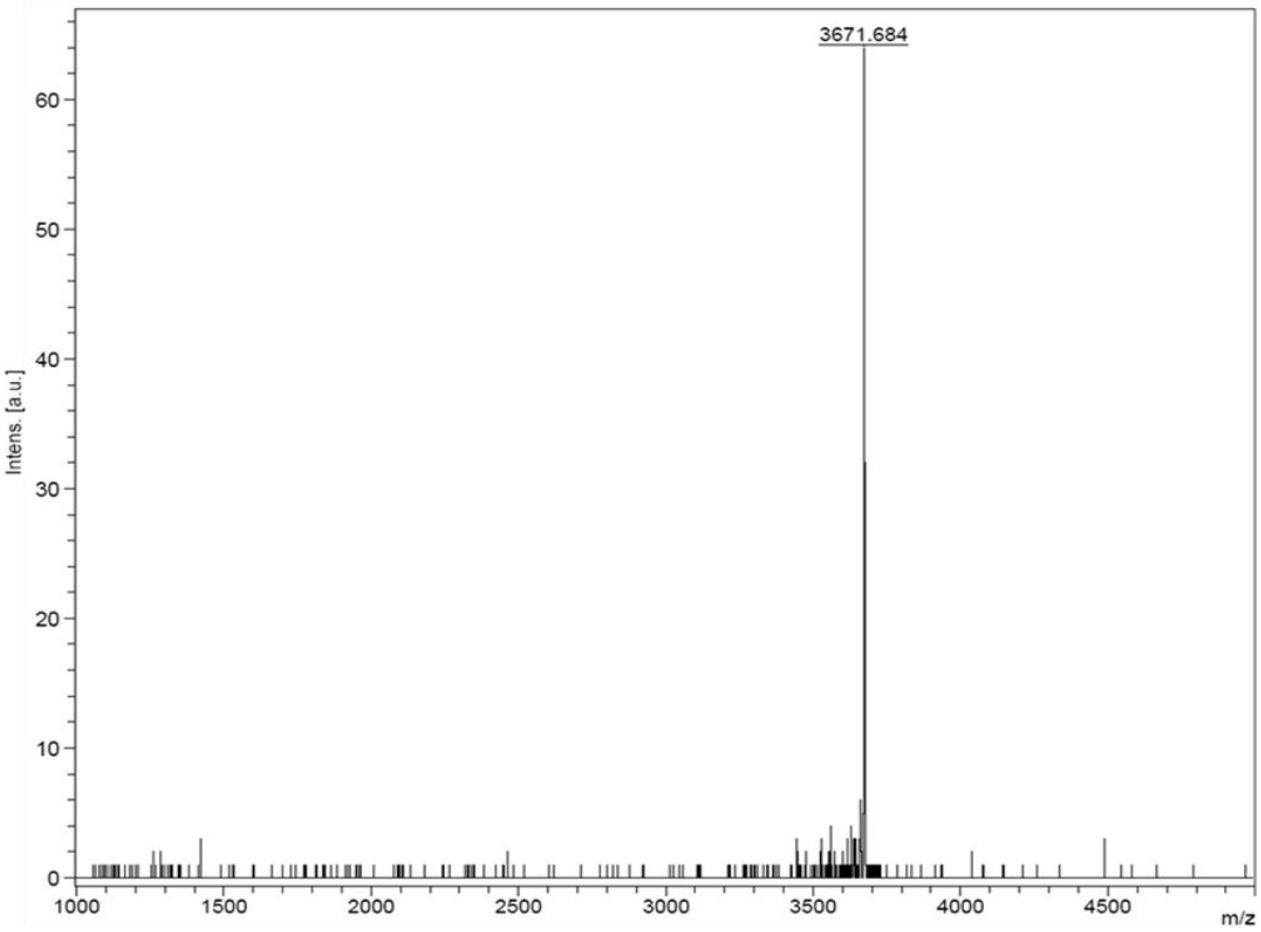

Figure 9 : Spectre de masse MALDI du p24TMD après synthèse et purification en phase inverse.

Par la suite nous avons utilisé ce peptide synthétique pour mener nos études sur l'interaction entre le p24TMD et la sphingomyéline. Les résultats obtenus sont présentés ci-dessous.

C) Caractérisation biophysique de l'interaction entre le peptide p24TMD et la SM C18

Le peptide p24TMD étant naturellement transmembranaire, il semblait donc primordial de reproduire un environnement proche des conditions biologiques afin de rendre sa caractérisation possible. Cette partie de mon travail a consisté à établir dans un premier temps les conditions expérimentales favorables à la reconstitution du peptide dans des membranes artificielles. Pour cela, des tests de solubilité du p24TMD ont été réalisés dans des conditions mimant les propriétés hydrophobes des membranes : solvants organiques (dichlorométhane, TFE, HFIP), différents détergents (SDS, DPC) et avec différents types de lipides (POPC, POPE, POPS) dans des liposomes ou des liposomes mixtes (mélange de différents lipides). Ces différentes conditions ont été étudiées par dichroïsme circulaire (CD) et par fluorescence du tryptophane (Trp). En effet, ces techniques permettent d'étudier le repliement des protéines dans leurs environnements. Nous avons montré que le peptide p24TMD en solution n'adopte pas une structure en hélice dans l'eau mais dans le mélange de solvants eau/HFIP (50/50, v/v) avec un pourcentage en hélice estimé à plus de 80%. La reconstitution du peptide préalablement préparé dans eau/HFIP (50/50, v/v) a ensuite été testée dans différentes membranes artificielles. Ces membranes ont été préparées à partir de lipides de taille et/ou groupes fonctionnels différents (POPC, POPE et DMPC) afin de tester l'effet sur l'insertion du peptide durant la reconstitution. Nous avons également des membranes préparées avec un mélange de lipides avec la sphingomyèline (POPC/SM (95/5) et POPC/POPE/SM (85/10/5) pour tester l'effet de cette dernière sur le p24TMD. Le spectre de dichroïsme circulaire obtenue montre

un spectre caractéristique prononcé d'une structure en hélice lors que le peptide est reconstitué dans le POPC/SM (95/5) comparé aux autres membranes (**Figure 10**). Ce résultat comparé à celui obtenu pour la membrane de POPC montre que la sphingomyèline influence la structure du peptide et donc interagit avec ce dernier. En revanche, le POPE semble favoriser l'agrégation du peptide. Ces résultats ont également été confirmés par les données expérimentales obtenues par fluorescence du Trp (non présenté)

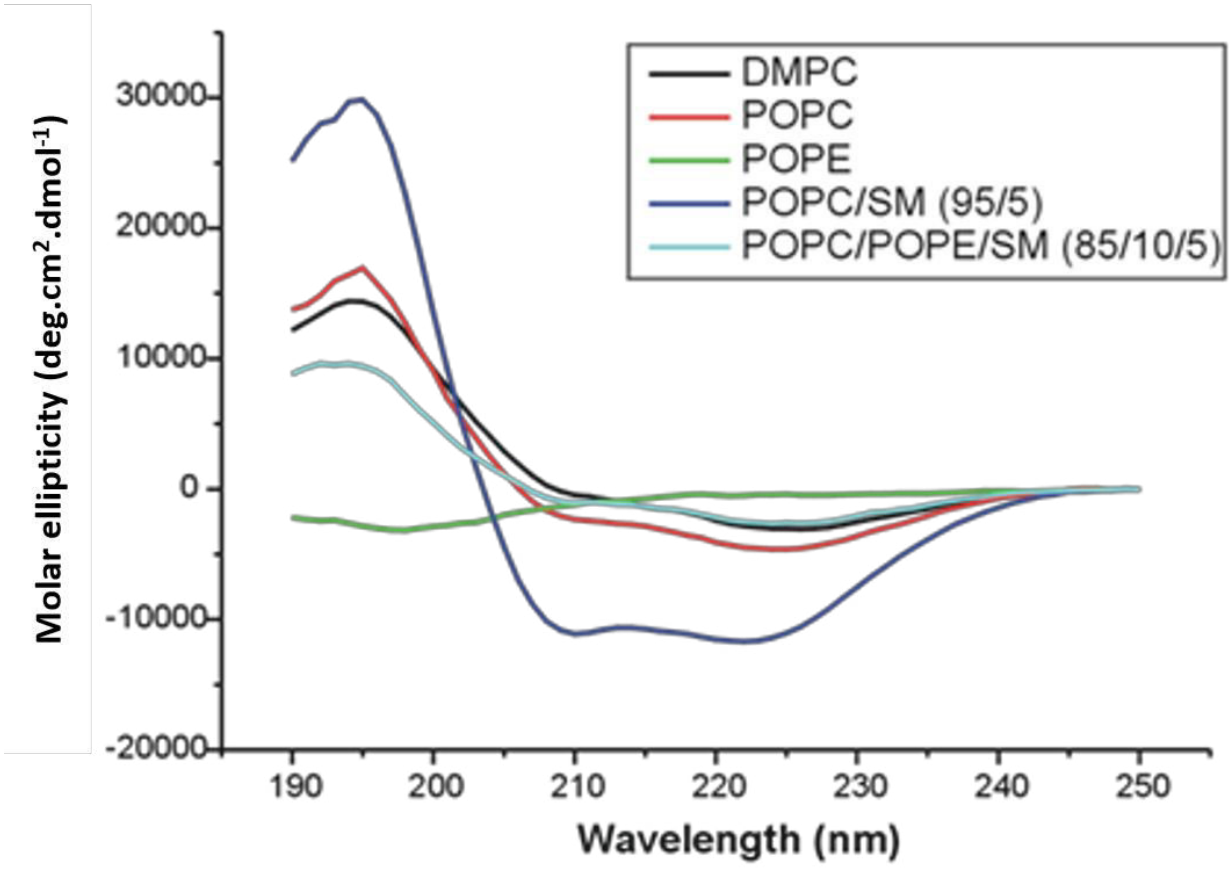

Figure 10 : Spectre de dichroïsme circulaire du p24TMD reconstitué dans différentes membranes.

Les résultats obtenus nous ont permis de mettre au point le protocole de reconstitution du p24TMD dans les membranes, et par la suite plus spécifiquement la préparation des échantillons orientés pour des études par RMN du solide (Kemayo Koumkoua et al., 2014).

La topologie et la dynamique des peptides membranaires peuvent être étudiées grâce à la spectroscopie RMN du solide de ^{15}N et du ^{2}H (Bechinger, 2001; Bechinger and Salnikov, 2012; Bechinger and Sizun, 2003; Bechinger et al., 2011). Cependant, comparé à la RMN du liquide qui donne un signal moyen avec des pics fins et bien définis dû aux mouvements rapides des molécules en solution, le signal en RMN du solide est large parce que les molécules sont quasi statiques voir immobiles. Afin d'obtenir des spectres mieux définis et exploitables, des approches ont été développées : la rotation à l'angle magique (MAS pour Magic Angle Spinning) et la RMN des échantillons statiques orientés entre lamelles de verre. Nous avons principalement utilisé la dernière méthode. Elle prend avantage du fait que le signal en RMN du solide dépend de l'orientation par rapport au champ magnétique B_0. En effet, l'échantillon est déposé sur des lamelles de verres et orienté avec la normale de la membrane parallèle par rapport au champ B_0. Dans cette condition, lorsque le déplacement chimique de l'azote 15 (^{15}N) est supérieur à 200ppm, le peptide est transmembranaire et en dessous de 100ppm le peptide a une orientation plane (sur la membrane)

(Bechinger and Sizun, 2003). L'orientation des membranes est contrôlée par RMN du phosphore (^{31}P) (Bechinger and Sizun, 2003).

Dans le cas du peptide p24TMD, ce dernier a été préparé dans le mélange eau/HFIP (50/50, v/v) et ajouté séquentiellement au POPC, POPC/SM (95/5) ou au POPC/SM (90/10) préalablement dissout dans du HFIP afin d'éviter de se retrouver uniquement en présence d'eau pour prévenir l'agrégation du peptide. L'échantillon a été préparé avec un ratio molaire final protéine/lipide (P/L) de 1%, déposé sur des lamelles de verre et orienté par rapport au champ B_0. Les spectres de ^{31}P ont donné un pic important autour de 25-30ppm et un autre moins important autour de -15ppm indiquant que les membranes sont bien orientées (**Figure 11**, à gauche). Les spectres de ^{15}N du peptide marqué à différentes positions (ici Leu 18) ont tous donné des pics avec déplacement chimique supérieur à 200ppm (**Figure 11**, à droite) indiquant que le peptide adopte une orientation transmembranaire dans les différentes membranes et donc que la SM C18 ne change pas la topologie de l'axe principale du peptide.

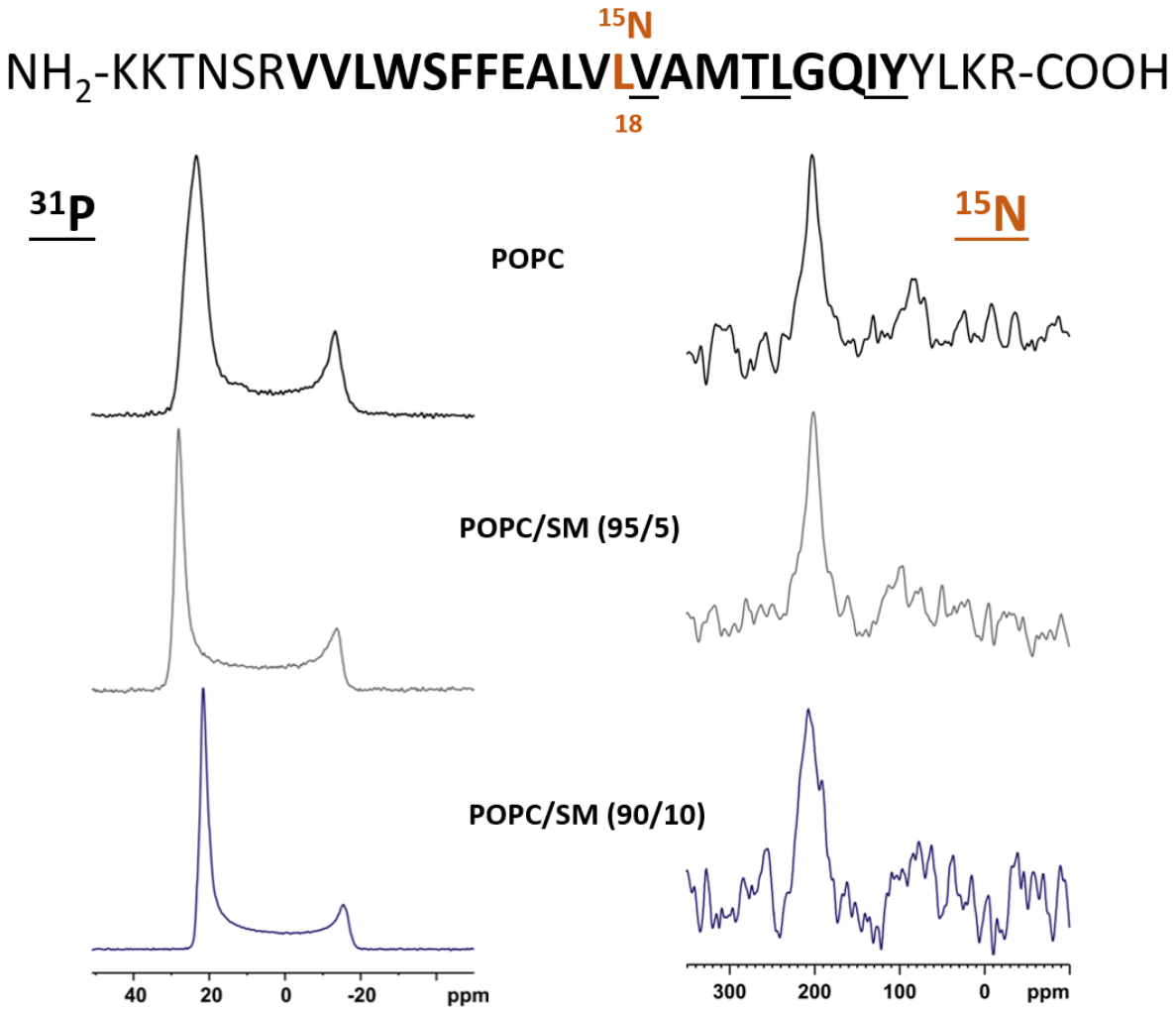

Figure 11 : Spectres RMN de ^{31}P des différentes membranes dans lesquelles le ^{15}NLeu18-p24TMD a été reconstitué ainsi que les spectres ^{15}N obtenus.

En plus de la RMN de ^{15}N, le peptide a également été marqué en 2H afin d'étudier la dynamique du peptide. En effet, la forme des spectres ^{2}H est un bon indicateur de la dynamique des peptides car elle est beaucoup plus sensible aux petites variations de mouvements du peptide dans les membranes. Les spectres ^{2}H expérimentaux obtenues lorsque le p24TMD est reconstitué dans les membranes de POPC et POPC/SM (95/5) sont larges (données non présentées) indiquant qu'il n'y

a pas une orientation mais une distribution autour de l'orientation principale. De plus, en présence de le SM C18, nous n'avons pas observé une différence significative, ce qui indique que la SM C18 n'affecte probablement pas de façon significative la dynamique du squelette peptidique.

Afin de proposer un modèle de la topologie du p24TMD dans les membranes, un diagramme a été généré à partir des valeurs de déplacement chimiques et de couplage quadripolaire obtenues pour différentes positions respectivement à partir des spectres ^{15}N et ^{2}H. Une seule courbe est générée pour chaque position donnée lorsque la valeur correspondante est introduite dans le programme MATHEMATICA avec les valeurs des coordonnées atomiques du résidu correspondant. Cette opération est réalisée pour chaque position et toutes les courbes générées sont superposées. Le point d'intercession par lequel toutes les courbes se touchent permet de lire les différents angles permettant de décrire la topologie du peptide dans les membranes. L'angle que fait l'axe principal du peptide par rapport à la normale de la bicouche a été estimé à 19° (**Figure 12**).

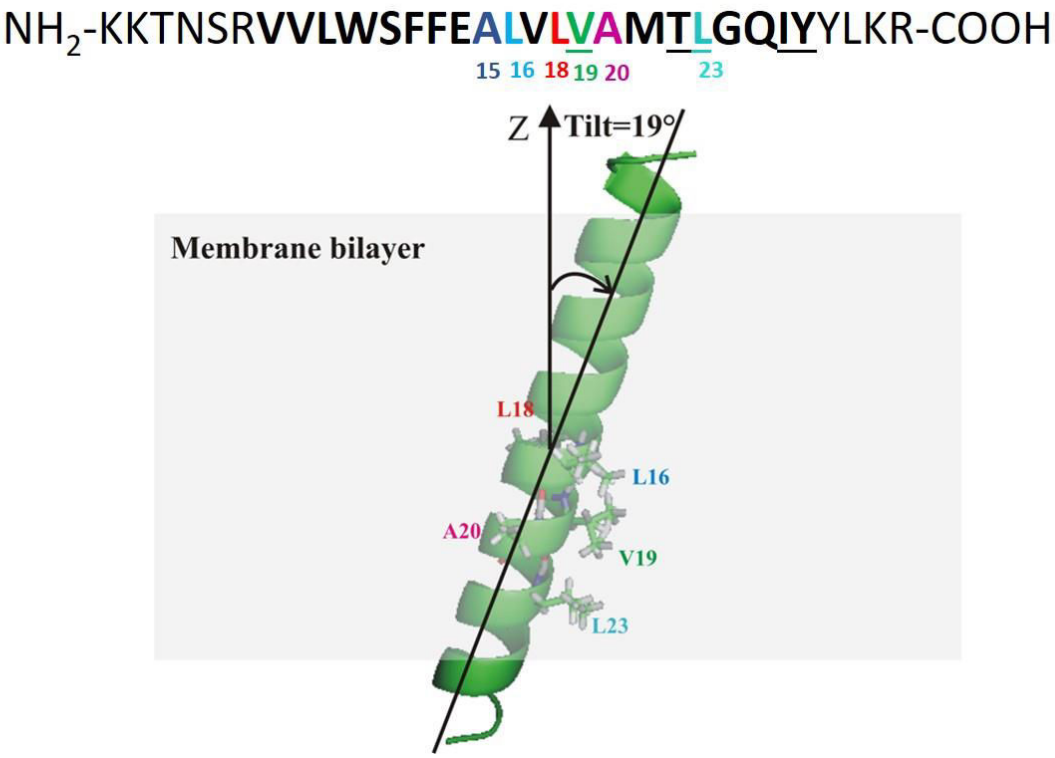

Figure 12 : Topologie du p24TMD dans des membranes de POPC/SM (95/5).

En résumé, nous avons montré par spectrométrie CD et fluorescence que la SM C18 interagit avec le peptide p24TMD probablement en affectant son repliement. Cependant, les études structurales réalisées par RMN du solide indiquent que cette interaction n'affecte vraisemblablement pas la topologie et la dynamique du squelette peptidique.

Nous avons également étudié l'effet de la SM C18 sur la dynamique de la chaîne latérale de la Leucine 23 (Leu 23) qui fait partie du motif responsable de l'interaction ce lipide. Nous avons pour cela utilisé la RMN du ^{2}H. Le peptide ^{2}HLeu23-p24TMD a été reconstitué dans les membranes de POPC et POPC/SM (95/5) avec un ratio molaire finale P/L de 1% et orienté avec la normale de la bicouche parallèle ou perpendiculaire au champ B_0. Dans les deux cas, à température ambiante (25°C) nous n'avons pas obtenu de signal (non présenté). En revanche à -20°C lorsque tous les mouvements sont figés, nous avons obtenus du signal ce qui indique qu'à température ambiante ce signal ne peut probablement pas être mesuré dans l'échelle de temps dans laquelle nous travaillons. La **Figure 13** montre la superposition des spectres ^{2}H obtenus lorsque l'échantillon est orienté parallèlement (en noir) ou perpendiculairement (en fushia) par rapport au champ B_0. Lorsque le peptide est reconstitué dans les membranes de POPC, on note une différence entre les spectres

superposés tandis que dans les membranes de POPC/SM (95/5) cette différence diminue considérablement. Ce résultat indique que les chaînes latérales de la Leu 23 présentent un certain degré d'alignement en l'absence et pas en présence de la SM C18. Ce qui suggère que la SM C18 affecte probablement la dynamique des chaînes latérales de la leucine 23.

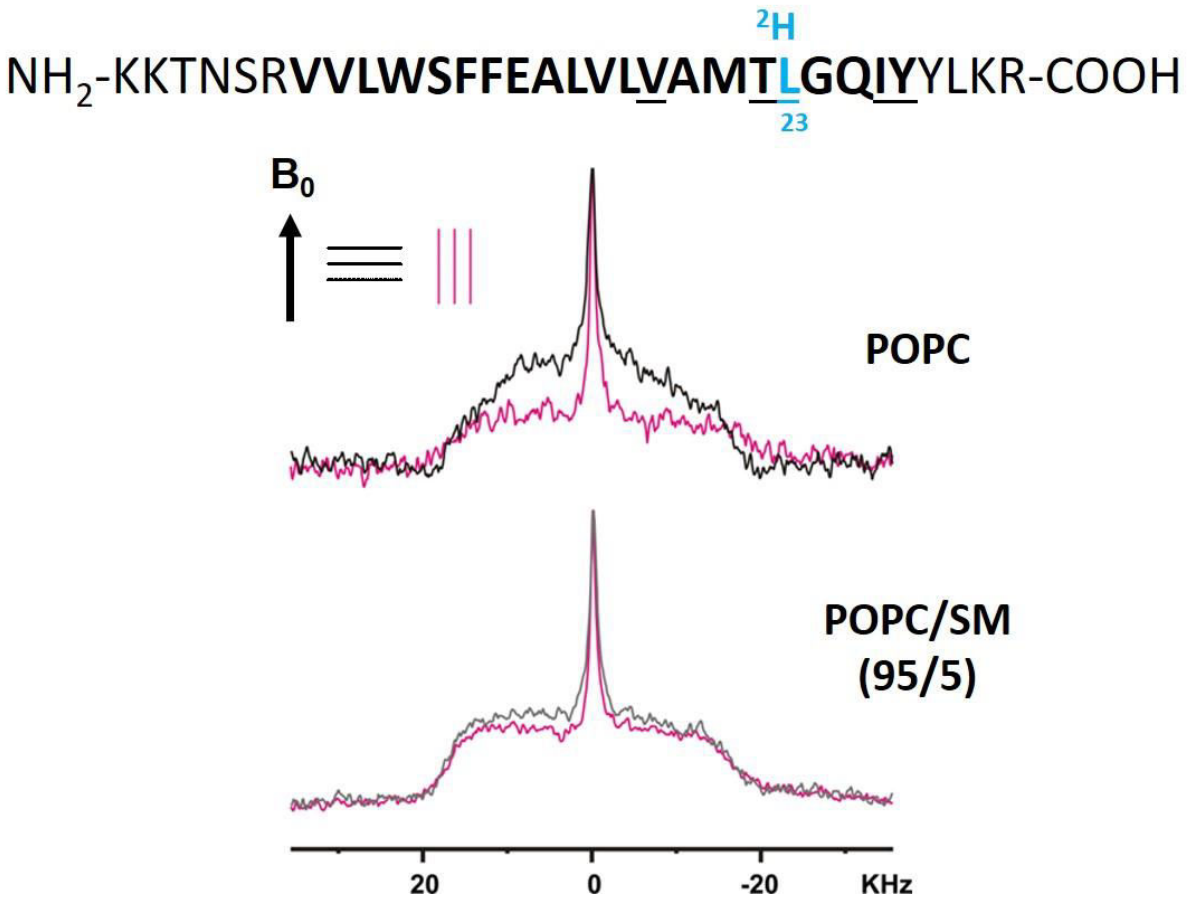

Figure 13 : Spectres ^{2}H du ^{2}HLeu23-p24TMD reconstitués dans des membranes de POPC et POPC/SM (95/5) mesurés à T -20°C lors que l'échantillon est orienté parallèlement (noir) ou perpendiculairement (fushia) par rapport au champ B_0.

Conclusions et perspectives

Ce travail de thèse avait pour objectif de caractériser l'interaction entre le domaine transmembranaire de la protéine p24 et la SM C14. Nous avons dans ce but voulut tout d'abord obtenir ce peptide. Et pour cela nous avons utilisé dans un premier temps l'expression en système bactérien puis la synthèse chimique. Concernant la première technique, nous avons utilisé deux systèmes d'expression (pMal c 5X-p24TMDH et pTIXP4-p24TMD) et avons pu mettre au point un protocol pour exprimer le peptide d'intérêt. Dans les deux cas, nous n'avons pas pu caractériser de peptide entier. Néanmoins en prenant en compte les différents problèmes rencontrés, nous avons proposé des deux systèmes de continuer à travailler avec le pTIXP4-p24TMD en améliorant la purification de la protéine de fusion TAF12-p24TMD ainsi que les techniques de détection du p24TMD. Nous avons néanmoins pu obtenir ce peptide par synthèse chimique.
Ensuite en utilisant la CD et la fluorescence du Trp nous avons pu mettre au point un protocole de reconstitution du pp24TMD dans les membranes. Nous avons également montré que la SM C18 interagit avec ce peptide en affectant sa structure. Cependant des études structurales poussées de la topologie et la dynamique dans les membranes par RMN du solide ont montré que la SM C18

n’affecte pas le squelette peptidique mais probablement la chaîne latérale de la Leu23 impliqué dans le motif d’interaction.

Ce travail a permis d’obtenir des informations structurales permettant de caractériser le peptide p24TMD dans un environnement membranaire. Cependant d’autres données structurales complémentaires doivent être obtenus. Particulièrement des expériences de PISEMA (Polarization Inversion Spin Exchange at the Magic Angle) qui permettrait d’avoir une topologie plus précise du peptide dans les membranes ainsi que le REDOR (Rotational Echo DOuble Resonance) qui permettrait de mesurer la distance inter atomique par exemple entre les chaines latérales de la Leu23 et la SM C18. La RMN du liquide dans les micelles est également complémentaire car elle permet d’obtenir comme pour la MAS des spectres mieux résolus. Toutes ces données sont indispensables pour pouvoir proposer un modèle pouvant être comparé au modèle proposé par *Contreras et al* et afin d’en tirer des conclusions.

Bibliographies:

Bechinger, B. (2001). Solid-state NMR investigations of interaction contributions that determine the alignment of helical polypeptides in biological membranes. FEBS Lett. *504*, 161–165.

Bechinger, B., and Salnikov, E.S. (2012). The membrane interactions of antimicrobial peptides revealed by solid-state NMR spectroscopy. Chem. Phys. Lipids *165*, 282–301.

Bechinger, B., and Sizun, C. (2003). Alignment and structural analysis of membrane polypeptides by 15N and 31P solid-state NMR spectroscopy. Concepts Magn. Reson. Part A *18A*, 130–145.

Bechinger, B., Resende, J.M., and Aisenbrey, C. (2011). The structural and topological analysis of membrane-associated polypeptides by oriented solid-state NMR spectroscopy: established concepts and novel developments. Biophys. Chem. *153*, 115–125.

Béthune, J., Wieland, F., and Moelleken, J. (2006). COPI-mediated transport. J. Membr. Biol. *211*, 65–79.

Brügger, B., Sandhoff, R., Wegehingel, S., Gorgas, K., Malsam, J., Helms, J.B., Lehmann, W.D., Nickel, W., and Wieland, F.T. (2000). Evidence for segregation of sphingomyelin and cholesterol during formation of COPI-coated vesicles. J. Cell Biol. *151*, 507–518.

Contreras, F.-X., Ernst, A.M., Haberkant, P., Björkholm, P., Lindahl, E., Gönen, B., Tischer, C., Elofsson, A., von Heijne, G., Thiele, C., et al. (2012). Molecular recognition of a single sphingolipid species by a protein's transmembrane domain. Nature *481*, 525–529.

Coskun, U., and Simons, K. (2010). Membrane rafting: from apical sorting to phase segregation. FEBS Lett. *584*, 1685–1693.

Coskun, U., and Simons, K. (2011). Cell membranes: the lipid perspective. Struct. Lond. Engl. 1993 *19*, 1543–1548.

Hanada, K., Kumagai, K., Yasuda, S., Miura, Y., Kawano, M., Fukasawa, M., and Nishijima, M. (2003). Molecular machinery for non-vesicular trafficking of ceramide. Nature *426*, 803–809.

Kamińska, J., Hoffman-Sommer, M., and Płachta, M. (2010). [The p24 family proteins--regulators of vesicular trafficking]. Postepy Biochem. *56*, 75–82.

Kemayo Koumkoua, P., Aisenbrey, C., Salnikov, E., Rifi, O., and Bechinger, B. (2014). On the design of supramolecular assemblies made of peptides and lipid bilayers. J. Pept. Sci. Off. Publ. Eur. Pept. Soc. *20*, 526–536.

van Meer, G., Voelker, D.R., and Feigenson, G.W. (2008). Membrane lipids: where they are and how they behave. Nat. Rev. Mol. Cell Biol. *9*, 112–124.

Popoff, V., Adolf, F., Brügger, B., and Wieland, F. (2011). COPI budding within the Golgi stack. Cold Spring Harb. Perspect. Biol. *3*, a005231.

Reinhard, C., Harter, C., Bremser, M., Brügger, B., Sohn, K., Helms, J.B., and Wieland, F. (1999). Receptor-induced polymerization of coatomer. Proc. Natl. Acad. Sci. U. S. A. *96*, 1224–1228.

Singer, S.J., and Nicolson, G.L. (1972). The fluid mosaic model of the structure of cell membranes. Science *175*, 720–731.

Vidovic, V., Prongidi-Fix, L., Bechinger, B., and Werten, S. (2009). Production and isotope labeling of antimicrobial peptides in Escherichia coli by means of a novel fusion partner that enables high-yield insoluble expression and fast purification. J. Pept. Sci. Off. Publ. Eur. Pept. Soc. *15*, 278–284.

Communications scientifiques

Publications :

Kemayo K P, Aisenbrey C, Salnikov E, Rifi O, Bechinger B. On the design of supramolecular assemblies made of peptides and lipid bilayers. Journal of Peptide Science. (2014, March) accepted.

Présentations poster

Kemayo K P, Aisenbrey C, Salnikov E, Brügger B, Bechinger B. NMR studies of highly specific lipid-protein interactions in lipid bilayers. Conference of the société française de biophysique (SFB) and the société française de biochimie et de biologie moléculaire (SFBBM). Grenoble, 21-23 November 2012 (**winner of poster prize**).

Communications orales:

Kemayo K P, Aisenbrey C, Salnikov E, Brügger B, Bechinger B. NMR studies of highly specific lipid-protein interactions in lipid bilayers. Réunion plénière GDR 3334 SupraMemBio : Assemblages supramoléculaires et membranes biologiques: Concepts, modèles et fonctions. Fournols, 14-17 October 2012.

Kemayo K P, Aisenbrey C, Glattard E, Salnikov E, and Bechinger B. Structural characterisation of highly specific membrane protein-lipid interactions involved in trafficking. A novel regulatory mechanism in membrane dynamics? Workshop of the German-French PhD College: "Membranes and Membrane Proteins" UFA 0407. Strasbourg, 30 November 2012.

Kemayo K P, Aisenbrey C, Glattard E, Salnikov E, and Bechinger B. Structural characterisation of highly specific membrane protein-lipid interactions involved in trafficking. A novel regulatory mechanism in membrane dynamics? ANR awardee mid-term workshop of the projects selected in 2010. Strasbourg, 7 December 2012.

Patricia KEMAYO KOUMKOUA

Structural characterisation of highly specific membrane protein-lipid interactions involved in cellular function.

Résumé

Les membranes cellulaires sont des systèmes complexes composés de lipides variés qui interagissent avec les protéines pour accomplir une fonction. Leur adressage spécifique dans la cellule est crucial pour le fonctionnement cellulaire. Les vésicules COP (**co**at **p**rotein) sont impliquées dans leur transport dans les premières étapes de la voie de sécrétion. Récemment, une interaction très spécifique a été identifiée entre le domaine transmembranaire de la protéine p24 (p24TMD) abondante dans la membrane des vésicules COP et la sphingomyéline C18:0. Cette spécificité a été identifiée dans le cas d'interaction protéine-protéine et protéine-acide nucléique comme impliquée dans la régulation de fonctions cellulaires, C'est pourquoi nous avons décidé d'étudier sur cette interaction. A cet effet, le p24TMD a été obtenu par synthèse chimique et sa structure étudiée par RMN du solide en présence de la sphingomyèline avec pour but ultime de comprendre la fonction.

Mots clés : interaction spécifique protéine-lipide, lipides, RMN, Protéine membranaire, CD.

Résumé en anglais

Cell membranes are complex systems composed of variety of lipids that interacts with proteins to trigger cellular function. The delivery of these lipids to the right compartment is crucial for cells to work efficiently. The **co**at **p**rotein (COP) complex vesicles are involved in lipids traffic in the early stages of the secretory pathway. Recently, a highly specific interaction has been found between the transmembrane domain of p24 protein (p24TMD) abundant in COPI membrane and sphingomyelin C18:0. As such highly specific interaction have been reported for protein-protein and protein-nucleic acid interactions to be involved in regulation of cell functions, we decide to investigate this specific interaction. The p24TMD was obtained chemically and investigated by solid state NMR in presence of sphingomyelin with the ultimately goal to understand the function behind.

Key words: specific protein-lipid interaction, lipid traffic, NMR, membrane protein, CD.